Title
Influence of Porous Materials on the Reactivity and Stability of Transition Metal Catalysts

Author
Lee, John Seonghyun

Publication Date
2019

Peer reviewed|Thesis/dissertation

Influence of Porous Materials on the Reactivity and Stability of Transition Metal Catalysts

By

John Seonghyun Lee

A dissertation submitted in partial satisfaction of the

requirements for the degree of

Doctor of Philosophy

in

Chemistry

in the

Graduate Division

of the

University of California, Berkeley

Committee in charge:

Professor F. Dean Toste, Chair
Professor Omar M. Yaghi
Professor Wenjun Zhang

Spring 2019

Abstract

Influence of Porous Materials on the Reactivity and Stability of Transition Metal Catalysts

by

John Seonghyun Lee

Doctor of Philosophy in Chemistry

University of California, Berkeley

Professor F. Dean Toste, Chair

Organometallic chemists have historically studied the influence of ligands and counteranions on homogeneous transition metal catalysts in order to improve their selectivities and reactivities. Recently, these interests have expanded to incorporate supramolecular hosts and heterogeneous porous materials as supports which can influence catalyst properties. This work encompasses such an integration of catalysts with heterogeneous supports, wherein two types of chiral porous materials are evaluated for their abilities to induce enantioselectivity with nano- and molecular-scale catalysts. Furthermore, the strategy of architectural stabilization is developed to improve a gold(III) catalyst *via* introduction into robust metal-organic frameworks.

Chapter 1. A variety of catalysts were immobilized in chiral mesoporous silica, and their reactivities were evaluated. Efforts towards the enantioenrichment of MOF-520 are described. Additionally, a novel post-synthetic metalation strategy is described for the introduction of a transition metal catalysts into metal-organic frameworks *via* oxidative addition.

Chapter 2. A novel architectural stabilization strategy is described with a structurally well-defined gold(III) catalyst in metal-organic frameworks. The robustness of IRMOF-10 and bio-MOF-100 were used to rigidify a gold(III) catalyst to suppress a unimolecular decomposition pathway – reductive elimination. Through this architectural stabilization strategy, decomposition of the incorporated gold(III) catalyst in the metal-organic frameworks was not observed; in contrast, the homogeneous analogue was prone to decomposition in solution. Stabilization of the gold(III) catalyst in these metal-organic frameworks precluded leaching and enabled recyclability, which is crucial for productive heterogeneous catalysis.

Influence of Porous Materials on the Reactivity and Stability of Transition Metal Catalysts

Table of Contents

Chapter 2. Suppression of a Unimolecular Decomposition Pathway by Architectural Stabilization of a Gold(III) Catalyst in Metal-Organic Frameworks

List of Figures

List of Schemes

List of Tables

Acknowledgements

So many individuals have played a pivotal role in my development as a person both before and during my time at Berkeley. I feel fortunate to have met people at every step of my life to help guide me as a scientist and help me enjoy my time both inside and outside of science.

I first want to thank Prof. Richard Brutchey and Dr. Daniel Ruddy for their mentorship and support during my undergraduate research experiences at the University of Southern California and the National Renewable Energy Laboratory, respectively. I also want to thank the Brutchey group as a whole for their involvement and support during my early growth as a chemist. I especially want to thank Prof. Federico Rabuffetti, Dr. Sean Culver, and Dr. Matthew Greaney for their mentorship and friendship during my time at USC.

I certainly would not have been about to have gone through graduate school without the amazing leadership and support of my advisor, Prof. Dean Toste. I thank him for his advice and patience to allow me to pursue challenging ideas. I also thank him for fostering an excellent group environment where everyone is supportive of one another.

I would like to thank Prof. Paul Alivisatos for his mentorship during my endeavors with chiral mesoporous silica. I would also like to thank my collaborators, Dr. Eugene Kapustin, Xiaokun Pei, and Prof. Omar Yaghi, for their helpful discussions and contributions.

During my time in the Toste group, I have met many individuals that I thank for their friendship and involvement in my growth as a scientist. I want to thank Dr. Dimitri Khrakovsky, Dr. Dillon Miles, Dr. Andrew Neel, Dr. Willie Wolf, Dr. Cindy Hong, Dr. David Kaphan, Dr. Mark Levin, Dr. Rebecca Triano, Dr. Drew Samant, and Dr. Carolina Avila for their guidance during my earlier years of graduate school. I want to thank my classmates Patrick Bohan, Suhong Kim, and Alec Christian for their friendship and support over the past five years. I also thank Dr. Jaime Coelho, Roman Sarott, Bread Miller, Dr. Patti Zhang, and Banruo Huang for their friendship and support both inside and outside of lab. I also want to thank my non-Toste group friends, Danny Thach, Jeff Derrick, Trevor Roberts, and Robinson Flaig, for their degeneracy, friendship, and support throughout the highs and lows of graduate school.

Finally, I would like to thank my parents, Young Lee and Prof. Kwan Lee, and my sister, Dr. Hannah Lee, for being great role models and for their unconditional love and support during my growth as a person and scientist.

Chapter 1

Immobilized Catalysts in Chiral Mesoporous Silica and a Chiral Metal-Organic Framework

1.1 Introduction

The synthesis of enantioenriched products is of great interest to organic chemists due to the ubiquity of stereocenters in biologically active compounds. Throughout this field, homogeneous catalysts bearing chiral ligands have typically been employed to kinetically bias the formation of one enantiomeric product over another. However, homogeneous catalysts are often difficult to separate from the reaction mixture, whereas their heterogeneous counterparts can be easily separated by filtration, centrifugation, etc. The ability to recover heterogeneous catalysts from reaction mixtures with ease offers advantages from an economical and environmental point of view; facile recovery can reduce the cost of utilizing catalysts derived from precious metals and also reduce the amount of waste that is produced from chemical processes.[1–3]

To this end, a plethora of heterogeneous catalysts bearing chiral ligands have been developed for a variety of enantioselective transformations.[4–16] However, due to the high cost of synthesizing chiral ligands, it remains highly desirable to prepare a chiral inorganic support comprised of achiral building blocks, in the presence of a recyclable chiral additive, towards enantioselective catalysis. A few examples have been reported for the synthesis of chiral materials in the presence of a chiral additive;[17–26] however, these materials have either not been applied towards enantioselective catalysis or catalyze reactions with poor selectivity.[24–26]

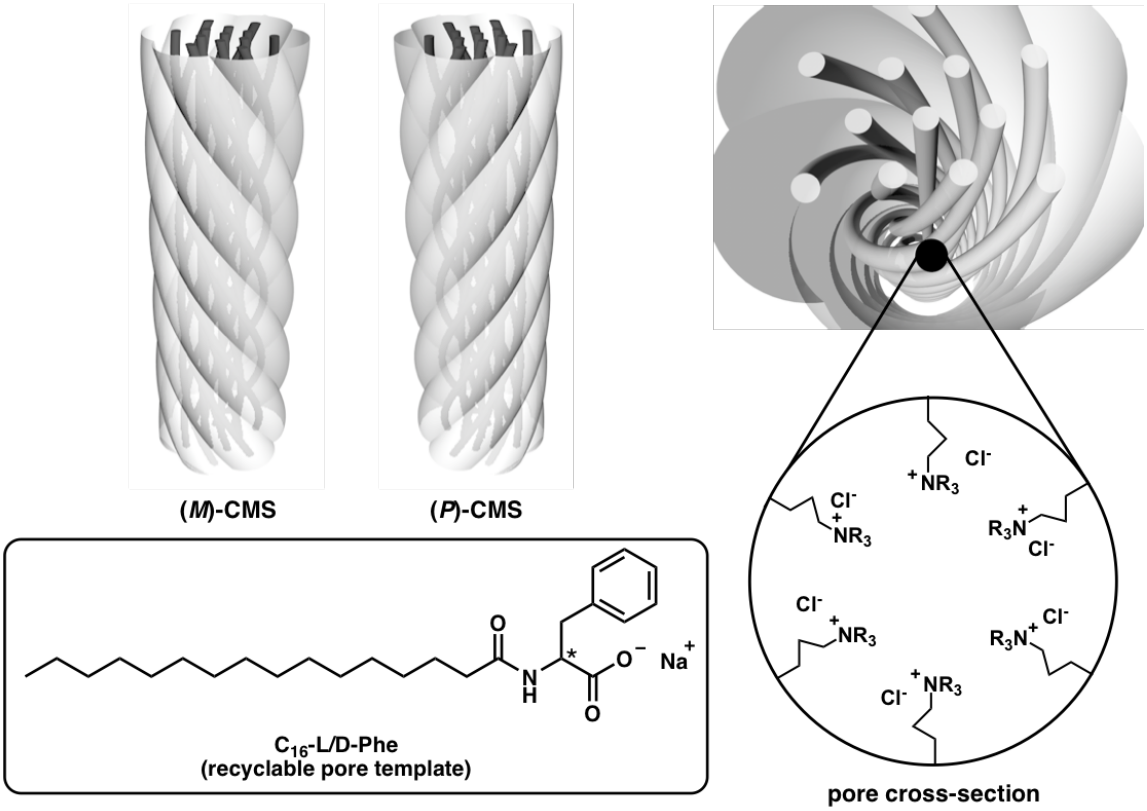

Figure 1.1. Chiral mesoporous silica.

Chiral mesoporous silica (CMS) is an attractive material to address these limitations because it can be synthesized with a recyclable, chiral surfactant and achiral silica precursors (Figure 1.1).[23,27] Although both (*P*) and (*M*) enantiomers of CMS can be targeted depending on the chirality of the surfactant that is employed during the self-assembly of the material,[27] there are no reports on the influence of CMS chirality on reaction enantioselectivity of supported catalysts. Additionally, we were interested in studying enantioinduction in a chiral metal-organic framework (MOF) composed of achiral building blocks, MOF-520.[28] MOF-520 can accommodate a wide variety of guests bearing alcohol or carboxylic acid groups, which can subsequently be characterized by single crystal X-ray diffraction (SXRD). Characterization of incorporated catalysts in MOF-520 by SXRD is an attractive feature because SXRD analysis could provide structural information that could potentially elucidate important interactions between the catalyst and the MOF for further catalyst development. Described here are the synthesis and reactivity of immobilized catalysts in CMS and MOF-520 and our efforts towards the enantioenrichment of MOF-520.

1.2 Results and Discussion

1.2.1 Immobilized Catalysts in Chiral Mesoporous Silica and Their Reactivity

We began our initial efforts towards evaluating the effectiveness of chirality transfer from a chiral material to a supported achiral catalyst with transition metal nanoparticle impregnated chiral mesoporous silica (M@CMS). CMS featuring trimethylammonium groups within the pores (CMS^{I}) was prepared according to a known literature procedure, where a phenylalanine-based surfactant was employed as a source of chirality (Scheme 1.1).[27] $Pt@CMS^{1}$ was prepared by addition of H_2PtCl_4 to CMS^{1} at elevated temperatures (Scheme 1.2, top). The impregnated platinum nanoparticles (NPs) are seen in the corresponding transmission electron microscopy (TEM) images (Scheme 1.2, bottom).

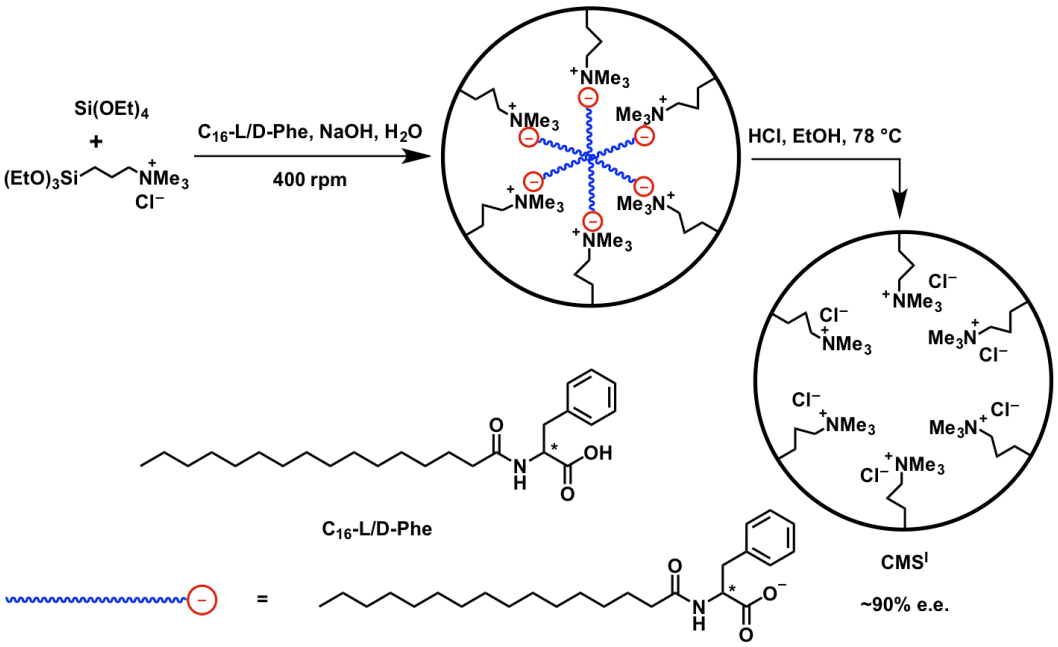

Scheme 1.1. Synthesis of CMS[I].

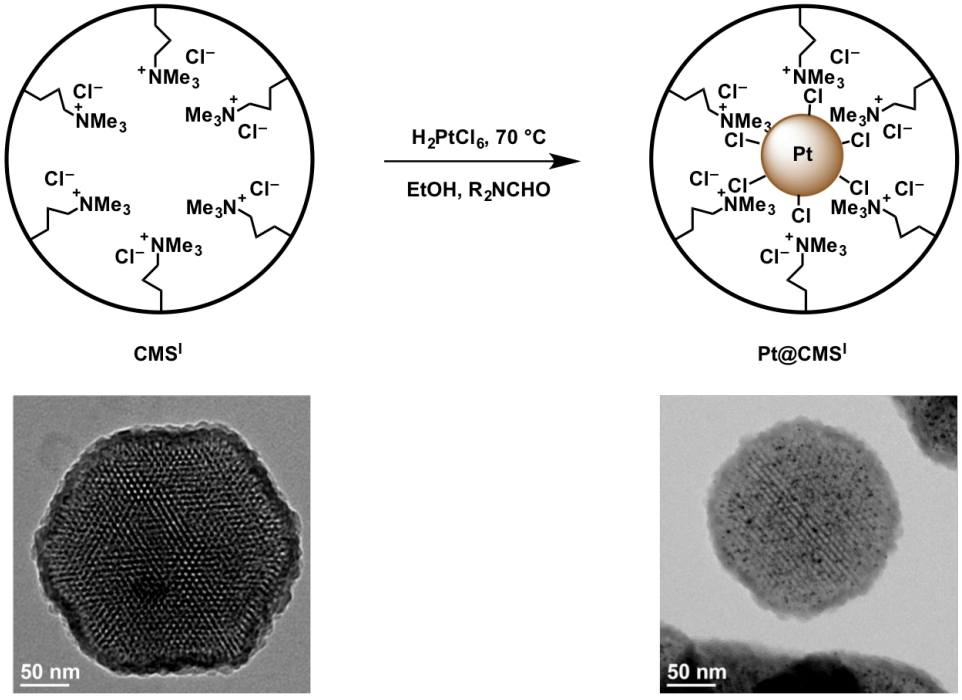

Scheme 1.2. Preparation of Pt@CMS[I]. TEM images before and after Pt deposition (bottom).

Pt@CMS^{I} was evaluated as a catalyst for the hydrogenation of olefin **1** and ketone **3**. Full conversion towards the corresponding products as racemates was observed in both cases (Scheme 1.3). We hypothesized that poor transfer of chirality could be due to the large size of the Pt NPs relative to the dimensions of the CMS pores. As a result, a new strategy was employed to decrease the size of the metal NPs during the impregnation process.

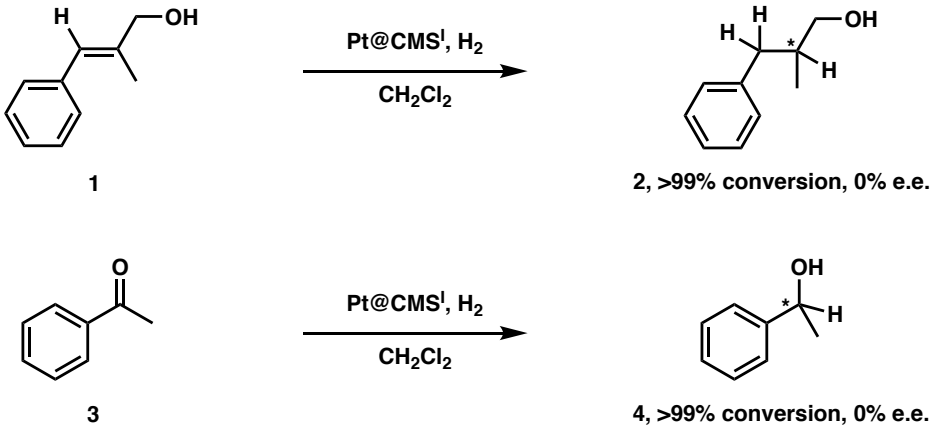

Scheme 1.3. Pt@CMS^{I}-catalyzed hydrogenation reactions.

Tetrabutylammonium chloride was introduced during the metal NP impregnation process to stabilize smaller NPs by additional electrostatic interactions within the CMS pores for the preparation of M@CMS^{I} (M = Pt or Au). M@CMS^{I} (M = Pt or Au) catalysts were then subjected to hydrogenation and hydrosilylation conditions, respectively. The desired product was observed in both cases. Smaller platinum and gold NPs were observed in Pt@CMS^{I} and Au@CMS^{I} prior to catalysis; however, agglomeration of the platinum and gold NPs was observed by TEM after catalysis (Figure 1.2). Due to the inability of electrostatic interactions to stabilize the platinum and gold NPs against agglomeration during catalysis, a strategy to stabilize smaller gold NPs by covalent bonds was pursued.

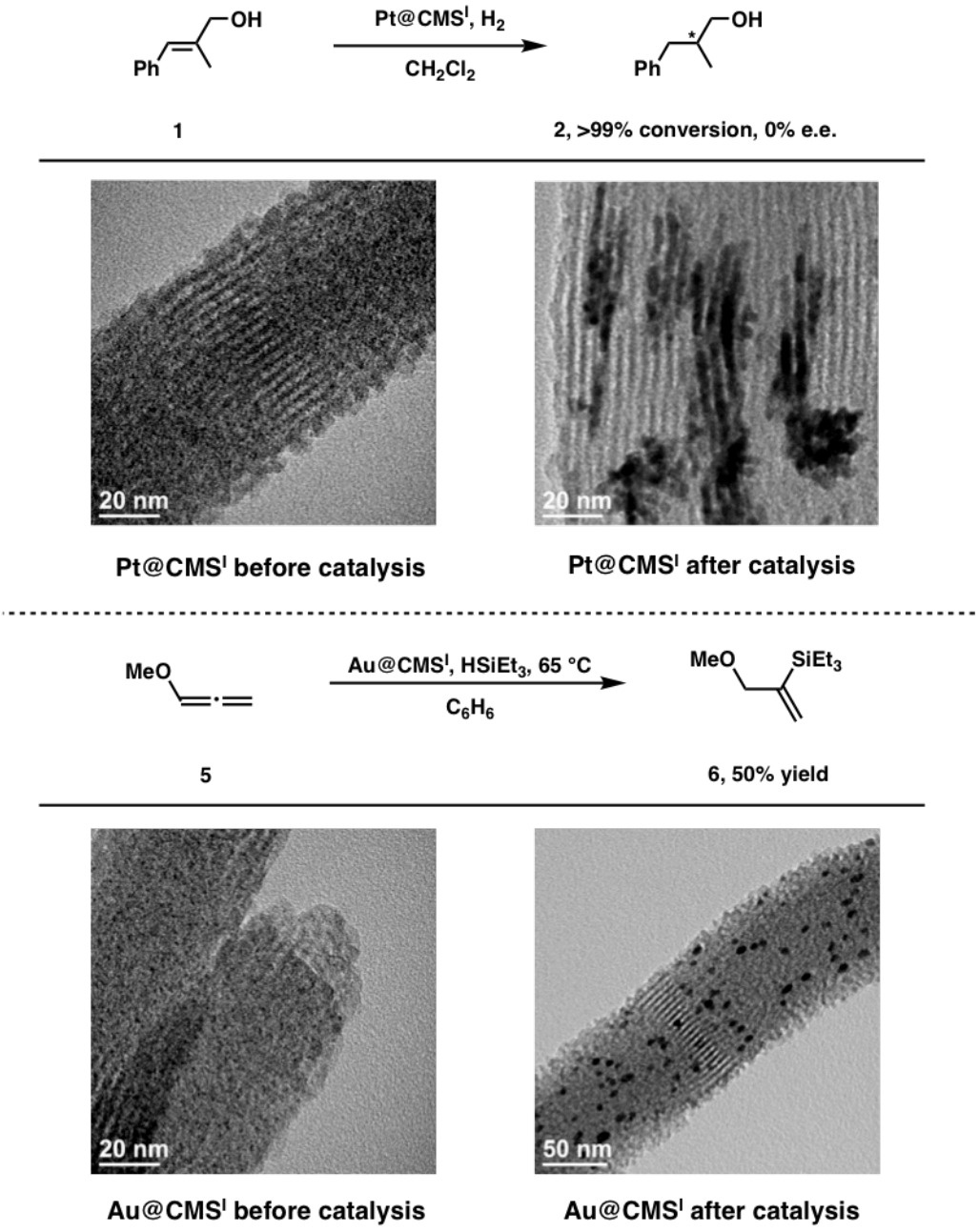

Figure 1.2. TEM images of M@CMS^{I} (M = Pt or Au) before and after catalysis.

In particular, we were interested in utilizing thiolate ligands, which are known to stabilize structurally well-defined 25 gold atom nanocluster catalysts.[29] Thus, we synthesized a new CMS material by introducing (3-mercaptopropyl)trimethoxysilane during the self-assembly of the material to introduce thiol groups into the pores (CMS^{II}, Scheme 1.4). CMS^{II} with 30% e.e. was obtained through this strategy. Inversion of the stereochemistry was observed upon utilizing chiral surfactant of the opposite chirality, as determined by scanning electron microscopy (SEM). Stabilized gold NPs were then prepared in CMS^{II} by addition of gold precursor and subsequent addition of thiol ligand and reductant to yield Au@CMS^{II} (Scheme 1.5).

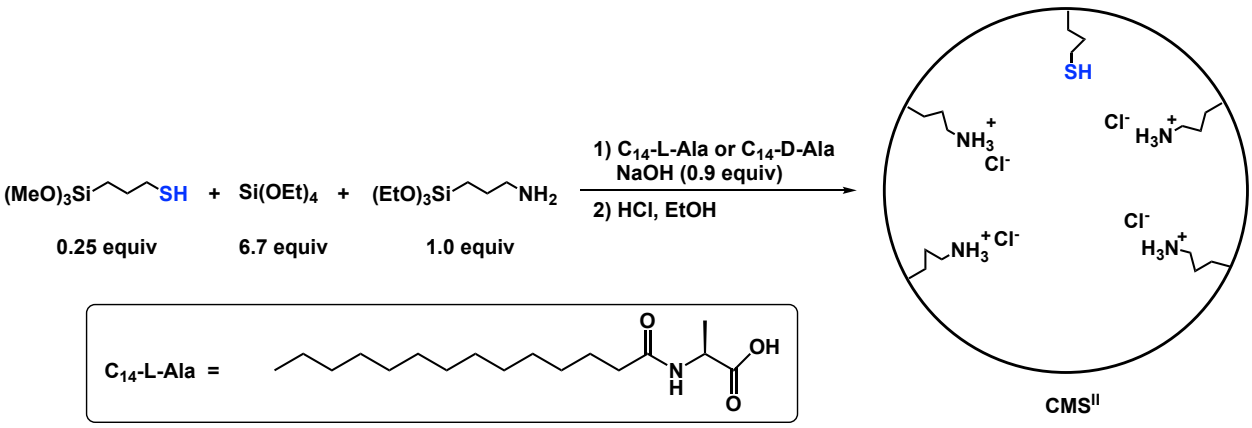

Scheme 1.4. Synthesis of CMS^{II}.

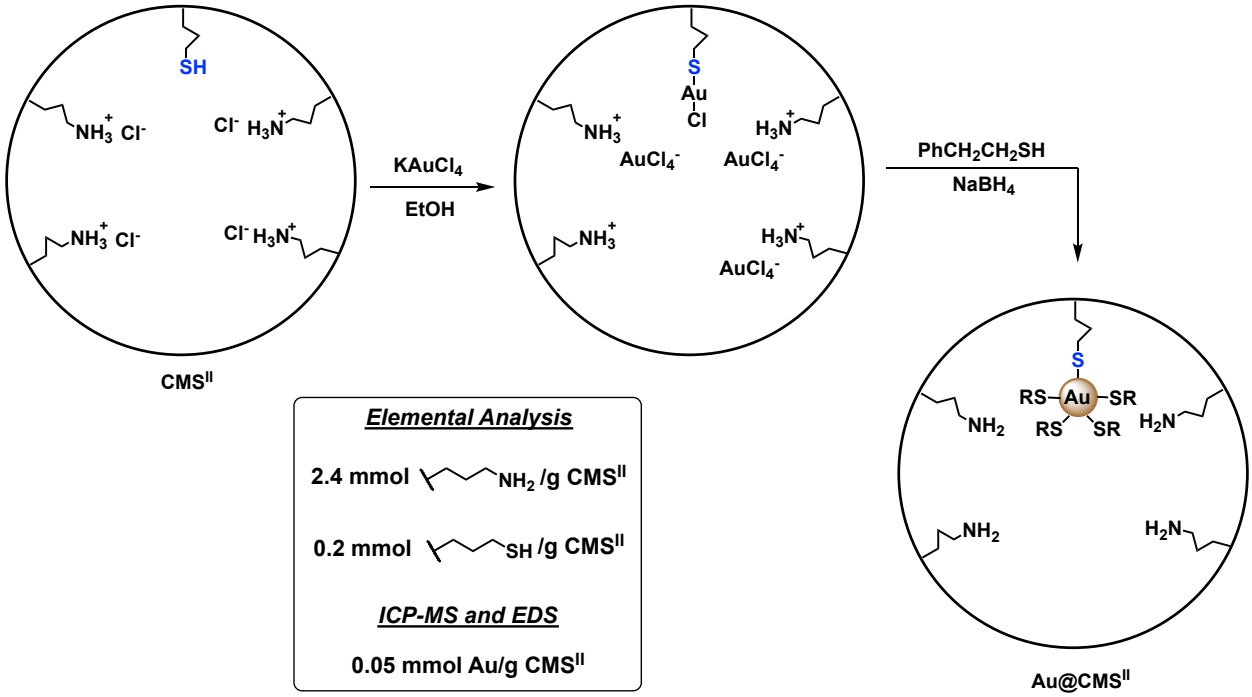

Scheme 1.5. Preparation of $Au@CMS^{II}$.

The stability of $Au@CMS^{II}$ under the hydrosilylation reaction conditions was then evaluated by high-resolution transmission electron microscopy (HRSTEM). Upon subjection of $Au@CMS^{II}$ to substrate **5**, hydrosilylated product **6** was observed with 50% yield. Additionally, no agglomeration of gold NPs was observed in $Au@CMS^{II}$ after catalysis, demonstrating the ability of thiolate ligands to stabilize these NPs during catalysis (Scheme 1.6).

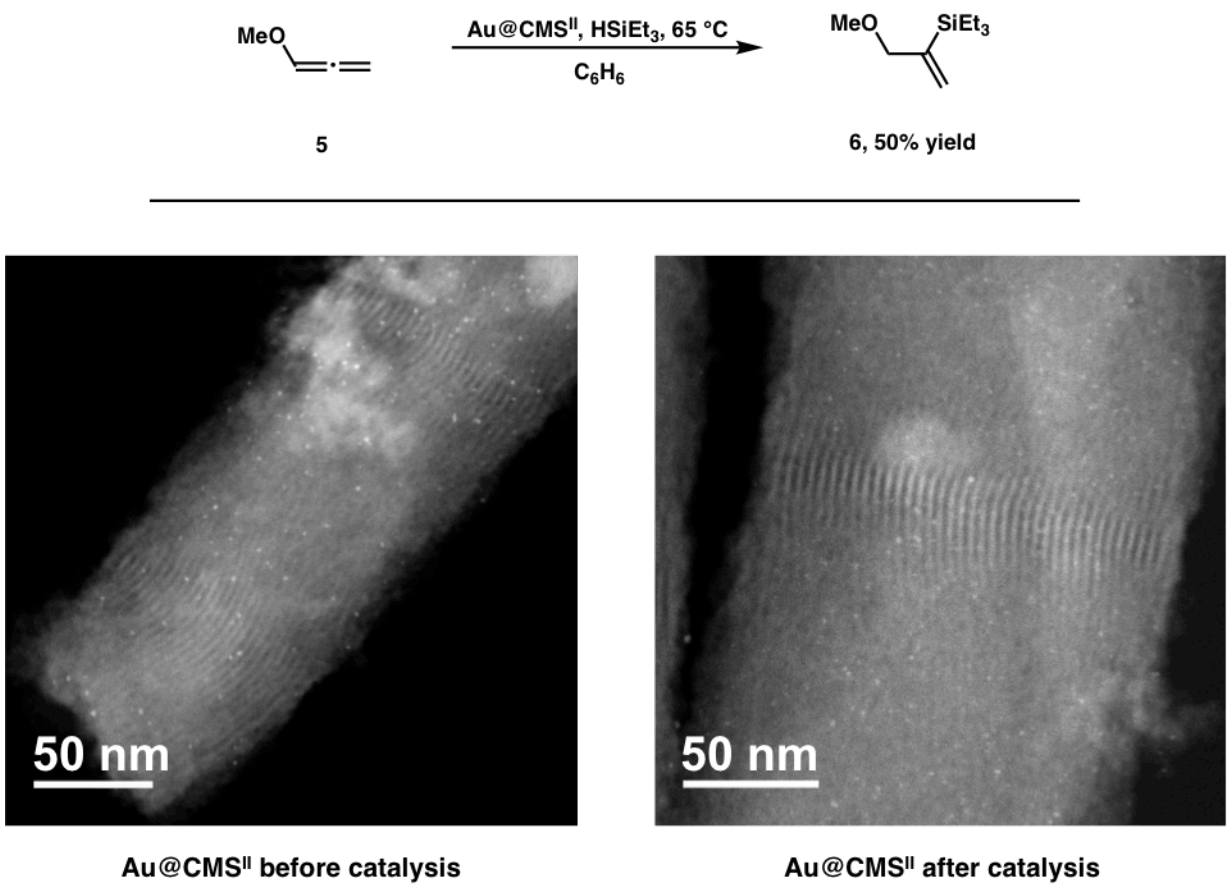

Scheme 1.6. HRSTEM images of Au@CMS^{II} before and after catalysis.

While developing Au@CMS^{II} system with stabilized gold NPs, we probed the possibility of chirality transfer from CMS to immobilized homogeneous catalysts. Cationic gold(I) catalysts were immobilized in CMS^{I} by hydrogen-bonding interactions and were tested towards a gold(I)-catalyzed cyclization of allenoic acid **7** (Table 1.1).[30] It was hypothesized that dinuclear gold complexes such as dppe$(AuBF_4)_2$ could adopt chiral conformations to induce a kinetic bias for the formation of enantioenriched **8**; however, racemic product was observed (entry 2). We probed whether CMS^{I} could diastereoselectively adsorb racemic BINAP complexes; however, racemic product distribution was observed, suggesting that diasteroeselective uptake of BINAP$(AuBF_4)_2$ did not occur (entry 3). We also tested for the possibility of synergetic interactions between the chirality of the support and that of the catalyst; however, no change in enantioselectivity of the reaction was detected upon introduction of (*R*)-DTBM-SEGPHOS$(AuBF_4)_2$ into CMS or an achiral mesoporous silica support, MCM-41 (entries 4 and 5). With these results, we concluded that these mesoporous materials may be inappropriate for molecular enantioinduction due to the drastic difference in pitch length (~1.5 μm) and pore size (~2 nm) of the support and the size of the catalyst and substrate. Additionally, due to the amorphous nature of CMS, it was difficult to ascertain potentially crucial support-catalyst interactions for enantioinduction. As a result, we continued our studies in a chiral, highly crystalline metal-organic framework, MOF-520, with smaller pore dimensions (~1 nm).

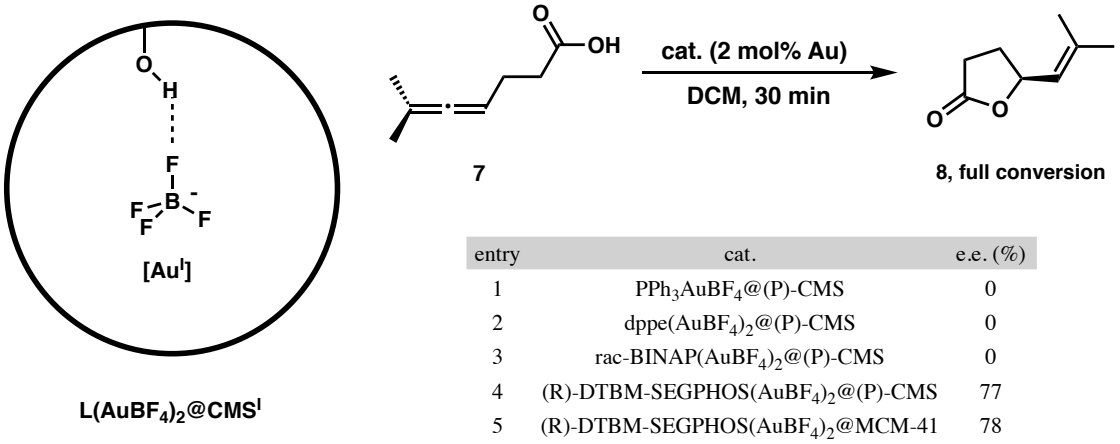

entry	cat.	e.e. (%)
1	PPh_3AuBF_4@(P)-CMS	0
2	dppe$(AuBF_4)_2$@(P)-CMS	0
3	rac-BINAP$(AuBF_4)_2$@(P)-CMS	0
4	(R)-DTBM-SEGPHOS$(AuBF_4)_2$@(P)-CMS	77
5	(R)-DTBM-SEGPHOS$(AuBF_4)_2$@MCM-41	78

Table 1.1. $L(AuBF_4)_2$@CMS^I-catalyzed lactonization reaction.

1.2.2 Efforts Towards the Enantioenrichment of MOF-520

Although MOF-520 is an attractive material for studying transfer of chirality from support to catalyst, there are no protocols for the isolation of enantioenriched MOF-520. We began our efforts by including chiral additives during the synthesis of MOF-520 (Table 1.2). L-lactic acid and D-lactic acid were introduced as chiral additives because they bear alcohol and carboxylic acid groups, both of which can interact with the secondary building unit (SBU) of MOF-520; however, the addition of lactic acid resulted in the formation of a racemic conglomerate of MOF-520, as determined by SXRD analysis of several crystals from the same batch. The addition of (*R*)-BINAP during the MOF synthesis resulted in the suppression of crystallization. We were then interested in cinchonidine and cinchonine as chiral additives because there is precedent for the self-assembly of chiral nanotubular architectures *via* the assembly of aluminum cinchonidine complexes.[31] However, the addition of either of the cinchona alkaloids resulted in the formation of a racemic conglomerate during the crystallization of MOF-520.

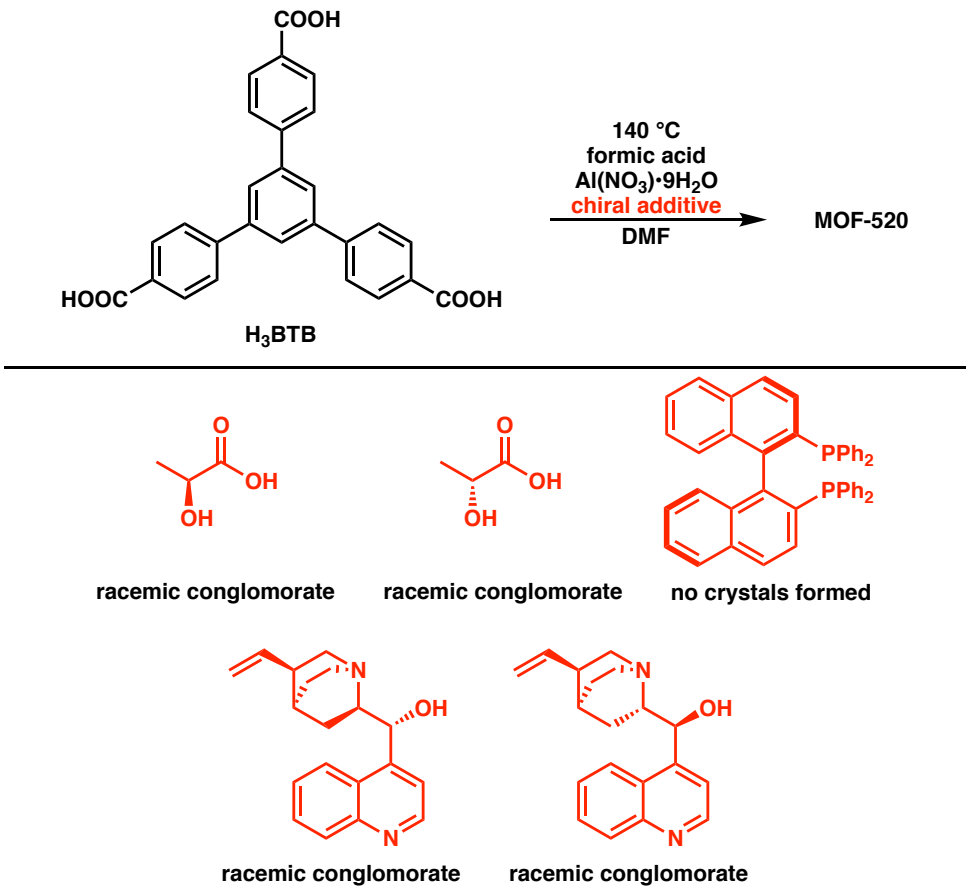

Table 1.2. Crystallization of MOF-520 in the presence of a chiral additive.

Due to the lack of success in obtaining enantioenriched MOF-520 crystals by addition of chiral additives, we explored the possibility of an enantioselective MOF-520 crystallization on a chiral surface. Crystallization of MOFs occurs on the inner surface of the reaction vessels, so we hypothesized that immobilizing a layer of cinchonidine on the surface of a vial would promote the necessary interactions between cinchonidine and the MOF precursors during the nucleation events to yield enantioenriched crystals. A cinchonidine-modified vial was prepared by hydrolysis and condensation of a hydrosilylated analogue of cinchonidine onto the inner surface of a glass vial (Scheme 1.7). However, crystallization of MOF-520 in the cinchonidine-modified vial resulted in the formation of a racemic conglomerate of MOF-520.

In addition to chiral additives and a chiral surface, we investigated whether substituting DMF with a chiral solvent could promote an enantioselective crystallization of MOF-520. A chiral solvent was prepared and was introduced under the MOF-520 crystallization conditions; however, a racemic conglomerate of MOF-520 was observed (Scheme 1.8).

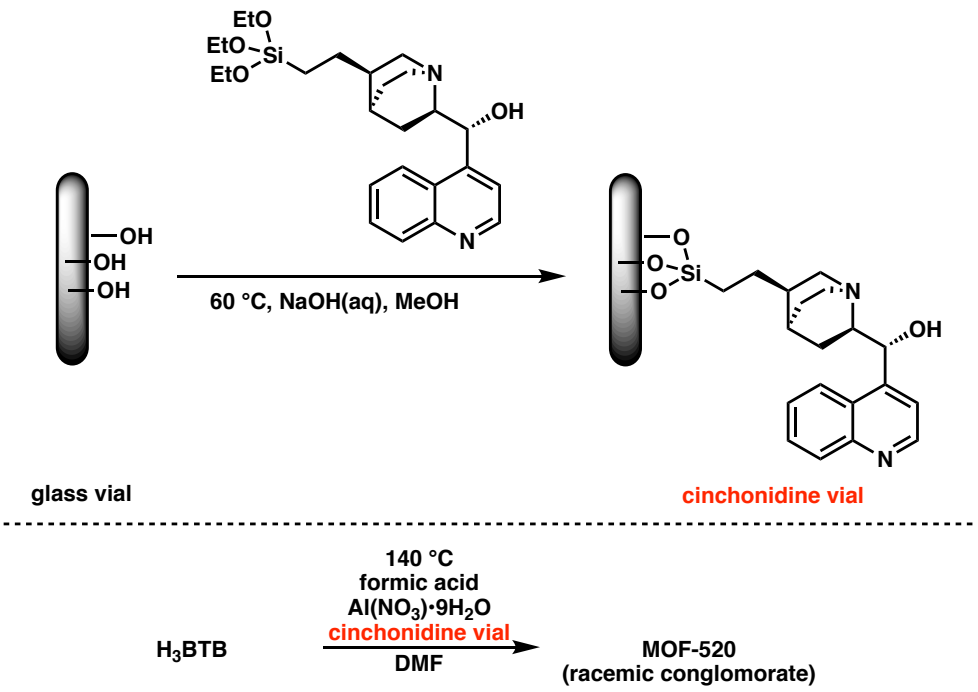

Scheme 1.7. Crystallization of MOF-520 on a cinchonidine-modified surface.

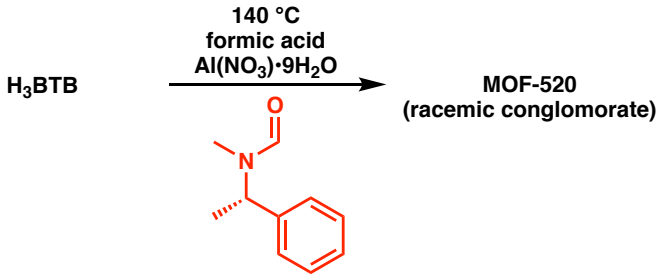

Scheme 1.8. Crystallization of MOF-520 in the presence of a chiral solvent.

1.2.3 Incorporation of a Gold(III) Catalyst into MOF-520 by Oxidative Addition and Their Reactivity

During our efforts towards the enantioenrichment of MOF-520, we were also interested in developing a novel post-synthetic metalation strategy for introducing a transition metal catalyst into a material under mild conditions. Typically, post-synthetic metalation of transition metal catalysts on materials relies on the use of L-type ligands, such as bipyridine and phosphines, to ligate metals. Despite the numerous strategies employing L-type ligands for the metalation of materials, no previous reports exploit the formation of M-X bonds to metalate materials *via* oxidative addition. In particular, we were interested in utilizing a known, mild

oxidative addition of a biphenylene C–C bond to gold(I) to yield the corresponding gold(III) complex (Scheme 1.9).[32]

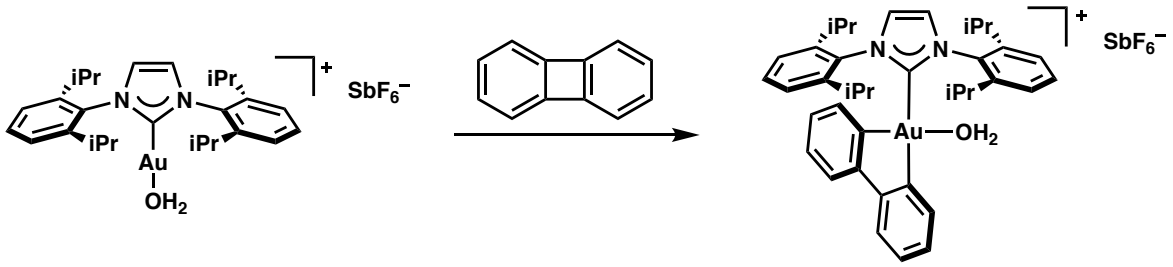

Scheme 1.9. Formation of gold(III) catalyst by oxidative addition of a C–C bond.

Towards this end, biphenylene-2-carboxylic acid (BPCA) was incorporated into MOF-520 by displacement of formate bound to the SBU, yielding MOF-520-BPCA (Scheme 1.10). Incorporation of BPCA into MOF-520 was confirmed by SXRD, through which the structure of incorporated biphenylene-2-carboxylate could be determined (Figure 1.3).

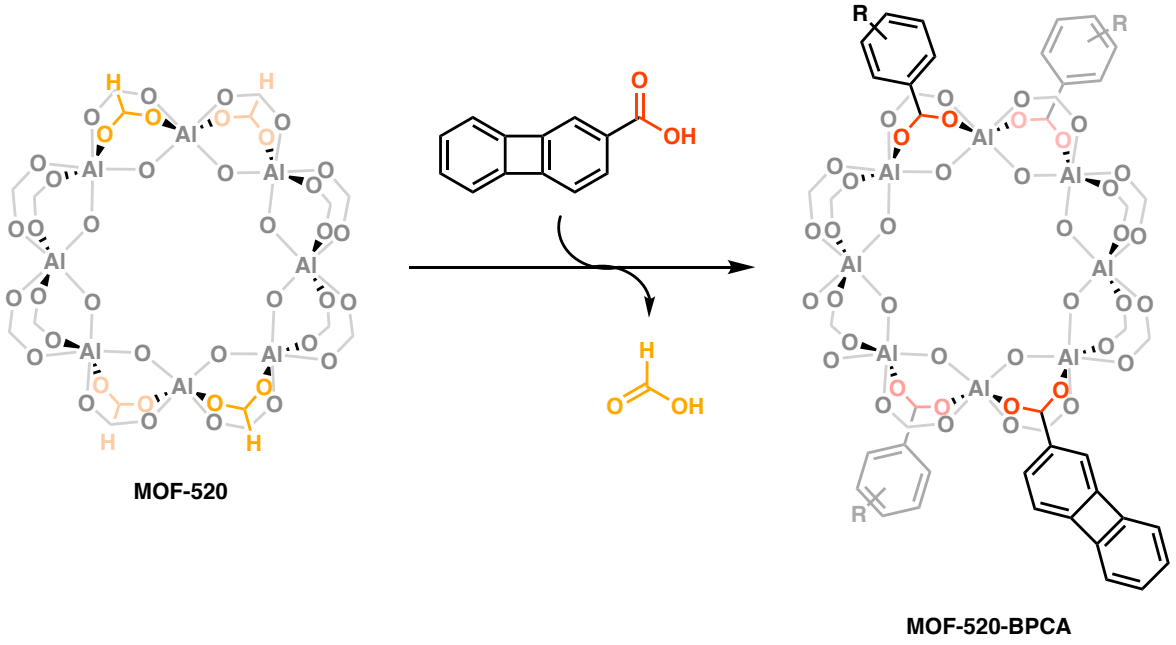

Scheme 1.10. Incorporation of biphenylene-2-carboxylic acid into MOF-520.

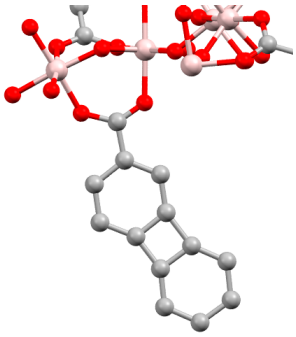

Figure 1.3. Crystal structure of MOF-520-BPCA.

MOF-520-BPCA was then subjected to a cationic gold(I) complex ($IPrAuSbF_6$), which yielded the corresponding immobilized gold(III) complex (MOF-520-BPCA-$IPrAuSbF_6$) shown in Scheme 1.11. The gold loading of MOF-520-BPCA-$IPrAuSbF_6$ was determined to be 0.17 wt% (6% of the theoretical maximum) by inductively coupled plasma atomic emission spectroscopy (ICP-OES). Due to the low gold loading of MOF-520-BPCA-$IPrAuSbF_6$, the occupancy of gold could not be assigned by SXRD analysis. We hypothesized that the low gold loading could be due to the bulky IPr ligand on the gold(I) complex, which would limit diffusion thought the material.

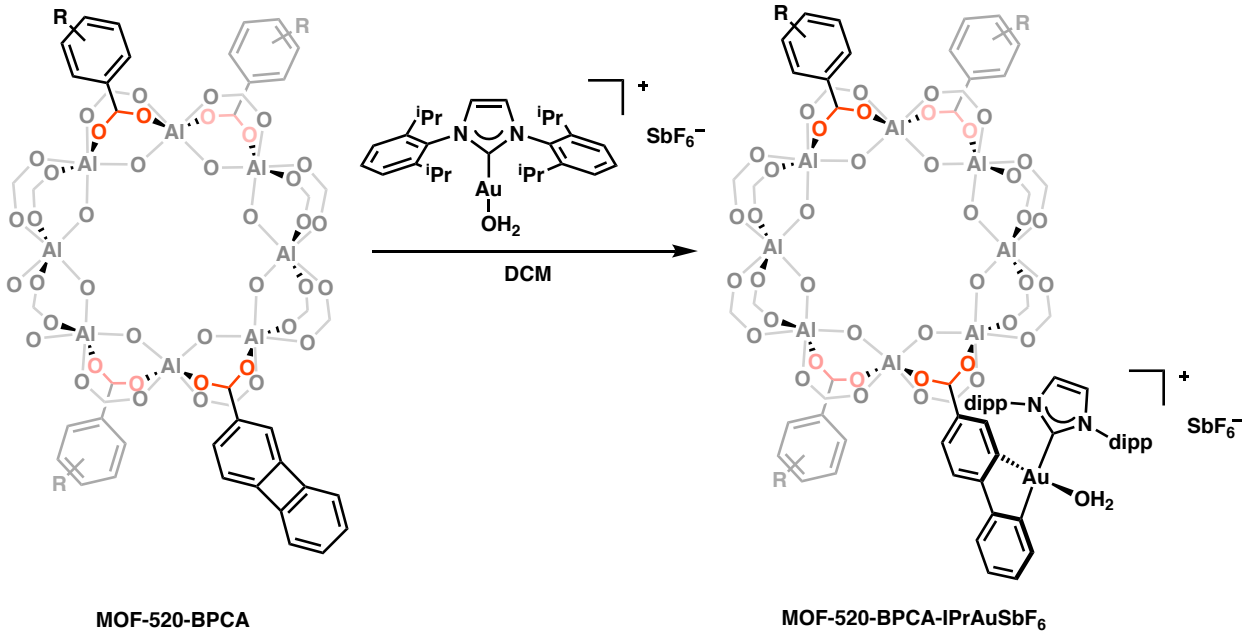

Scheme 1.11. Preparation of MOF-520-BPCA-$IPrAuSbF_6$ *via* oxidative addition.

Due to the low gold loading of MOF-520-BPCA-$IPrAuSbF_6$, gold(I) complexes bearing smaller carbene ligands were then examined under the oxidative addition conditions. However, when gold(I) complexes bearing carbene ligands smaller than IPr were employed, decomposition to gold(0) was observed (Table 1.3). No gold occupancy was detected in the treated MOF-520-

BPCA crystals by SXRD analysis, which suggests that decomposition precludes the possibility of oxidative addition.

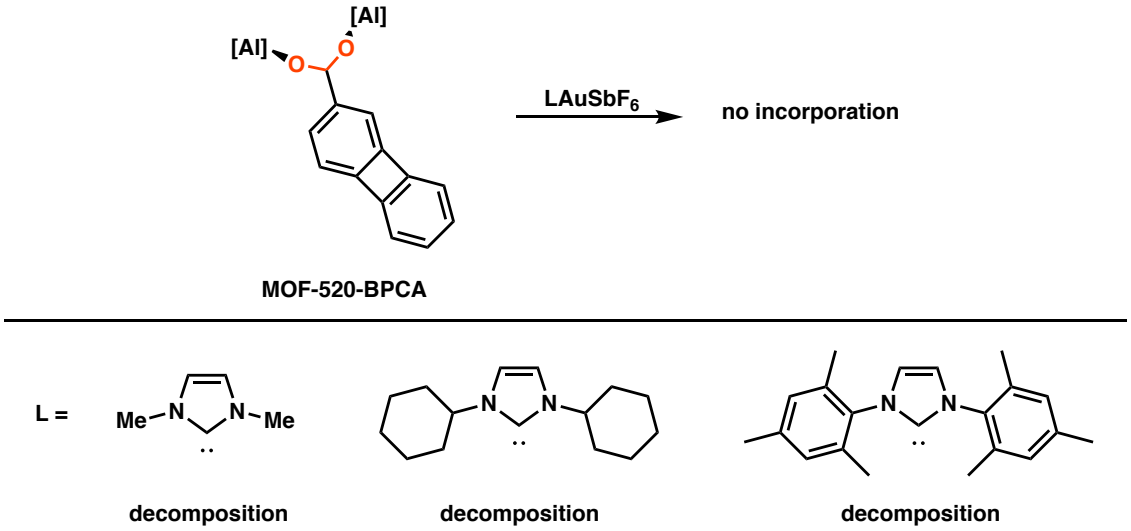

Table 1.3. Attempted oxidative addition to MOF-520-BPCA with gold(I) complexes.

The Mukaiyama-Michael addition reactivity of MOF-520-BPCA-IPrAuSbF$_6$ was then compared to that of the homogeneous gold(I) and gold(III) complexes: IPrAuSbF$_6$ and IPrAu(biphenyl)SbF$_6$ (Table 1.4). The homogeneous gold(I) complex favored the formation of the 1,2 adduct while the homogenous gold(III) complex preferentially catalyzed generation of the 1,4 adduct (entries 1 and 2), which is consistent with previously reported reactivity.[32] In contrast, employing MOF-520-BPCA treated with IPrAuSbF$_6$ as a catalyst for the Mukaiyama-Michael addition resulted in a 50:50 ratio of 1,4/1,2 adducts (entry 3). These results suggested that both gold(I) and gold(III) species are present in MOF-520-BPCA-IPrAuSbF$_6$. This intermediate selectivity can either be attributed to gold(I) species that were not fully removed from the crystals after the post-synthetic metalation or to the dynamic equilibrium between gold(I) and gold(III) species due to reversible oxidative addition and reductive elimination. As a control experiment, 2-naphthoic acid was incorporated into MOF-520 (MOF-520-NA), to emulate the pore environment of MOF-520-BPCA while being inert towards oxidative addition. MOF-520-NA treated with IPrAuSbF$_6$ yielded reactivity consistent with gold(I) species when used as a catalyst for the Mukaiyama-Michael addition reaction (entry 4). This result suggests that the pore environment of MOF-520-BPCA does not influence the reactivity of gold(I) species; therefore, some of the reactivity observed in entry 3 can be attributed to gold(III) species. As an additional control experiment, MOF-520-NA was subjected to Mukaiyama-Michael addition conditions, which resulted in poor reactivity (entry 5). This poor reactivity demonstrates that the SBU of MOF-520 does not have a major contribution to the reactivity observed with MOF-520-BPCA-IPrAuSbF$_6$.

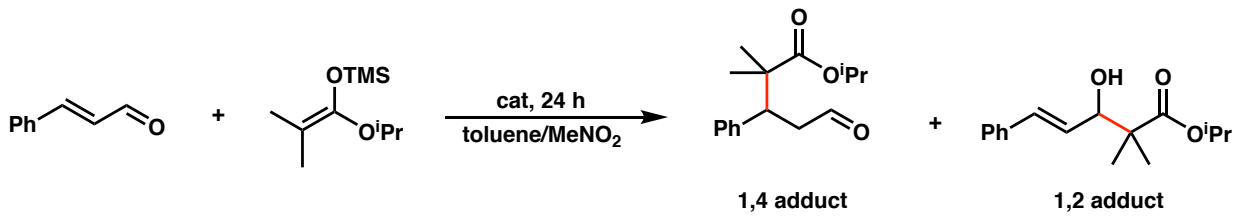

entry	cat.	1,4/1,2 adduct	conversion (%)
1	IPrAu(biphenyl)SbF_6	72:25	>98
2	IPrAuSbF_6	25:75	50
3	MOF-520-BPCA-IPrAuSbF_6	50:50	50
4	MOF-520-NA + IPrAuSbF_6	25:75	>98
5	MOF-520-NA	<2:98	5

Table 1.4. MOF-520-BPCA-IPrAuSbF_6-catalyzed Mukaiyama-Michael and control experiments.

To further confirm the presence of gold(III) species in MOF-520-BPCA-IPrAuSbF_6, the MOF was used as a catalyst for the previously reported conjugate addition conditions where gold(I) species exhibit no catalytic activity (Table 1.5). Consistent with previous reports, gold(III) species catalyzed the δ-selective thiol addition, while gold(I) species under the same conditions gave no desired product (entries 1 and 2).[32] Selectivity observed with MOF-520-BPCA-IPrAuSbF_6 under the same conditions was consistent with that of the homogeneous gold(III) catalyst (entry 3). As a control experiment, MOF-520 and homogeneous gold(I) catalyst were tested under otherwise identical reaction conditions and yielded no desired product (entry 4). The lack of reactivity in the control experiment suggests that gold(III) species are present in MOF-520-BPCA-IPrAuSbF_6 and are responsible for the reactivity observed in entry 3.

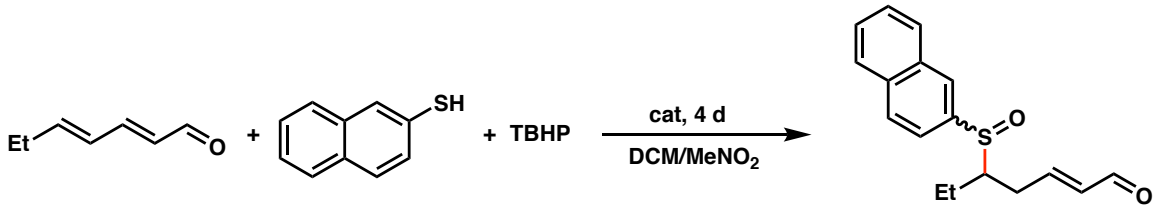

entry	cat.	δ-selectivity	conversion (%)
1	IPrAu(biphenyl)SbF_6	>98:2	60
2	IPrAuSbF_6	—	<2
3	MOF-520-BPCA-IPrAuSbF_6	>98:2	25
4	MOF-520 + IPrAuSbF_6	—	<2

Table 1.5. MOF-520-BPCA-IPrAuSbF_6-catalyzed δ-selective thiol addition and control experiments.

1.3 Conclusions

In conclusion, the development of immobilized catalysts in CMS and MOF-520 have attempted to take steps towards addressing the challenge of chiral induction from chiral porous materials, derived from achiral building blocks, to immobilized catalysts. We determined that chiral induction from currently known CMS materials to catalysts is extremely challenging, which may be attributed to the disparity in size between the pores, catalysts, and substrates. A new strategy was developed for the post-synthetic metalation of MOFs *via* oxidative addition. Although initial efforts towards the enantioenrichment of MOF-520 were not successful, further development of an oxidative addition post-synthetic metalation approach may open doors for interesting opportunities to gain insights into enantioselective catalysis in MOF-520.

1.4 Supporting Information

1.4.1 General Methods

Unless noted, all reactions and manipulations were performed at 24 °C with no rigorous effort to exclude water or air, and reaction solutions were magnetically stirred. All reagents were purchased from commercial suppliers and were used without further purification. The morphology of the particles was characterized using a 200 kV LaB6 FEI G20 Tecnai transmission electron microscope, FEI TitanX 60-300 microscope, and/or a FEI Nova NanoSEM 650 scanning electron microscope. TEM samples were prepared by drop-casting dilute dispersions of sample in ethanol onto amorphous carbon on 400 mesh Cu grids from Electron Microscopy Sciences. SEM samples were prepared by drop-casting dilute dispersions of sample in ethanol onto silicon wafers. Organic reactions were monitored by thin layer chromatography (TLC) on Silicycle Siliaplate^{TM} glass backed TLC plates (250 μm, 60 Å porosity, F-254 indicator) and visualized by UV irradiation. Volatile solvents were removed under reduced pressure with a rotary evaporator and subsequent high vacuum on a Schlenk line. ^{1}H-NMR spectra were taken with Bruker spectrometers operating at 300, 400, or 500 MHz. Chemical shifts are reported relative to the residual solvent signal. NMR data are reported as follows: chemical shift (multiplicity, coupling constants where applicable, number of hydrogens). Splitting is reported with the following symbols: s = singlet, d = doublet, t = triplet, q = quartet, quint = quintet, hept = heptet, dd = doublet of doublets, td = triplet of doublets, tt = triplet of triplets, and m = multiplet. Chiral phase high performance liquid chromatography (HPLC) was performed on Shimadzu VP and Shimadzu prominence series instruments using the specified column (5μm, 4.6 mm x 250 mm). Single-crystal X-ray diffraction (SXRD) data was collected using a Bruker D-8-Venture diffractometer. The Bruker D8-Venture diffractometer is equipped with a PHOTON100 CMOS detector and a micro-focus X-ray tube with a Cu-target (λ = 1.54178 Å) and Mo-target (λ = 0.71073 Å). Inductively coupled plasma optical emission spectra (ICP-OES) were obtained with an ICP Optima 7000 DV instrument at the Microanalytical Facility at the University of California, Berkeley.

The following compounds and materials were prepared according to previously published procedures and their characterization match those reported in literature: CMS^{I},[27] C_{16}-L/D-Phe,[33] C_{14}-L/D-Ala,[33] 6-methylhepta-4,5-dienoic acid,[30] (R)-quinolin-4-yl((1S,2R,4S,5R)-5-(2-(triethoxysilyl)ethyl)quinuclidin-2-yl)methanol,[34] (S)-N-methyl-N-(1-phenylethyl)formamide,[35] biphenylene-2-carboxylic acid,[36] MOF-520,[28] Me_2ImAuCl,[37] Cy_2ImAuCl,[37] IMesAuCl,[37] IPrAuCl,[38] and ((1-isopropoxy-2-methylprop-1-en-1-yl)oxy)trimethylsilane.[32]

1.4.2 Synthetic Procedures for Previously Unreported Materials

Pt@CMS^{I}

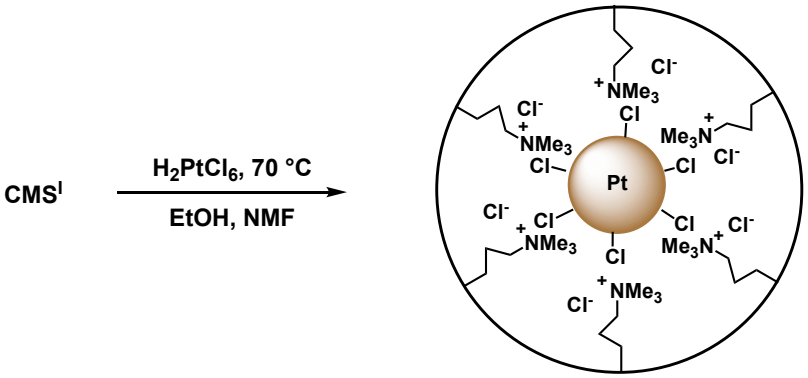

Pt@CMS^{I}

To a 20 mL vial was added CMS^{I} (25 mg) and a mixture of ethanol (3 mL) and N-methylformamide (3 mL) followed by sonication for 5 min. The dispersion was heated to 70 °C followed by the addition of a solution of H_2PtCl_4 (8 wt% in water, 0.36 mL, 0.07 mmol). After stirring the reaction mixture for 14 hours, the mixture was cooled to room temperature and centrifuged at 8000 rpm for 15 min. The supernatant was discarded, and the black solid was washed with ethanol (45 mL x 3) and centrifuged. Residual solvent was removed from Pt@ CMS^{I} under reduced pressure.

Au@CMS^{I}

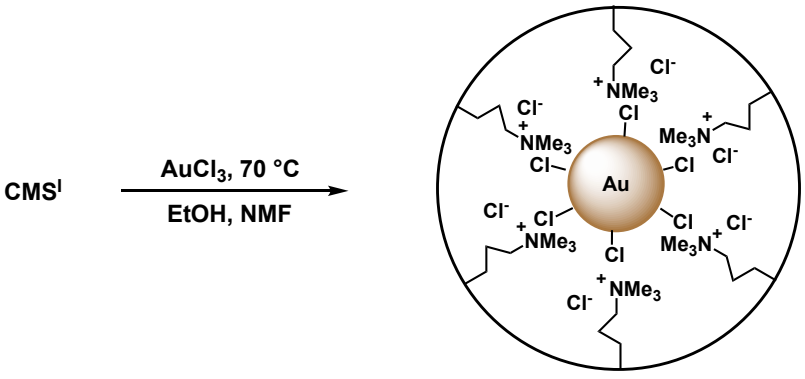

Pt@CMS^{I}

To a 20 mL vial was added CMS^{I} (25 mg) and a mixture of ethanol (3 mL) and N-methylformamide (3 mL) followed by sonication for 5 min. The dispersion was heated to 70 °C followed by the addition of $AuCl_3$ (21 mg, 0.07 mmol). After stirring the reaction mixture for 14 hours, the mixture was cooled to room temperature and centrifuged at 8000 rpm for 15 min. The supernatant was discarded, and the purple solid was washed with ethanol (45 mL x 3) and centrifuged. Residual solvent was removed from Au@CMS^{I} under reduced pressure.

Pt@CMS^{I} with Bu_4NCl

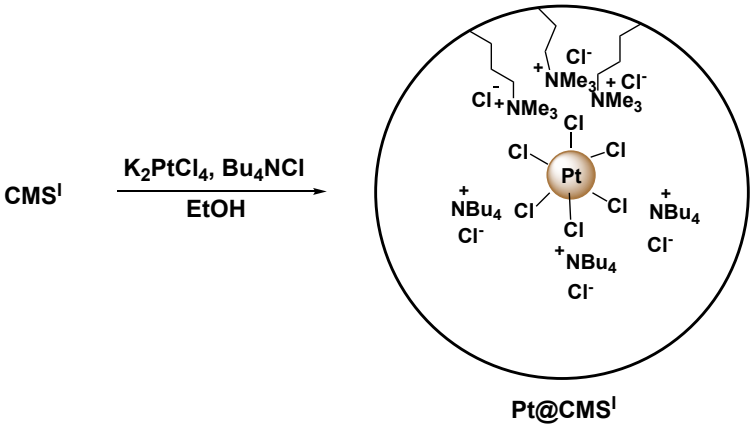

Pt@CMS^{I}

To a 20 mL vial was added CMS^{I} (20 mg) and ethanol (5 mL), which was sonicated for 5 min, followed by the addition of a solution of K_2PtCl_4 (0.25 M in water, 0.2 mL, 0.05 mmol) and Bu_4NCl (0.42 g, 1.5 mmol). After stirring the reaction mixture for 14 hours, the mixture was centrifuged at 8000 rpm for 15 min. The supernatant was discarded, and the solid was washed with ethanol (45 mL x 3) and centrifuged. Residual solvent was removed from Pt@ CMS^{I} under reduced pressure.

Au@CMS^{I} with Bu_4NCl

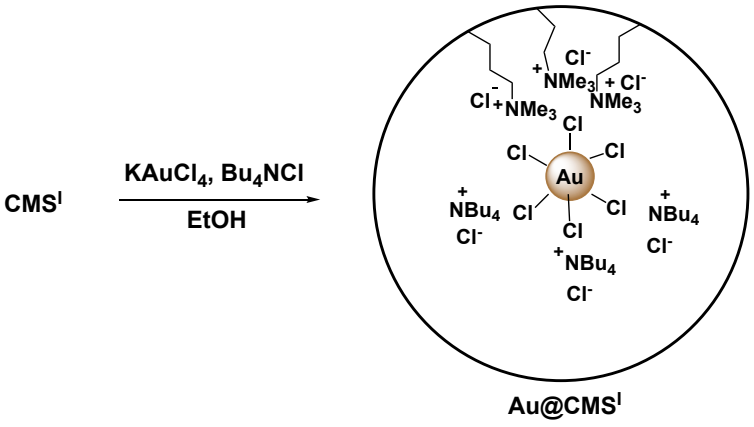

Au@CMS^{I}

To a 20 mL vial was added CMS^{I} (20 mg) and ethanol (5 mL), which was sonicated for 5 min, followed by the addition of a solution of $KAuCl_4$ (0.25 M in water, 0.2 mL, 0.05 mmol) and Bu_4NCl (0.42 g, 1.5 mmol). After stirring the reaction mixture for 14 hours, the mixture was centrifuged at 8000 rpm for 15 min. The supernatant was discarded, and the solid was washed with ethanol (45 mL x 3) and centrifuged. Residual solvent was removed from Pt@ CMS^{I} under reduced pressure.

CMS^{II}

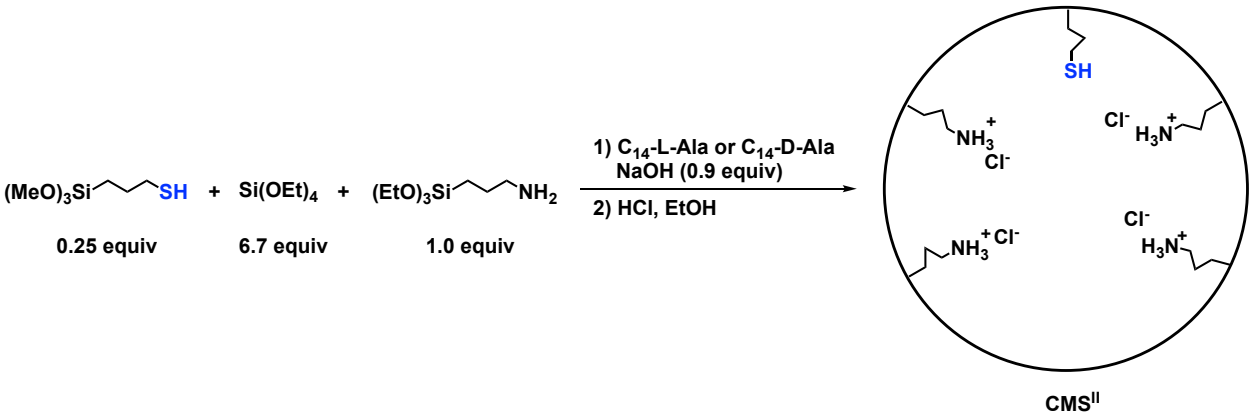

To a 100 mL glass beaker with a stir bar (3.2 cm x 0.80 cm) was added C_{14}-L-Ala or C_{14}-D-Ala (0.30 g, 1.0 mmol, 1.0 equiv.), H_2O (22.0 mL), and a solution of NaOH (0.099 M in water, 9.09 mL, 0.90 mmol, 0.9 equiv.). The mixture was heated to 60 °C and stirred until complete dissolution of starting materials. Upon complete dissolution, the reaction mixture was cooled to room temperature, and (3-mercaptopropyl)trimethoxysilane (47.3 μL, 0.25 mmol, 0.25 equiv.), (3-aminopropyl)triethoxysilane (234 μL, 1.0 mmol, 1.0 equiv.), and tetraethyl orthosilicate (1480 μL, 6.7 mmol, 6.7 equiv.) were added sequentially while stirring at 300 rpm. After stirring for 10 minutes at 300 rpm, the stir bar was removed from the reaction mixture, and the reaction mixture was left under static conditions for an additional 26 h. The mixture was then centrifuged at 7000 rpm for 20 min, washed with ethanol (45 mL), centrifuged at 7000 rpm for 20 min, and dried at 90 °C for 6 h. The dried solid was then dispersed in a mixture of ethanol (110 mL) and concentrated aqueous HCl (11 mL) and stirred at 85 °C for 11 h. The mixture was then centrifuged at 7000 rpm for 20 min, and the colorless solid was washed with ethanol (45 mL x 3) and centrifuged. Residual solvent was removed from CMS^{II} under reduced pressure.

Au@CMS^{II}

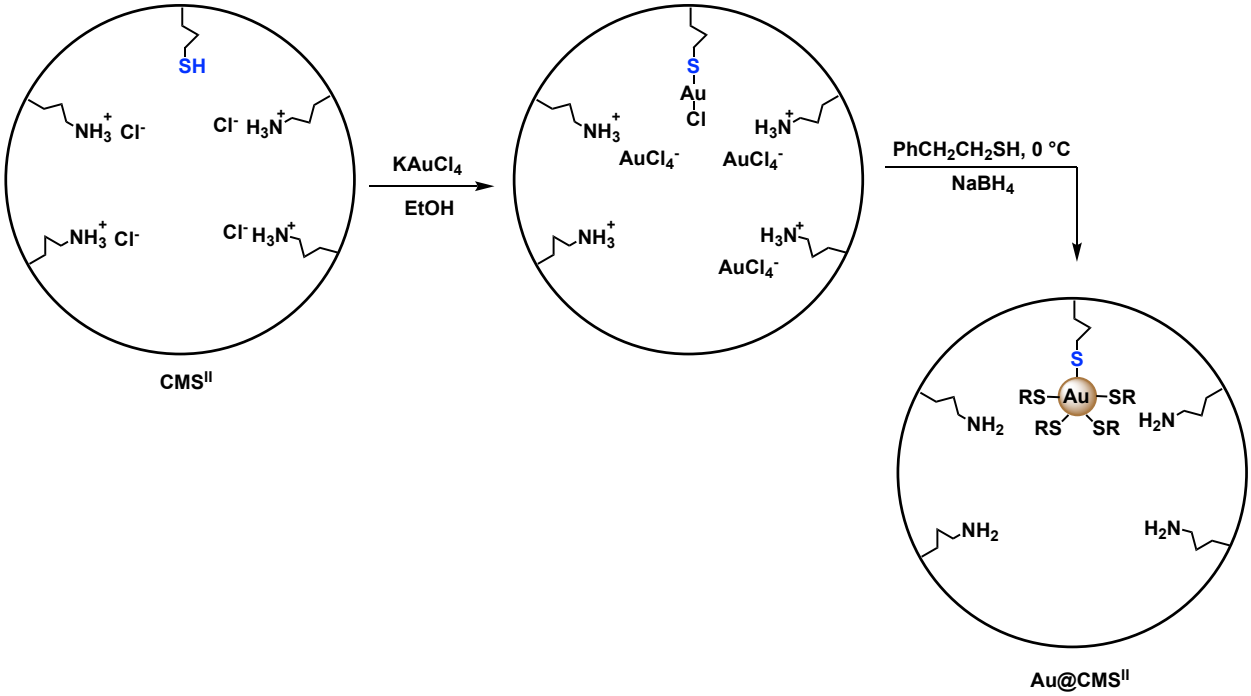

To a 100 mL round bottom flask was added CMS^{II} (200 mg) and a solution of Bu_4NCl (0.03 M in ethanol, 50 mL) which was sonicated for 5 min, followed by the addition of a solution of $KAuCl_4$ (0.25 M in water, 0.5 mL, 1.0 equiv.). After stirring the reaction mixture for 3 h, the mixture was centrifuged at 7000 rpm for 20 min, washed with ethanol (45 mL x 3), and the residual solvent was removed from the solid under reduced pressure. To the dried solid was then added toluene (30 mL), and the mixture was cooled to 0 °C. 2-phenylethanethiol (54 μL, 0.40 equiv.) was added to the reaction mixture. After stirring the reaction mixture for an additional 1 h, a solution of $NaBH_4$ (0.25 M in diglyme, 2.0 mL, 10 equiv.) was added to the reaction mixture. After stirring the reaction mixture for an additional 14 h, the reaction mixture was diluted with ethanol (40 mL) and centrifuged at 7000 rpm for 20 min. The solid was then washed with ethanol (30 mL), toluene (10 mL), and ethanol (10 mL) sequentially. Residual solvent was removed from Au@CMS^{II} under reduced pressure.

A general procedure for the synthesis of $L(AuBF_4)_2$@CMS^I

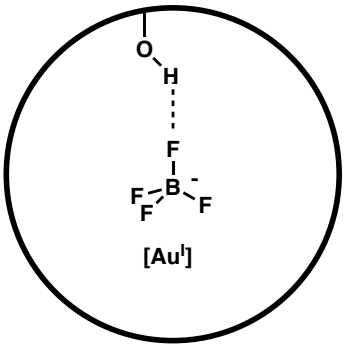

$L(AuBF_4)_2$@CMS^I

$L(AuBF_4)_2$@CMS^I was synthesized according to a reported procedure[30] with CMS^1 instead of SBA-15.

Cinchonidine vial

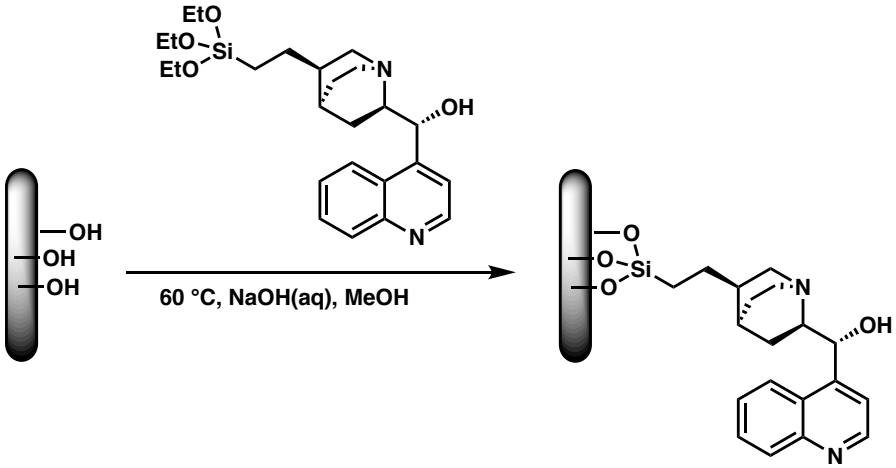

glass vial **cinchonidine vial**

To a 20 mL vial was added (R)-quinolin-4-yl((1S,2R,4S,5R)-5-(2-(triethoxysilyl)ethyl)quinuclidin-2-yl)methanol (0.14 g) and methanol (10 mL). To the mixture was added a solution of NaOH (0.1 M in water, 10 mL). After shaking the vial, the mixture was heated to 60 °C. After 14 h, the solution was discarded, and the inner surface of the vial was washed with methanol (10 mL x 3). The vial was then heated at 100 °C under reduced pressure to remove residual solvent.

MOF-520-BPCA

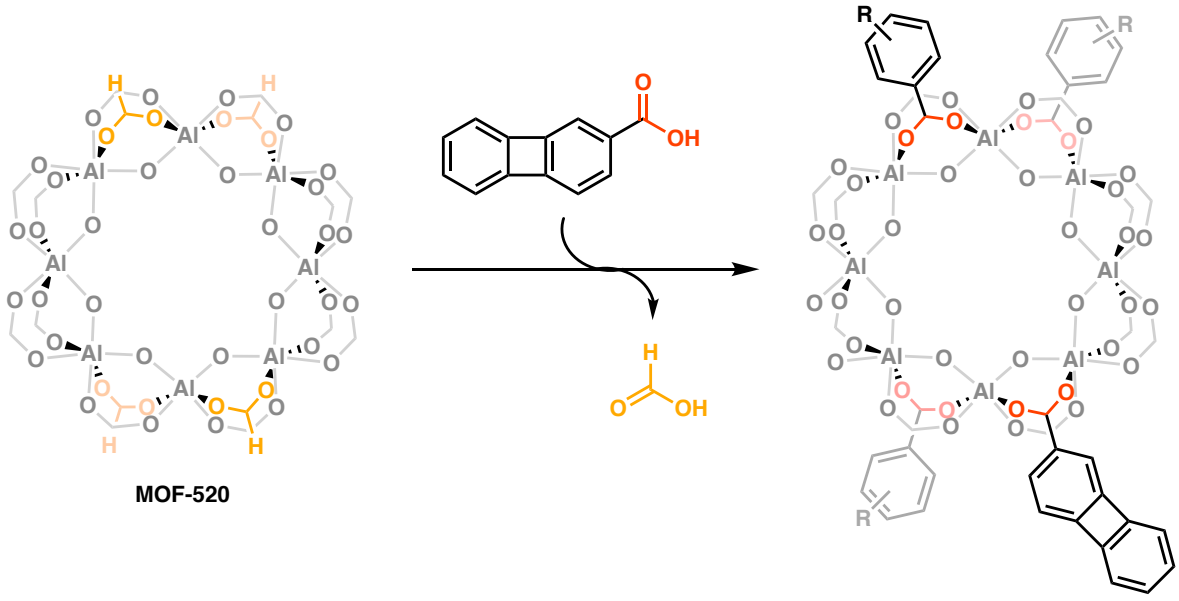

MOF-520-BPCA was synthesized according to a reported inclusion procedure[28] with biphenylene-2-carboxylic acid and MOF-520.

A general procedure for the oxidative addition of gold(III) complexes into MOF-520-BPCA

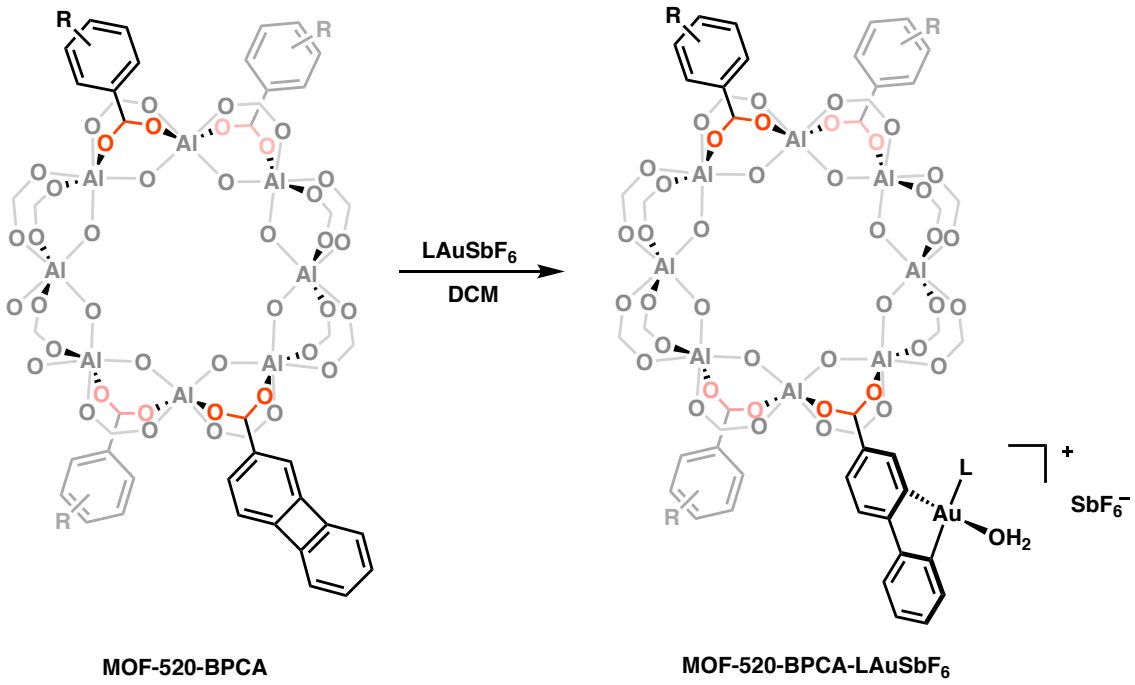

To a 1 dram vial was added gold(1) complex (0.025 mmol), $AgSbF_6$ (0.028 mmol), and DCM (2 mL). The mixture was sonicated for 10 min then filtered through a glass fiber filter. The filtered solution was then added to MOF-520-BPCA (25 mg) immersed in DCM (2 mL). After 8 days, the supernatant was removed and the crystals were washed with DCM (4 mL x 10).

1.4.3 Procedures for Catalysis

A general procedure for Pt@CMS^{I}-catalyzed hydrogenation reactions

To Pt@CMS^{I} (4 mg) was added substrate (0.4 mmol) and DCM (3 mL). After stirring for 24 h under 1 atm H_2, catalyst was removed by centrifugation and the organic supernatant was concentrated under reduced pressure. ^{1}H NMR spectra of 2-methyl-3phenylpropan-1-ol (**2**) and 1-phenylethan-1-ol (**4**) match those previously reported.[39,40]

A general procedure for Au@CMS-catalyzed hydrosilylation reactions

To Au@CMS^{I} (4 mg) was added substrate **5** (0.2 mmol), benzene (1 mL), and triethylsilane (0.4 mmol). The reaction mixture was heated to 65 °C. After stirring for 16 h, catalyst was removed by centrifugation and the organic supernatant was concentrated under reduced pressure.

A general procedure for L(AuBF$_4$)$_2$@CMS^{I}-catalyzed lactonization reactions

Reported reaction conditions[30] were used except with L(AuBF$_4$)$_2$@CMS^{1} instead of L(AuBF$_4$)$_2$@SBA-15. ^{1}H NMR spectrum of (*S*)-5-(2-methylprop-1-en-1-yl)dihydrofuran-2(3*H*)-one (**8**) matches previously reported spectrum.[30]

A general procedure for MOF-520-BPCA-IPrAuSbF$_6$-catalyzed conjugate additions

Reported reaction conditions[32] were used except with MOF-520-BPCA-IPrAuSbF$_6$ instead of IPrAu(biphenyl)SbF$_6$. ^{1}H NMR spectra of products match those previously reported.[32]

1.4.4 Scanning Electron Microscopy Images of CMS^{II}

The enantiopurity of CMS^{II}, prepared with C_{14}-L-Ala or C_{14}-D-Ala, was determined by SEM analysis.

CMS^{II} prepared from C_{14}-L-Ala (-31% e.e.)

86 (*P*)-CMS and 163 (*M*)-CMS

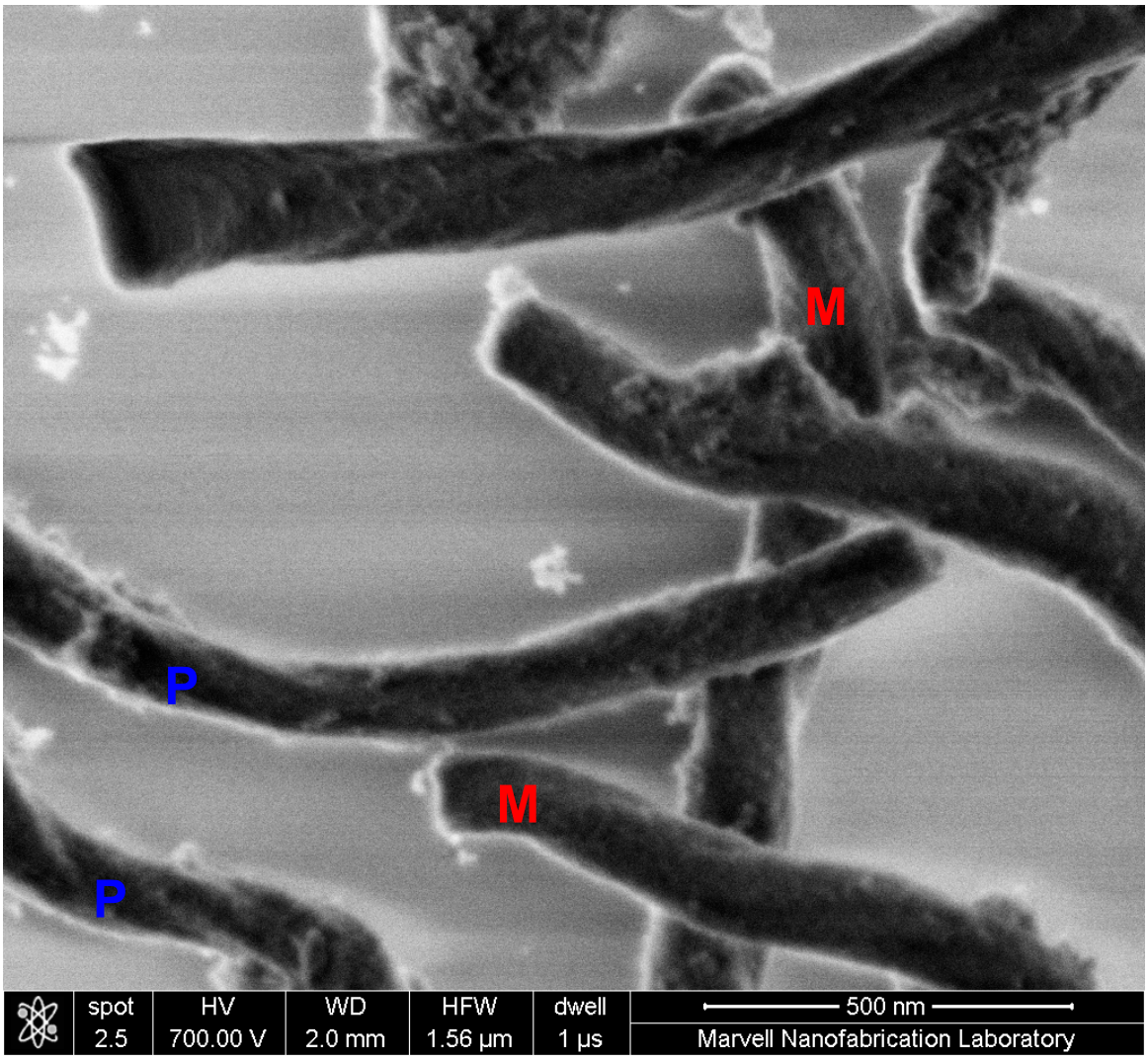

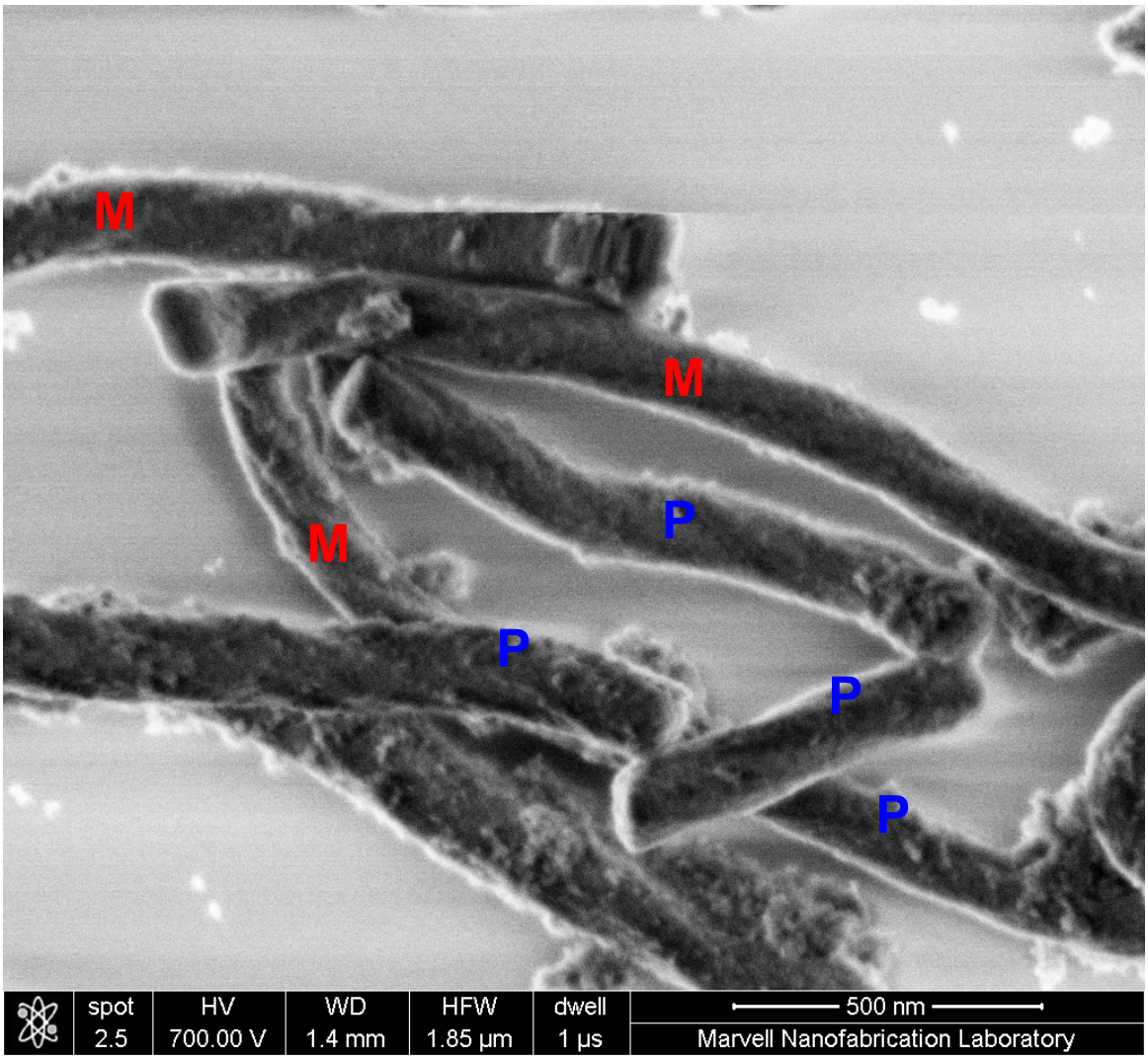
M
M
M
P
P
P
P
spot
2.5
HV
700.00 V
WD
1.4 mm
HFW
1.85 µm
dwell
1 µs
500 nm
Marvell Nanofabrication Laboratory

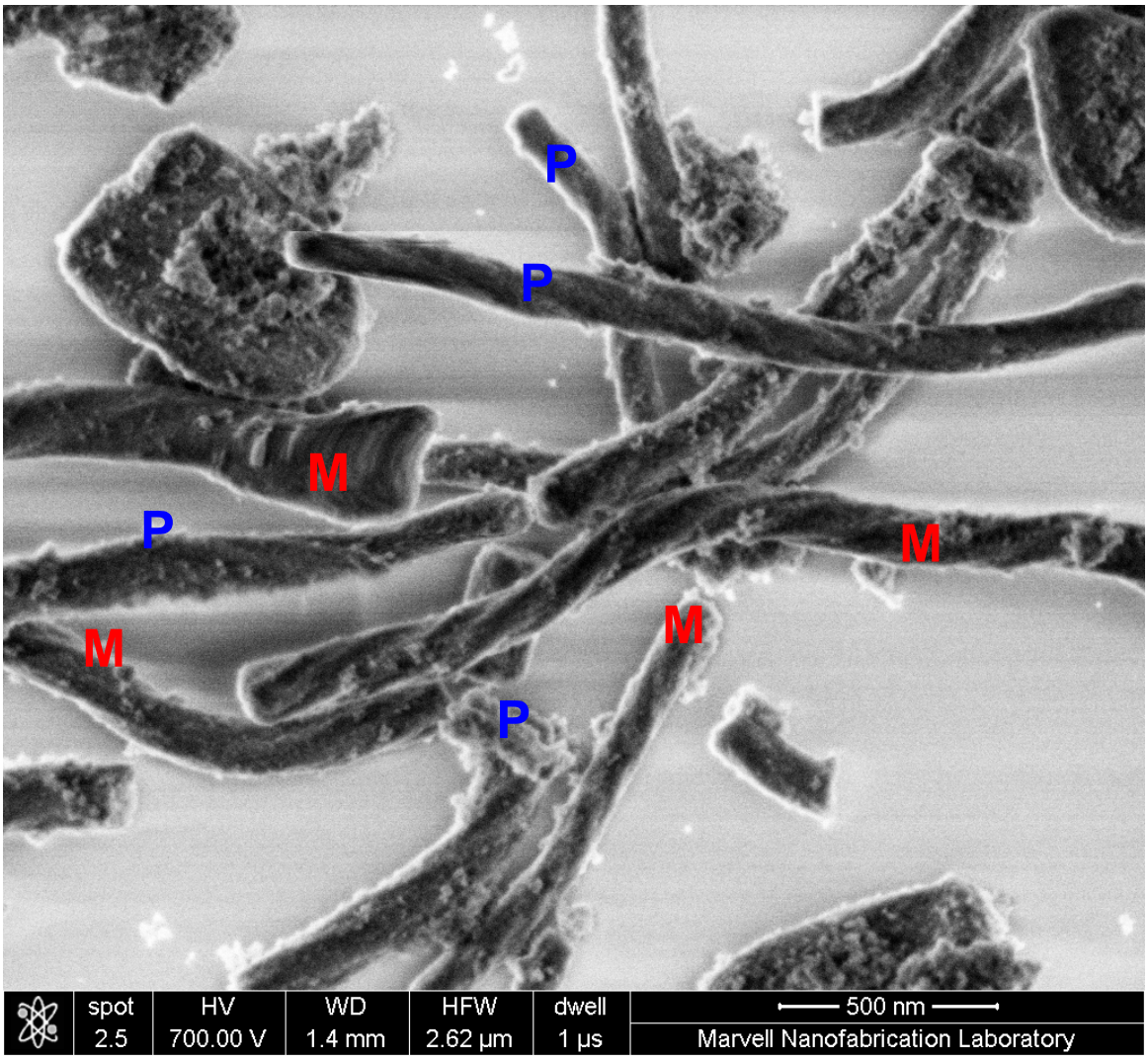
P
P
M
P
M
M
M
P
spot
2.5
HV
700.00 V
WD
1.4 mm
HFW
2.62 µm
dwell
1 µs
500 nm
Marvell Nanofabrication Laboratory

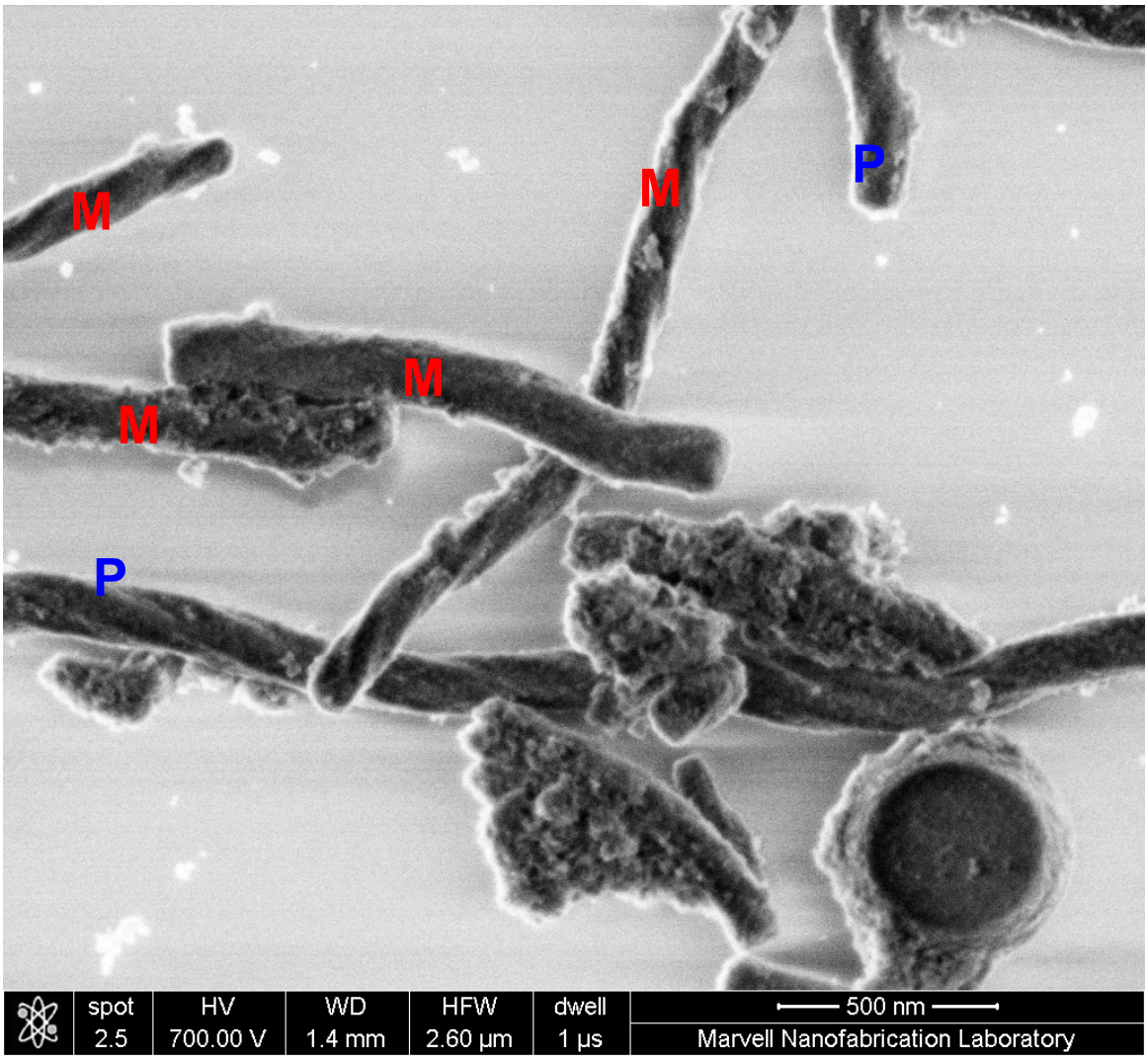
M
M
M
P
M
P
spot
2.5
HV
700.00 V
WD
1.4 mm
HFW
2.60 µm
dwell
1 µs
500 nm
Marvell Nanofabrication Laboratory

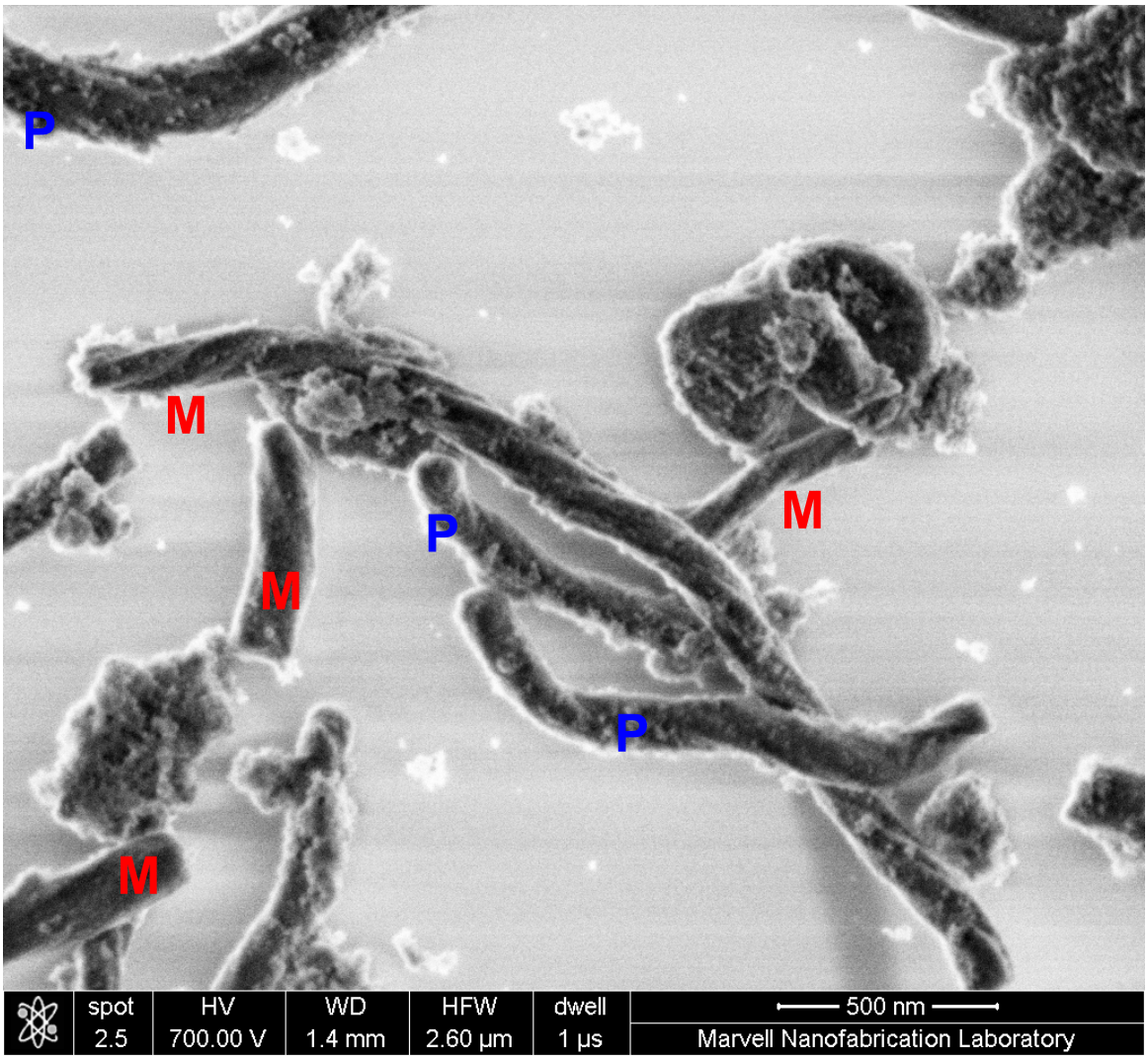
P
M
P
M
M
P
M
spot
2.5
HV
700.00 V
WD
1.4 mm
HFW
2.60 µm
dwell
1 µs
500 nm
Marvell Nanofabrication Laboratory

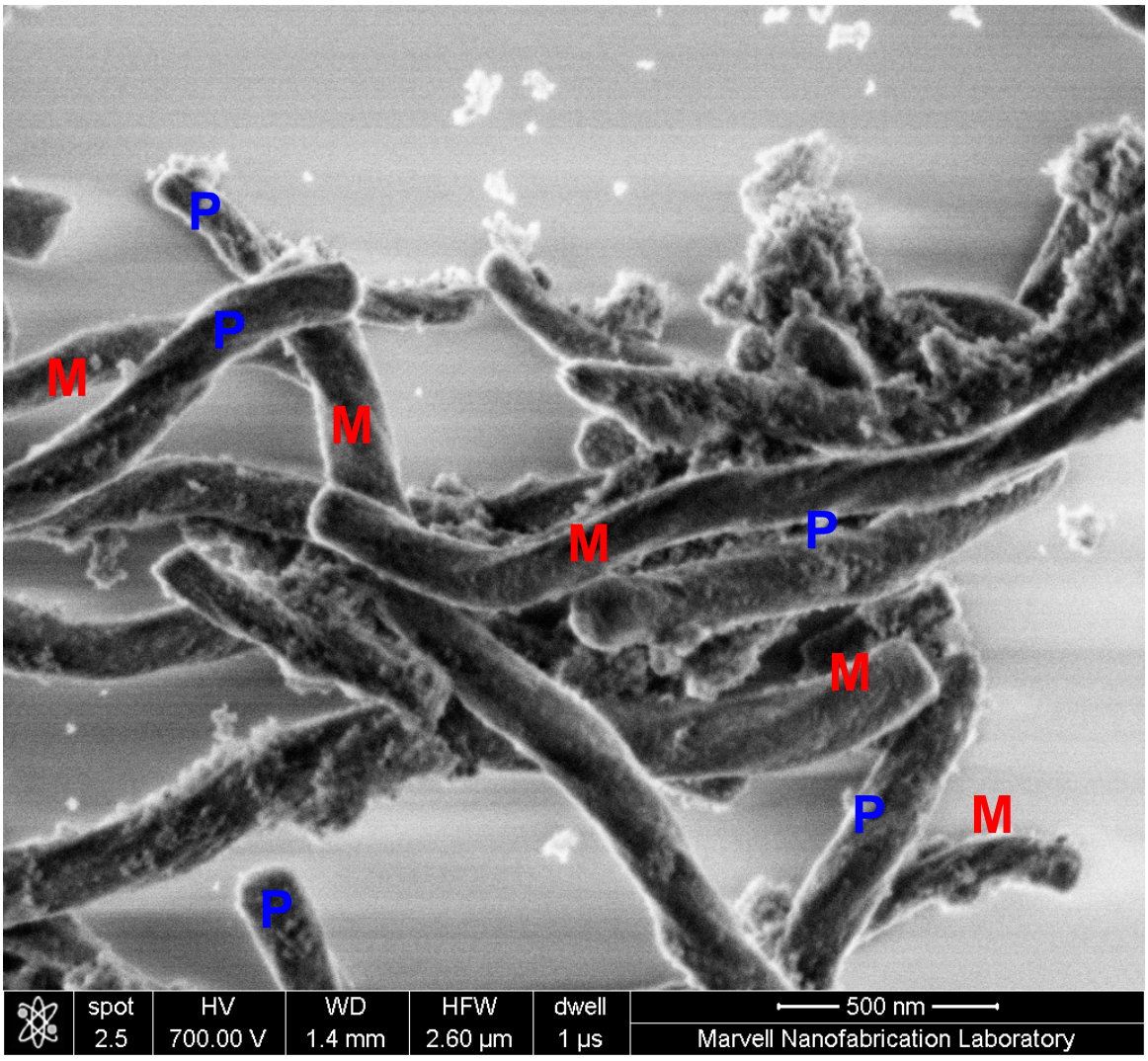
P
P
M
M
M
P
M
P
M
P
spot
2.5
HV
700.00 V
WD
1.4 mm
HFW
2.60 µm
dwell
1 µs
500 nm
Marvell Nanofabrication Laboratory

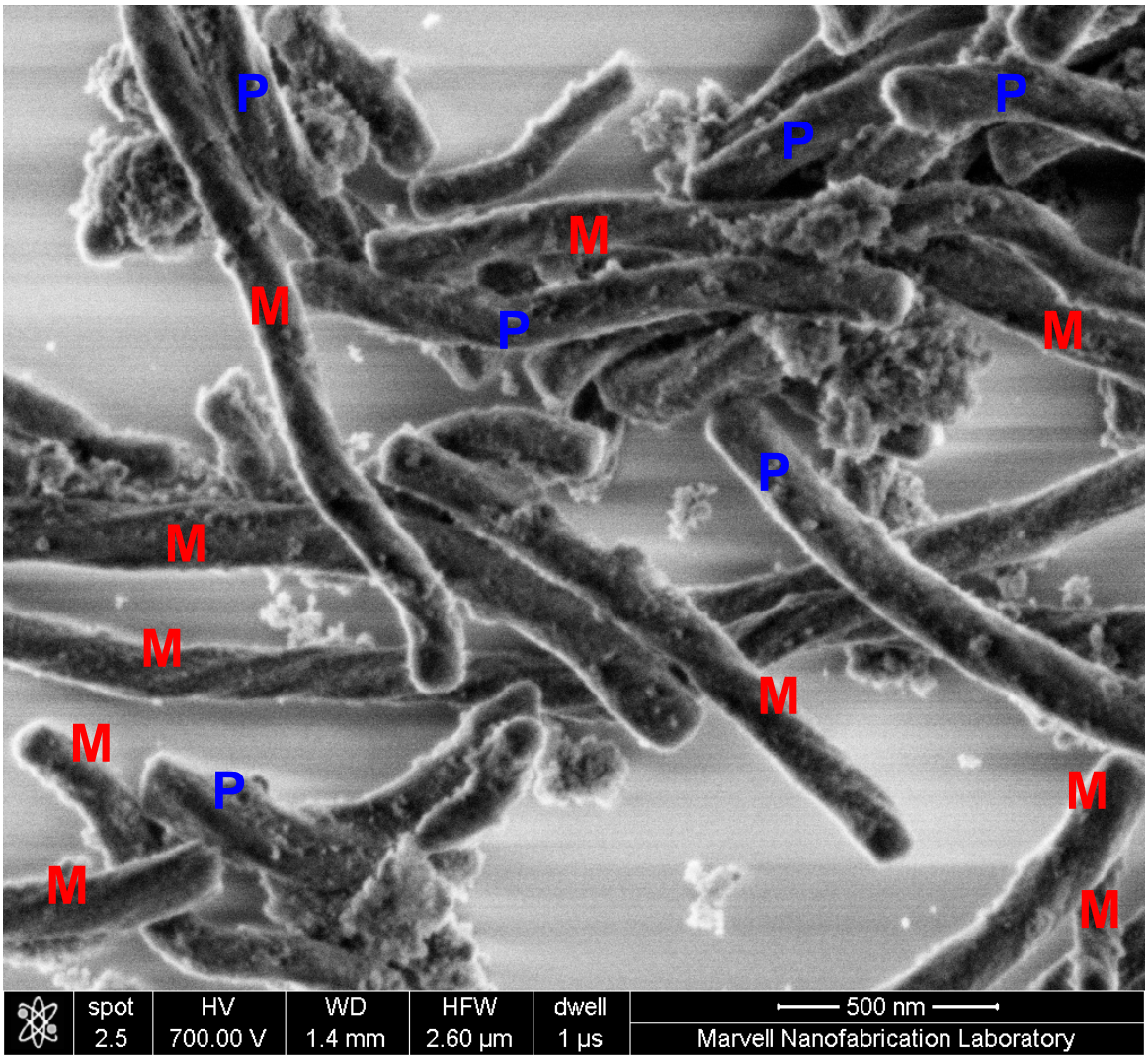
P
P
P
M
M
P
M
P
M
M
M
M
P
M
M
spot
2.5
HV
700.00 V
WD
1.4 mm
HFW
2.60 µm
dwell
1 µs
500 nm
Marvell Nanofabrication Laboratory

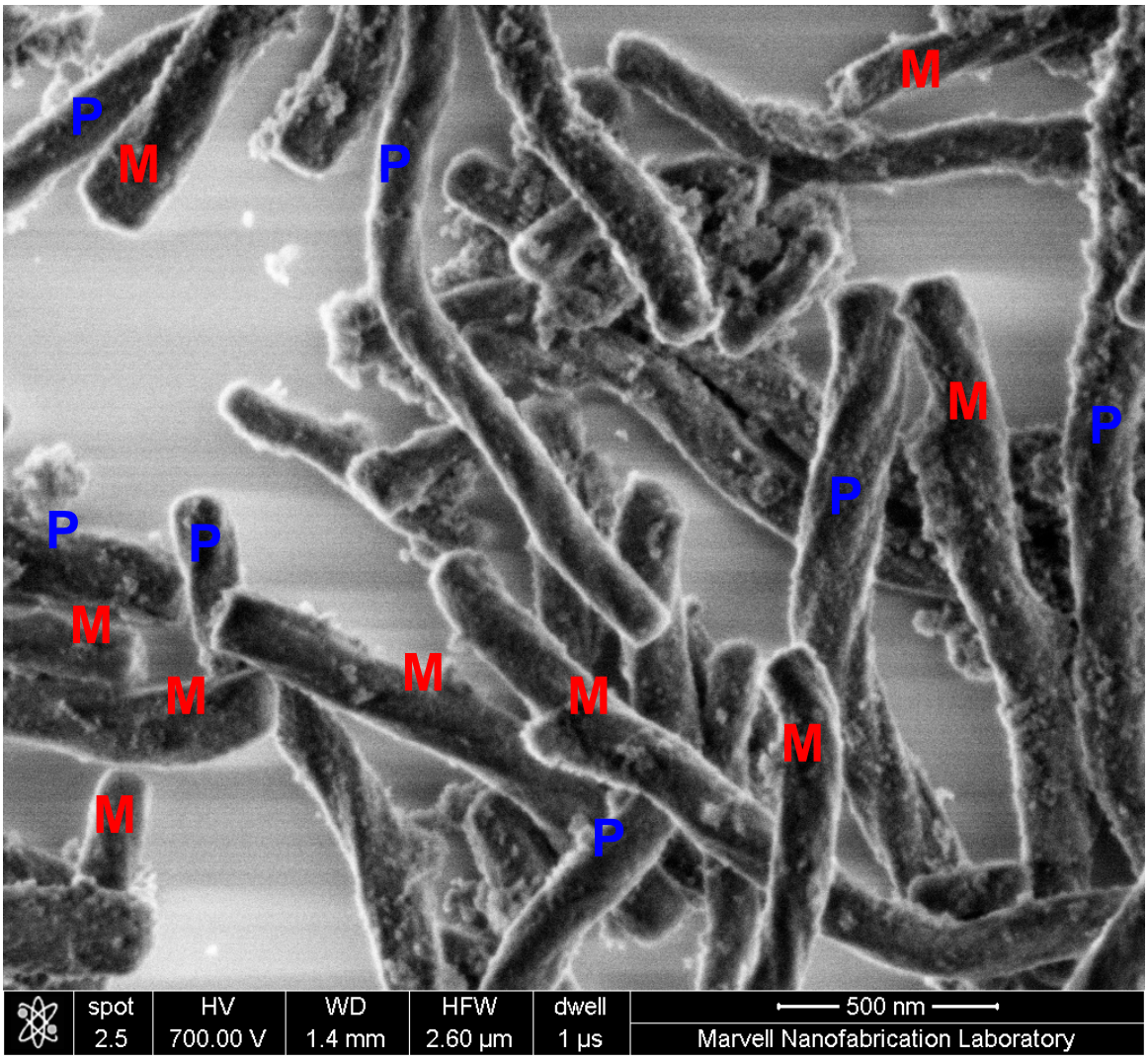
P
M
P
M
P
M
P
P
M
M
M
M
M
P
spot
2.5
HV
700.00 V
WD
1.4 mm
HFW
2.60 µm
dwell
1 µs
500 nm
Marvell Nanofabrication Laboratory

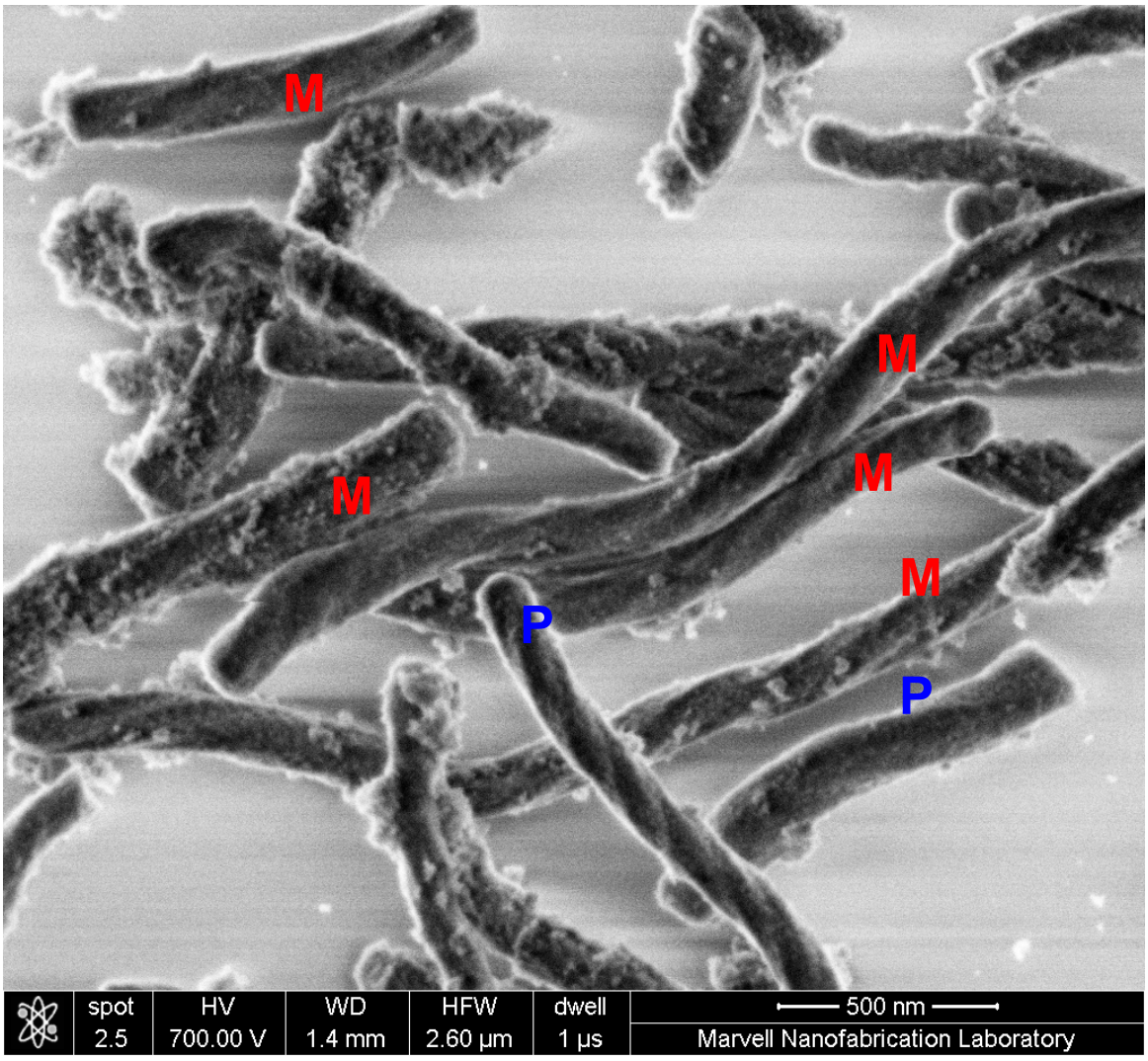
M
M
M
M
M
P
P
spot
2.5
HV
700.00 V
WD
1.4 mm
HFW
2.60 µm
dwell
1 µs
500 nm
Marvell Nanofabrication Laboratory

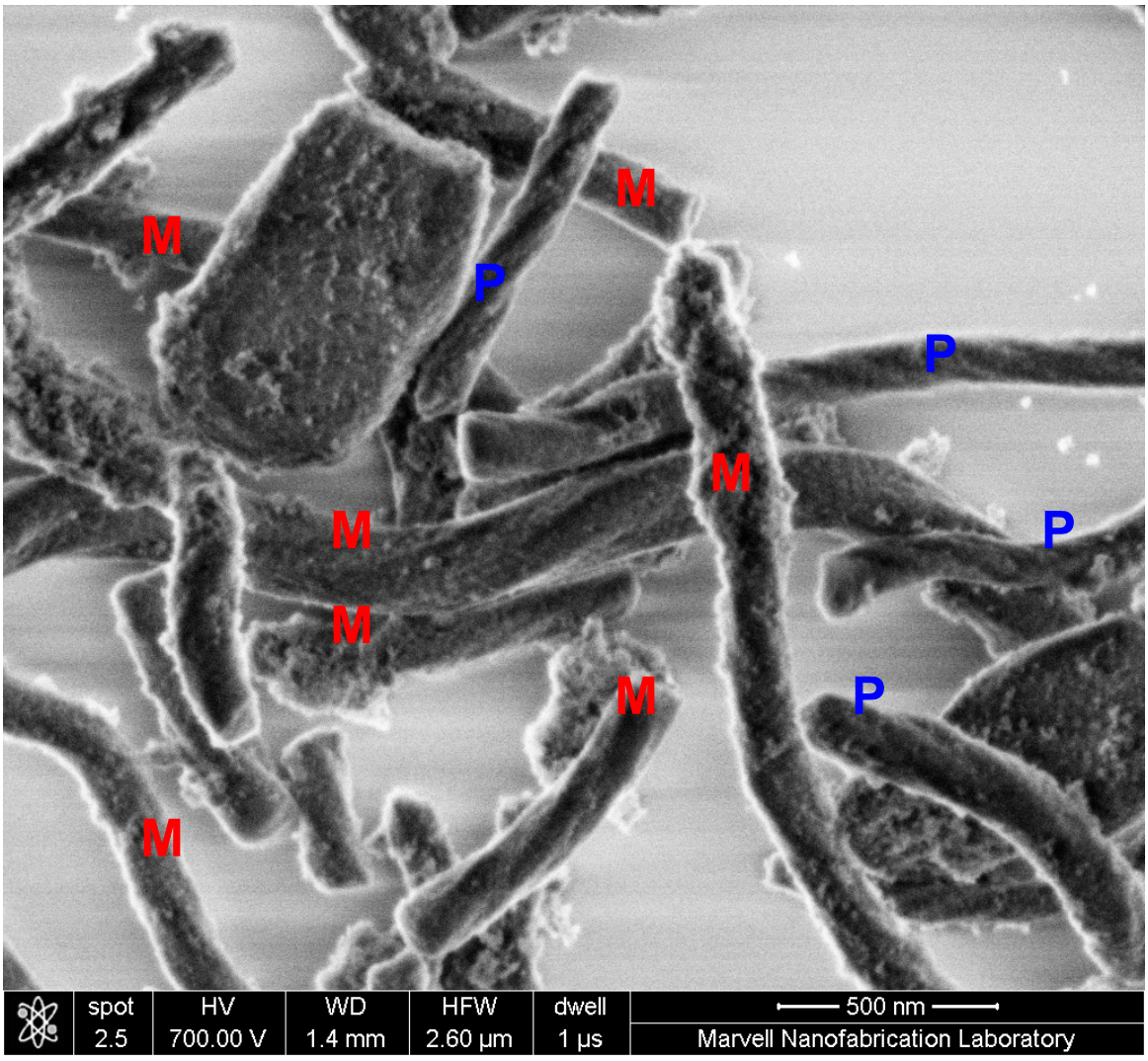
M
M
P
P
M
M
P
M
P
M
spot
2.5
HV
700.00 V
WD
1.4 mm
HFW
2.60 µm
dwell
1 µs
500 nm
Marvell Nanofabrication Laboratory

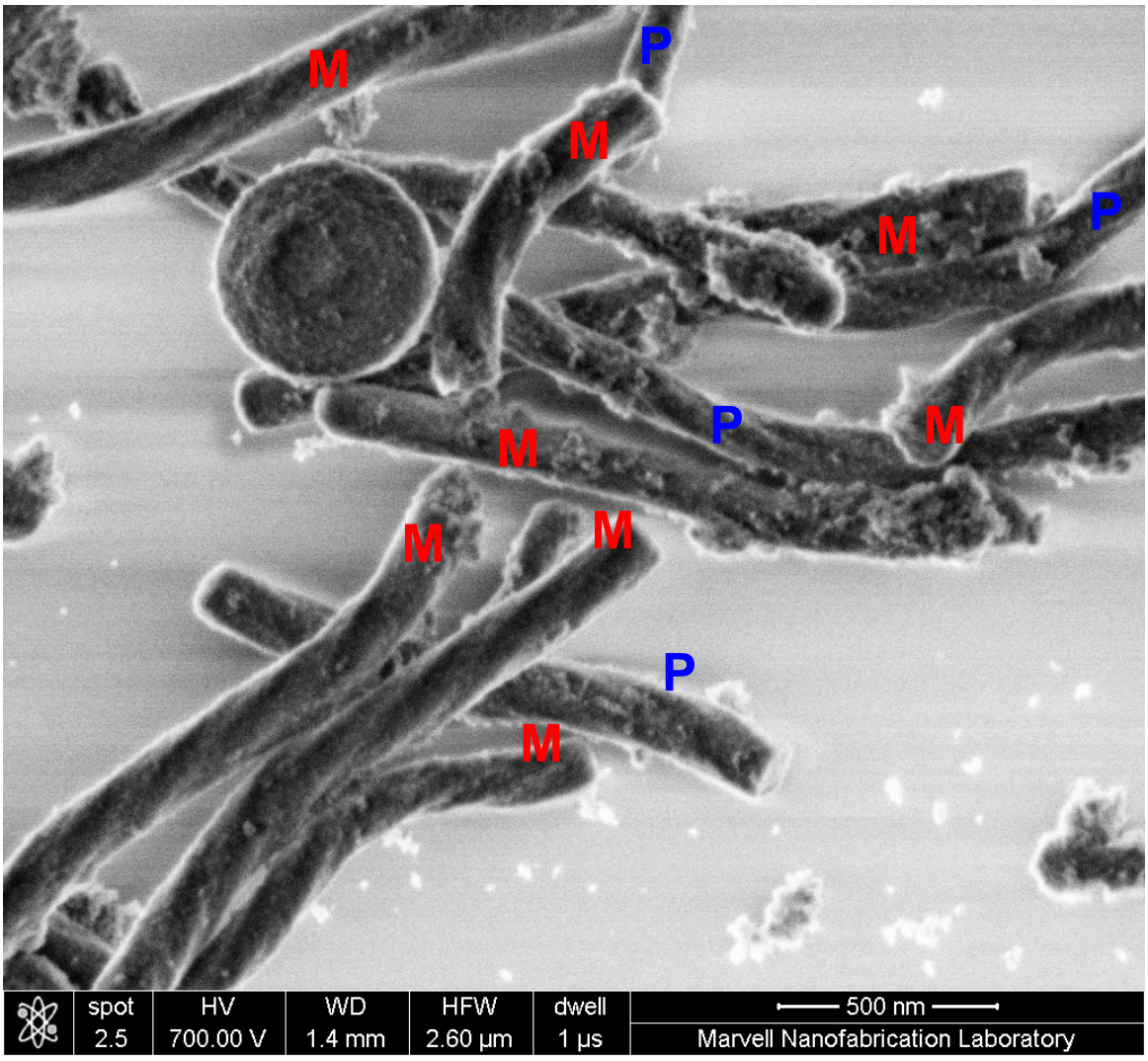
M
P
M
M
P
P
M
M
M
M
P
M
spot
2.5
HV
700.00 V
WD
1.4 mm
HFW
2.60 µm
dwell
1 µs
500 nm
Marvell Nanofabrication Laboratory

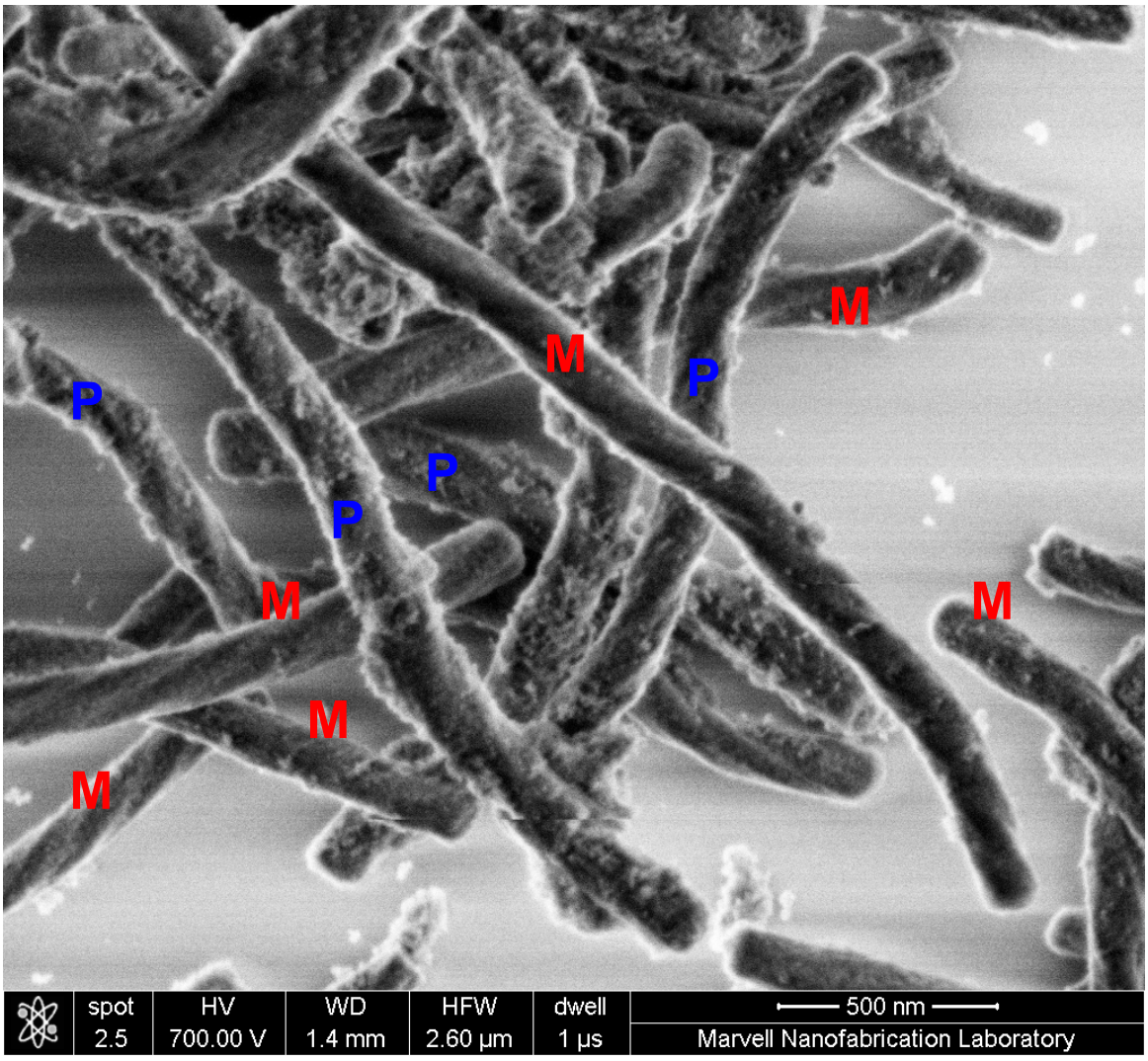
M
M
P
P
P
P
M
M
M
M
spot
2.5
HV
700.00 V
WD
1.4 mm
HFW
2.60 µm
dwell
1 µs
500 nm
Marvell Nanofabrication Laboratory

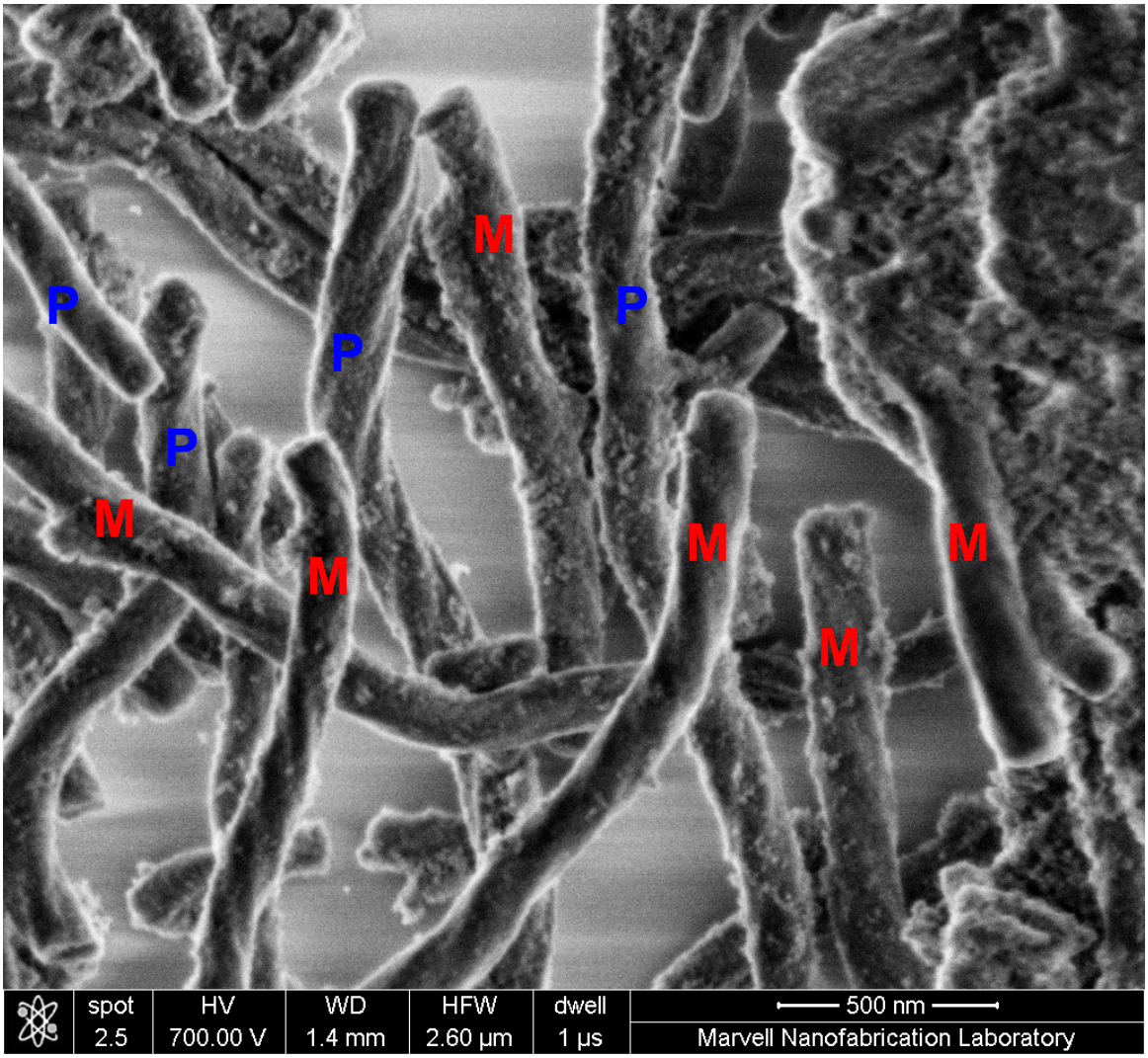
P
P
P
P
M
M
M
M
M
spot
2.5
HV
700.00 V
WD
1.4 mm
HFW
2.60 µm
dwell
1 µs
500 nm
Marvell Nanofabrication Laboratory

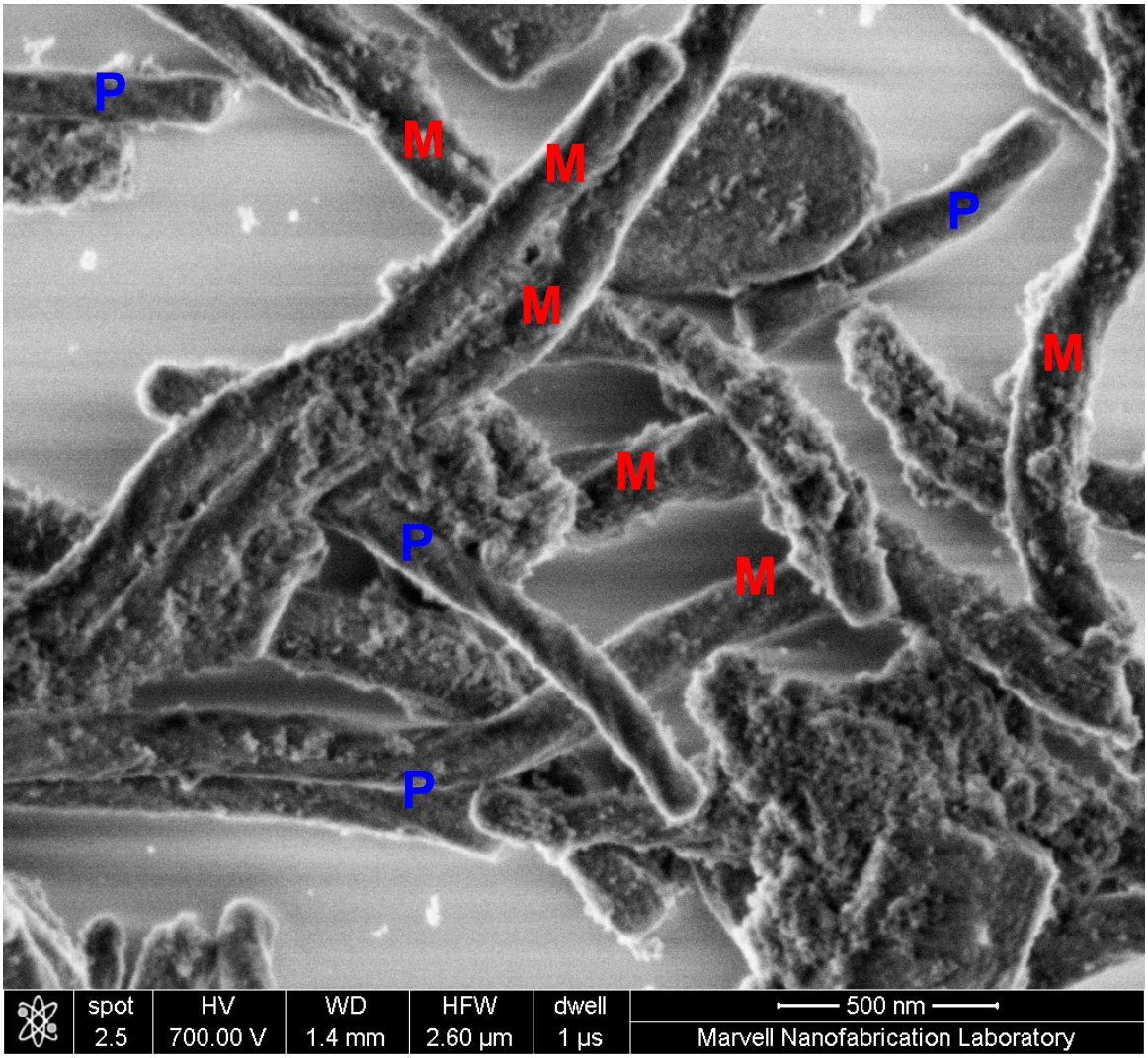
P
M
M
P
M
M
P
M
P
M
spot
2.5
HV
700.00 V
WD
1.4 mm
HFW
2.60 µm
dwell
1 µs
500 nm
Marvell Nanofabrication Laboratory

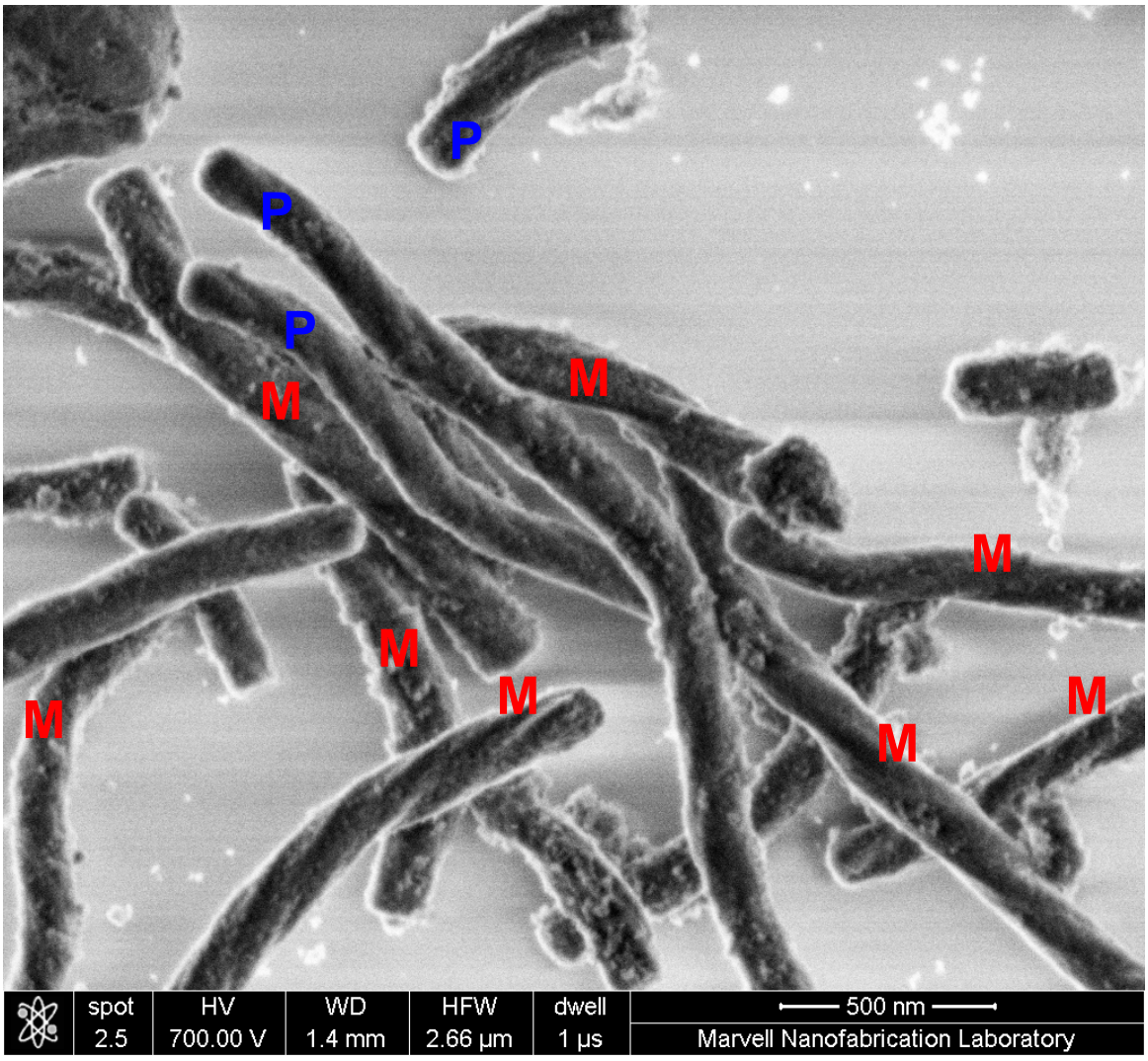
P
P
P
M
M
M
M
M
M
M
M
spot
2.5
HV
700.00 V
WD
1.4 mm
HFW
2.66 µm
dwell
1 µs
500 nm
Marvell Nanofabrication Laboratory


spot
2.5
HV
700.00 V
WD
1.4 mm
HFW
2.60 µm
dwell
1 µs
500 nm
Marvell Nanofabrication Laboratory

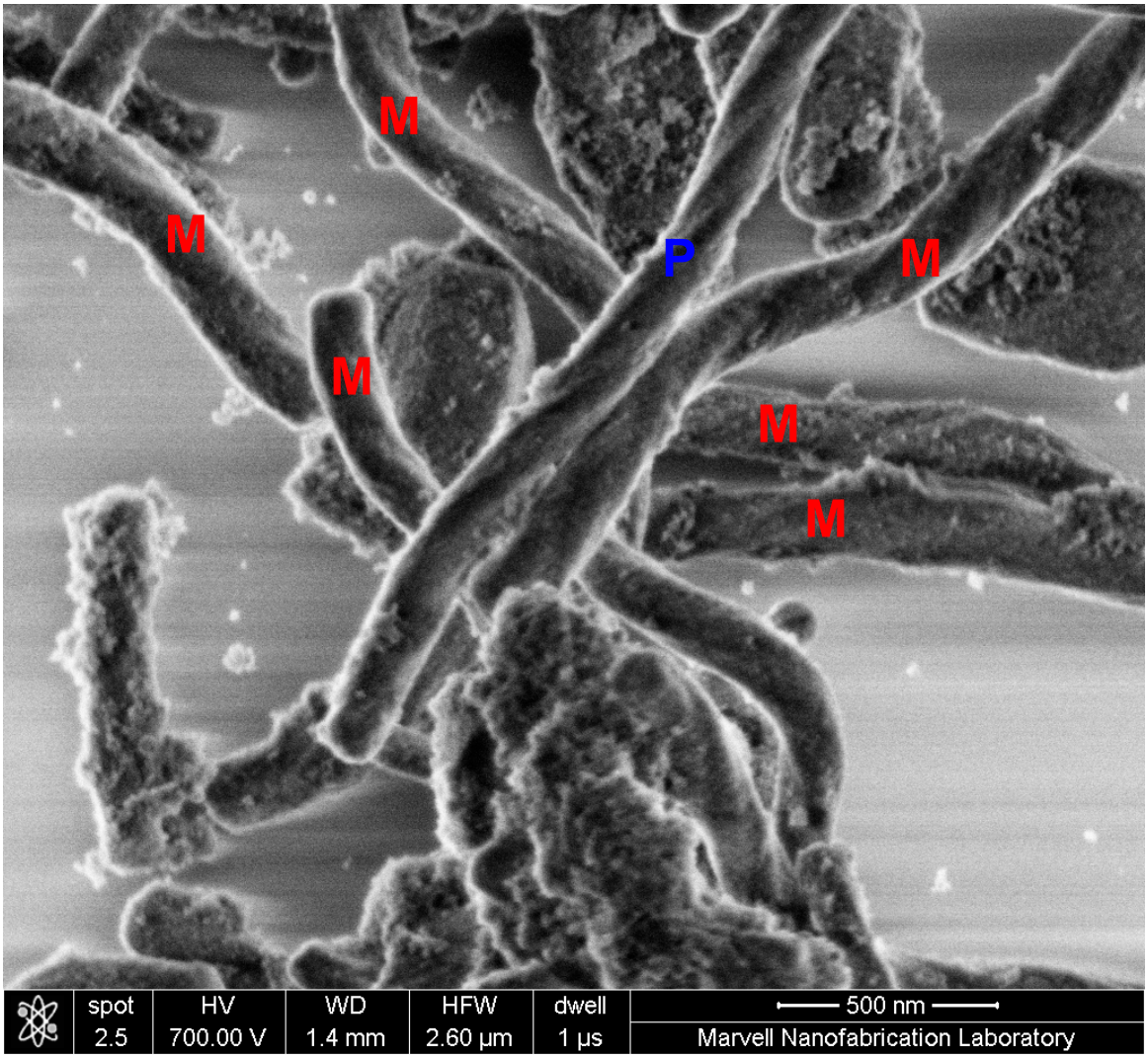
M
M
P
M
M
M
M
spot
2.5
HV
700.00 V
WD
1.4 mm
HFW
2.60 µm
dwell
1 µs
500 nm
Marvell Nanofabrication Laboratory

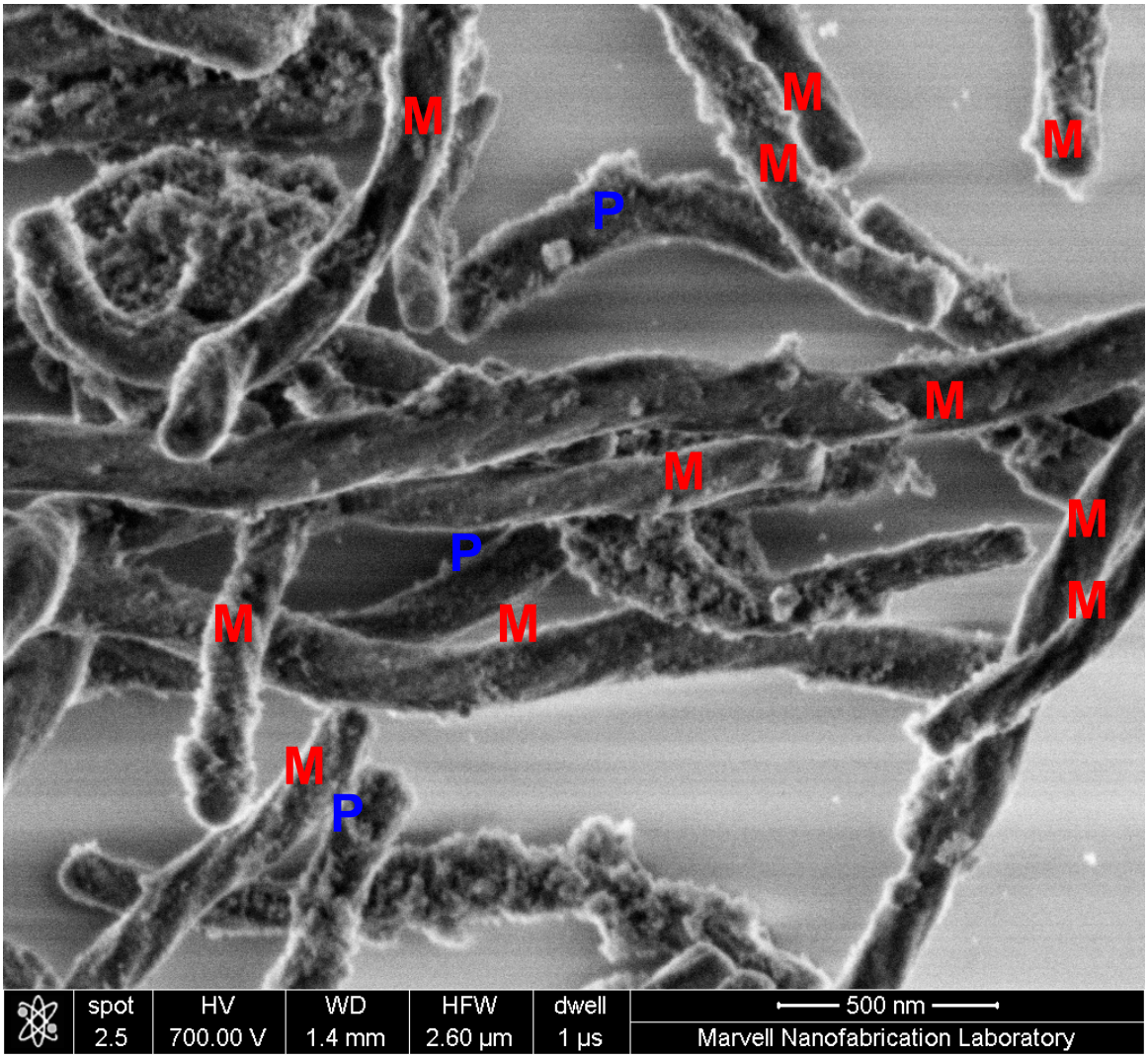
M
M
M
M
P
M
M
M
P
M
M
M
P
spot
2.5
HV
700.00 V
WD
1.4 mm
HFW
2.60 µm
dwell
1 µs
500 nm
Marvell Nanofabrication Laboratory

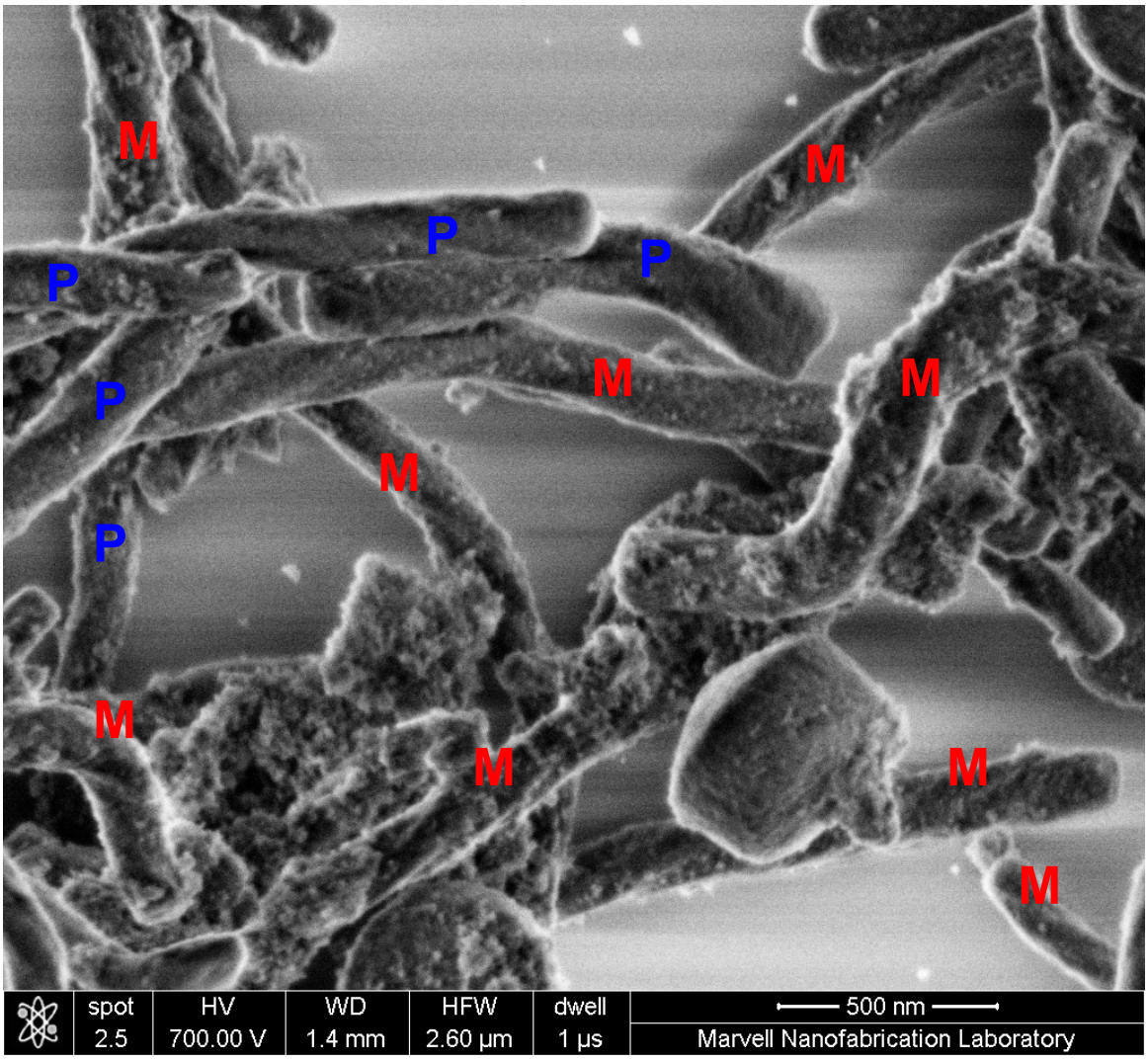
M
M
P
P
P
P
M
M
M
P
M
M
M
M
spot
2.5
HV
700.00 V
WD
1.4 mm
HFW
2.60 µm
dwell
1 µs
500 nm
Marvell Nanofabrication Laboratory

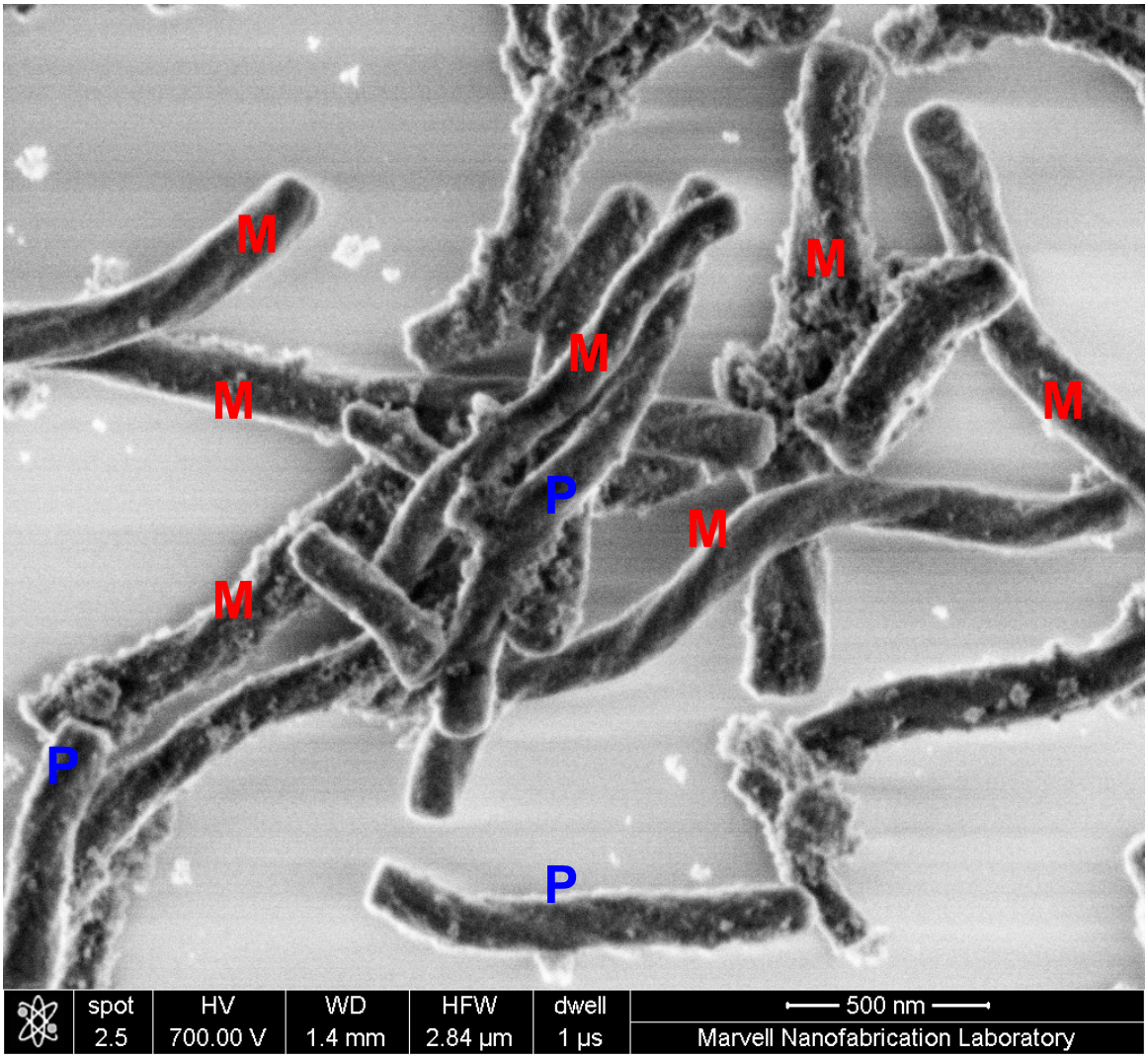
M
M
M
M
M
M
P
P
P
spot
2.5
HV
700.00 V
WD
1.4 mm
HFW
2.84 µm
dwell
1 µs
500 nm
Marvell Nanofabrication Laboratory

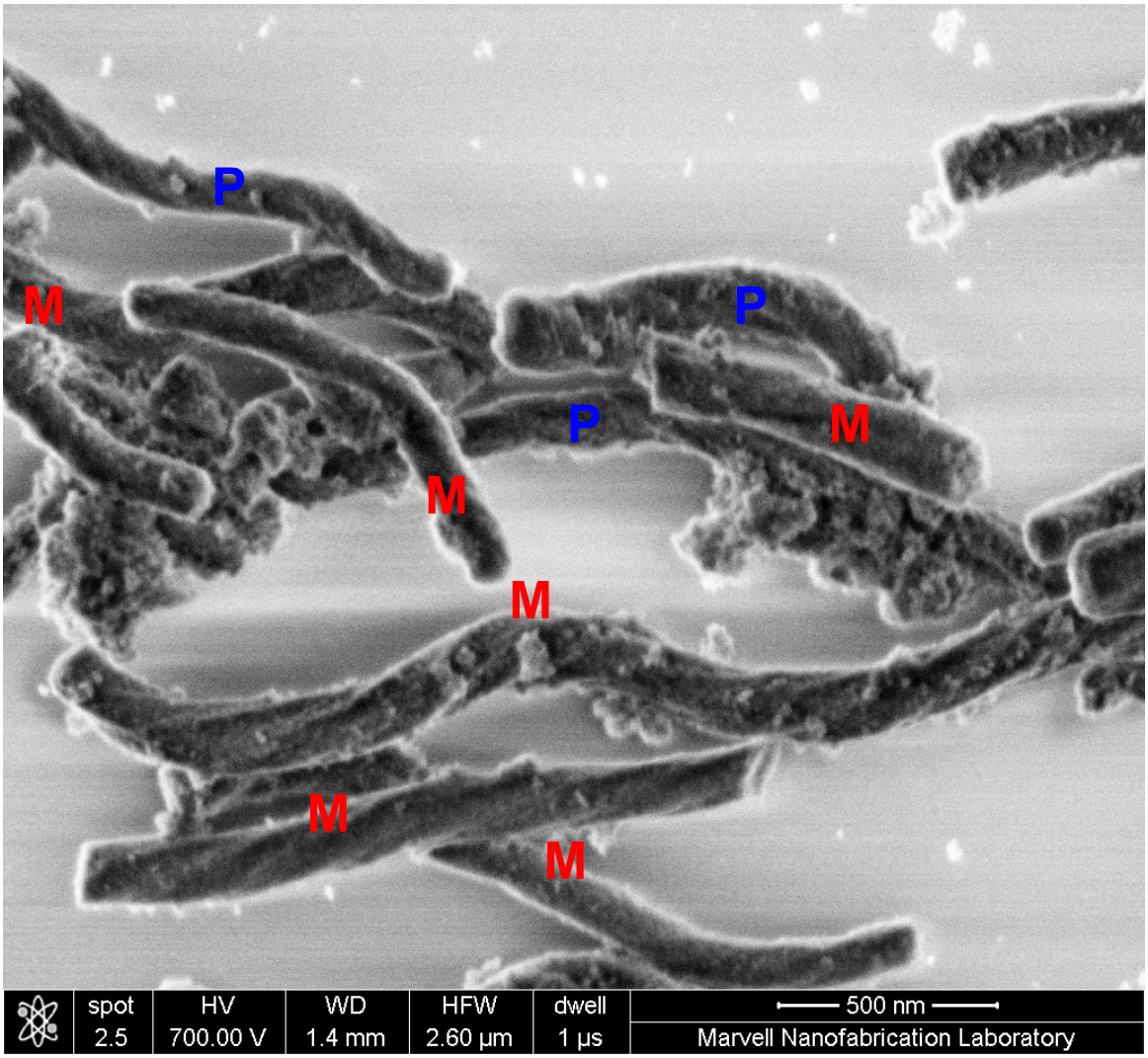
P
M
P
P
M
M
M
M
M
spot
2.5
HV
700.00 V
WD
1.4 mm
HFW
2.60 µm
dwell
1 µs
500 nm
Marvell Nanofabrication Laboratory

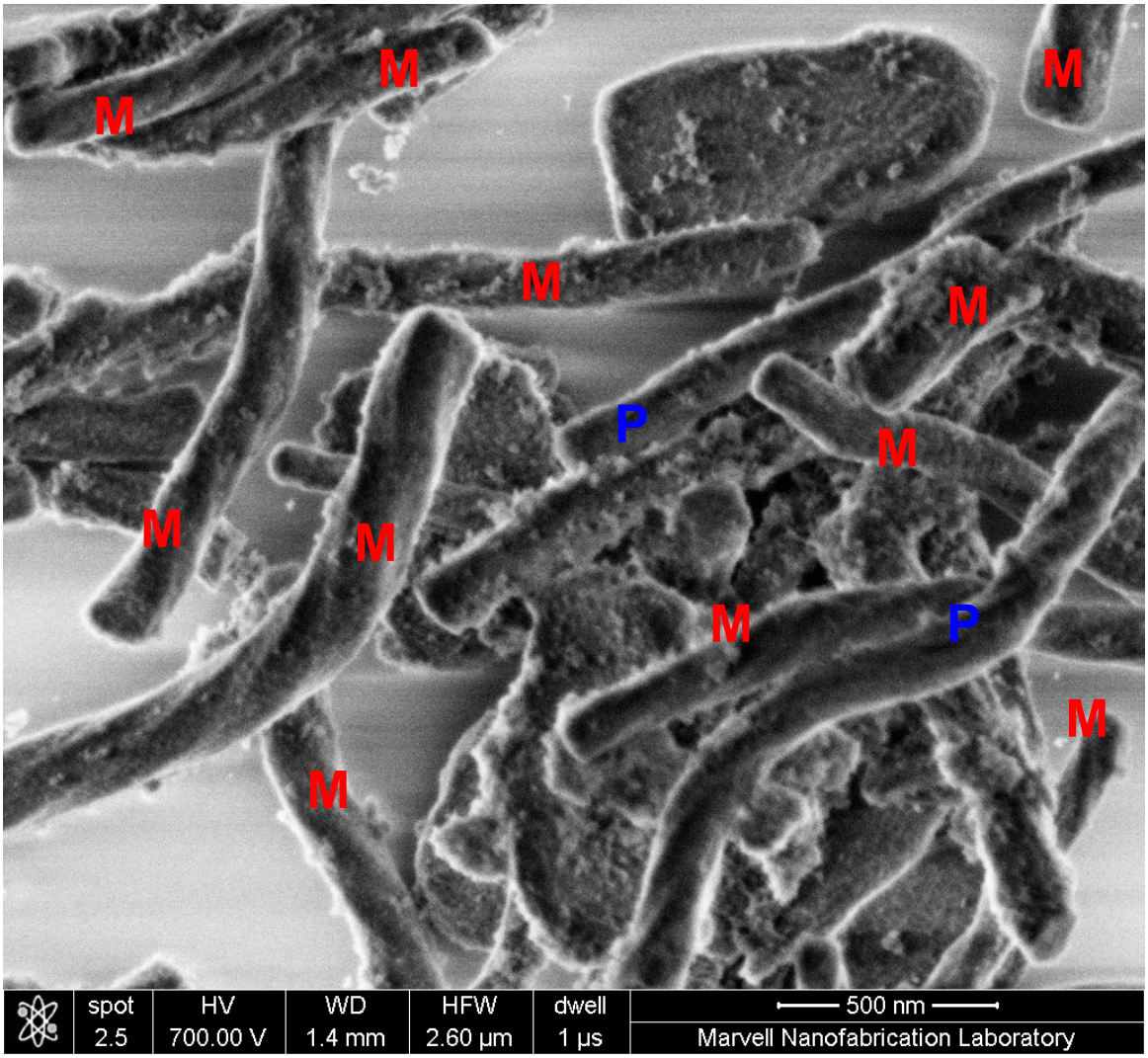
M
M
M
M
M
M
P
M
M
M
M
P
M
M
spot
2.5
HV
700.00 V
WD
1.4 mm
HFW
2.60 µm
dwell
1 µs
500 nm
Marvell Nanofabrication Laboratory

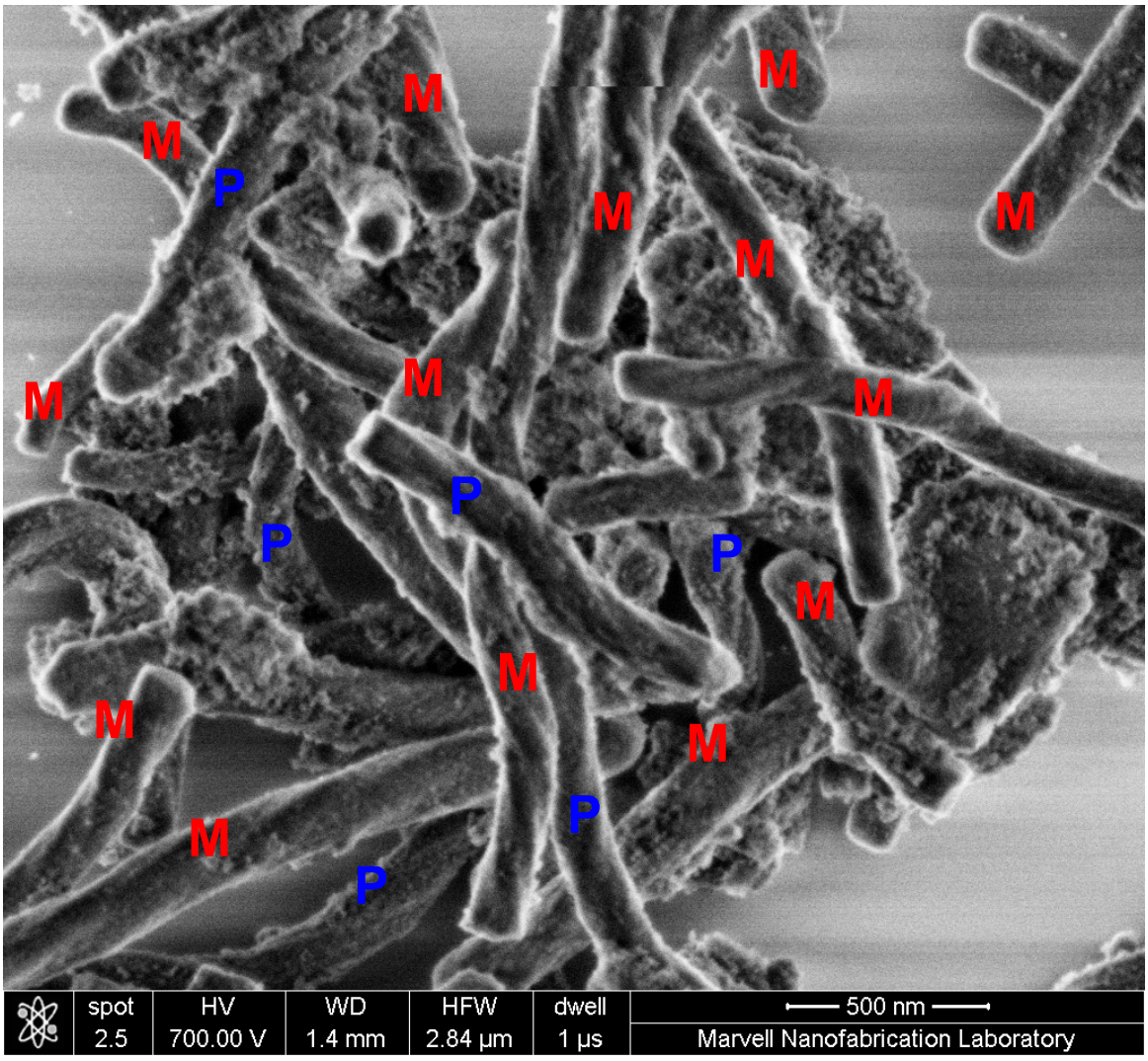
M
M
P
M
M
M
M
M
M
M
P
P
P
M
M
M
M
P
M
P
spot
2.5
HV
700.00 V
WD
1.4 mm
HFW
2.84 µm
dwell
1 µs
500 nm
Marvell Nanofabrication Laboratory

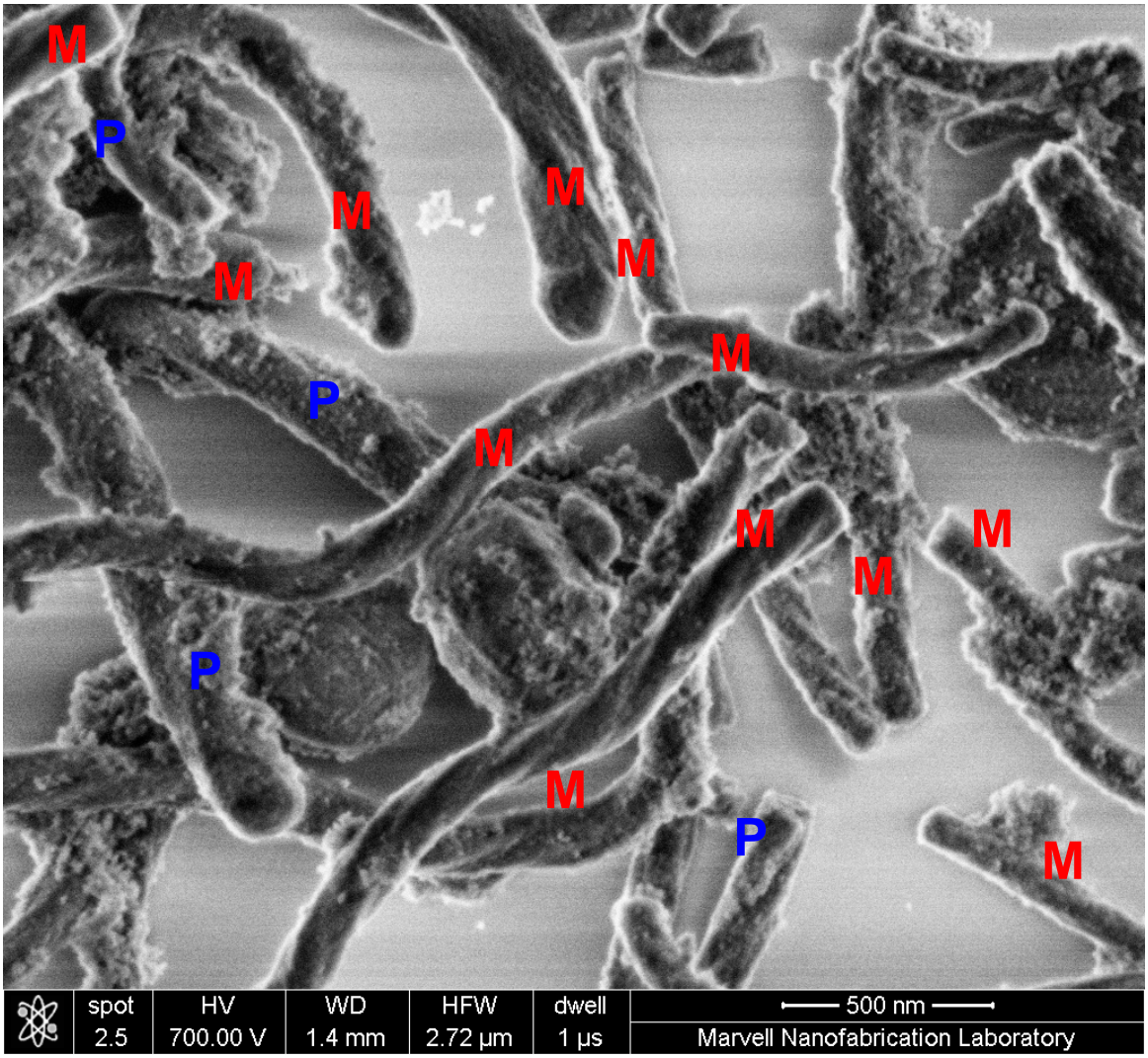
M
P
M
M
M
M
P
M
M
M
M
P
M
P
M
spot
2.5
HV
700.00 V
WD
1.4 mm
HFW
2.72 µm
dwell
1 µs
500 nm
Marvell Nanofabrication Laboratory

CMS^{II} prepared from C_{14}-D-Ala (29% e.e.)

271 (*P*)-CMS and 150 (*M*)-CMS

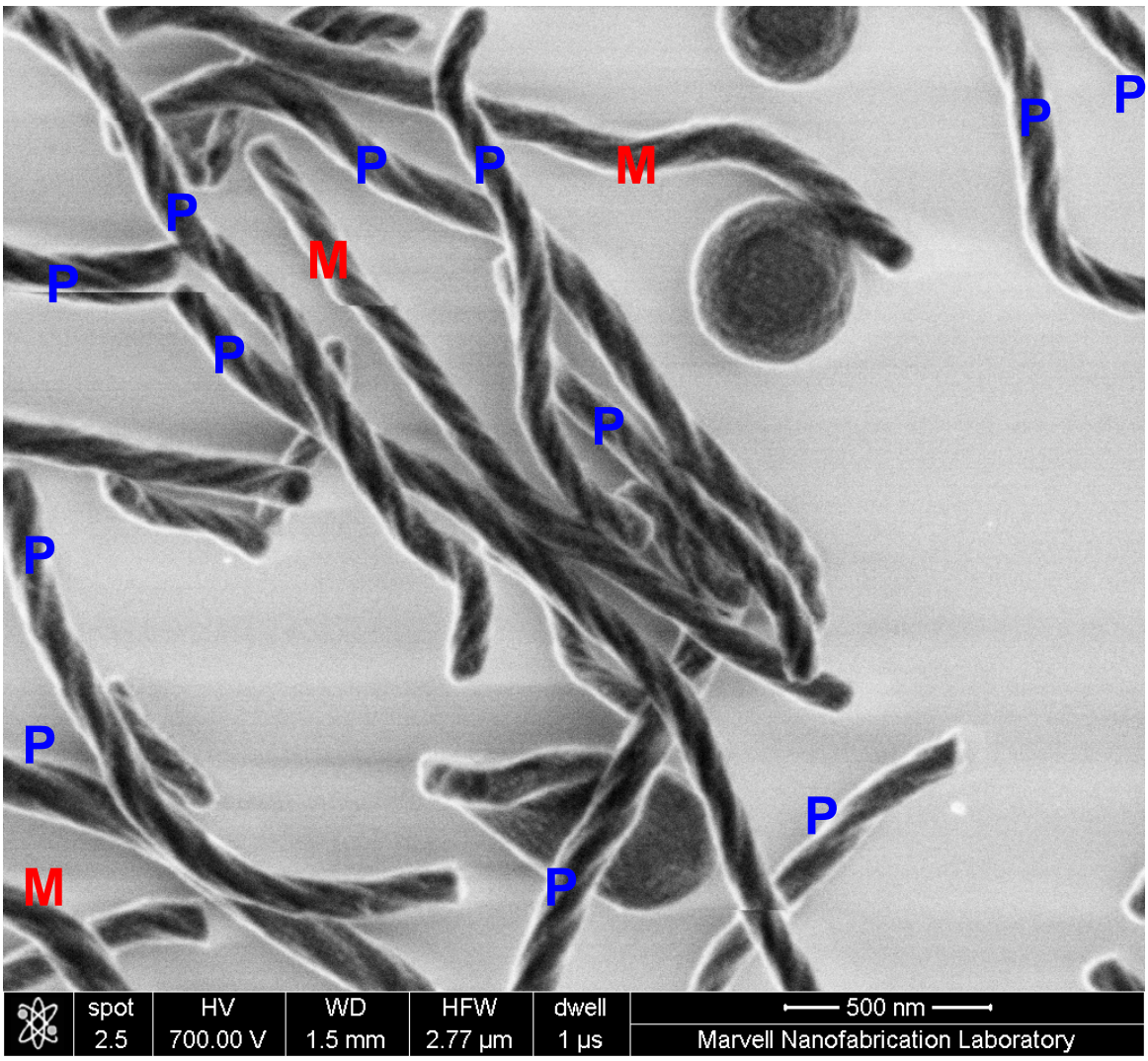

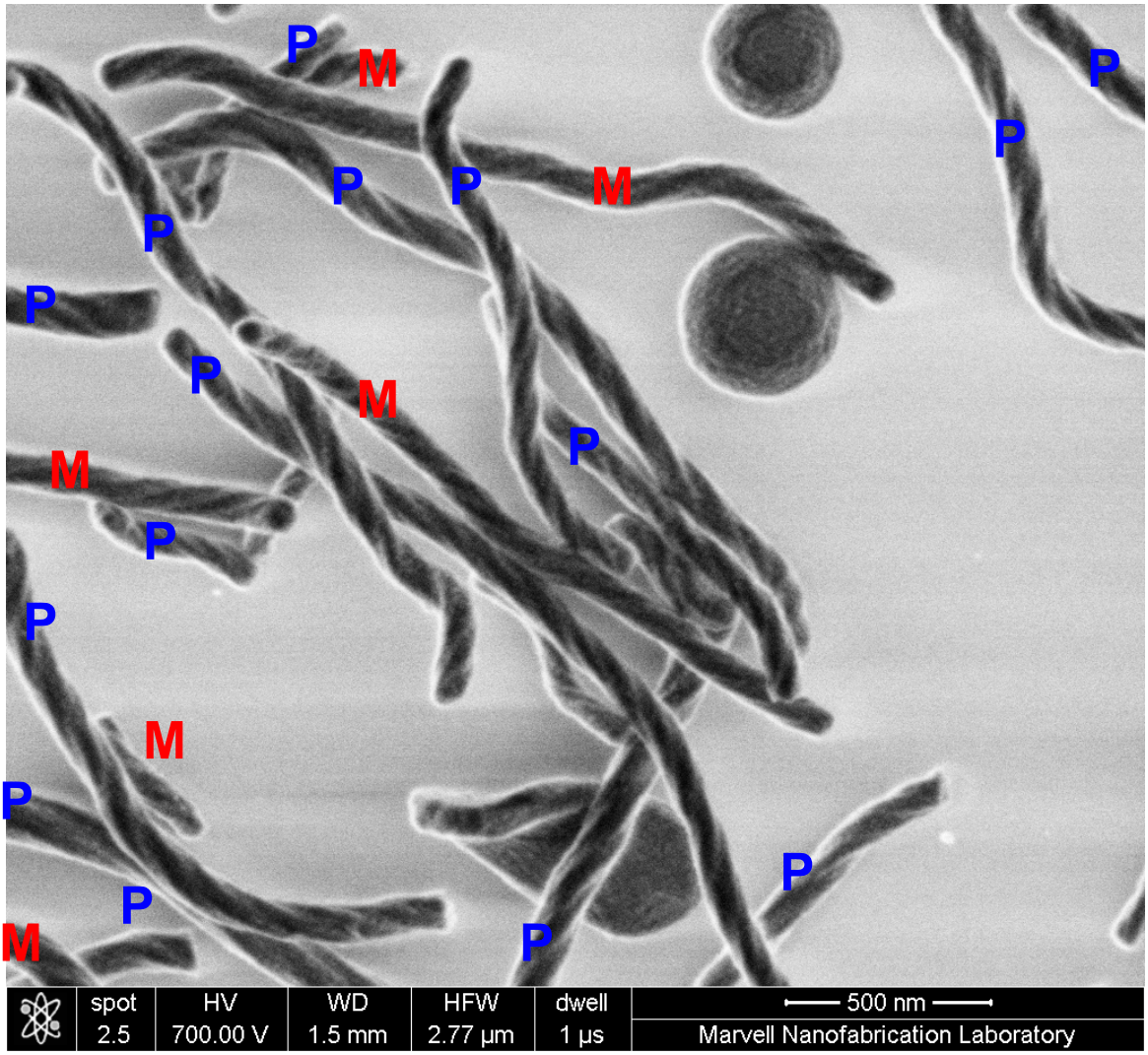
P
M
P
P
M
P
P
P
P
M
M
P
P
P
M
P
P
M
P
P
spot
2.5
HV
700.00 V
WD
1.5 mm
HFW
2.77 µm
dwell
1 µs
500 nm
Marvell Nanofabrication Laboratory

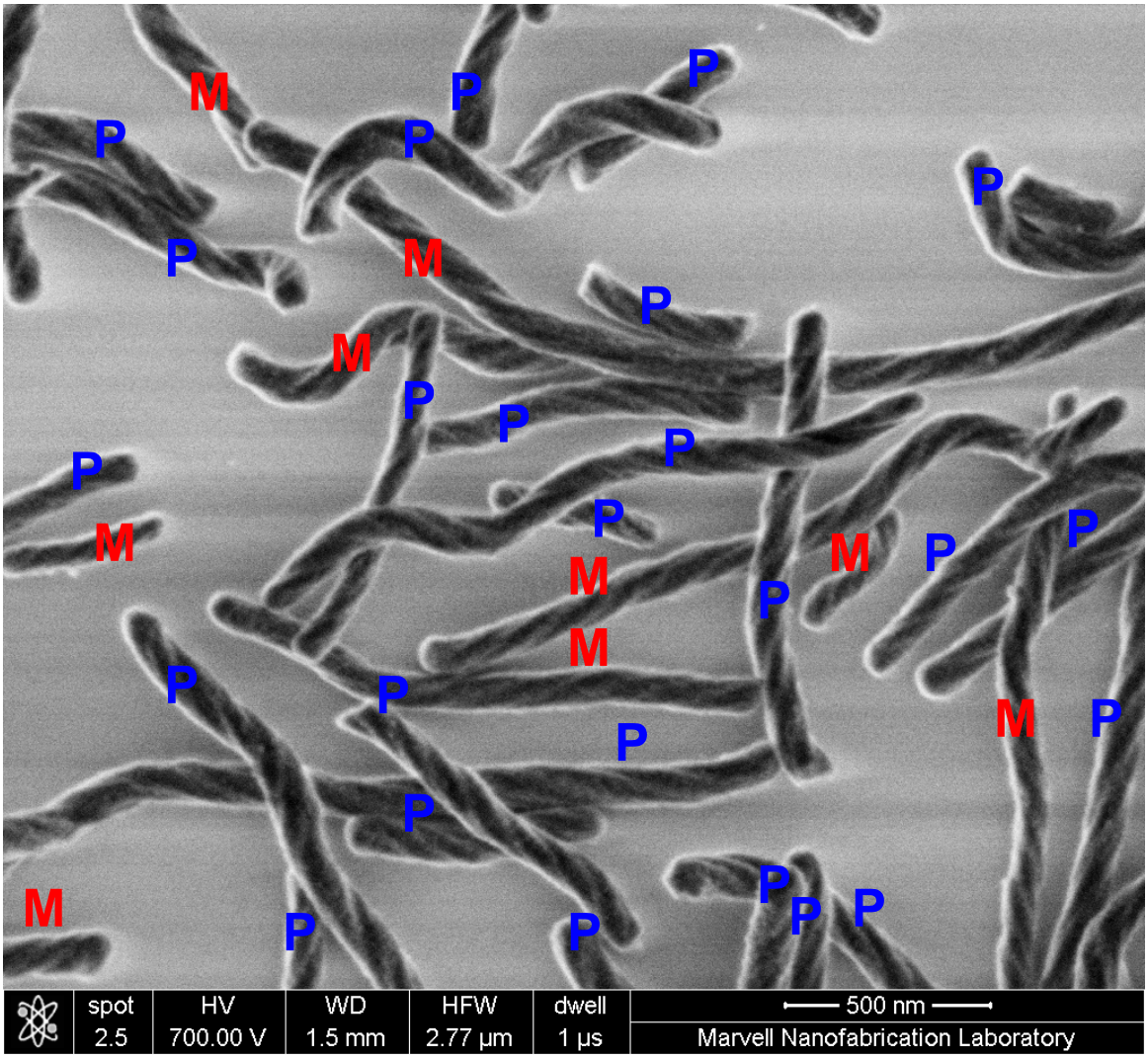
M
P
P
P
P
P
P
M
P
M
P
P
P
P
P
M
P
M
P
M
P
P
P
M
P
P
P
P
M
P
P
P
spot
2.5
HV
700.00 V
WD
1.5 mm
HFW
2.77 µm
dwell
1 µs
500 nm
Marvell Nanofabrication Laboratory

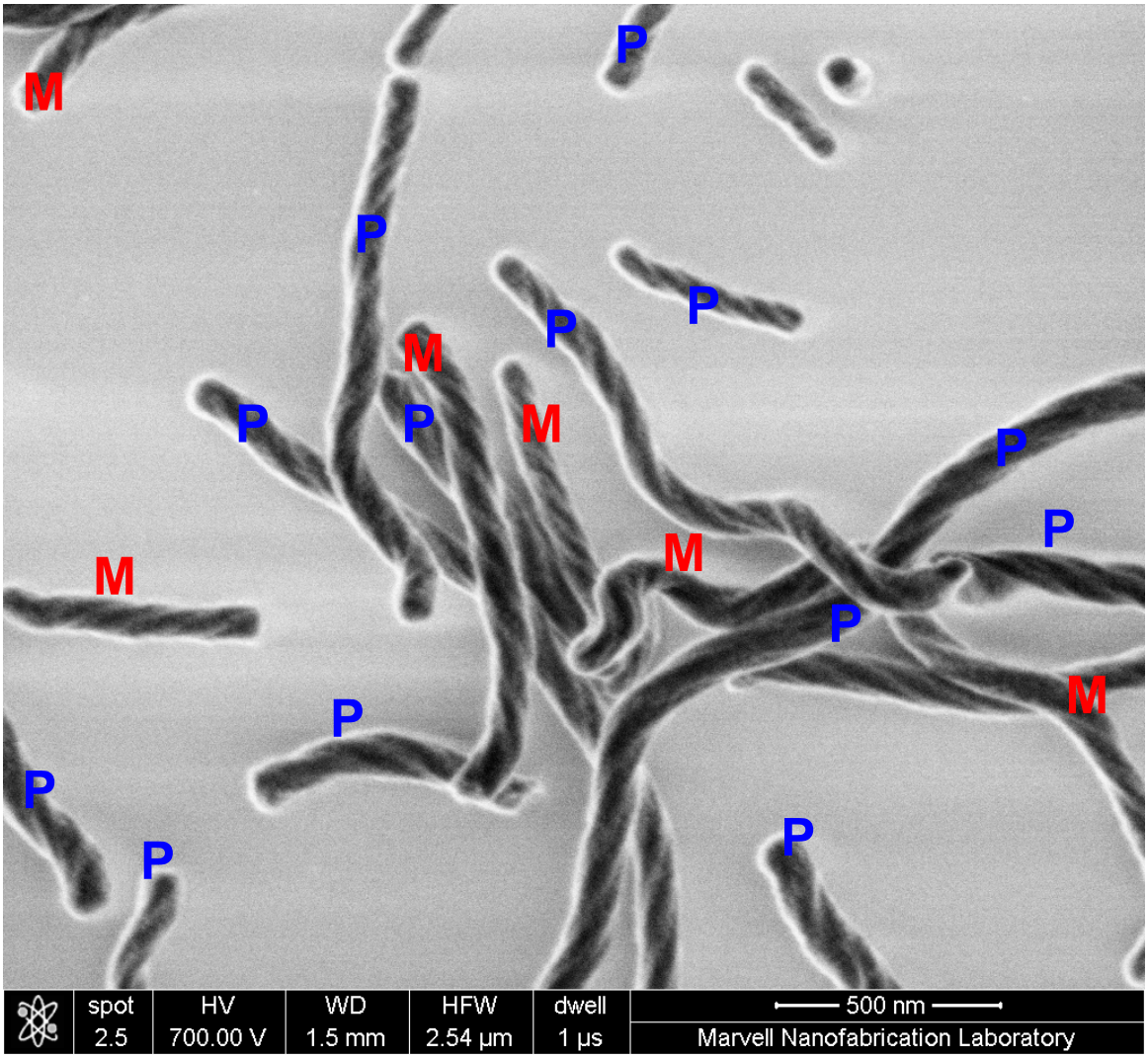
M
P
P
P
P
M
P
P
M
P
P
M
M
P
P
P
M
P
P
P
spot
2.5
HV
700.00 V
WD
1.5 mm
HFW
2.54 µm
dwell
1 µs
500 nm
Marvell Nanofabrication Laboratory

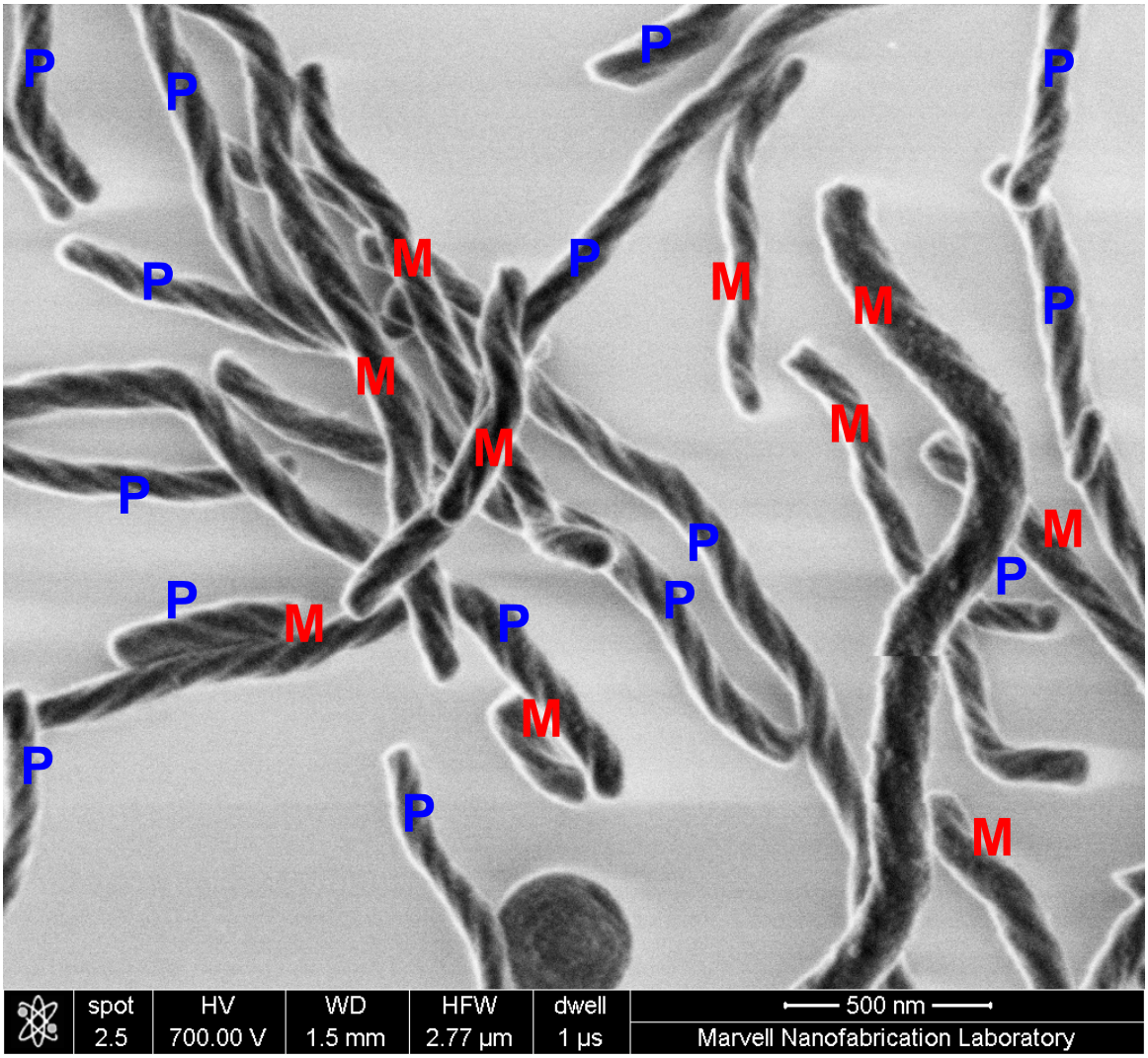
P
P
P
P
P
M
P
M
M
M
M
P
M
M
P
P
M
P
P
P
M
P
M
P
P
M
M
spot
2.5
HV
700.00 V
WD
1.5 mm
HFW
2.77 µm
dwell
1 µs
500 nm
Marvell Nanofabrication Laboratory

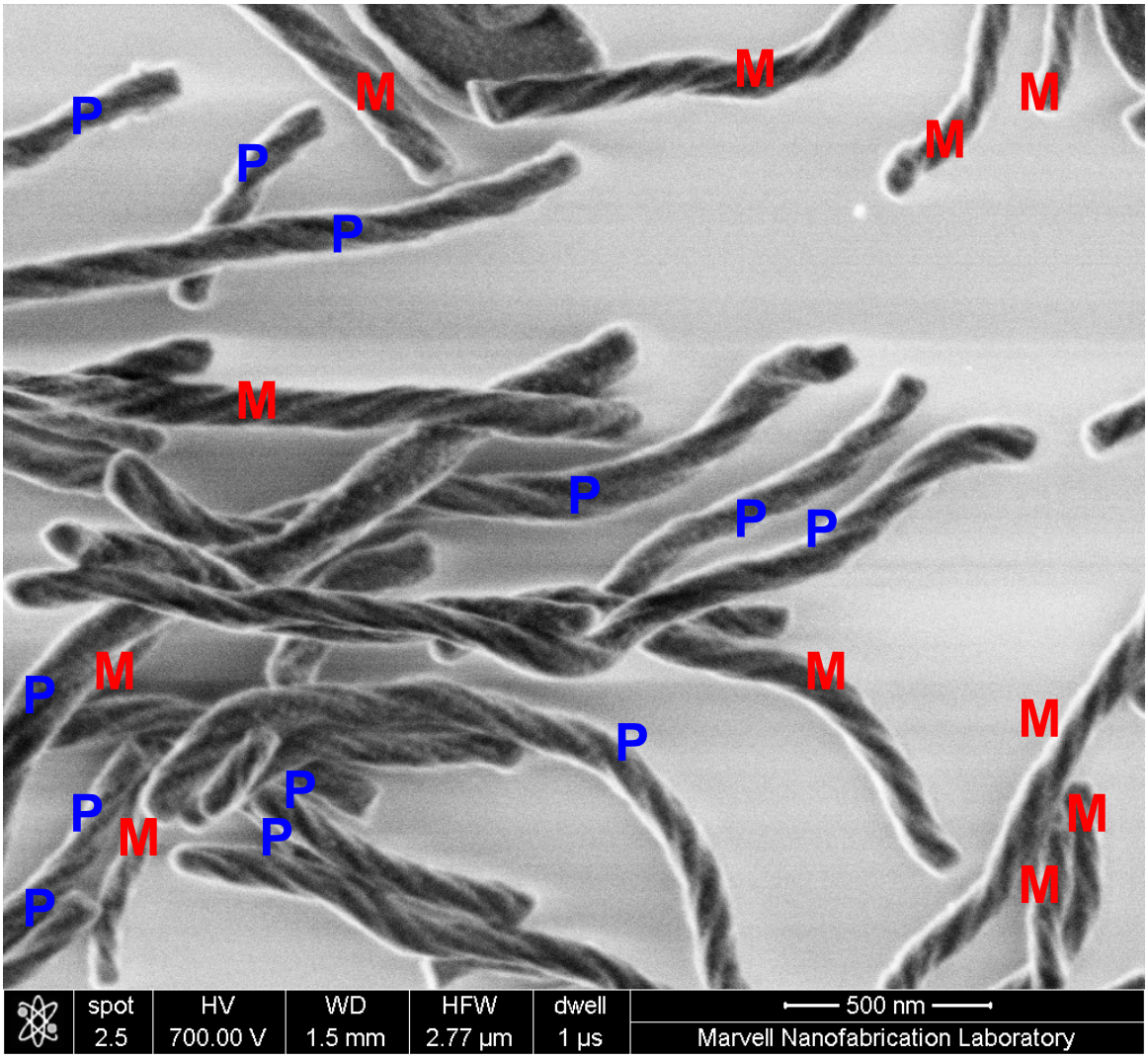
P
M
P
P
M
M
M
M
P
P
P
M
M
P
M
P
P
M
P
P
M
M
M
spot
2.5
HV
700.00 V
WD
1.5 mm
HFW
2.77 µm
dwell
1 µs
500 nm
Marvell Nanofabrication Laboratory

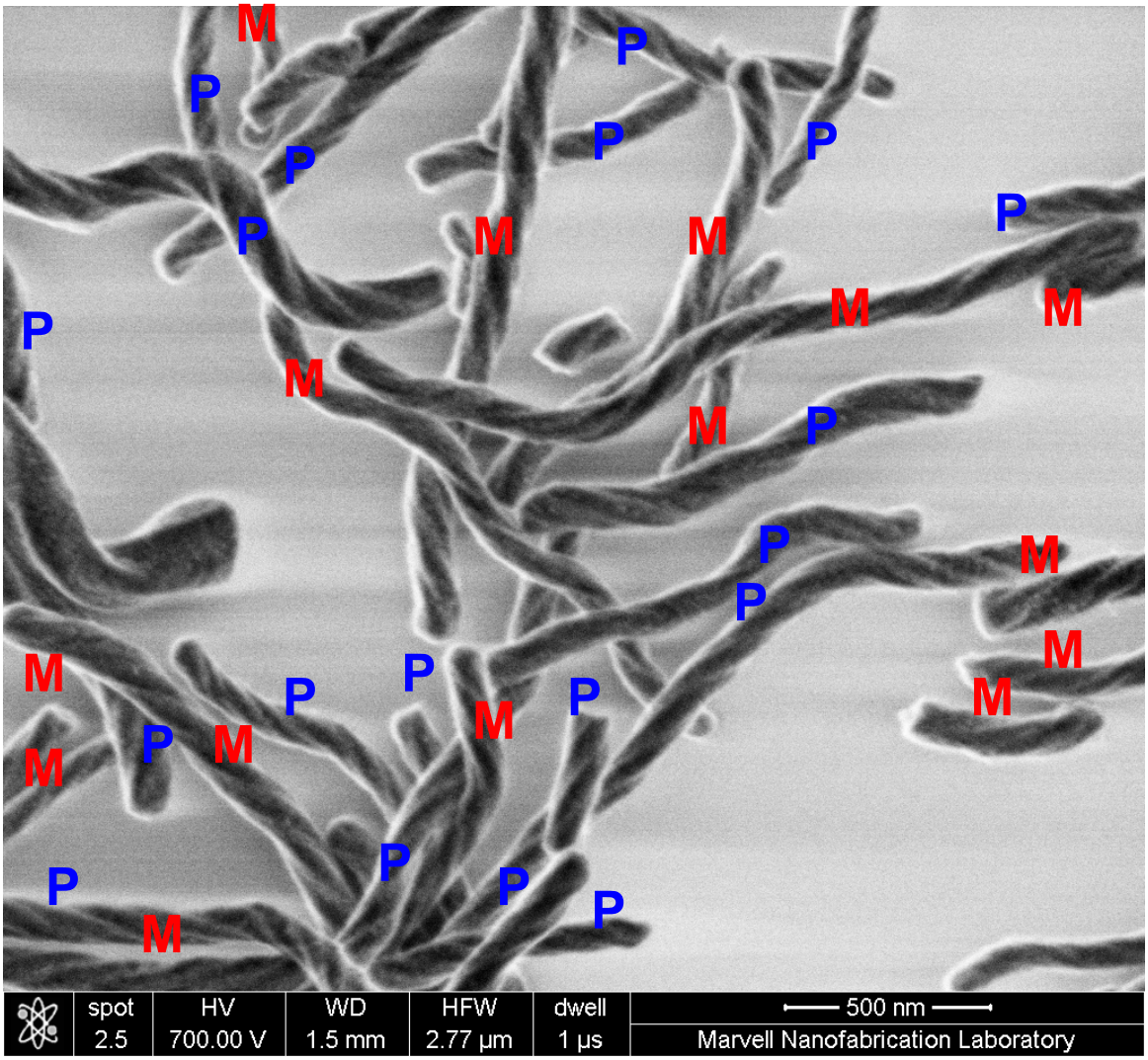
M
P
P
P
P
P
M
M
P
P
M
M
M
P
M
P
P
M
P
P
M
M
M
P
P
M
M
P
M
P
P
P
M
spot
2.5
HV
700.00 V
WD
1.5 mm
HFW
2.77 µm
dwell
1 µs
500 nm
Marvell Nanofabrication Laboratory

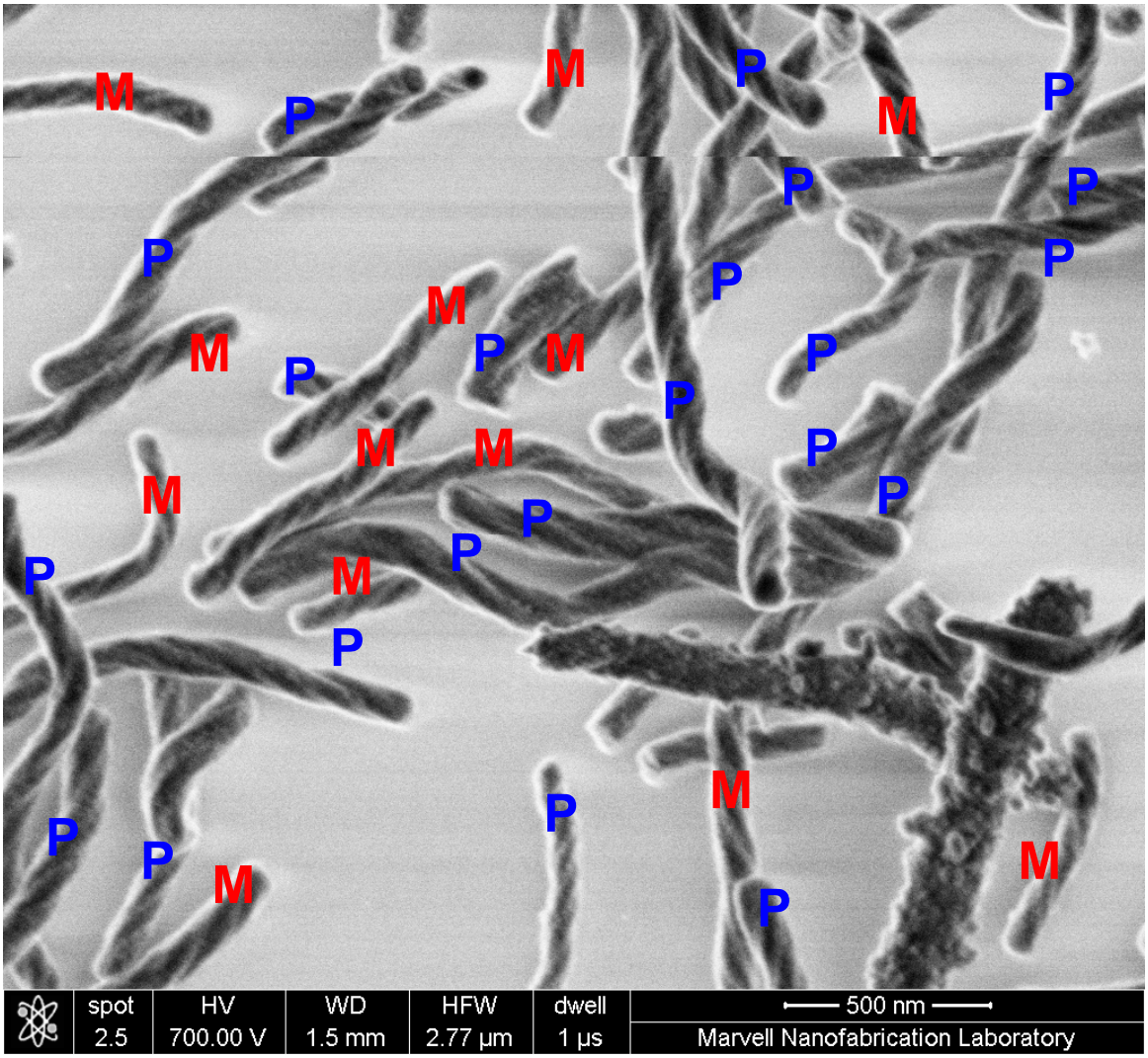
M
P
M
P
M
P
P
P
P
P
P
M
M
P
M
P
M
P
P
M
M
P
P
P
P
M
P
P
P
M
P
M
P
P
M
spot
2.5
HV
700.00 V
WD
1.5 mm
HFW
2.77 µm
dwell
1 µs
500 nm
Marvell Nanofabrication Laboratory

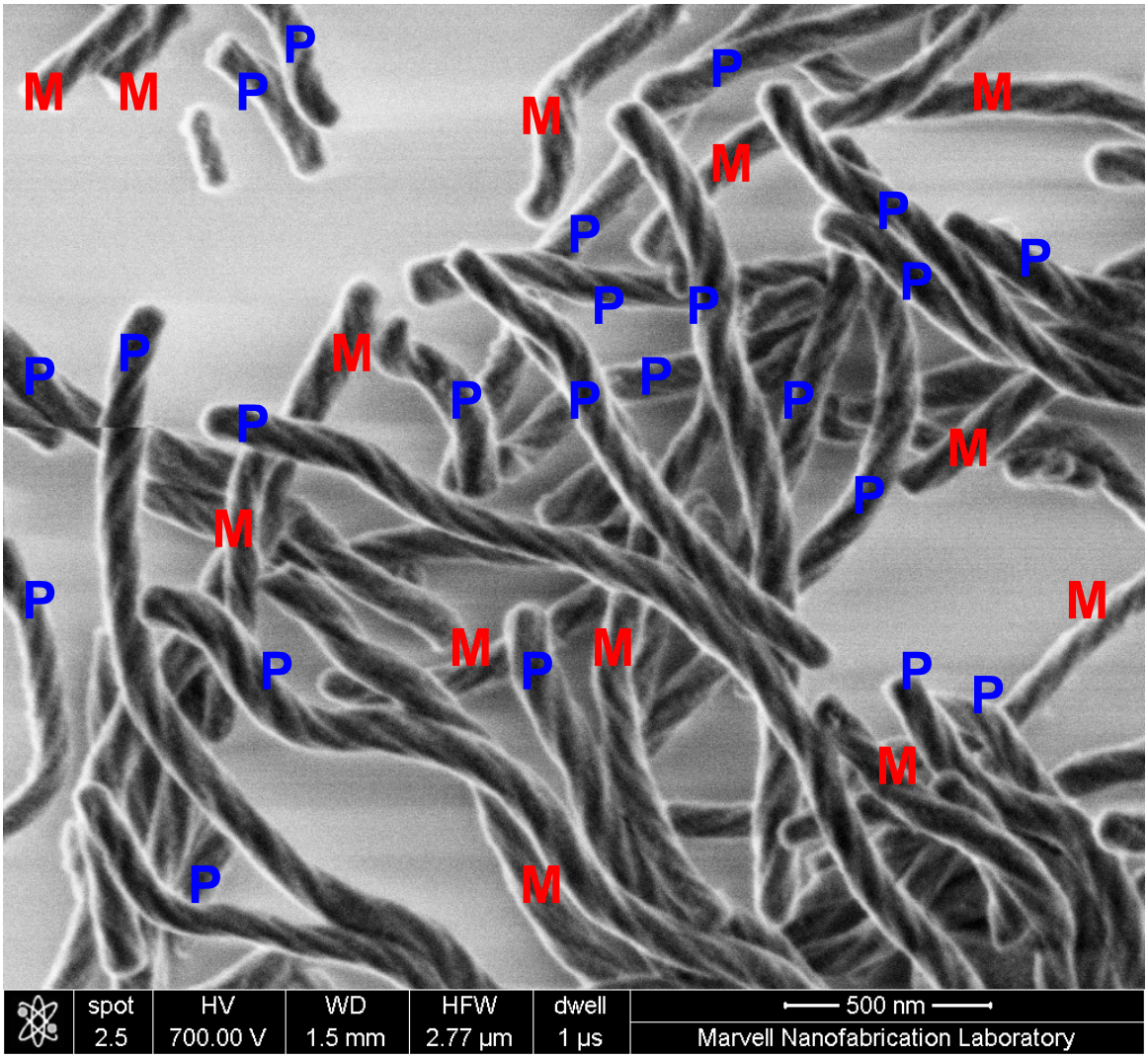
M
M
P
P
M
P
M
M
P
P
P
P
P
P
M
P
P
P
P
P
P
M
M
P
M
P
M
P
M
P
P
M
P
M
spot
2.5
HV
700.00 V
WD
1.5 mm
HFW
2.77 µm
dwell
1 µs
500 nm
Marvell Nanofabrication Laboratory

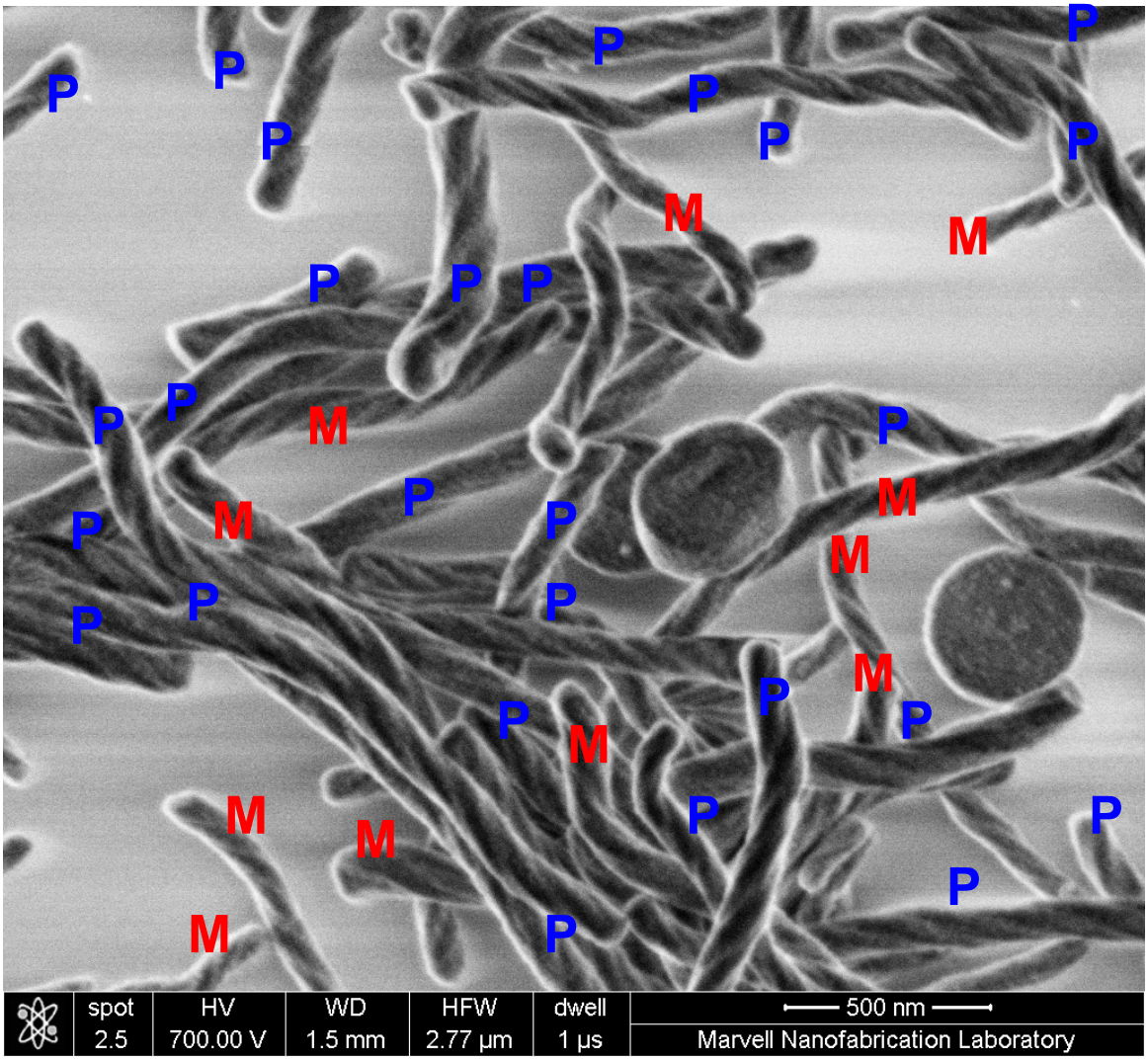
P
M
spot
2.5
HV
700.00 V
WD
1.5 mm
HFW
2.77 µm
dwell
1 µs
500 nm
Marvell Nanofabrication Laboratory

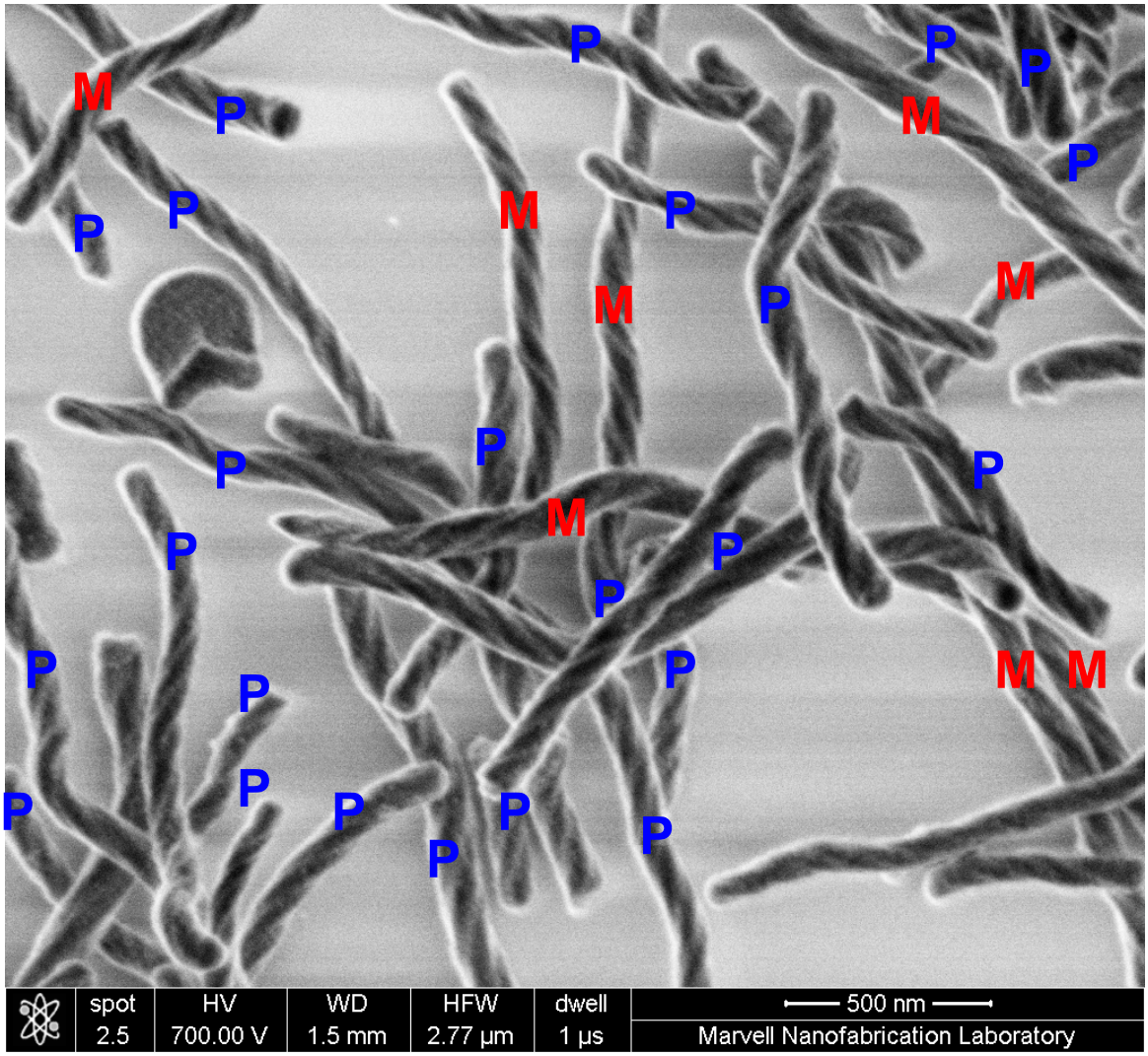
P
P
P
P
P
M
P
M
P
P
M
P
M
P
M
P
P
P
M
P
P
P
P
P
P
P
P
P
P
M
M
spot
2.5
HV
700.00 V
WD
1.5 mm
HFW
2.77 µm
dwell
1 µs
500 nm
Marvell Nanofabrication Laboratory

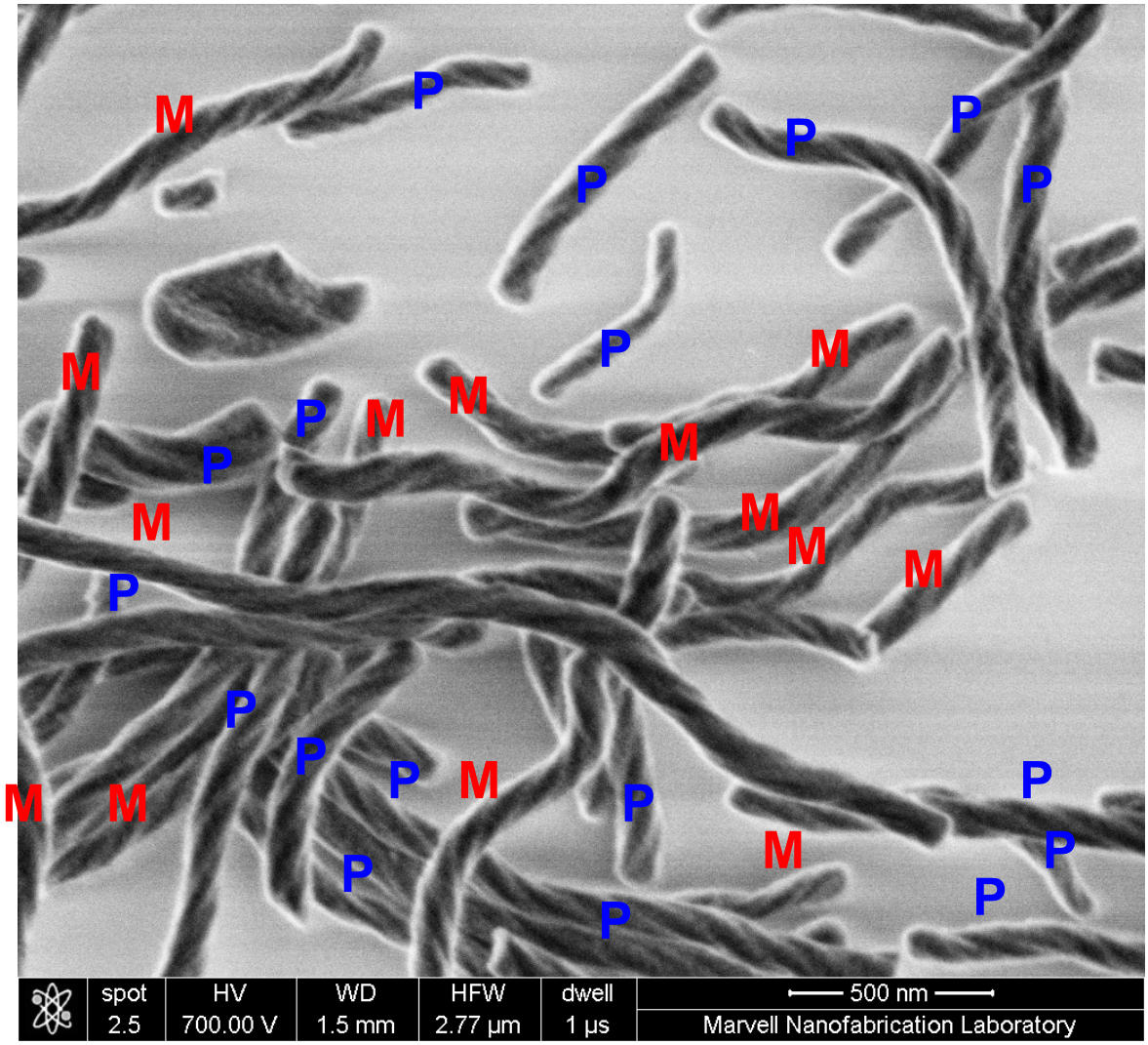
M
P
P
P
P
P
P
M
M
M
P
M
M
P
P
M
M
M
M
P
P
P
P
M
M
P
M
P
P
M
P
P
P
spot
2.5
HV
700.00 V
WD
1.5 mm
HFW
2.77 µm
dwell
1 µs
500 nm
Marvell Nanofabrication Laboratory

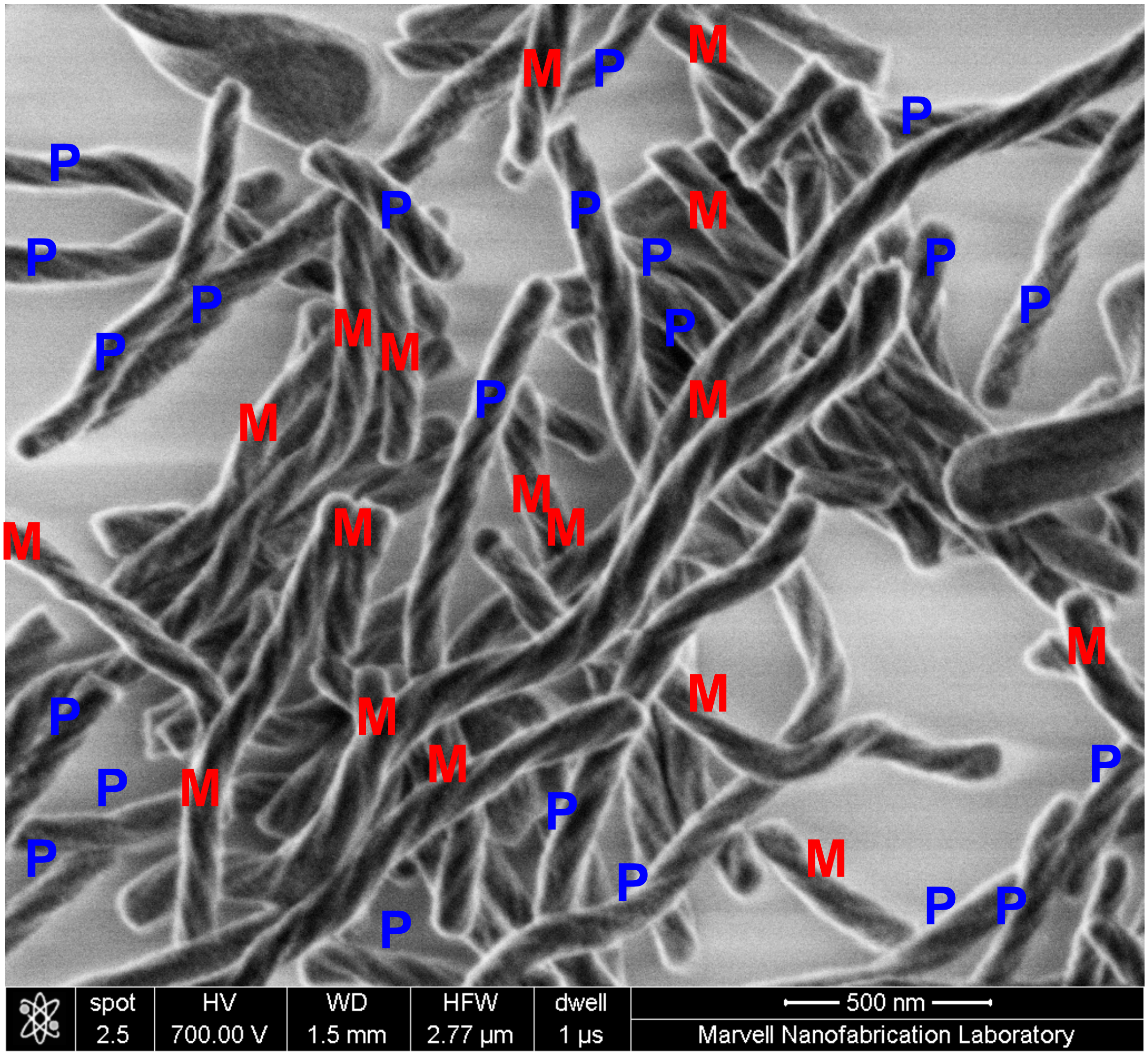
spot
2.5
HV
700.00 V
WD
1.5 mm
HFW
2.77 µm
dwell
1 µs
500 nm
Marvell Nanofabrication Laboratory

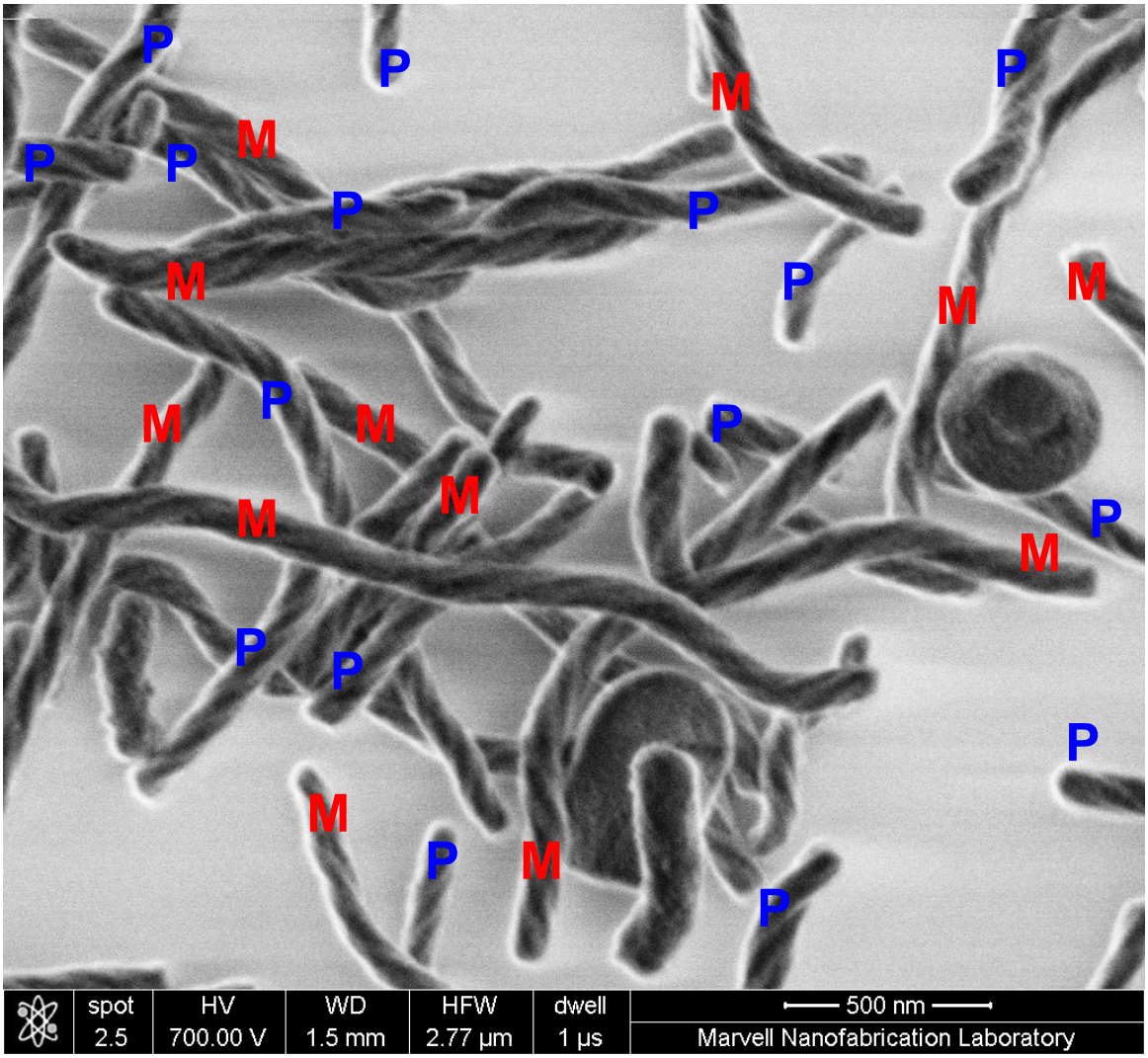
P
P
M
P
P
M
P
P
P
M
P
M
M
P
M
M
P
M
M
P
P
M
P
P
M
P
P
M
P
spot
2.5
HV
700.00 V
WD
1.5 mm
HFW
2.77 µm
dwell
1 µs
500 nm
Marvell Nanofabrication Laboratory

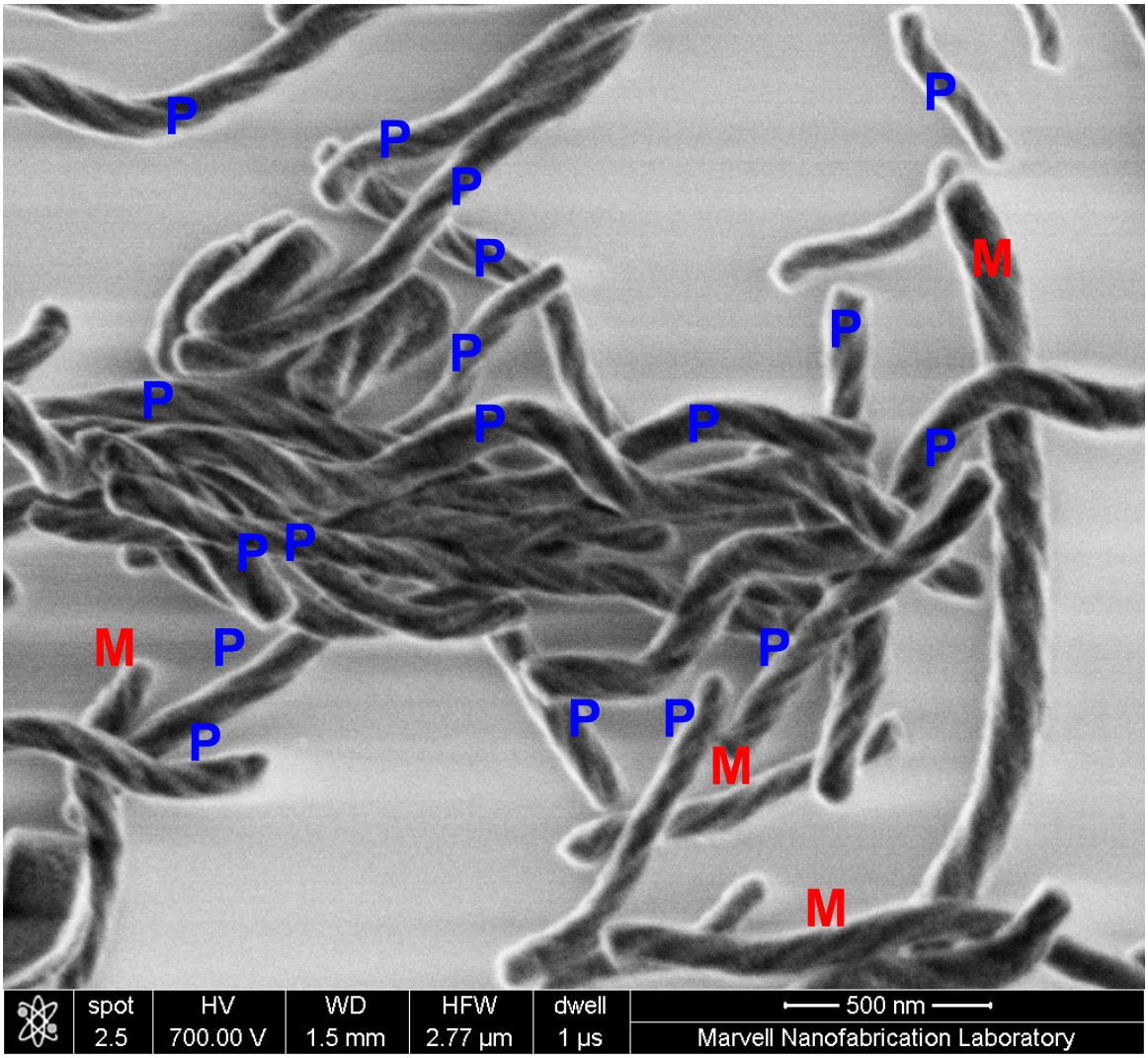
P
P
P
P
P
P
P
P
P
P
P
P
P
P
P
P
P
P
M
M
M
spot
2.5
HV
700.00 V
WD
1.5 mm
HFW
2.77 µm
dwell
1 µs
500 nm
Marvell Nanofabrication Laboratory

1.4.5 Single Crystal X-ray Diffraction Data for MOF-520-BPCA

Table S1. Crystal data, data collection, and structure refinement parameters for **MOF-510-BPCA**.

Name	**MOF-520-BPCA**
Chemical composition	$C_{34.43}H_{20.46}Al_2O_{10}$ [+ solvent]
Formula mass	648.13
Crystal system	Tetragonal
Space group	$P4_22_12$
a, Å	18.865(2)
V, Å^3	36.859(5)
d, g cm^{-3}	0.656
μ, mm^{-1}	0.646
Z	8
Measured reflections	34667
Independent reflections	6867
Observed reflections	4854
θ_{min} , º	2.397
θ_{max} , º	50.427
h	-18 to 18
k	-18 to 8
l	-33 to 36
R int	0.0819
R [$F^2>2\sigma(F^2)$]	0.0486

$wR(F^2)$	0.1184
S	0.970
Parameters	447
Restraints	107
$\Delta\rho_{max}$, e Å^{-3}	0.178
$\Delta\rho_{min}$, e Å^{-3}	-0.203
Crystal size, μm^3	80 x 80 x 80
Radiation, Å	CuKa
Temperature, K	100

Table S2. Atomic coordinates of **MOF-520-BPCA**.

Al1	0.66391(9)	0.33609(9)	0
Al2	0.63064(9)	0.40429(9)	0.08127(4)
Al3	0.5	0.5	0.11528(5)
O1AA	0.56678(18)	0.47780(16)	0.08075(8)
H1AA	0.568424	0.507375	0.060576
O0AA	0.60591(17)	0.37387(16)	0.03551(7)
H0AA	0.558209	0.378053	0.0295
O1	0.6952(2)	0.3297(2)	0.08518(9)
O2	0.6998(2)	0.26914(19)	0.03321(9)
C10	0.7065(3)	0.2063(3)	0.08863(14)
C12	0.5395(4)	-0.2837(4)	0.12528(15)
C13	0.7027(4)	0.2101(3)	0.12626(14)
H13	0.701207	0.253728	0.137955

C14	0.5009(5)	-0.3478(3)	0.11393(13)
C15	0.8727(4)	-0.0450(3)	0.34466(16)
C16	0.7018(4)	0.0821(3)	0.12951(15)
C17	0.7101(4)	0.1406(4)	0.07127(16)
H17	0.713833	0.138082	0.046141
C18	0.7011(4)	0.1481(4)	0.14584(15)
H18	0.699554	0.15059	0.171026
C19	0.7309(4)	-0.0457(4)	0.20628(17)
C20	0.7007(3)	0.2739(3)	0.06766(15)
C21	0.7737(5)	-0.0789(3)	0.30492(16)
H21	0.752695	-0.101248	0.324656
C22	0.8375(4)	-0.0464(3)	0.30958(16)
C23	0.5121(4)	-0.2163(4)	0.12129(14)
H23	0.467652	-0.210433	0.110815
C24	0.7696(5)	-0.0465(4)	0.24237(17)
C25	0.6984(5)	0.0190(4)	0.15220(17)
C26	0.6058(4)	-0.2924(3)	0.14125(17)
H26	0.624461	-0.33766	0.144261
C27	0.6591(5)	-0.0418(4)	0.14051(17)
H27	0.636817	-0.040881	0.117995
C28	0.6926(5)	-0.1040(4)	0.19465(18)
H28	0.69288	-0.145115	0.20859
C30	0.8672(4)	-0.0128(4)	0.27963(16)
H30	0.909823	0.011587	0.281968

C31	0.6532(5)	-0.1025(4)	0.16206(17)
C32	0.7383(4)	-0.0797(4)	0.27119(18)
H32	0.694814	-0.102295	0.268629
C33	0.6438(5)	-0.2344(4)	0.15255(18)
H33	0.689128	-0.240075	0.16208
C34	0.5498(5)	-0.1571(4)	0.13267(17)
H34	0.531566	-0.112017	0.128692
C35	0.7335(4)	0.0142(4)	0.18490(16)
H35	0.760038	0.052751	0.192826
C36	0.7081(4)	0.0792(3)	0.09181(16)
H36	0.711052	0.035341	0.080337
C37	0.8339(5)	-0.0157(4)	0.24684(18)
H37	0.856104	0.004196	0.226769
C38	0.6132(5)	-0.1649(4)	0.14955(19)
O5	0.9343(3)	-0.0206(2)	0.34689(9)
O6	0.8390(2)	-0.0711(2)	0.37180(10)
O2AA	0.4377(2)	-0.34153(19)	0.10189(9)
O4	0.5326(2)	-0.4057(2)	0.11725(9)
O3AA	0.7027(2)	0.4638(2)	0.06229(11)
O4AA	0.73427(19)	0.4046(2)	0.01194(10)
C3	0.7417(4)	0.4536(4)	0.0343(2)
C4	0.8407(7)	0.4949(8)	-0.0056(3)
H4	0.818679	0.472953	-0.025133
C1	0.8082(5)	0.4951(5)	0.0283(3)

C5	0.8412(7)	0.5279(7)	0.0575(2)
H5	0.819483	0.528054	0.080175
C2AA	0.9067(7)	0.5605(6)	0.0529(4)
C0AA	0.9392(5)	0.5603(8)	0.0191(5)
C1AA	0.9062(8)	0.5275(10)	-0.0102(3)
H1AB	0.927968	0.527319	-0.032803
C7AA	0.9973(9)	0.6013(10)	0.0295(5)
C44	0.9719(8)	0.5917(10)	0.0645(6)
C3AA	1.0086(12)	0.6199(12)	0.0939(4)
H3AA	0.991577	0.613462	0.117305
C6AA	1.0708(10)	0.6577(11)	0.0881(5)
H6AA	1.095441	0.676614	0.107754
C5AA	1.0963(7)	0.6674(10)	0.0531(6)
H5AA	1.137957	0.692667	0.049267
C4AA	1.0596(10)	0.6391(11)	0.0238(4)
H4AA	1.076609	0.645568	0.000331

1.5 References

(1) Barbaro, P.; Liguori, F.; Linares, N.; Marrodan, C. M. *Eur. J. Inorg. Chem.* **2012**, 3807.

(2) Lucarelli, C.; Vaccari, A. *Green Chem.* **2011**, *13*, 1941.

(3) Yin; Liebscher, J. *Chem. Rev.* **2007**, *107*, 133.

(4) Yasukawa, T.; Miyamura, H.; Kobayashi, S. *Chem. Soc. Rev.* **2014**, *43*, 1450.

(5) Gross, E.; Liu, J. H.-C.; Alayoglu, S.; Marcus, M. a; Fakra, S. C.; Toste, F. D.; Somorjai, G. A. *J. Am. Chem. Soc.* **2013**, *135*, 3881.

(6) Hu, A.; Ngo, H. L.; Lin, W. *Angew. Chem. Int. Ed.* **2003**, *42*, 6000.

(7) Cho, S.-H.; Ma, B.; Nguyen, S. T.; Hupp, J. T.; Albrecht-Schmitt, T. E. *Chem. Commun.* **2006**, 2563.

(8) Ma, L.; Abney, C.; Lin, W. *Chem. Soc. Rev.* **2009**, *38*, 1248.

(9) Heitbaum, M.; Glorius, F.; Escher, I. *Angew. Chem. Int. Ed.* **2006**, *45*, 4732.

(10) Ajellal, N.; Carpentier, J.-F.; Guillaume, C.; Guillaume, S. M.; Helou, M.; Poirier, V.; Sarazin, Y.; Trifonov, A. *Dalton Trans.* **2010**, *39*, 8363.

(11) Roy, S.; Pericàs, M. A. *Org. Biomol. Chem.* **2009**, *7*, 2669.

(12) Mallat, T.; Orglmeister, E.; Baiker, A. *Chem. Rev.* **2007**, *107*, 4863.

(13) Akiyama, R.; Kobayashi, S. *Angew. Chem. Int. Ed.* **2001**, *40*, 3469.

(14) Sawai, K.; Tatumi, R.; Nakahodo, T.; Fujihara, H. *Angew. Chem. Int. Ed.* **2008**, *47*, 6917.

(15) Ranganath, K. V. S.; Kloesges, J.; Schäfer, A. H.; Glorius, F. *Angew. Chem. Int. Ed.* **2010**, *49*, 7786.

(16) Yasukawa, T.; Miyamura, H.; Kobayashi, S. *J. Am. Chem. Soc.* **2012**, *134*, 16963.

(17) Morris, R. E.; Bu, X. *Nat. Chem.* **2010**, *2*, 353.

(18) Lin, Z.; Slawin, A. M. Z.; Morris, R. E. *J. Am. Chem. Soc.* **2007**, *129*, 4880.

(19) Zhang, J.; Chen, S.; Wu, T.; Feng, P.; Bu, X. *J. Am. Chem. Soc.* **2008**, *130*, 12882.

(20) Zhang, J.; Chen, S.; Nieto, R. A.; Wu, T.; Feng, P.; Bu, X. *Angew. Chem. Int. Ed.* **2010**, *49*, 1267.

(21) Zhang, J.; Chen, S.; Bu, X. *Angew. Chem. Int. Ed.* **2009**, *48*, 6049.

(22) Qiu, H.; Che, S. *Chem. Soc. Rev.* **2011**, *40*, 1259.

(23) Che, S.; Liu, Z.; Ohsuna, T.; Sakamoto, K.; Terasaki, O.; Tatsumi, T. *Nature* **2004**, *429*, 281.

(24) Switzer, J. A.; Kothari, H. M.; Poizot, P.; Nakanishi, S.; Bohannan, E. W. *Nature* **2003**, *425*, 490.

(25) Bohannan, E. W.; Kothari, H. M.; Nicic, I. M.; Switzer, J. A. *J. Am. Chem. Soc.* **2004**, *126*, 488.

(26) Han, X.; Zhang, J.; Huang, J.; Wu, X.; Yuan, D.; Liu, Y.; Cui, Y. *Nat. Commun.* **2018**, *9*, 1294.

(27) Qiu, H.; Wang, S.; Zhang, W.; Sakamoto, K.; Terasaki, O.; Inoue, Y.; Che, S. *J. Phys. Chem. C* **2008**, *112*, 1871.

(28) Lee, S.; Kapustin, E. A.; Yaghi, O. M. *Science* **2016**, *353*, 808.

(29) Li, G.; Jin, R. *Acc. Chem. Res.* **2013**, *46*, 1749.

(30) Shu, X.-Z.; Nguyen, S. C.; He, Y.; Oba, F.; Zhang, Q.; Canlas, C.; Somorjai, G. A.; Alivisatos, A. P.; Toste, F. D. *J. Am. Chem. Soc.* **2015**, *137*, 7083.

(31) Kaczorowski, T.; Justyniak, I.; Lipińska, T.; Lipkowski, J.; Lewiński, J. *J. Am. Chem. Soc.* **2009**, *131*, 5393.

(32) Wu, C.-Y.; Horibe, T.; Jacobsen, C. B.; Toste, F. D. *Nature* **2014**, *517*, 449.

(33) Takehara, M.; Yoshimura, I.; Takizawa, K.; Yoshida, R. *J. Am. Oil Chem. Soc.* **1972**, *49*, 157.

(34) Lindholm, A.; Maki-Arvela, P.; Toukoniitty, E.; Pakkanen, T. A.; Hirvi, J. T.; Salmi, T.; Murzin, D. Y.; Sjoholm, R.; Leino, R. *J. Chem. Soc. Trans. 1* **2002**, 2605.

(35) Ganapati Reddy, P.; Kishore Kumar, G. .; Baskaran, S. *Tetrahedron Lett.* **2000**, *41*, 9149.

(36) Baker, W.; Barton, J. W.; McOmie, J. F. W. *J. Chem. Soc.* **1958**, 2666.

(37) Baker, M. V; Barnard, P. J.; Berners-price, S. J.; Brayshaw, S. K.; Hickey, J. L.; Skelton, B. W.; White, A. H. *J. Organomet. Chem.* **2005**, *690*, 5625.

(38) Michalska, M.; Grela, K. *Synlett* **2015**, *27*, 599.

(39) Zhang, B.; Li, H.; Ding, Y.; Yan, Y.; An, J. *J. Org. Chem.* **2018**, *83*, 6006.

(40) Hornung, C. H.; Hallmark, B.; Mackley, M. R.; Baxendale, I. R.; Ley, S. V. *Adv. Synth. Catal.* **2010**, *352*, 1736.

Chapter 2

Suppression of a Unimolecular Decomposition Pathway by Architectural Stabilization of a Gold(III) Catalyst in Metal-Organic Frameworks

2.1 Introduction

In mechanochemistry, tensile forces have traditionally been utilized to promote various bond cleavage events,[1–3] which can enable productive chemistry through ring opening,[4–6] rearrangement,[7] and catalyst activation.[8,9] More recently, this strategy has been applied towards preserving chemical bonds by suppressing an undesired unimolecular decomposition pathway – a retro-Michael pathway of a maleimide-thiol adduct (Scheme 1a).[10] Despite these advances in mechanochemistry, the static force provided by rigid materials has, to the best of our knowledge, previously not been utilized towards the stabilization of ligand geometry. In cases where reductive elimination is problematic in transition-metal catalysis,[11–13] rigidification of ligands could potentially suppress such unimolecular decomposition pathways [for examples of suppressed bimolecular decomposition pathways with solid supports see ref. 14–16].

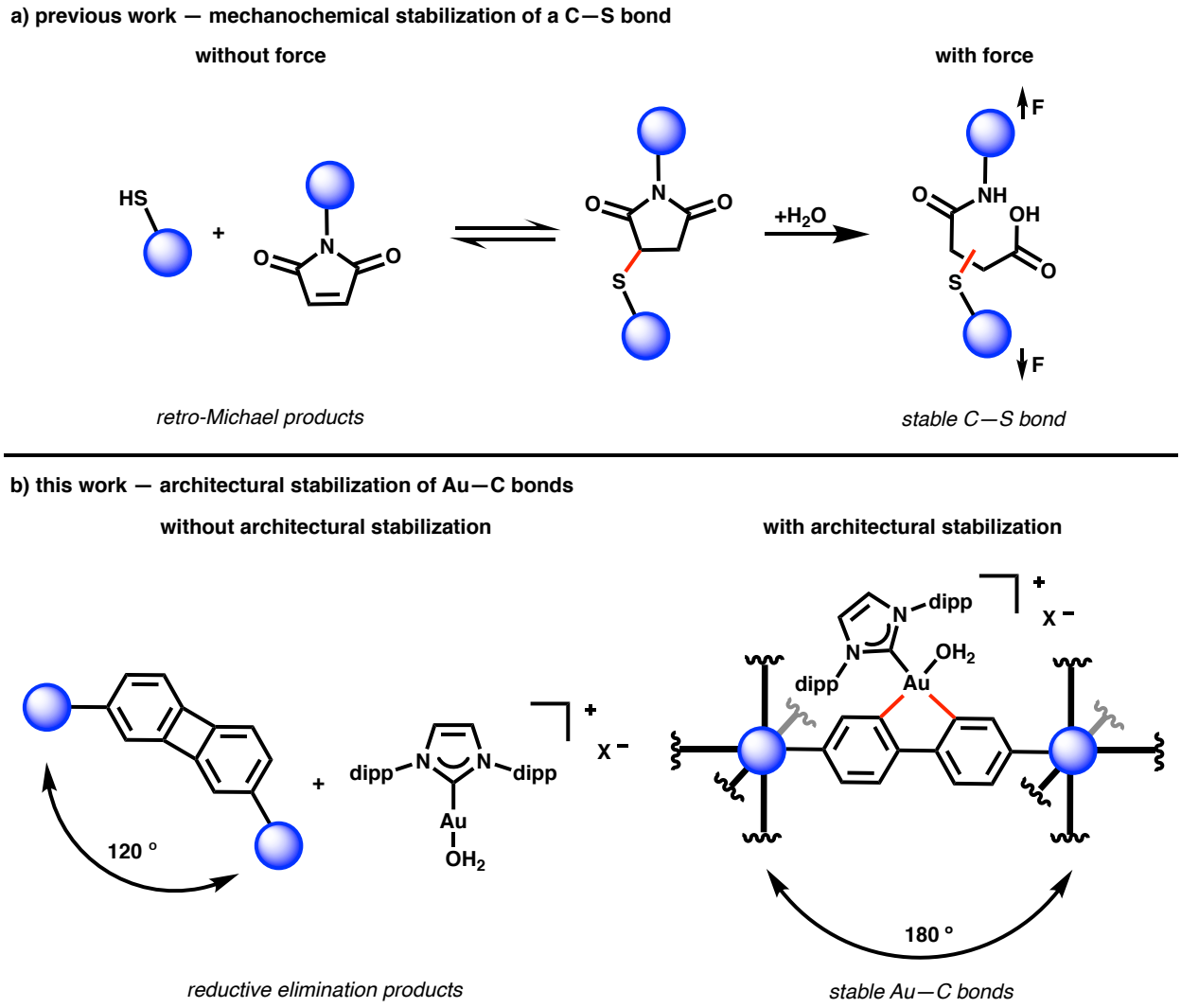

Scheme 2.1. Mechanochemical and architectural stabilization of chemical bonds.

As a model system, we were interested in leveraging architectural stabilization to prevent a unimolecular decomposition pathway of IPrAu(III)(biphenyl)X (where IPr is [1,3-bis(2,6-

diisopropylphenyl)imidazole-2-ylidene] and X is a non-coordinating counteranion), which is known to undergo reductive elimination to yield biphenylene and IPrAu(I)X (Scheme 1b).[13] We reasoned that a bifunctionalized IPrAu(III)(biphenyl)X catalyst might be incorporated into a robust porous material to architecturally lock the geometry of the catalyst. Contrary to common solid-state supports, metal-organic frameworks (MOFs) allow for the precise placement of molecules in a well-ordered fashion[17–19] [for reviews on MOFs as catalysts see ref. 20–23], which can constrain the geometry of incorporated guests within the framework. In this chapter, studies establishing that a unimolecular decomposition pathway of IPrAu(III)(biphenyl)X catalyst is prohibited due to architectural stabilization in MOFs by preserving the geometry of the gold(III) complex such that the linear geometry of the biphenyl ligand is maintained (Scheme 1b). Deviation of its linear geometry is architecturally forbidden because reductive elimination in a rigid MOF would either necessitate the formation of a defect site or result in strain throughout the material. In particular, two strategies are described for introducing a gold(III) catalyst into MOFs with two distinct biphenyldicarboxylate (BPDC) binding modes, which resulted in no observation of the reductive elimination products in contrast to its homogeneous analogues.

2.2 Results and Discussion

2.2.1 Efforts Towards the Incorporation of Gold(III) Linkers into MOF-520

MOF-520 was an attractive material for our efforts to incorporate a biphenyl-based gold(III) catalyst because this material is known to accommodate 4,4'-biphenyldicarboxylate (BPDC) *via* incorporation to yield a bridging guest.[18] Additionally, the low symmetry of MOF-520 would enable facile structural characterization of incorporated catalysts by single crystal X-ray diffraction (SXRD).

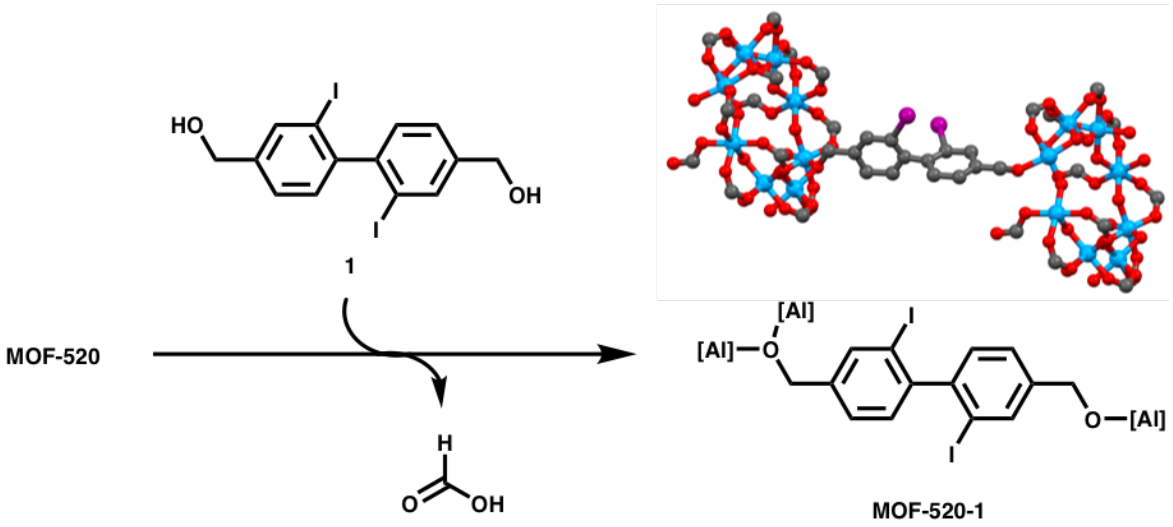

Scheme 2.2. Incorporation of **1** into MOF-520.

In addition to BPDC, we hypothesized that MOF-520 would also be able to accommodate a diol analogue of BPDC, **1**. Subjection of a **1** to MOF-520 under incorporation conditions[17]

yielded the incorporated dialkoxide in MOF-520, which was characterized *via* SXRD (Scheme 2.2). From the crystal structure, we were able to observe incorporation of both alcohol groups on the guest, yielding a rigidified biphenyl moiety, which could be amenable for the suppression of reductive elimination when ligated to a transition-metal complex.

Knowing that both diols and dicarboxylic acids would be suitable bridging guests for MOF-520, we targeted the synthesis of both diol- and dicarboxylic acid-based gold(III) complexes (Scheme 2.3). Dimethyl biphenyl-4,4'-dicarboxylate was iodinated to the corresponding diiodide according to a reported procedure.[24] Due to the intolerance of ester groups under lithium-halogen exchange conditions, the diester was reduced to the corresponding diol followed by TBS protection. Lithium-halogen exchange with the corresponding diiodide, followed by nBu_2SnCl_2 afforded the corresponding stannane. Transmetallation of the stannane with (THT)AuCl followed by addition of NHC or (NHC)AgCl yielded the corresponding gold(III) complex. TBS deprotection of the gold(III) complex yielded the targeted diol based gold(III) linkers **2** and **3**. MnO_2 oxidation followed by a Pinnick oxidation furnished the targeted dicarboxylic acid based gold(III) linkers **4** and **5**.

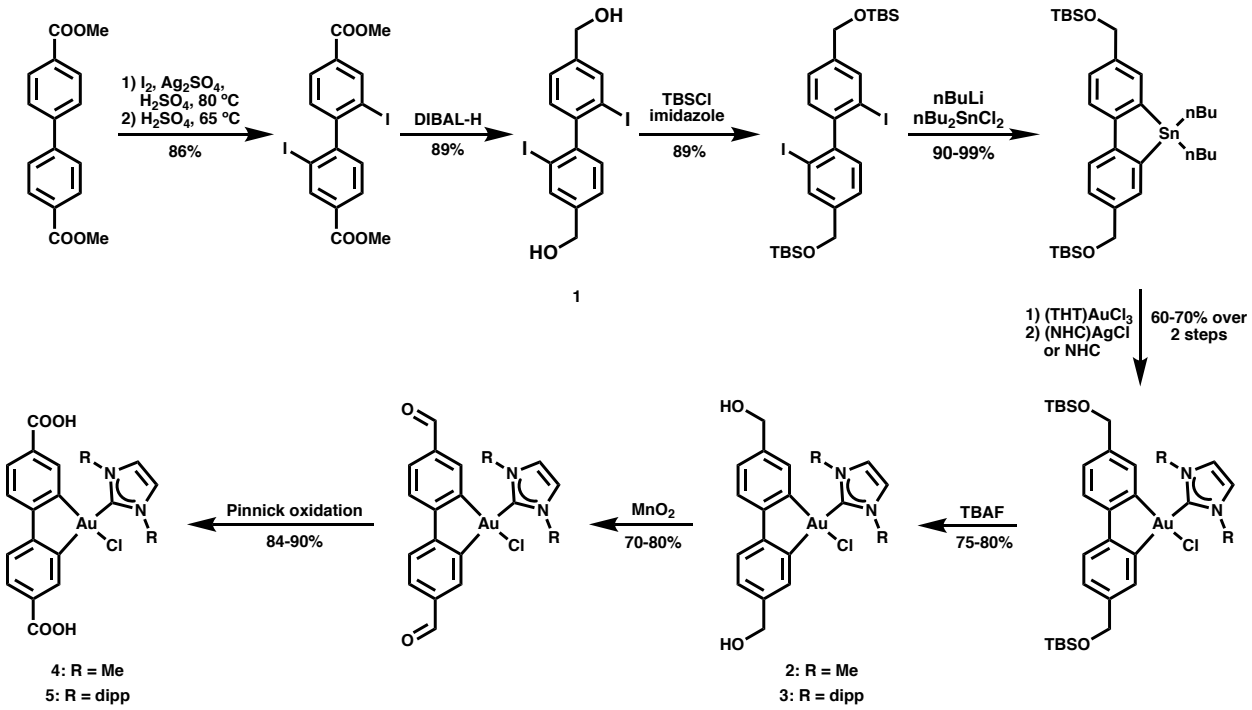

Scheme 2.3. Synthesis of gold(III) linkers.

The prepared gold(III) linkers were then subjected to incorporation conditions with MOF-520 (Table 2.1). Diol-based gold(III) linker **2** incorporated into MOF-520; however, only one of the alcohol groups incorporated into the structure, yielding a dangling guest in MOF-520, which was not amenable for architectural stabilization of the corresponding cationic complex. Diol based gold(III) linker **3** did not incorporate into MOF-520, which might be attributed to the steric bulk of the IPr ligand. Both dicarboxylic acid-based gold(III) linkers **4** and **5** resulted in the incorporation of BPDC without gold; however, no decomposition of the gold(III) complexes were detected in the supernatant by ^{1}H nuclear magnetic resonance (NMR) spectroscopy. These

data suggested two possibilities: (1) minor formation of H_2BPDC as a result of protodeauration, where H_2BPDC outcompetes the gold(III) linkers for incorporation or (2) incorporation of the gold(III) linker followed by protodeauration. Due to the incompatibility of the MOF-520 incorporation conditions with the gold(III) linkers, an alternate strategy was pursued.

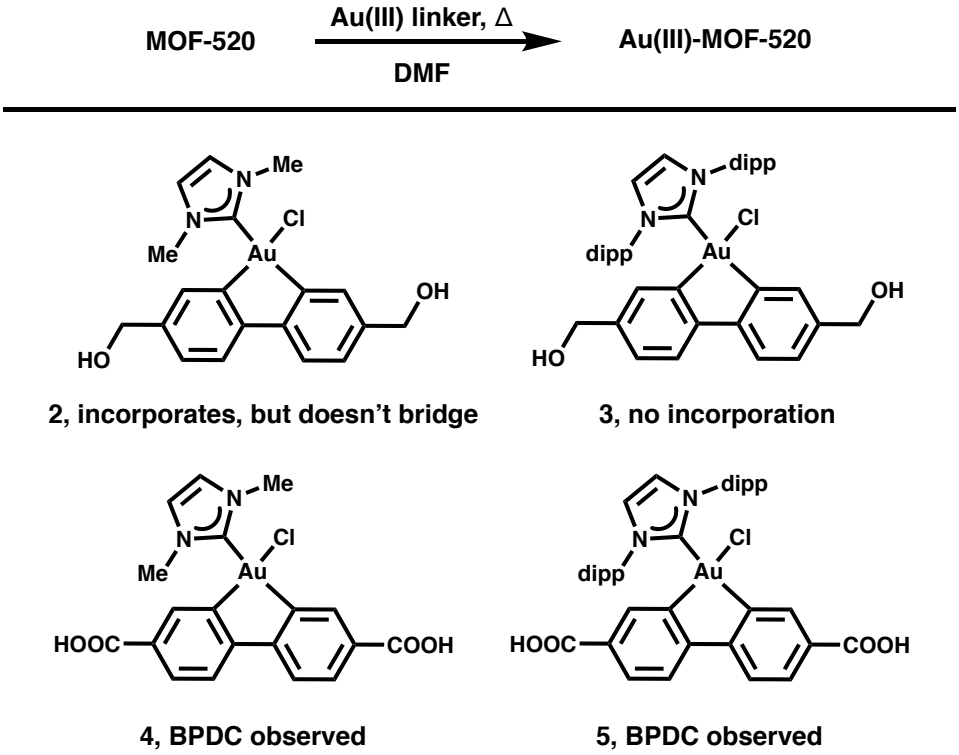

Table 2.1. Attempted gold(III) linker incorporation into MOF-520.

2.2.2 Synthesis and Reactivity of a Gold(III) Catalyst in UiO-67

UiO-67 was chosen as an ideal support for introducing gold(III) linkers for catalysis as several groups have reported the robustness of biphenyl and bipyridine based catalysts incorporated in UiO-67, which were prepared by mixed linker synthesis or solvent assisted linker exchange.[16,25–28] In particular, Yaghi and coworkers have prepared large single crystals of Re catalyst-incorporated UiO-67 *via* a mixed linker synthesis and obtain a crystal structure of their incorporated catalyst.[16] Thus, we hypothesized that UiO-67 would be a suitable platform for the incorporation of our dicarboxylic acid-based Au(III) linkers and characterization of the precatalyst and catalyst by SXRD analysis.

Due to anticipated issues with steric bulk, we began our efforts with gold(III) linker **4** to determine the feasibility of introducing a dicarboxylic acid-based gold(III) complex into a MOF *via* a mixed linker synthesis strategy. Through a mixed linker synthesis strategy, we were able to obtain Me_2ImAu(III)Cl-UiO-67 crystals with gold occupancy ranging from 10 to 100% (Figure 2.1). Synthesis of Me_2ImAu(III)Cl-UiO-67 with 20% gold occupancy yielded the largest crystals that were suitable for SXRD analysis, by which the gold atom and chloride ligand could be assigned in the structure (Scheme 2.4, bottom left). Upon subjection of Me_2ImAu(III)Cl-UiO-67

to $AgSbF_6$, the electron density of the chloride ligand in the precatalyst structure was no longer observed by SXRD analysis, which was attributed to chloride abstraction by the silver salt to yield the corresponding active catalyst in the MOF, $Me_2ImAu(III)SbF_6$-UiO-67 (Scheme 2.4, bottom right).

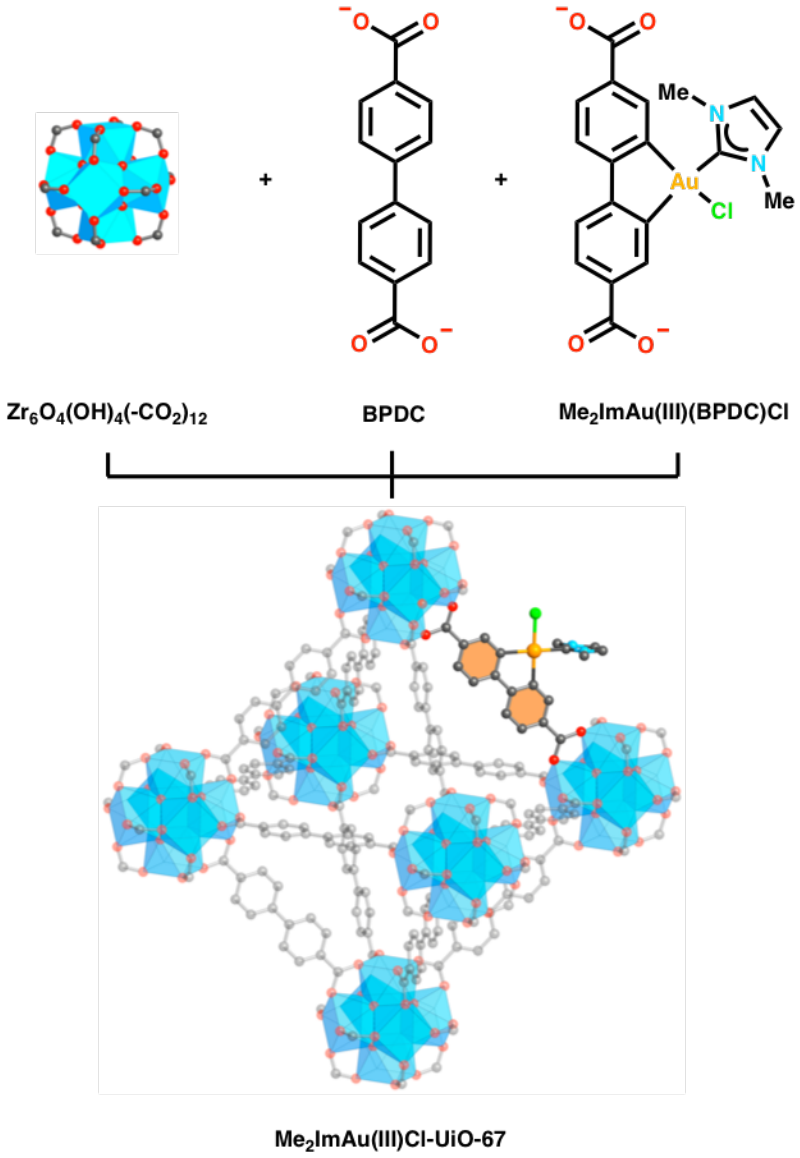

Figure 2.1. Structure of $Me_2ImAu(III)Cl$-UiO-67 obtained from SXRD and subsequent modeling.

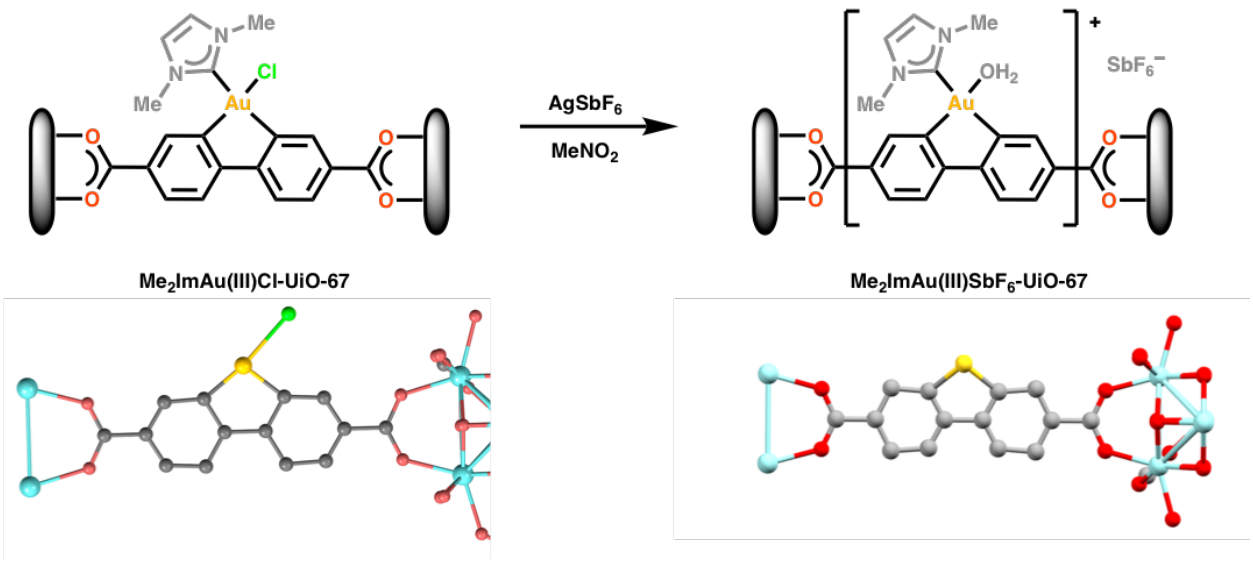

Scheme 2.4. Activation of a gold(III) precatalyst in UiO-67.

After activation of the gold(III) precatalyst in UiO-67, the reactivity of the catalyst was evaluated as further evidence of chloride abstraction. $Me_2ImAu(III)SbF_6$-UiO-67 was reactive towards gold-catalyzed cycloisomerization of 1,5-enyne substrate **6** to yield the corresponding bicyclohexene product **7** (Table 2.2, entry 1). In contrast, addition of substrate **6** to $Me_2ImAu(III)Cl$-UiO-67 without $AgSbF_6$ treatment, under otherwise equivalent conditions, resulted in no background reactivity (entry 2). Additionally, subjection of pristine UiO-67, with or without $AgSbF_6$ treatment, to substrate **6** did not yield any product, which supports the assumption that the Zr-based secondary building units (SBUs) and silver salt are not responsible for the reactivity observed with $Me_2ImAu(III)SbF_6$-UiO-67 (entries 3 and 4).

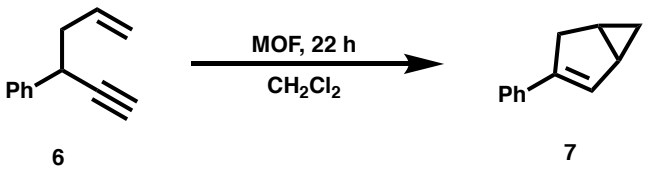

6 **7**

entry	MOF	conversion (%)
1	$Me_2ImAu(III)SbF_6$-UiO-67 (1 mol% Au)	47
2	$Me_2ImAu(III)Cl$-UiO-67 (1 mol% Au)	<1
3	UiO-67-$AgSbF_6$	<1
4	UiO-67	<1

Table 2.2. Control experiments with UiO-67.

After running the appropriate control experiments, silver salts were screened for a gold-catalyzed 1,5-enye cycloisomerization (Table 2.3). Higher reactivity was observed with less coordinating counteranions (entries 1 and 2) when compared to more coordinating counteranions (entries 3 and 4).

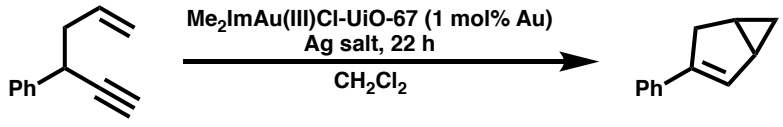

6 7

entry	Ag salt	conversion (%)
1	$AgSbF_6$	47
2	$AgNTf_2$	57
3	AgOTf	19
4	$AgBF_4$	<1

Table 2.3. Silver salt screen with Me_2ImAu(III)Cl-UiO-67.

After screening silver salts, a few solvents were screened under otherwise equivalent conditions with Me_2ImAu(III)SbF_6-UiO-67 as catalyst (Table 2.4). Similar to the trends observed with counteranions, higher reactivity was observed with less coordinating solvents (entries 1 and 2) when compared to more coordinating solvents (entries 4 and 5).

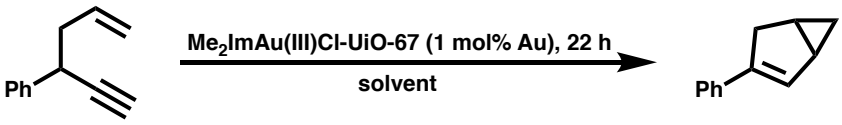

6 7

entry	solvent	conversion (%)
1	CH_2Cl_2	47
2	toluene	33
3	$MeNO_2$	13
4	THF	<1
5	MeCN	<1

Table 2.4. Solvent screen with Me_2ImAu(III)SbF_6-UiO-67.

With the data obtained with Me_2ImAu(III)Cl-UiO-67, we determined that it was feasible to introduce BPDC-based gold(III) linkers into MOFs by a mixed linker synthesis strategy, activate the gold(III) precatalyst incorporated into the framework with a halide abstractor, and observe gold(III)-catalyzed reactivity within the framework. However, the homogeneous gold(III) analogue of Me_2ImAu(III)SbF_6-UiO-67 decomposed *via* a bimolecular decomposition pathway – ligand exchange (Scheme 2.5). Thus we continued our efforts towards the incorporation of gold(III) linker **5** into MOFs to evaluate the feasibility of architectural stabilization of gold(III) catalysts in MOFs.

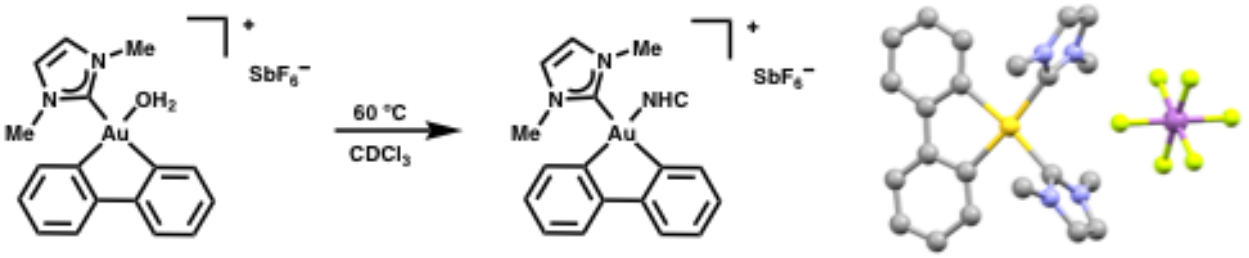

Scheme 2.5. Bimolecular decomposition pathway of $Me_2ImAu(biphenyl)SbF_6$.

Attempted mixed linker synthesis of IPrAu(III)Cl-UiO-67 with gold(III) linker **5**, however, resulted in no observed gold occupancy in the resulting UiO-67 crystals both by SXRD and digestion ^{1}H NMR analysis (Scheme 2.6). We hypothesized that gold(III) linker **5** could not be introduced into UiO-67 due to the steric clash between the bulky IPr ligand and the potentially neighboring linkers. Thus, MOFs that could mitigate this potential steric clash were pursued for the incorporation of gold(III) linker **5**.

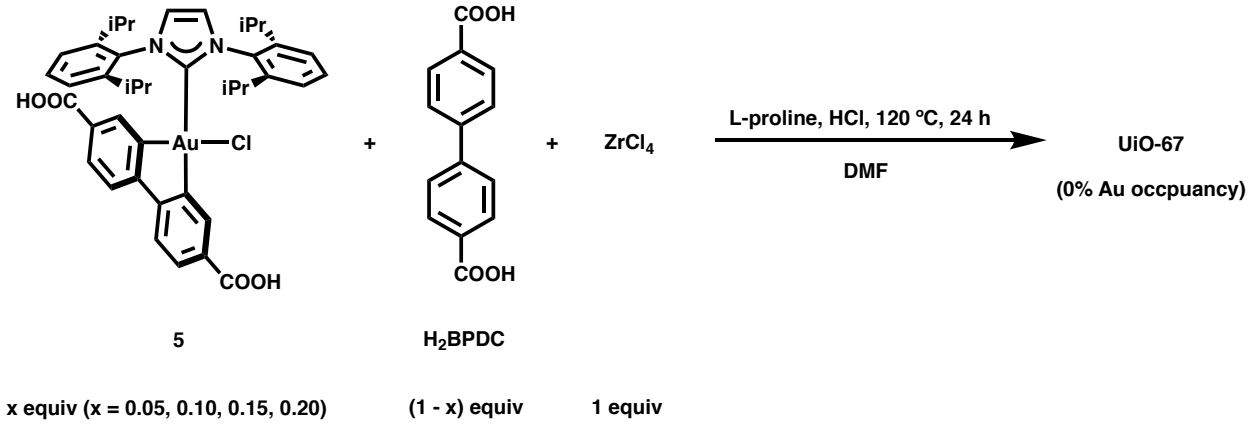

Scheme 2.6. Attempted mixed linker synthesis of IPrAu(III)Cl-UiO-67.

2.2.3 Architectural Stabilization of a Gold(III) Catalyst in IRMOF-10 and bio-MOF-100

In order to probe the architectural stabilization of a gold(III) catalyst in MOFs, we then targeted the incorporation of gold(III) linker IPrAu(III)(BPDC)Cl into IRMOF-10 and bio-MOF-100 through a mixed linker synthesis and a solvent-assisted linker exchange, respectively (see SI for details). IPrAu(III)(BPDC)Cl was encompassed into a microporous IRMOF-10 system through a mixed linker synthesis strategy with 5% occupancy of gold(III) precatalyst to yield IPrAu(III)Cl-IRMOF-10 (Figure 2.2). A partial structure of IPrAu(III)Cl-IRMOF-10 with primitive cubic (**pcu**) topology was confirmed *via* SXRD and powder X-ray diffraction (PXRD). The chemical composition of IPrAu(III)Cl-IRMOF-10 was determined by ^{1}H nuclear magnetic resonance (NMR) of digested samples with an observed IPrAu(III)(BPDC)Cl to BPDC ratio of 5:95. Mixed linker syntheses with a targeted H_2IPrAu(III)(BPDC)Cl/H_2BPDC ratio >5:95 in IRMOF-10 yielded crystals that were not suitable for SXRD characterization due to an increase

in defects, which affected the overall crystallinity; an increase in defects was attributed to steric clash in the framework between gold(III) complexes bearing bulky IPr ligands. Low gold(III) loading and high symmetry of the IRMOF-10 system precluded the possibility of obtaining a crystal structure of the precatalyst in IPrAu(III)Cl-IRMOF-10 *via* SXRD to ensure that the catalytic moiety was indeed geometrically constrained between SBUs.

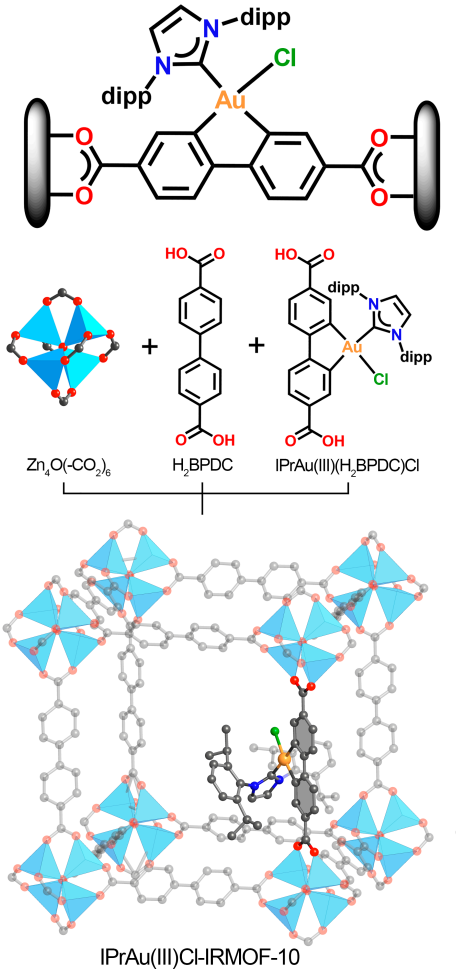

Figure 2.2. Structure of IPrAu(III)Cl-IRMOF-10 obtained from modeling.

In order to mitigate steric clash and increase the occupancy of the gold(III) species in MOFs, bio-MOF-100,[29] a mesoporous MOF featuring larger pores (~4.5 nm), was chosen as a support for SXRD characterization of the gold(III) precatalyst and catalyst. Interestingly, bio-MOF-100 features two symmetrically distinct BPDC moieties in its asymmetric unit. This feature offers the opportunity to selectively displace one type of BPDC in the framework and thus make it amenable to low guest loading with high occupancy and as a consequence, enable SXRD characterization. Additionally, bio-MOF-100 possesses a unique binding mode of BPDC to the SBU compared to that of IRMOF, which offers an alternative strategy of rigidifying the biphenyl ligand. IPrAu(III)(BPDC)Cl was incorporated into mesoporous bio-MOF-100 through a solvent-assisted linker exchange with up to 40% occupancy of gold(III) precatalyst per substitutable site to yield IPrAu(III)Cl-bio-MOF-100 (Figure 2.3), where the occupancy of gold(III) precatalyst was assigned *via* SXRD. With 40% occupancy of gold(III) precatalyst, gold,

chloride, and 7 atoms of the IPr ligand could be assigned in the IPrAu(III)Cl-bio-MOF-100 SXRD crystal structure. The chemical composition of IPrAu(III)Cl-bio-MOF-100 was further confirmed by ^{1}H NMR of digested samples.

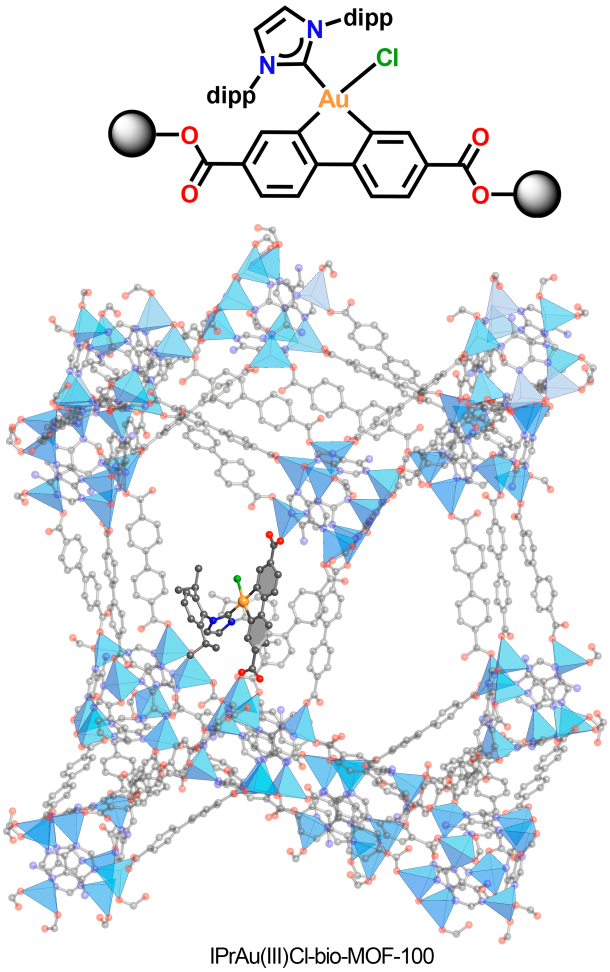

Figure 2.3. Structure of IPrAu(III)Cl-bio-MOF-100 obtained from SXRD analysis and subsequent modeling.

The catalytically active, cationic gold(III) species in the IRMOF-10 system were accessed by treatment of IPrAu(III)Cl-IRMOF-10 with 1 equivalent of $AgSbF_6$ (relative to gold) to access IPrAu(III)SbF_6-IRMOF-10, which is analogous to the conditions for activation of homogeneous complex.[30] Chloride abstraction was evidenced by the reactivity observed in the IPrAu(III)SbF_6-IRMOF-10-catalyzed cycloisomerization reaction of 1,5-enyne substrate **6** to yield the corresponding bicyclohexene product **7** (Table 2.5). In contrast, addition of substrate **6** to IPrAu(III)Cl-IRMOF-10 without $AgSbF_6$ treatment, under otherwise equivalent conditions, resulted in no background reactivity. Additionally, subjecting pristine IRMOF, with or without $AgSbF_6$ treatment, to substrate **6** did not yield any product. These observations support the conclusion that the Zn-based SBUs and Ag salt are not responsible for the reactivity observed with IPrAu(III)SbF_6-IRMOF-10.

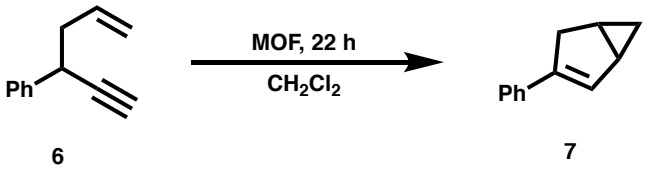

6 7

entry	MOF	conversion (%)
1	IPrAu(III)SbF_6-IRMOF-10 (3 mol% Au)	44
2	IPrAu(III)Cl-IRMOF-10 (3 mol% Au)	<1
3	IRMOF-9-$AgSbF_6$	<1
4	IRMOF-9	<1

Table 2.5. Control experiments with IRMOF.

Efforts towards accessing cationic gold(III) species in the bio-MOF-100 system through $AgSbF_6$ treatment resulted in a decrease in crystallinity. We posited that this MOF degradation might be attributed to protonation of the BPDC linkers by $HSbF_6$ generated from the hydrolysis of $AgSbF_6$ in the presence of adventitious water. Addition of $NaBAr^F{}_4$, a common halide-abstracting agent that is less prone to hydrolysis,[31] also yielded poorly crystalline frameworks, presumably due to hard acid – hard base interactions between sodium cations and the carboxylate-based linkers. Thus, $TlPF_6$ was chosen as the halide-abstracting agent, as it is less sensitive towards hydrolysis and features a soft thallium cation. After $TlPF_6$ treatment of IPrAu(III)Cl-bio-MOF-100, the sample retained crystallinity, yielding the desired IPrAu(III)PF_6-bio-MOF-100. SXRD measurement revealed preservation of 40% gold(III) occupancy in the framework, which is consistent with that of the precatalyst structure. In the crystal structure of IPrAu(III)PF_6-bio-MOF-100, the chloride ligand was no longer observed, which indicates successful halide abstraction from the precatalyst to form the desired cationic catalyst.

IPrAu(III)PF_6-bio-MOF-100 had very low reactivity towards the cycloisomerization reaction of substrate **6** to product **7**; this low reactivity was attributed to a potential decrease in rate of diffusion of nonpolar substrates through the intrinsically anionic bio-MOF-100 framework. Raising the temperature to increase the rate of diffusion of **6** was, however, not compatible with this cycloisomerization reaction due to the thermal instability of substrate **6**. Thus, alkynyl cylcoheptatriene substrate **8** was chosen as a model substrate, as it has higher thermal stability than **1** and is known to undergo a cycloisomerization reaction in the presence of cationic gold complexes to yield the corresponding indene products **9** and **10**.[32] Addition of **8** to IPrAu(III)PF_6-bio-MOF-100 resulted in formation of desired products **9** and **10** at elevated temperatures (Table 2.6, entry 1). Similar to the IRMOF-based gold(III) reactivity, no product was observed in the corresponding control experiments with the bio-MOF-100 system (entries 2–4). These data further demonstrate that chloride abstraction from the gold(III) precatalyst was successful by $TlPF_6$ treatment of IPrAu(III)Cl-bio-MOF-100.

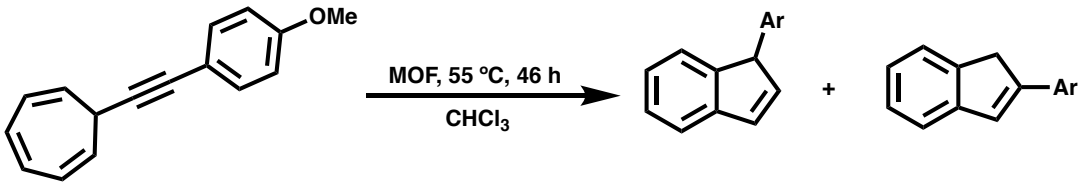

8 **9** **10**

entry	MOF	conversion (%)	**9**/**10**
1	IPrAu(III)PF_6-bio-MOF-100 (7 mol% Au)	96	60:40
2	IPrAu(III)Cl-Ibio-MOF-100 (7 mol% Au)	<1	—
3	bio-MOF-100-TlPF_6	<1	—
4	bio-MOF-100	<1	—

Table 2.6. Control experiments with bio-MOF.

The chemical stability of this cationic gold(III) catalyst in IRMOF-10 and bio-MOF-100 was compared with the stability of their homogeneous counterparts. Reductive elimination of IPrAu(III)(biphenyl)SbF_6 is known to be exacerbated in the presence of a trap for cationic gold(I) species, 1,3,5-trimethoxybenzene (TMB), to yield a Au(I)-TMB adduct (Table 2.7, entry 3).[13] In contrast, no 2,7-biphenylene dicarboxylic acid or Au(I)-TMB adduct was observed with the MOF analogues under equivalent conditions in the supernatant or by digestion ^{1}H NMR (entries 1 and 2). Additionally, we observed 78% decomposition of a homogeneous gold(III) analogue to the corresponding reductive elimination products when heated to 55°C (entry 5). In bio-MOF-100, the gold(III) occupancy remained unperturbed under these conditions and no reductive elimination products were observed in the supernatant by ^{1}H NMR (entry 4). These results are consistent with the hypothesis that the architectural stabilization afforded by IRMOF-10 and bio-MOF-100 is robust enough to prevent this unimolecular decomposition.

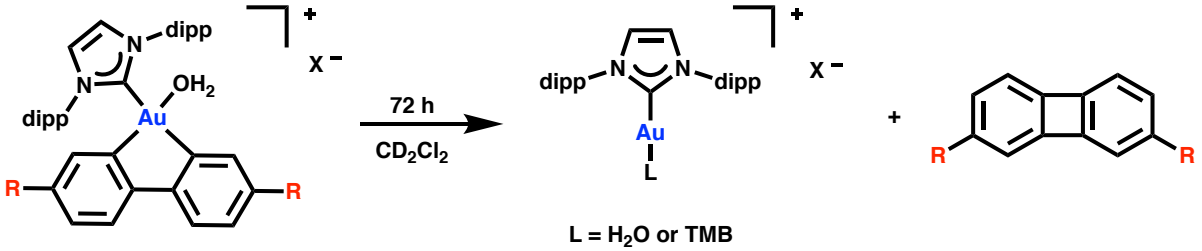

entry	catalyst	T (°C)	additive	decomposition (%)
1	IPrAu(III)SbF_6-IRMOF-10	25	TMB (10 equiv.)	0
2	IPrAu(III)PF_6-bio-MOF-100	25	TMB (10 equiv.)	0
3	IPrAu(III)(biphenyl)SbF_6	25	TMB (10 equiv.)	68
4	IPrAu(III)PF_6-bio-MOF-100[a]	55	none	0
5	IPrAu(III)(Me_2BPDC)SbF_6[a]	55	none	78

[a]$CDCl_3$ was used instead of CD_2Cl_2

Table 2.7. Stability of homogeneous gold(III) complexes vs. MOF analogues.

As a further evaluation that catalysis was occurring in the pores of the framework rather than at the surface or in bulk solution, the impact of substrate size was evaluated in IRMOF-10, as it features smaller pore dimensions than bio-MOF-100 (Table 4). The Au(III)-IRMOF-10-catalyzed reaction of 1,5-enyne substrate **11**, which is slightly larger along one dimension, did not show a substantial decrease in reactivity compared to substrate **6**. On the other hand, when the steric bulk was extended along two dimensions with substrate **12**, a decrease in reactivity to 2% conversion after 22 h was observed. Further extension of steric bulk along these two dimensions with substrate **13** resulted in no observed product formation by ^{1}H NMR. In contrast, full conversion was observed with substrates **6**, **11**, **12**, and **13** with 4 mol% homogeneous IPrAu(biphenyl)SbF_6, after 22 hours (see SI). These data are consistent with the hypothesis that the catalysis observed with IPrAu(III)SbF_6-IRMOF-10 occurs within the pores, and the leaching of catalytically active species into solution is unlikely. The lack of catalytically active species in solution further highlights the effectiveness of architectural stabilization to prohibit the formation of undesired gold(I) species in bulk solution.

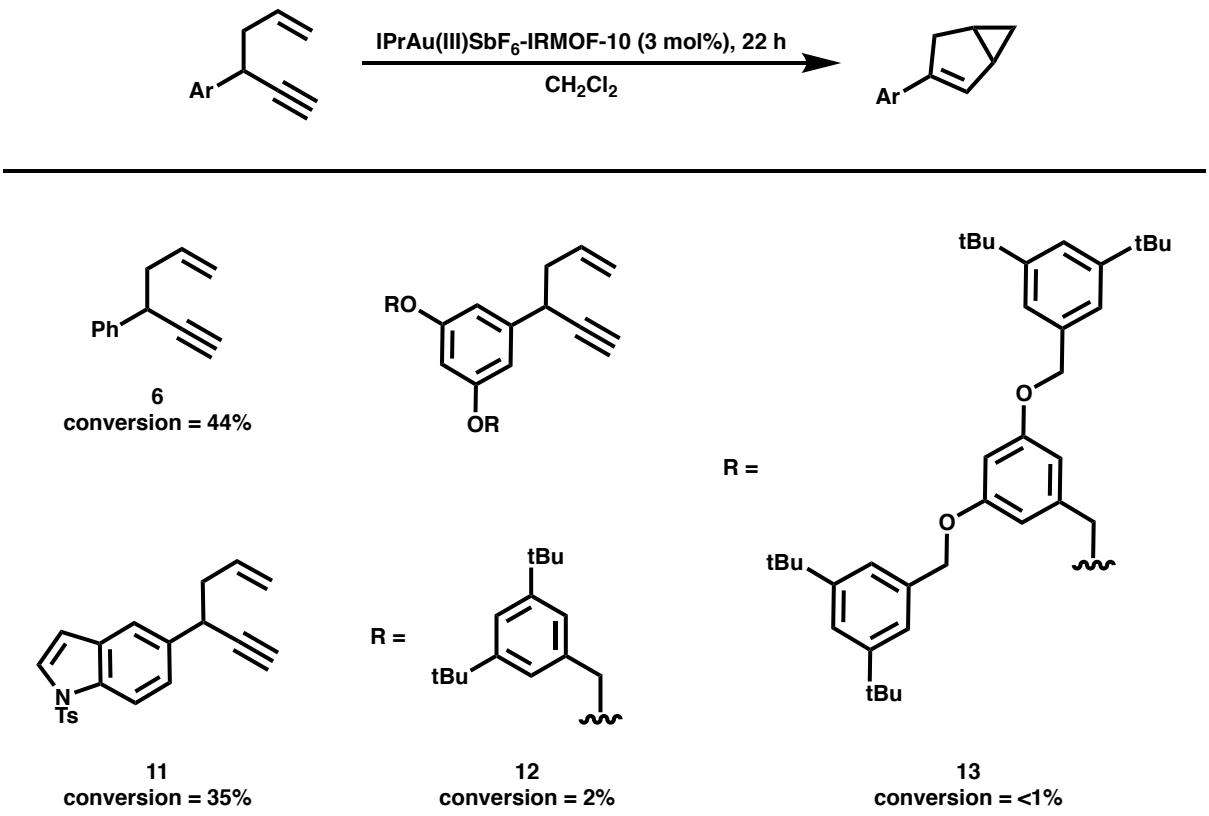

Table 2.8. Impact of substrate size on catalysis with Au(III)-IRMOF-10.

For solid-supported homogeneous catalysts to be implemented in industry, these catalysts must be recyclable for long-term use. Thus, after evaluating the stability of both Au(III)-MOF systems towards reductive elimination, the reuse of both systems was evaluated to further assess the impact of the architectural stability of these frameworks on the catalyst recyclability and longevity. To this end, employing IPrAu(III)SbF_6-IRMOF-10 with 3 mol% gold loading as a catalyst, 44% and 46% conversion of enyne **6** to bicyclohexene **7** was observed in cycles 1 and 2, respectively (Figure 2a). Reactivity towards the cycloisomerization of **6** continued to persist in cycles 3–5, albeit at lower conversions. We hypothesized that this decrease in reactivity might be attributed to the slow trapping of Au(III)Cl species in the presence of AgCl within the pores, which is a phenomenon that has previously been observed with solid-supported cationic gold species.[33] Indeed, we observed a rebound in reactivity upon treatment of IPrAu(III)SbF_6-IRMOF-10 with 1 equivalent of $AgSbF_6$ (relative to gold) in cycle 6 with continued reactivity over the subsequent cycle. Recyclable reactivity over 7 cycles was also observed with IPrAu(III)PF_6-bio-MOF-100-catalyzed cycloisomerization reaction of **8** to yield **9** and **10** (Figure 2.4). Additionally, no loss in reactivity of IPrAu(III)PF_6-bio-MOF-100 was observed after storing the catalyst for 29 days, demonstrating that catalyst deactivation does not occur even after long-term storage. The recyclability reactivity in both the IRMOF-10 and bio-MOF-100 systems further demonstrates the robustness of these systems engendered by architectural stabilization.

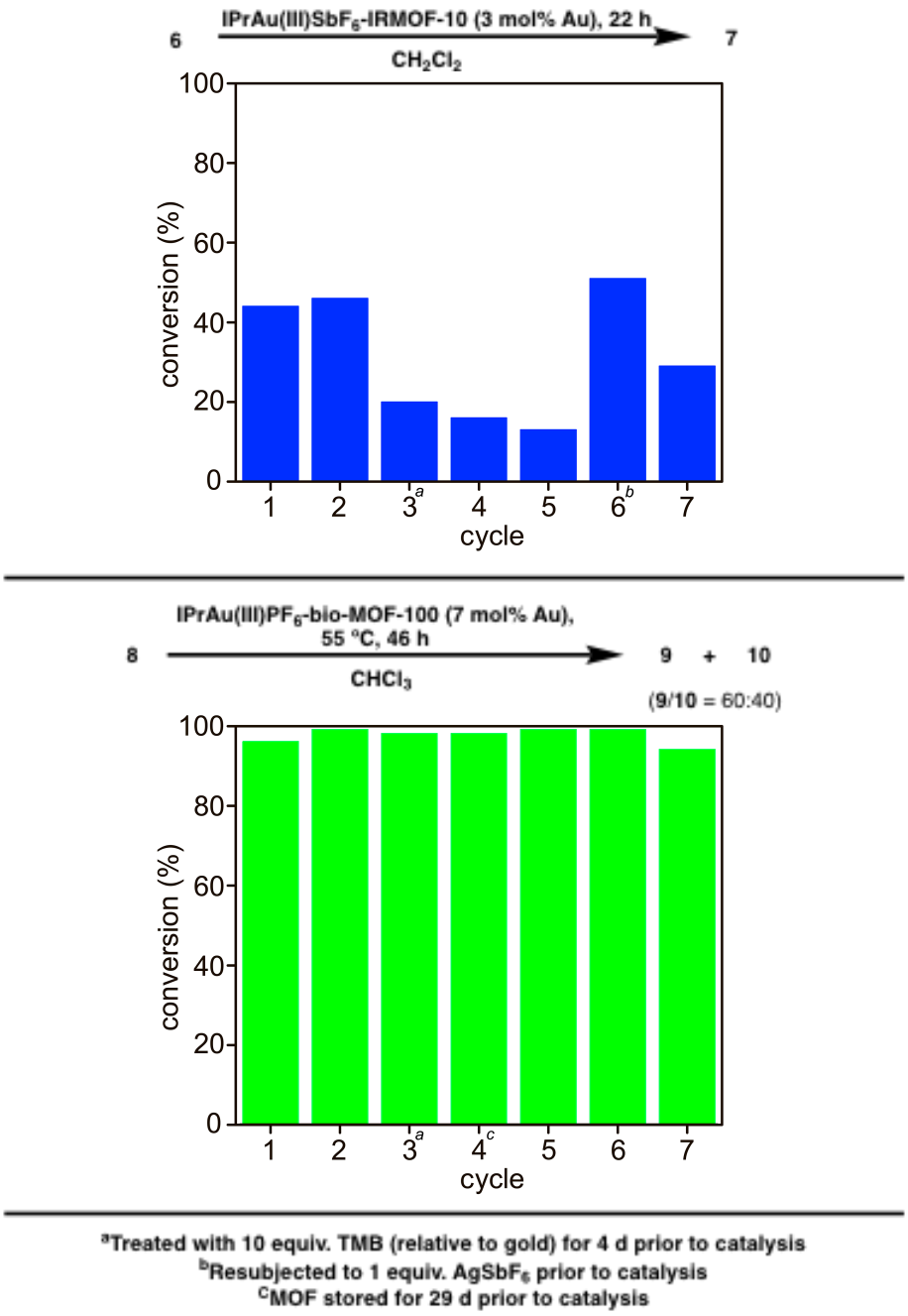

Figure 2.4. Recyclability of IPrAu(III)SbF_6-IRMOF-10 and IPrAu(III)PF_6-bio-MOF-100.

2.3 Conclusions

In conclusion, we have developed the first strategy for suppressing a unimolecular decomposition pathway with a solid support by architectural stabilization. The late-stage divergent synthesis developed for gold(III) linkers should facilitate diversification of L-type ligands bound to gold for the further development of Au(III)-MOF catalysts. This architectural

stabilization strategy should prove general to access other immobilized transition-metal catalysts that are otherwise prone to unimolecular decomposition pathways and are consequently unstable or inaccessible in solution.

2.4 Supporting Information

2.4.1 General Methods

Unless stated otherwise, all reactions were performed in oven-dried or flame-dried glassware. Reactions were sealed with rubber septa under a nitrogen atmosphere and were stirred with Teflon-coated magnetic stir bars. Dry tetrahydrofuran (THF), dimethylformamide (DMF), diethyl ether (Et_2O), and dichloromethane (DCM) were obtained by passing these previously degassed solvents through activated alumina columns. All other reagents were used as received. For all reactions conducted in a glove box, reagents were thoroughly dried and degassed by standard methods prior to use. Reactions were monitored by thin layer chromatography (TLC) on Silicycle Siliaplate^{TM} glass backed TLC plates (250 μm, 60 Å porosity, F-254 indicator) and visualized by UV irradiation. Volatile solvents were removed under reduced pressure with a rotary evaporator and subsequent high vacuum on a Schlenk line. ^{1}H- and ^{13}C-NMR spectra were taken with Bruker spectrometers operating at 300, 400, 500, 600, or 900 MHz. Chemical shifts are reported relative to the residual solvent signal. NMR data are reported as follows: chemical shift (multiplicity, coupling constants where applicable, number of hydrogens). Splitting is reported with the following symbols: s = singlet, d = doublet, t = triplet, q = quartet, quint = quintet, hept = heptet, dd = doublet of doublets, td = triplet of doublets, tt = triplet of triplets, and m = multiplet. High-resolution mass spectra (HRMS) were obtained with a Thermo LTQ-FT-ICR (7T, ESI) by the QB3 mass spectral facility at the University of California, Berkeley. Single-crystal X-ray diffraction (SXRD) data was collected using a Bruker D-8-Venture diffractometer. The Bruker D8-Venture diffractometer is equipped with a PHOTON100 CMOS detector and a micro-focus X-ray tube with a Cu-target (λ = 1.54178 Å) and Mo-target (λ = 0.71073 Å). Powder X-ray diffraction (PXRD) patterns were acquired with a Bruker D8 Advance diffractometer (Cu Kα radiation, λ = 1.54056 Å). FTIR measurements were taken on a Bruker Vertex 80 in the Center for Catalysis at University of California, Berkeley.

The following compounds and materials were prepared according to previously published procedures and their characterization match those reported in literature: dimethyl 2,2'-diiodo-[1,1'-biphenyl]-4,4'-dicarboxylate,[24] hex-5-en-1-yn-3-ylbenzene,[34] 5-(hex-5-en-1-yn-3-yl)-1-tosyl-1H-indole,[34] (3,5-bis((3,5-di-*tert*-butylbenzyl)oxy)phenyl)methanol,[35] (3,5-bis((3,5-bis((3,5-di-*tert*-butylbenzyl)oxy)benzyl)oxy)phenyl)methanol,[35] Au(biphenyl)Cl dimer,[30] Me_2ImAgCl,[36] IPrAu(biphenyl)Cl,[30] 7-((4-methoxyphenyl)ethynyl)cyclohepta-1,3,5-triene,[32] UiO-67,[37] IRMOF-9,[38] and bio-MOF-100.[39]

2.4.2 Synthetic Procedures for Gold(III) Complexes

(2,2'-diiodo-[1,1'-biphenyl]-4,4'-diyl)dimethanol, 1

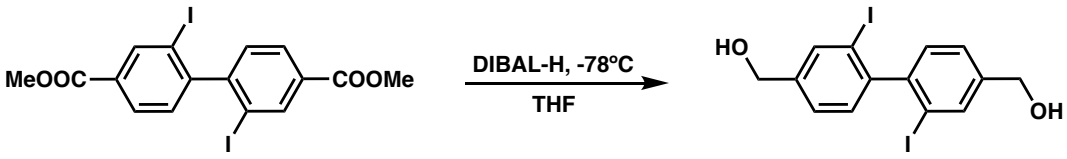

To a flame dried 500 mL round bottom flask was added dimethyl 2,2'-diiodo-[1,1'-biphenyl]-4,4'-dicarboxylate (7.9 g, 15 mmol, 1 equiv.) and THF (80 mL, 0.19 M). The reaction mixture was cooled to -78°C and a solution of DIBAL-H (1 M in heptane, 90 mL, 6 equiv) was added dropwise. After addition of DIBAL-H, the reaction mixture was allowed to warm to room temperature and stir for 12 h. The reaction mixture was then diluted with 100 mL Et_2O. The reaction mixture was then quenched at 0°C with the sequential addition of 3.6 mL H_2O, 3.6 mL 15% NaOH(aq), and 9.0 mL H_2O. After warming to room temperature, the quenched reaction mixture was dried over $MgSO_4$, filtered through a pad of celite, and concentrated under reduced pressure. The crude product was then purified by column chromatography (15:1 DCM/MeOH), yielding the title compound as a colorless solid (6.3 g, 89%).

^{1}H NMR (300 MHz, Methanol-d_4) δ 7.95 (s, 2H), 7.42 (dd, J = 7.92, 1.6 Hz, 2H), 7.13 (d, J = 7.8 Hz, 2H), 4.63 (s, 4H)

^{13}C NMR (126 MHz, Methanol-d_4) δ 148.97, 144.43, 138.18, 130.93, 127.55, 100.30, 63.86

HRMS (ESI−) *m/z* calcd for $C_{14}H_{11}O_2I_2$ $[M-H]^-$: 464.8854, found: 464.8849

IR (neat, cm^{-1}) 3288, 2868, 1596, 1549, 1465, 1390, 1263, 1196, 1138, 1071, 1036, 997, 887, 817, 735, 702, 660, 628, 560

(((2,2'-diiodo-[1,1'-biphenyl]-4,4'-diyl)bis(methylene))bis(oxy))bis(tert-butyldimethylsilane), SI 1

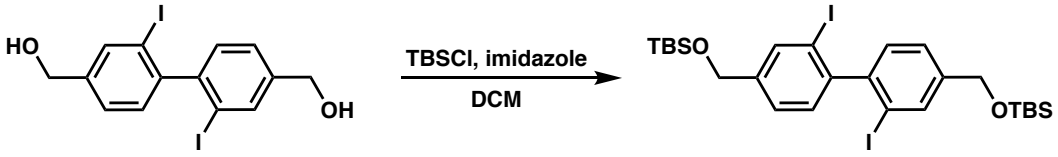

To a flame dried 250 mL round bottom flask was added **1** (6.3 g, 14 mmol, 1 equiv.), TBSCl (6.1 g, 41 mmol, 3 equiv.), imidazole (3.7 g, 54 mmol, 4 equiv.), and 3:10 THF/DCM (130 mL, 0.10 M). The reaction mixture was allowed to stir for 24 h. The reaction mixture was then poured into 100 mL H_2O and extracted three times with DCM (100 mL x 3). The combined organic layers were dried over $MgSO_4$, filtered, and concentrated under reduced pressure. The crude product

was then purified by column chromatography (20:1 Hexanes/EtOAc), yielding the title compound as a colorless oil (8.3 g, 89%).

^{1}H NMR (500 MHz, Chloroform-*d*) δ 7.89 (d, *J* = 1.6 Hz, 2H), 7.36 (dd, *J* = 7.86, 1.8 Hz, 2H), 7.13 (d, *J* = 7.8 Hz, 2H), 4.76 (s, 4H), 0.96 (s, 18H), 0.13 (s, 12H)

^{13}C NMR (126 MHz, Chloroform-*d*) δ 147.45, 143.01, 136.40, 129.86, 125.75, 99.74, 63.92, 26.11, 26.15, 18.57, -5.07

HRMS (EI) *m/z* calcd: 694.0656, found: 694.0654

IR (neat, cm^{-1}) 2953, 2929, 2856, 1697, 1591, 1549, 1470, 1362, 1288, 1251, 1098, 1037, 999, 939, 833, 771, 739, 670, 571

(((5,5-dibutyl-5H-dibenzo[b,d]stannole-3,7-diyl)bis(methylene))bis(oxy))bis(tert-butyldimethylsilane), SI 2

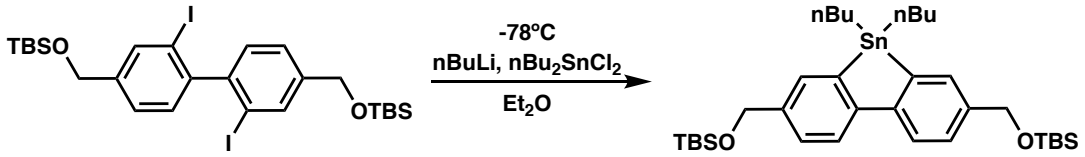

To a flame dried 250 mL round bottom flask was added **SI 1** (8.3 g, 12 mmol, 1 equiv.) and Et_2O (60 mL, 0.2 M). The reaction mixture was cooled to -78°C and a solution of n-butyllithium (1.6 M in hexanes, 19 mL, 2.5 equiv.) was added in a dropwise fashion. The reaction mixture was stirred warming to room temperature for 2 h resulting in a light brown slurry. A solution of dibutyl tin chloride (4.7 g, 15 mmol, 1.3 equiv.) in Et_2O (30 mL, 0.5 M) was then added to the reaction mixture. The reaction mixture was then allowed to stir for 12 h resulting in a pale yellow slurry. The reaction mixture was then quenched at 0°C with 10 mL H_2O. The organic layer was diluted with 200 mL Et_2O and washed with H_2O (200 mL x 3). The combined organic layers were dried over $MgSO_4$, filtered, and concentrated under reduced pressure. The crude product was then purified by column chromatography (10:1 Hexanes/EtOAc), yielding the title compound as a colorless oil (6.3 g, 77%).

^{1}H NMR (300 MHz, Chloroform-*d*) δ 7.89 (d, *J* = 8.1 Hz, 2H), 7.65 – 7.47 (m, 2H), 7.32 (dd, *J* = 8.1, 2.0 Hz, 2H), 4.77 (s, 4H), 1.69 – 1.57 (m, 4H), 1.39 – 1.26 (m, 8H), 0.95 (s, 18H), 0.87 (t, *J* = 7.5 Hz, 6H), 0.11 (s, 12H)

^{13}C NMR (101 MHz, Chloroform-*d*) δ 147.71, 141.22, 140.05, 134.47, 127.19, 122.31, 65.33, 29.22, 27.36, 18.60, 13.79, 12.11, -4.99

HRMS (ESI+) *m/z* calcd for $C_{34}H_{59}O_2Si_2Sn$ $[M+H]^+$: 675.3070, found: 675.3074

IR (neat, cm^{-1}) 2954, 2927, 2855, 1462, 1361, 1252, 1201, 1080, 1005, 939, 833, 813, 774, 715, 664, 596

TBS-protected Me_2ImAu(III)(biphenyl)Cl complex, SI 3

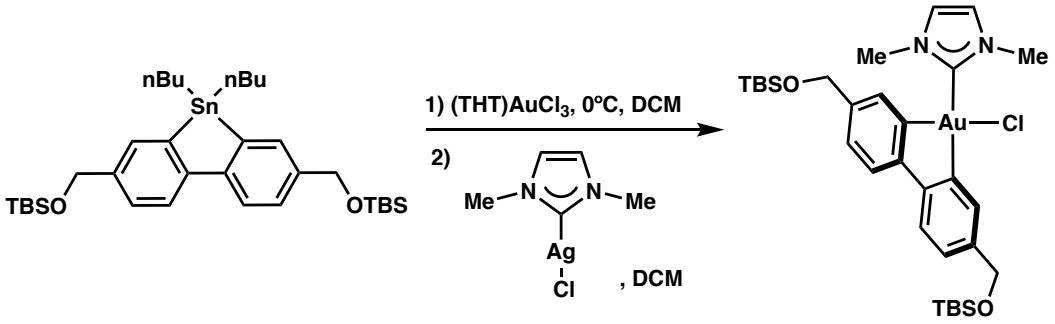

To a 20 mL vial was added **SI 2** (0.57 g, 0.85 mmol, 1 equiv.) and DCM (7 mL, 0.12 M). The reaction mixture was cooled to 0°C and (THT)$AuCl_3$ (0.33 g, 0.85 mmol, 1 equiv.) was added in one portion. The reaction mixture was stirred for 10 min at 0°C resulting in a black slurry. The reaction mixture was then stirred for an additional 10 min while warming to room temperature. The reaction mixture was then concentrated to 1 mL under reduced pressure. The resulting reaction mixture was then filtered through a pad of celite and concentrated under reduced pressure to yield crude TBS-protected Au(biphenyl)Cl dimer as a yellow oil. To a 20 mL vial was added crude gold dimer, Me_2ImAgCl (0.20 g, 0.85 mmol, 1 equiv.) and DCM (9 mL, 0.1 M). The reaction mixture was then stirred for 14 h, filtered through a pad of celite, and concentrated under reduced pressure. The crude product was then purified by column chromatography (70:1 to 35:1 DCM/MeOH), yielding the title compound as a colorless solid (0.27 g, 42%).

^{1}H NMR (500 MHz, Methylene Chloride-d_2) δ 8.03 (d, J = 1.7 Hz, 1H), 7.41 (dd, J = 7.8, 5.4 Hz, 2H), 7.26 – 7.21 (m, 1H), 7.17 (s, 2H), 7.12 – 7.08 (m, 1H), 6.54 (d, J = 1.7 Hz, 1H), 4.77 (s, 2H), 4.59 (s, 2H), 3.89 (s, 6H), 1.01 (s, 9H), 0.92 (s, 9H), 0.18 (s, 6H), 0.08 (s, 6H)

^{13}C NMR (101 MHz, Methylene Chloride-d_2) δ 183.71, 159.75, 153.02, 151.66, 150.60, 140.33, 139.88, 131.02, 130.90, 125.37, 125.18, 123.12, 121.38, 120.38, 65.48, 64.84, 37.52, 25.88, 25.76, 18.42, 18.25, -5.39, -5.51

Diol Me_2ImAu(III)(biphenyl)Cl complex, 2

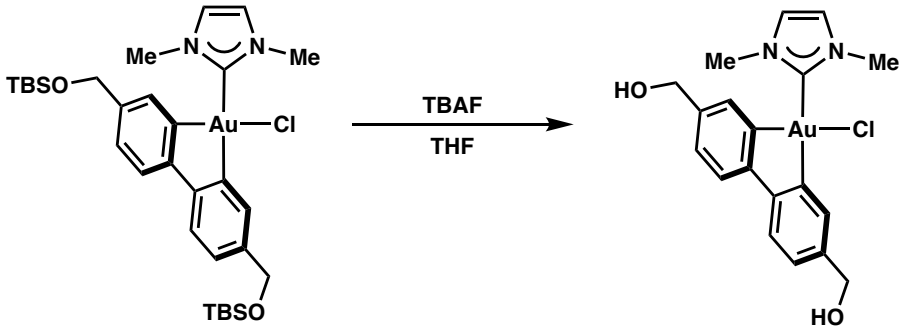

To a flame dried 20 mL vial was added **SI 3** (0.27 g, 0.36 mmol, 1.0 equiv.) and THF (13 mL, 0.028 M). TBAF (1 M in THF, 0.78 mL, 2.2 equiv.) was then added to the reaction mixture. After stirring for 22 h, the reaction mixture was then diluted with H_2O (30 mL) extracted with DCM (30 mL x 4). The combined organic fractions were concentrated under reduced pressure, and the crude product was then purified by column chromatography (10:1 DCM/MeOH), yielding the title compound as a colorless solid (0.16 g, 82%).

^{1}H NMR (400 MHz, Methanol-d_4) δ 8.04 (d, J = 1.6 Hz, 1H), 7.43 (s, 2H), 7.42 – 7.37 (m, 2H), 7.16 (d, J = 7.7 Hz, 1H), 7.12 (d, J = 7.7 Hz, 1H), 6.45 (s, 1H), 4.57 (s, 2H), 4.38 (s, 2H), 3.84 (s, 6H)

Dialdehyde Me_2ImAu(III)(biphenyl)Cl complex, SI 4

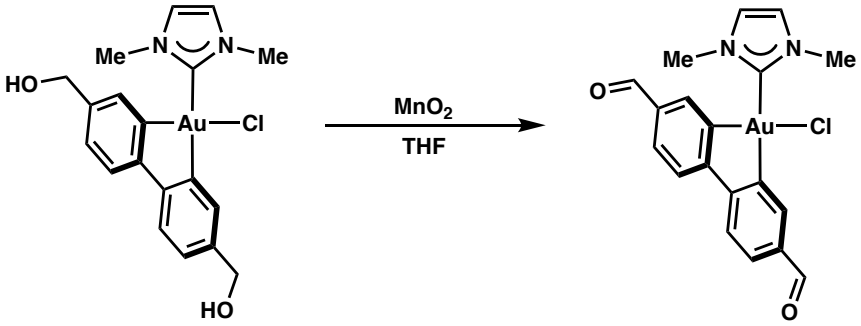

To a flame dried 20 mL vial was added **2** (0.16 g, 0.29 mmol, 1.0 equiv.) and THF (5 mL, 0.058 M). Activated MnO_2 (4.3 g, 49 mmol, 60 equiv.) was then added to the reaction mixture in one portion. After stirring for 21 h, the reaction mixture was filtered through a pad of celite and concentrated under reduced pressure. The crude product was then purified by column chromatography (10:1 DCM/MeOH), yielding the title compound as a pale yellow solid (0.14 g, 90%).

^{1}H NMR (300 MHz, Chloroform-d) δ 10.06 (s, 1H), 9.78 (s, 1H), 8.73 (d, J = 1.7 Hz, 1H), 7.82 (dd, J = 8.0, 1.7 Hz, 1H), 7.71 (s, 2H), 7.63 (d, J = 8.0 Hz, 1H), 7.18 (s, 2H), 6.99 (s, 1H), 3.89 (s, 6H)

$Me_2ImAu(III)(H_2BPDC)Cl$, 4

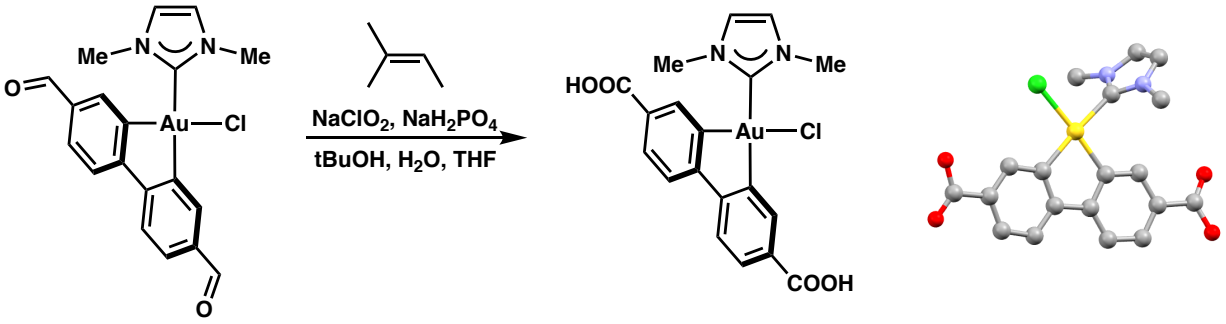

To a 250 mL round bottom flask was added **SI 4** (0.14 g, 0.26 mmol, 1.0 equiv.), tBuOH (5 mL), H_2O (5 mL), and THF (18 mL). 2-Methyl-2-butene (2.8 mL. 26 mmol. 100 equiv.), $NaH_2PO_4 \bullet H_2O$ (0.72 g, 5.2 mmol, 20 equiv.), and $NaClO_2$ (0.47 g, 5.2 mmol, 20 equiv.) were added sequentially to the reaction mixture. After stirring for 19 h, organic solvents were removed from the reaction mixture under reduced pressure. The pale yellow precipitate was recovered by centrifugation, and the precipitate was further washed with H_2O (10 mL x 5) with sonication and centrifugation. The washed precipitate was dried under reduced pressure, yielding the title compound as a pale yellow solid (94 mg, 42%).

^{1}H NMR (300 MHz, DMSO-d_6) δ 8.63 (d, J = 1.7 Hz, 1H), 7.78 (dd, J = 7.9, 1.7 Hz, 2H), 7.72 – 7.64 (m, 4H), 7.02 (d, J = 1.6 Hz, 1H), 3.76 (s, 7H)

$Me_2ImAu(III)(biphenyl)Cl$, SI 5

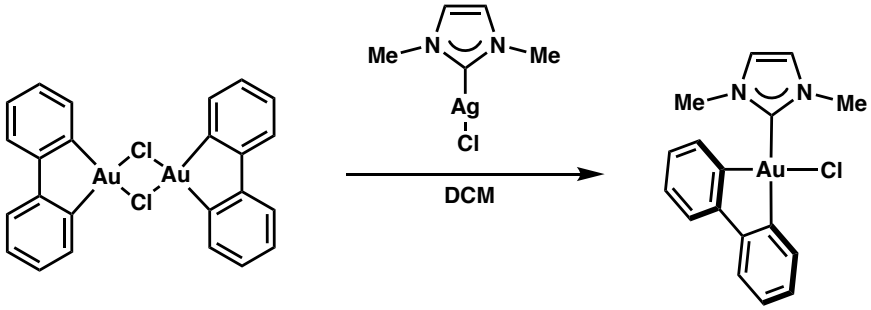

To a 1 dram vial was added $Me_2ImAgCl$ (32 mg, 0.13 mmol, 1 equiv), Au(biphenyl)Cl dimer (50 mg, 0.065 mmol, 0.5 equiv.), and DCM (2 mL, 0.065 M). The reaction mixture was stirred for 3 h, filtered through a pad of celite, and concentrated under reduced pressure. The crude product was then purified by column chromatography (50:1 DCM/MeOH), yielding the title compound as a colorless solid (57 mg, 91%).

^{1}H NMR (300 MHz, Chloroform-d) δ 8.23 – 8.14 (m, 1H), 7.48 – 7.36 (m, 2H), 7.23 – 7.12 (m, 3H), 7.10 (s, 2H), 6.80 – 6.71 (m, 1H), 6.38 (d, J = 7.7 Hz, 1H), 3.88 (s, 6H)

TBS-protected IPrAu(III)(biphenyl)Cl complex, SI 6

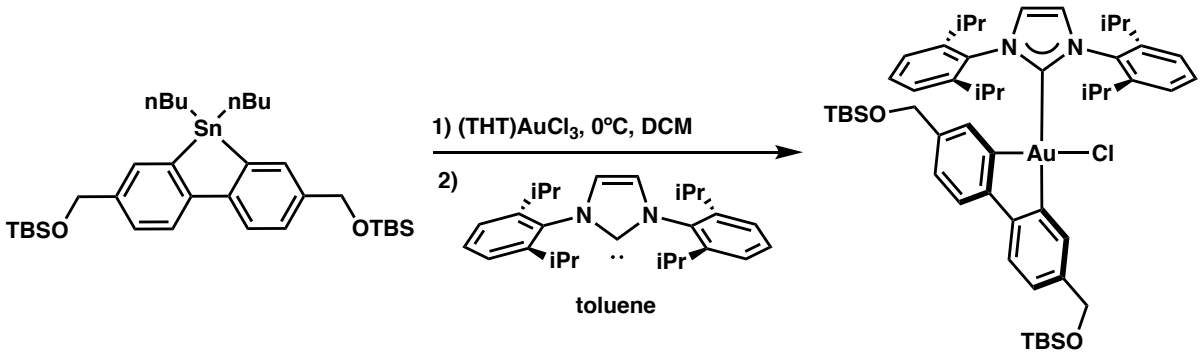

To a 20 mL vial was added **SI 2** (0.80 g, 1.2 mmol, 1.0 equiv.) and DCM (9 mL, 0.13 M). The reaction mixture was cooled to 0°C and (THT)$AuCl_3$ (0.46 g, 1.2 mmol, 1.0 equiv.) was added in one portion. The reaction mixture was stirred for 10 min at 0°C resulting in a black slurry. The reaction mixture was then stirred for an additional 10 min while warming to room temperature. The reaction mixture was then concentrated to 1 mL under reduced pressure. The resulting reaction mixture was then filtered through a pad of celite and concentrated under reduced pressure to yield crude TBS-protected Au(biphenyl)Cl dimer as a yellow oil, which was used without further purification. In a glovebox, to crude gold dimer and DCM (12 mL, 0.10 M) in an oven dried 20 mL vial was added free IPr carbene (1,3-bis(2,6-diisopropylphenyl)-1,3- dihydro-2H-imidazol-2-ylidene) (0.46 g, 1.2 mmol, 1.0 equiv) in one portion. The reaction mixture was then stirred for 12 h and was then taken out of the glovebox. The reaction mixture was then filtered through a pad of celite and concentrated under reduced pressure. The crude product was then purified by column chromatography (3:2 DCM/Hexanes), yielding the title compound as a colorless solid (0.70 g, 56%).

^{1}H NMR (500 MHz, Methylene Chloride-d_2) δ 7.75 (d, J = 1.7 Hz, 1H), 7.42 (d, J = 7.9 Hz, 2H), 7.41 (s, 2H), 7.30 (dd, J = 7.8, 1.5 Hz, 2H), 7.24 (d, J = 7.9 Hz, 1H), 7.20 (dd, J = 7.8, 1.5 Hz, 2H), 7.15 (d, J = 7.8 Hz, 1H), 7.09 (dd, J = 7.9, 1.5 Hz, 1H), 7.02 (dd, J = 7.7, 1.7 Hz, 1H), 6.71 (s, 1H), 4.61 (s, 2H), 4.56 (s, 2H), 3.20 (hept, J = 7.1 Hz, 2H), 2.95 (hept, J = 6.5 Hz, 2H), 1.44 (d, J = 6.6 Hz, 6H), 1.17 (d, J = 6.8 Hz, 6H), 1.04 (d, J = 6.9 Hz, 6H), 0.97 (s, 9H), 0.88 (s, 9H), 0.69 (d, J = 6.7 Hz, 6H), 0.16 (s, 6H), 0.04 (s, 6H).

^{13}C NMR (101 MHz, Methylene Chloride-d_2) δ 188.40, 158.90, 153.23, 151.99, 151.93, 147.92, 145.50, 139.53, 138.96, 134.53, 131.72, 131.11, 130.87, 126.52, 125.13, 124.98, 124.69, 121.37, 120.41, 65.73, 65.51, 29.48, 29.06, 26.90, 26.64, 26.36, 26.17, 18.90, 18.71, -5.04, -5.15

HRMS (ESI+) *m/z* calcd for $C_{53}H_{76}O_2N_2AuClNaSi_2$ $[M+Na]^+$: 1083.4692, found: 1083.4716

IR (neat, cm^{-1}) 2957, 2929, 2858, 1592, 1462, 1402, 1363, 1325, 1255, 1200, 1092, 1006, 939, 837, 804, 777, 757, 706, 667

Diol IPrAu(III)(biphenyl)Cl complex, 3

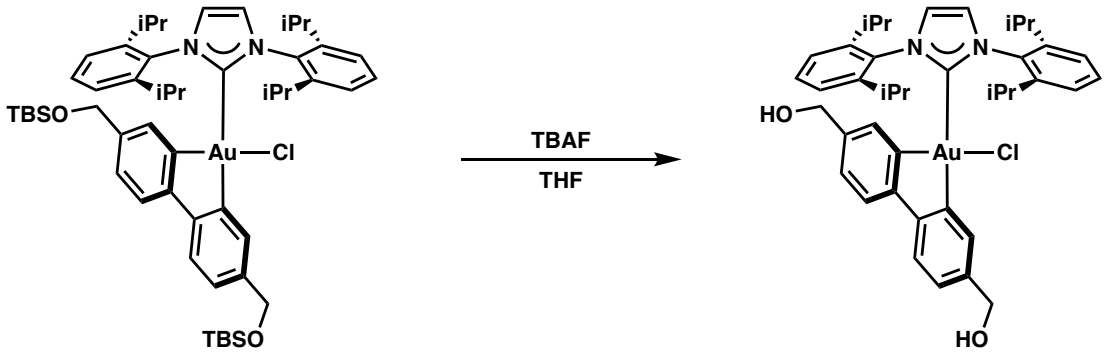

To a flame dried 20 mL vial was added **SI 6** (0.81 g, 0.76 mmol, 1.0 equiv.) and THF (16 mL, 0.048 M). TBAF (1 M in THF, 1.9 mL, 2.5 equiv.) was then added to the reaction mixture. After stirring for 14 h, the reaction mixture was then diluted with H_2O (50 mL) extracted with DCM (50 mL x 4). The combined organic fractions were concentrated under reduced pressure, and the crude product was then purified by column chromatography (25:1 DCM/MeOH), yielding the title compound as a colorless solid (0.61 g, 96%).

^{1}H NMR (500 MHz, Methylene Chloride-d_2) δ 7.90 (s, 1H), 7.48 – 7.40 (m, 4H), 7.32 (d, J = 7.7 Hz, 2H), 7.26 (d, J = 7.8 Hz, 1H), 7.21 (d, J = 7.8 Hz, 2H), 7.19 (d, J = 7.7 Hz, 1H), 7.08 (d, J = 7.8 Hz, 1H), 7.01 (d, J = 7.7 Hz, 1H), 6.88 (s, 1H), 4.58 (s, 2H), 4.47 (s, 2H), 3.24 (hept, J = 6.8 Hz, 2H), 3.02 (hept, J = 6.9 Hz, 2H), 1.46 (d, J = 6.5 Hz, 6H), 1.18 (d, J = 6.8 Hz, 6H), 1.05 (d, J = 6.8 Hz, 6H), 0.70 (d, J = 6.7 Hz, 6H)

^{13}C NMR (126 MHz, Chloroform-d) δ 187.61, 159.14, 153.47, 152.45, 151.91, 147.85, 145.41, 139.38, 138.88, 134.50, 132.88, 131.72, 131.09, 126.56, 126.13, 125.70, 124.94, 124.63, 121.53, 120.69, 65.89, 65.38, 29.45, 29.02, 26.88, 26.39, 22.97, 22.71

HRMS (ESI+) *m/z* calcd for $C_{41}H_{48}O_2N_2AuClNa$ $[M+Na]^+$: 855.2962, found: 855.2980

IR (neat, cm^{-1}) 3423, 2967, 2928, 2867, 1591, 1559, 1461, 1403, 1387, 1364, 1325, 1280, 1203, 1121, 1046, 943, 905, 804, 757, 707, 667, 635, 523

Dialdehyde IPrAu(III)(biphenyl)Cl complex, SI 7

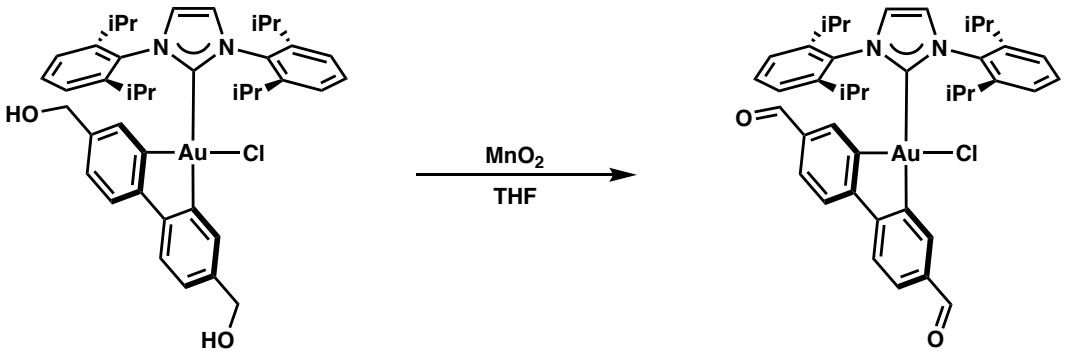

To a flame dried 20 mL vial was added **3** (0.68 g, 0.82 mmol, 1.0 equiv.) and THF (15 mL, 0.055 M). Activated MnO_2 (4.3 g, 49 mmol, 60 equiv.) was then added to the reaction mixture in one portion. After stirring for 13 h, the reaction mixture was filtered through a pad of celite and concentrated under reduced pressure. The crude product was then purified by column chromatography (100% DCM), yielding the title compound as a pale yellow solid (0.53 g, 78%).

^{1}H NMR (500 MHz, Methylene Chloride-d_2) δ 9.88 (s, 1H), 9.85 (s, 1H), 8.51 (d, J = 1.7 Hz, 1H), 7.65 (dd, J = 8.0, 1.5 Hz, 1H), 7.61 (dd, J = 7.9, 1.7 Hz, 1H), 7.56 (d, J = 7.8 Hz, 1H), 7.52 (s, 1H), 7.50 (s, 2H), 7.47 (d, J = 8.6 Hz, 1H), 7.44 (t, J = 8.0 Hz, 2H), 7.33 (dd, J = 7.8, 1.5 Hz, 2H), 7.19 (dd, J = 7.8, 1.5 Hz, 2H), 3.19 – 3.04 (m, 4H), 1.46 (d, J = 6.6 Hz, 6H), 1.16 (d, J = 6.8 Hz, 6H), 1.05 (d, J = 6.9 Hz, 6H), 0.58 (d, J = 6.7 Hz, 6H).

^{13}C NMR (126 MHz, Methylene Chloride-d_2) δ 192.65, 191.41, 184.79, 159.59, 159.45, 157.74, 151.51, 147.78, 145.37, 135.78, 135.65, 135.52, 134.27, 132.84, 132.03, 131.26, 128.00, 126.79, 124.93, 124.69, 123.03, 122.40, 29.54, 28.94, 26.83, 26.47, 22.88, 22.62.

HRMS (ESI+) *m/z* calcd for $C_{41}H_{44}O_2N_2AuClNa$ $[M+Na]^+$: 851.2649, found: 851.2672

IR (neat, cm^{-1}) 2968, 2868, 1686, 1582, 1463, 1405, 1384, 1325, 1294, 1192, 854, 819, 803, 757, 708, 666

IPrAu(III)(H_2BPDC)Cl, 5

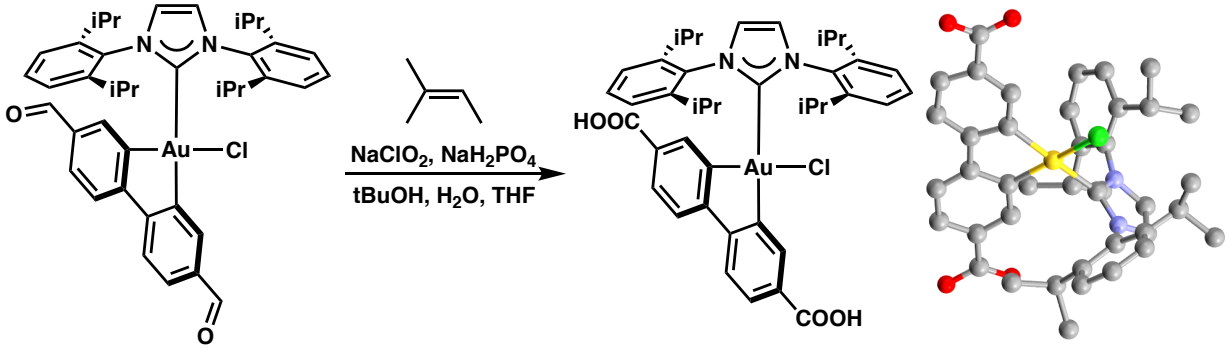

To a 250 mL round bottom flask was added **SI 7** (0.53 g, 0.64 mmol, 1.0 equiv.), tBuOH (22 mL), H_2O (22 mL), and THF (63 mL). 2-Methyl-2-butene (6.8 mL. 64 mmol. 100 equiv.), NaH_2PO_4•H_2O (1.77 g, 12.8 mmol, 20 equiv.), and $NaClO_2$ (1.16 g, 12.8 mmol, 20 equiv.) were added sequentially to the reaction mixture. After stirring for 16 h, organic solvents were removed from the reaction mixture under reduced pressure. The pale yellow precipitate was recovered by centrifugation, and the precipitate was further washed with H_2O (40 mL x 5) with sonication and centrifugation. The washed precipitate was dried under reduced pressure, yielding the title compound as a pale yellow solid (0.49 g, 86%).

^{1}H NMR (600 MHz, DMSO-d_6) δ 8.45 (d, J = 1.7 Hz, 1H), 8.26 (s, 2H), 7.75 (d, J = 8.1 Hz, 1H), 7.64 (dd, J = 7.9, 1.7 Hz, 1H), 7.60 (s, 1H), 7.58 (d, J = 8.0 Hz, 1H), 7.51 (d, J = 8.0 Hz, 1H), 7.46 (t, J = 7.7 Hz, 2H), 7.33 (d, J = 7.8 Hz, 2H), 7.26 (d, J = 7.8 Hz, 2H), 3.16 (hept, J =

7.4, 6.7 Hz, 2H), 2.98 (hept, J = 6.0 Hz, 2H), 1.39 (d, J = 6.6 Hz, 6H), 1.14 (d, J = 6.6 Hz, 6H), 1.02 (d, J = 6.8 Hz, 6H), 0.51 (d, J = 6.6 Hz, 6H)

^{13}C NMR (226 MHz, DMSO-d_6) δ 182.35, 167.41, 166.80, 158.15, 156.65, 155.85, 149.32, 146.91, 144.88, 135.18, 133.99, 133.46, 130.67, 129.51, 128.76, 128.69, 128.54, 127.68, 124.45, 123.89, 122.18, 121.47, 28.68, 28.13, 26.37, 25.79, 22.45, 22.27

HRMS (ESI+) *m/z* calcd for $C_{41}H_{44}O_4N_2AuClNa$ [M+Na]$^+$: 883.2547, found: 883.2558

IR (neat, cm^{-1}) 2966, 2868, 1676, 1586, 1558, 1459, 1440, 1405, 1363, 1319, 1280, 1244, 1198, 1122, 1056, 932, 839, 799, 767, 754, 732, 705, 688, 631, 577, 528

IPrAu(III)(Me$_2$BPDC)Cl, SI 9

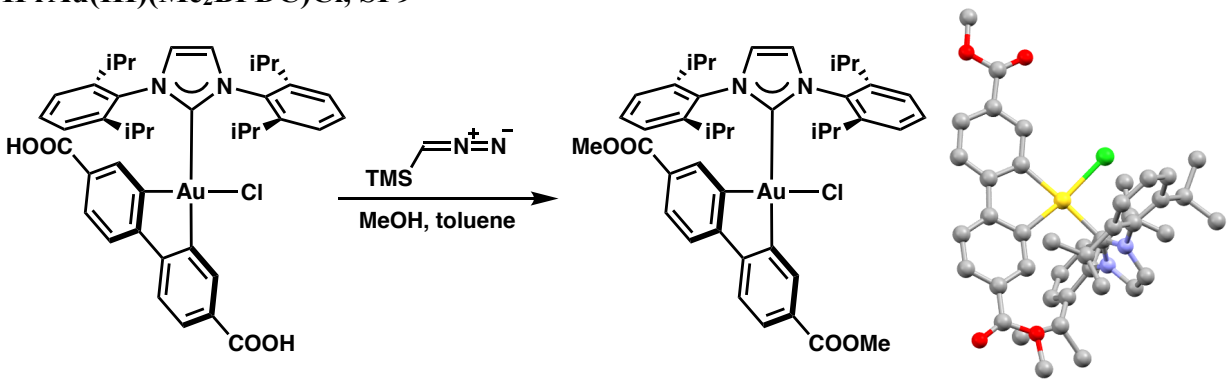

To a 2 dram vial was added **5** (20.0 mg, 0.023 mmol, 1 equiv.) and 10:1 MeOH/toluene (2.2 mL, 0.10 M). A solution of trimethylsilyldiazomethane (2 M in hexanes, 0.50 mL, 43 equiv.) was added in 4 portions over 15 h. After stirring the reaction mixture for an additional 24 h, the mixture was quenched with acetic acid (0.05 mL), concentrated, then purified by column chromatography (4:1 DCM/Hexanes) to yield the title compound as a pale yellow solid (16 mg, 80% yield).

^{1}H NMR (600 MHz, Methylene Chloride-d_2) δ 8.56 (d, J = 1.7 Hz, 1H), 7.81 (dd, J = 8.0, 1.6 Hz, 1H), 7.72 (dd, J = 8.0, 1.8 Hz, 1H), 7.62 (d, J = 1.7 Hz, 1H), 7.47 (s, 2H), 7.44 (t, J = 7.8 Hz, 2H), 7.41 (d, J = 8.1 Hz, 1H), 7.35 (d, J = 8.1 Hz, 1H), 7.33 (dd, J = 7.9, 1.4 Hz, 2H), 7.20 (dd, J = 7.8, 1.5 Hz, 2H), 3.89 (s, 3H), 3.81 (s, 3H), 3.20 (hept, J = 6.4 Hz, 2H), 3.10 (hept, J = 6.8 Hz, 2H), 1.47 (d, J = 6.6 Hz, 6H), 1.16 (d, J = 6.8 Hz, 6H), 1.05 (d, J = 6.9 Hz, 6H), 0.61 (d, J = 6.7 Hz, 6H)

^{13}C NMR (226 MHz, Methylene Chloride-d_2) δ 185.50, 167.54, 166.67, 158.80, 158.27, 156.66, 150.75, 147.82, 145.45, 135.48, 134.39, 133.70, 131.24, 129.08, 128.94, 128.83, 126.67, 124.93, 124.69, 122.20, 121.43, 52.31, 52.17, 30.09, 29.54, 29.03, 26.82, 26.41, 22.85, 22.65

HRMS (ESI+) *m/z* calcd for $C_{43}H_{48}O_4N_2AuClNa$ [M+Na]$^+$: 911.2860, found: 911.2885

IR (neat, cm^{-1}) 2924, 2852, 1714, 1587, 1462, 1405, 1383, 1278, 1244, 1110, 971, 944, 803, 763, 707

2.4.3 Synthetic Procedures for Au(III)-MOFs

Me_2ImAu(III)Cl-UiO-67 (6% Au occupancy)

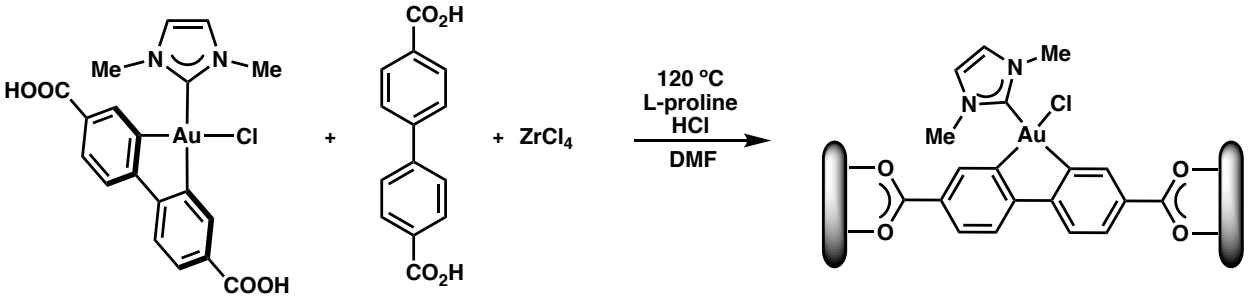

H_2BPDC Me_2ImAu(III)Cl-UiO-67

To a 20 mL vial was added Me_2ImAu(III)(H_2BPDC)Cl (25.6 mg, 0.045 mmol, 0.1 equiv.), H_2BPDC (98.1 mg, 0.41 mmol, 0.9 equiv.), $ZrCl_4$ (105 mg, 0.45 mmol, 1.0 equiv.), L-proline (250 mg, 2.2 mmol, 5 equiv.), concentrated aqueous HCl (40 μL), and DMF (10.0 mL). The reaction mixture was capped, sonicated for 10 minutes, then heated at 120 °C in an oven for 17 h h. This yielded colorless crystals, which were washed with DMF (15 mL x 5), DCM (15 mL x 15), then $MeNO_2$ (15 mL x 5). Residual solvent was removed from Me_2ImAu(III)Cl-UiO-67 under reduced pressure. 6% loading IPrAu(BPDC)Cl vs BPDC (digestion ^{1}H NMR).

Me_2ImAu(III)Cl-UiO-67 (20% Au occupancy)

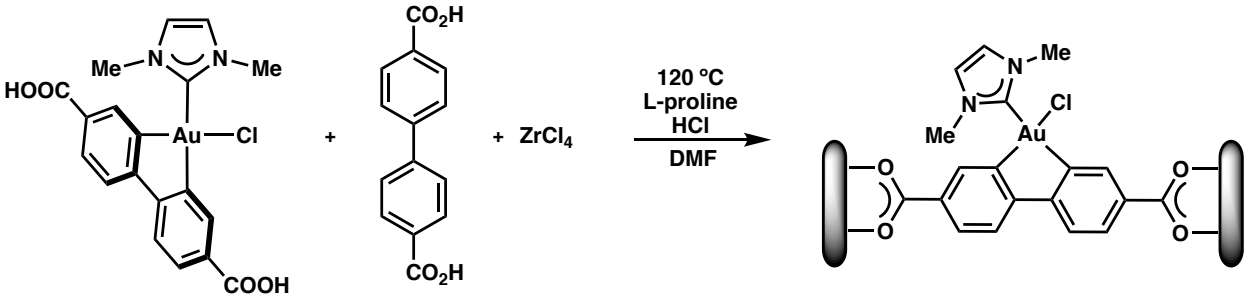

H_2BPDC Me_2ImAu(III)Cl-UiO-67

To a 1 dram vial was added Me_2ImAu(III)(H_2BPDC)Cl (5.1 mg, 0.0090 mmol, 0.4 equiv.), H_2BPDC (3.4 mg, 0.030 mmol, 0.75 equiv.), $ZrCl_4$ (5.3 mg, 0.023 mmol, 1.0 equiv.), L-proline (12.5 mg, 0.11 mmol, 4.8 equiv.), concentrated aqueous HCl (2 μL), and DMF (500 μL). The reaction mixture was capped, sonicated for 10 minutes, then heated at 120 °C in an oven for 17 h h. This yielded colorless crystals, which were washed with DMF (6 mL x 5), DCM (6 mL x 15), then $MeNO_2$ (6 mL x 5). Me_2ImAu(III)Cl-UiO-67 was immersed in $MeNO_2$ prior to SXRD analysis and chloride abstraction. 20% loading IPrAu(BPDC)Cl vs BPDC (SXRD).

$Me_2ImAu(III)SbF_6$-UiO-67 (20% Au occupancy)

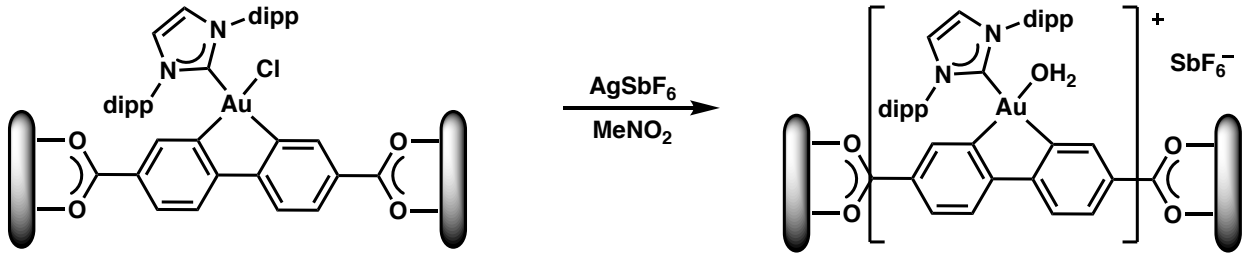

IPrAu(III)Cl-IRMOF-10 **IPrAu(III)SbF_6-IRMOF-10**

To a 2 mL vial was added $Me_2ImAu(III)Cl$-UiO-67 (20% $Me_2ImAu(BPDC)Cl$ loading, 0.2 mg, 1 equiv.) immersed in $MeNO_2$ (0.1 mL), followed by the addition of a solution of $AgSbF_6$ (0.11 M in $MeNO_2$, 0.3 mL). After 72 h, the crystals were washed with $MeNO_2$ (2 mL x 3) then DCM (2 mL x 5). $Me_2ImAu(III)SbF_6$-UiO-67 was immersed in $MeNO_2$ prior to SXRD analysis and catalysis.

IPrAu(III)Cl-IRMOF-10 (5% Au occupancy)

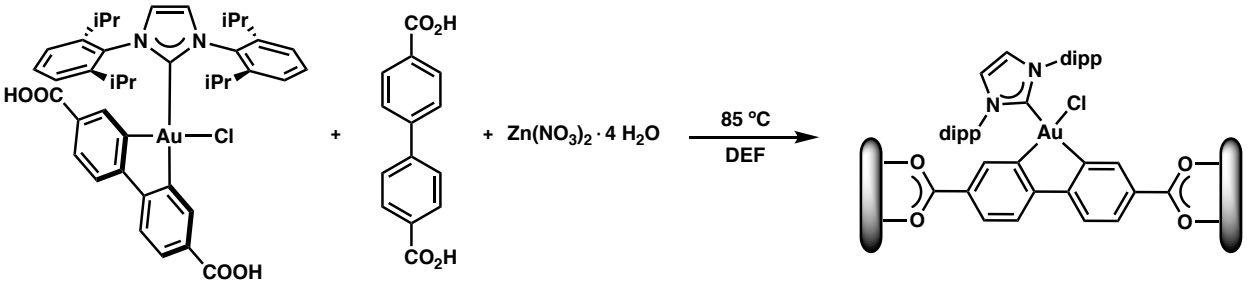

SI 8 **H_2BPDC** **IPrAu(III)Cl-IRMOF-10**

To a 2 dram vial was added SI 8 (8.6 mg, 0.010 mmol, 0.25 equiv.), H_2BPDC (7.3 mg, 0.030 mmol, 0.75 equiv.), $Zn(NO_3)_2$•4 H_2O (42 mg, 0.16 mmol, 4.0 equiv.), and diethyl formamide (2.14 mL). The reaction mixture was capped, sonicated for 5 minutes, then heated at 85°C in an oven for 24 h. This yielded yellow crystals, which were washed with DMF (6 mL x 5), DCM (6 mL x 15), then $MeNO_2$ (6 mL x 5). Due to a loss of crystallinity of IPrAu(III)Cl-IRMOF-10 in the absence of solvent, the crystals were immersed in solvent prior to $AgSbF_6$ treatment. 5% loading IPrAu(BPDC)Cl vs BPDC (digestion ^1H NMR).

IPrAu(III)SbF_6-IRMOF-10 (5% Au occupancy)

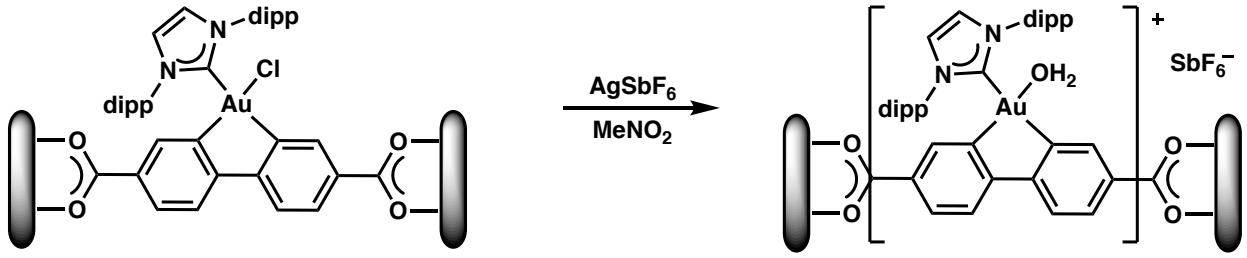

IPrAu(III)Cl-IRMOF-10 IPrAu(III)SbF_6-IRMOF-10

To a 2 mL vial was added IPrAu(III)Cl-IRMOF-10 (5% IPrAu(BPDC)Cl loading, 4 mg, 1 equiv.) immersed in $MeNO_2$ (0.1 mL), followed by the addition of a solution of $AgSbF_6$ (7 mM in $MeNO_2$, 0.13 mL, 1 equiv.). After 48 h, the crystals were washed with $MeNO_2$ (2 mL x 3) then DCM (2 mL x 5). Due to a loss of crystallinity of IPrAu(III)SbF_6-IRMOF-10 in the absence of solvent, the crystals were immersed in solvent prior to catalysis.

IPrAu(III)Cl-bio-MOF-100 (24% Au occupancy)

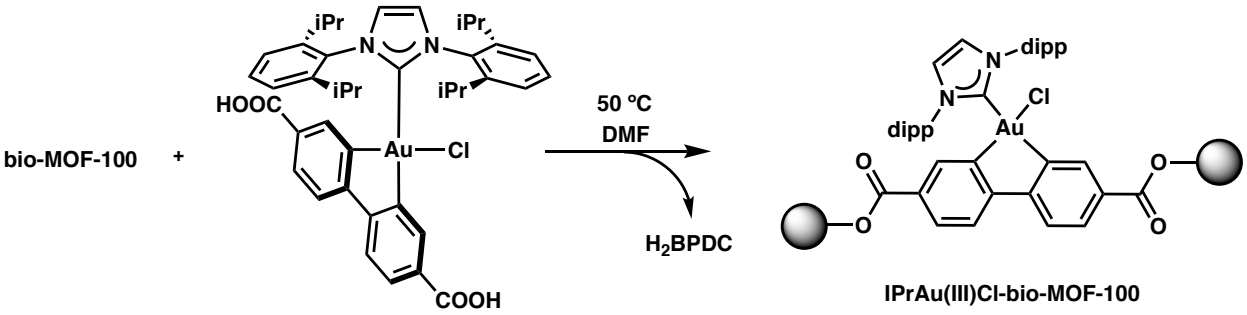

SI 8 IPrAu(III)Cl-bio-MOF-100

To a 1 dram vial was added bio-MOF-100 (20 mg), SI 8 (20 mg), and DMF (0.9 mL). The reaction mixture was capped, then heated at 50°C in an oven for 96 h. This yielded colorless crystals, which were washed with DMF (3 mL x 7), DCM (3 mL x 15), then $MeNO_2$ (3 mL x 5). Due to a loss of crystallinity of IPrAu(III)Cl-bio-MOF-100 in the absence of solvent, the crystals were immersed in solvent prior to $TlPF_6$ treatment. 16% loading IPrAu(BPDC)Cl vs BPDC was observed by digestion ^1H NMR.

IPrAu(III)PF_6-bio-MOF-100 (24% Au occupancy)

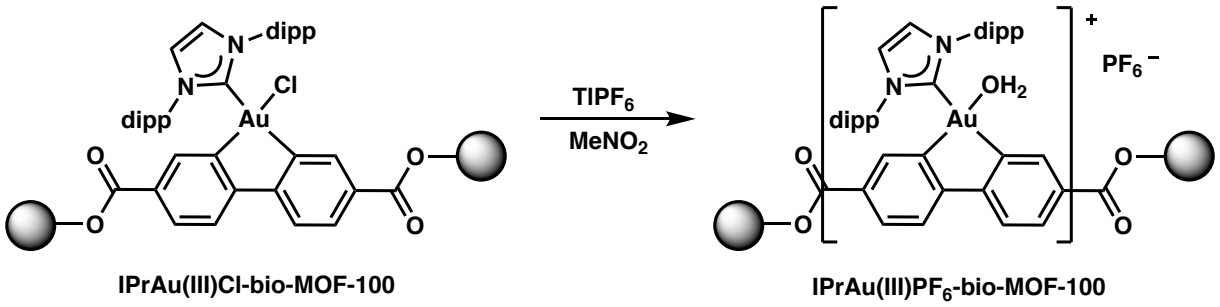

IPrAu(III)Cl-bio-MOF-100 IPrAu(III)PF_6-bio-MOF-100

To a 2 mL vial was added IPrAu(III)Cl-bio-MOF-100 (16% IPrAu(BPDC)Cl loading, 5 mg, 1 equiv.) immersed in $MeNO_2$ (0.1 mL), followed by the addition of a solution of $TlPF_6$ (15 mM in $MeNO_2$, 0.10 mL, 1 equiv.). After 48 h, the crystals were washed with $MeNO_2$ (2 mL x 3) then $CHCl_3$ (2 mL x 5). Due to a loss of crystallinity of IPrAu(III)PF_6-bio-MOF-100 in the absence of solvent, the crystals were immersed in solvent prior to catalysis.

IPrAu(III)Cl-bio-MOF-100 (40% Au occupancy)

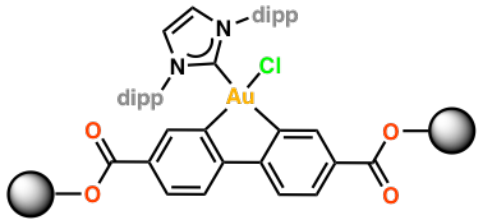

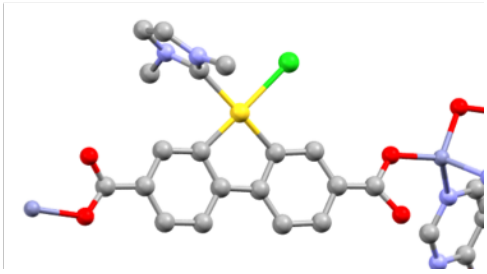

To a 2 mL vial was added IPrAu(III)Cl-bio-MOF-100 (24% IPrAu(BPDC)Cl occupancy, 1 mg), SI 8 (9 mg), and DMF (0.2 mL). The reaction mixture was capped, then heated at 50°C in an oven for 96 h. This yielded colorless crystals, which were washed with DMF (2 mL x 4), DCM (2 mL x 15), then $MeNO_2$ (2 mL x 5). Due to a loss of crystallinity of IPrAu(III)Cl-bio-MOF-100 in the absence of solvent, the crystals were immersed in solvent prior to $TlPF_6$ treatment.

IPrAu(III)PF_6-bio-MOF-100 (40% Au occupancy)

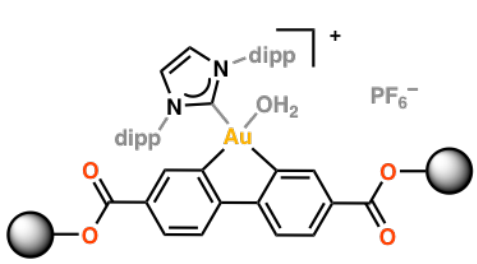

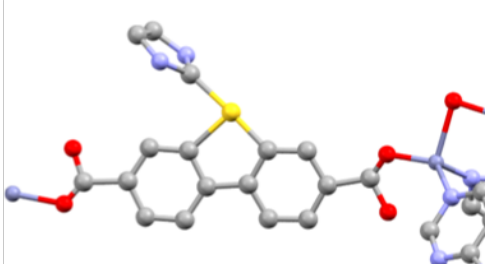

To a 2 mL vial was added IPrAu(III)Cl-bio-MOF-100 (40% IPrAu(BPDC)Cl occupancy, 1 mg, 1 equiv.) immersed in $MeNO_2$ (0.1 mL), followed by the addition of a solution of $TlPF_6$ (3 mM in $MeNO_2$, 0.14 mL, 1 equiv.). After 48 h, the crystals were washed with $MeNO_2$ (2 mL x 10).

2.4.4 Decomposition of Homogeneous Gold(III) Complexes

To a 1 dram vial was added Au(III) complex, IPrAu(III)(biphenyl)Cl or SI 9 (1 equiv.), $AgSbF_6$ (1 equiv.), and CD_2Cl_2 (4 mM). The vial was capped and sonicated for 10 minutes. The reaction mixture was passed through a glass fiber filter and collected in a 1 dram vial. For conditions in the presence of a cationic Au(I) trap, TMB (10 equiv.) was added to the reaction mixture. For conditions without TMB, $CDCl_3$ was used as solvent instead of CD_2Cl_2 and reactions mixtures were heated to 55°C. After 4 days, the reaction mixture was treated with Et_4NCl (1.3 equiv.). Conversion was determined by ^1H NMR spectroscopy. ^1H NMR spectra of IPrAu(I)Cl, biphenylene, and dimethyl biphenylene-2,7-dicarboxylate match those previously reported.[24,40,41]

2.4.5 Synthetic Procedures for Unreported 1,5-Enyne Substrates

3,5-bis((3,5-di-tert-butylbenzyl)oxy)benzaldehyde, SI 10

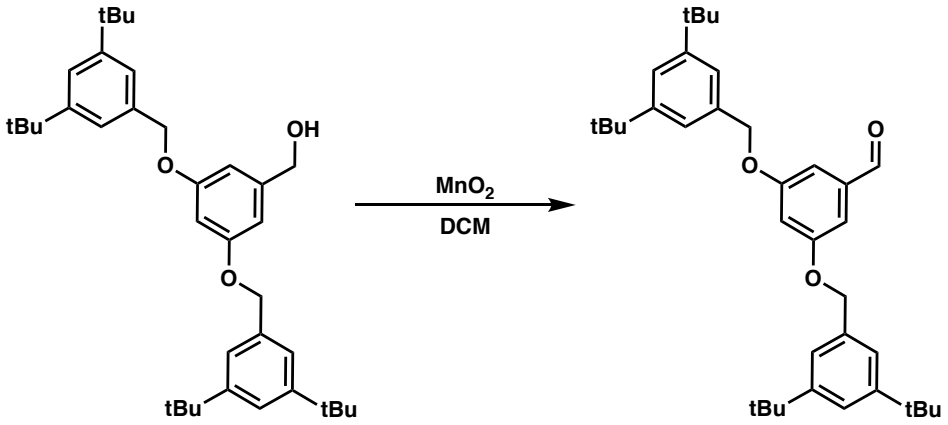

To a flame dried 20 mL vial was added (3,5-bis((3,5-di-tert-butylbenzyl)oxy)phenyl)methanol (0.85 g, 1.6 mmol, 1.0 equiv.) and DCM (12 mL, 0.13 M). Activated MnO_2 (4.0 g, 47 mmol, 30 equiv.) was then added to the reaction mixture in one portion. After stirring for 16 h, the reaction mixture was filtered through a pad of celite and concentrated under reduced pressure to yield the title compound as a white solid, which was used in the subsequent reaction without further purification.

1-(3,5-bis((3,5-di-tert-butylbenzyl)oxy)phenyl)prop-2-yn-1-yl acetate, SI 11

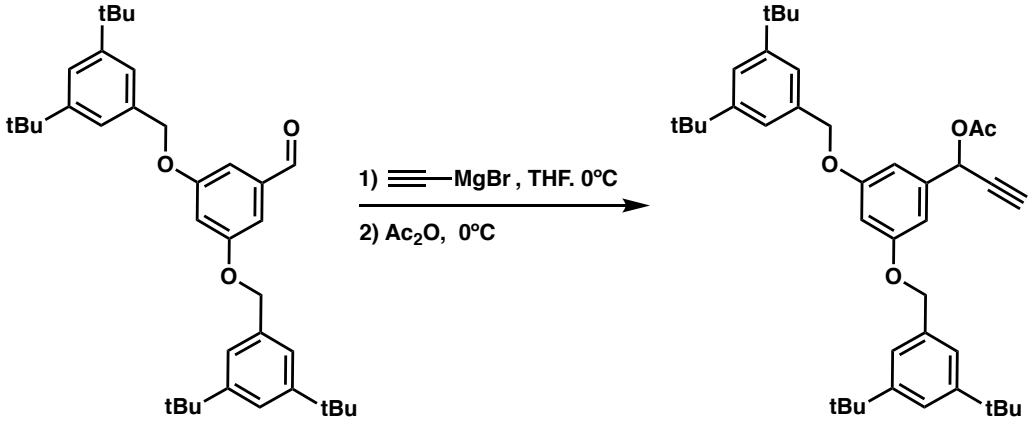

To a flame dried 2 dram vial was added **SI 10** (0.20 g, 0.37 mmol, 1 equiv.) and THF (2.2 mL, 0.17 M). The reaction mixture was cooled to 0°C, and a solution of ethynylmagnesium bromide (0.5 M in THF, 1.1 mL, 1.5 equiv.) was added in a dropwise fashion. The reaction mixture was stirred warming to room temperature for 1 h. The reaction mixture was then cooled to 0°C, and acetic anhydride (0.090 mL, 0.95 mmol, 2.6 equiv) was added in a dropwise fashion. The reaction mixture was stirred warming to room temperature for 1 h, quenched with a saturated aqueous NH_4Cl solution, extracted three times with DCM (5 mL x 3), dried over sodium sulfate,

filtered, and concentrated under reduced pressure to yield the title compound as a white solid, which was used in the subsequent reaction without further purification.

5,5'-(((5-(hex-5-en-1-yn-3-yl)-1,3-phenylene)bis(oxy))bis(methylene))bis(1,3-di-tert-butylbenzene), 12

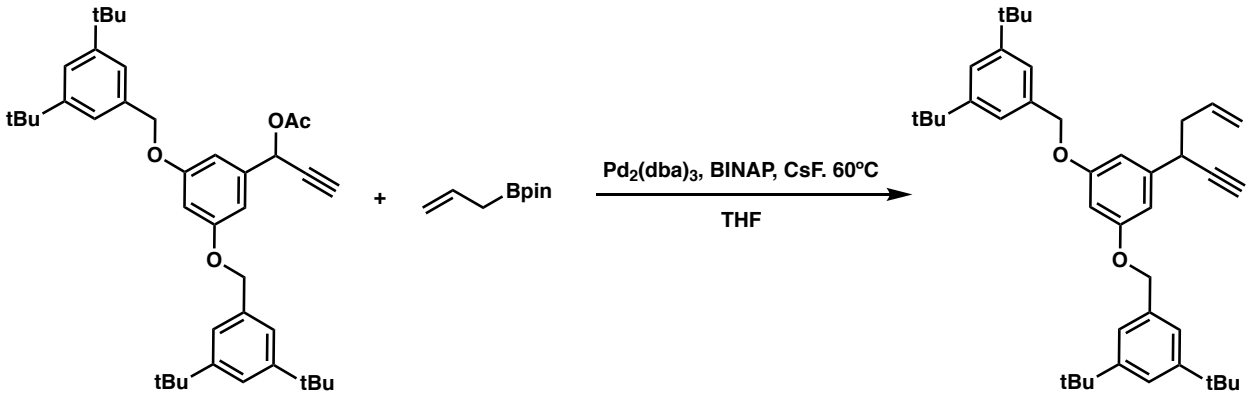

The title compound was synthesized according to a modification of a literature procedure.[42] To a flame dried 1 dram vial was added $Pd_2(dba)_3$ (5.5 mg, 0.006 mmol, 0.02 equiv.), BINAP (7.5 mg, 0.012 mmol, 0.04 equiv.), and THF (0.2 mL), and the reaction mixture was stirred for 5 min. To the reaction mixture was added a solution of **SI 11** (0.38 M in THF, 0.80 mL, 1 equiv.), CsF (0.15 g, 0.99 mmol, 3.3 equiv.), and allylboronic acid pinacol ester (0.068 mL, 0.36 mmol, 1.2 equiv.). The reaction mixture was then stirred at 60°C for 14 h, diluted with Et_2O (10 mL), passed through a pad of silica, then concentrated under reduced pressure. The crude product was then purified by column chromatography (50:1 Hexanes/EtOAc), yielding the title compound as a white solid (0.16 g, 90%).

^{1}H NMR (500 MHz, Methylene Chloride-d_2) δ 7.47 (t, J = 1.8 Hz, 2H), 7.34 (d, J = 1.9 Hz, 4H), 6.69 (d, J = 2.2 Hz, 2H), 6.61 (t, J = 2.3 Hz, 1H), 5.89 (ddt, J = 17.2, 10.2, 7.0 Hz, 1H), 5.15 – 5.07 (m, 2H), 3.70 (td, J = 7.1, 2.5 Hz, 1H), 2.56 (tt, J = 7.1, 1.3 Hz, 2H), 2.38 (d, J = 2.4 Hz, 1H), 1.39 (s, 36H)

^{13}C NMR (151 MHz, Methylene Chloride-d_2) δ 160.66, 151.57, 143.62, 136.44, 135.68, 122.79, 122.62, 117.32, 107.16, 100.78, 85.59, 71.85, 71.40, 42.56, 38.28, 35.22, 31.70

HRMS (EI+) m/z calcd: 592.4280, found: 592.4279

IR (neat, cm^{-1}) 3310, 2954, 2867, 1593, 1458, 1393, 1363, 1286, 1248, 1202, 1156, 1054, 994, 916, 894, 869, 830, 738, 711, 693, 634, 533

3,5-bis((3,5-bis((3,5-di-tert-butylbenzyl)oxy)benzyl)oxy)benzaldehyde, SI 12

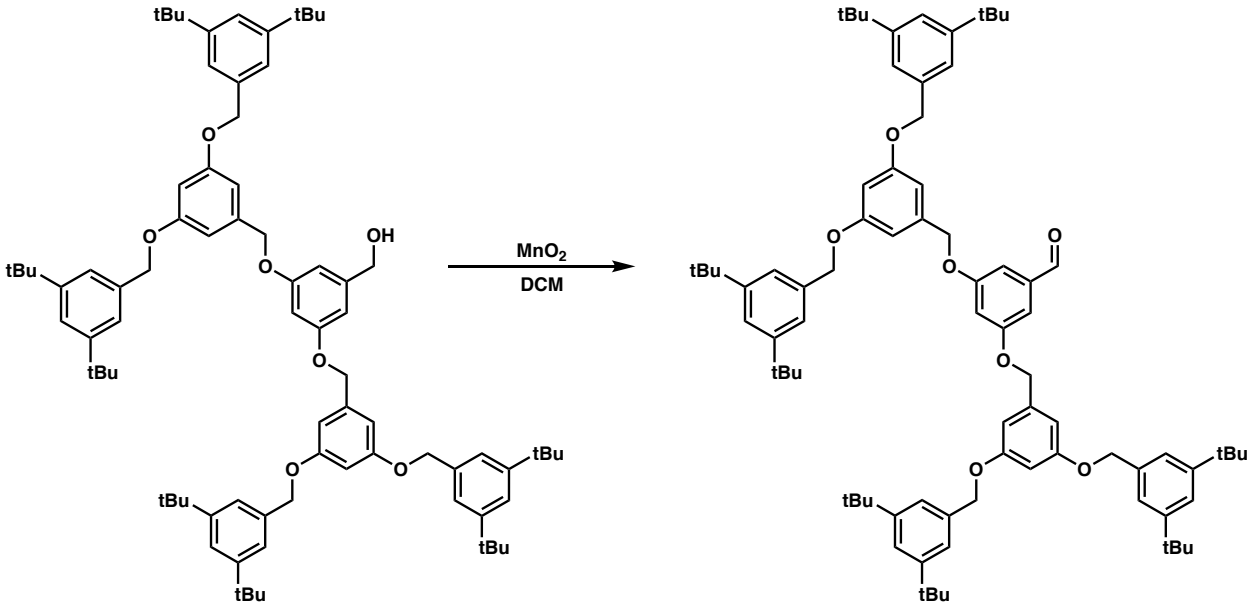

To a flame dried 2 dram vial was added (3,5-bis((3,5-di-tert-butylbenzyl)oxy)phenyl)methanol (0.29 g, 0.25 mmol, 1.0 equiv.) and DCM (4 mL, 0.06 M). Activated MnO_2 (0.65 g, 7.5 mmol, 30 equiv.) was then added to the reaction mixture in one portion. After stirring for 12 h, the reaction mixture was filtered through a pad of celite and concentrated under reduced pressure to yield the title compound as a white solid, which was used in the subsequent reaction without further purification.

1-(3,5-bis((3,5-bis((3,5-di-tert-butylbenzyl)oxy)benzyl)oxy)phenyl)prop-2-yn-1-ol, SI 13

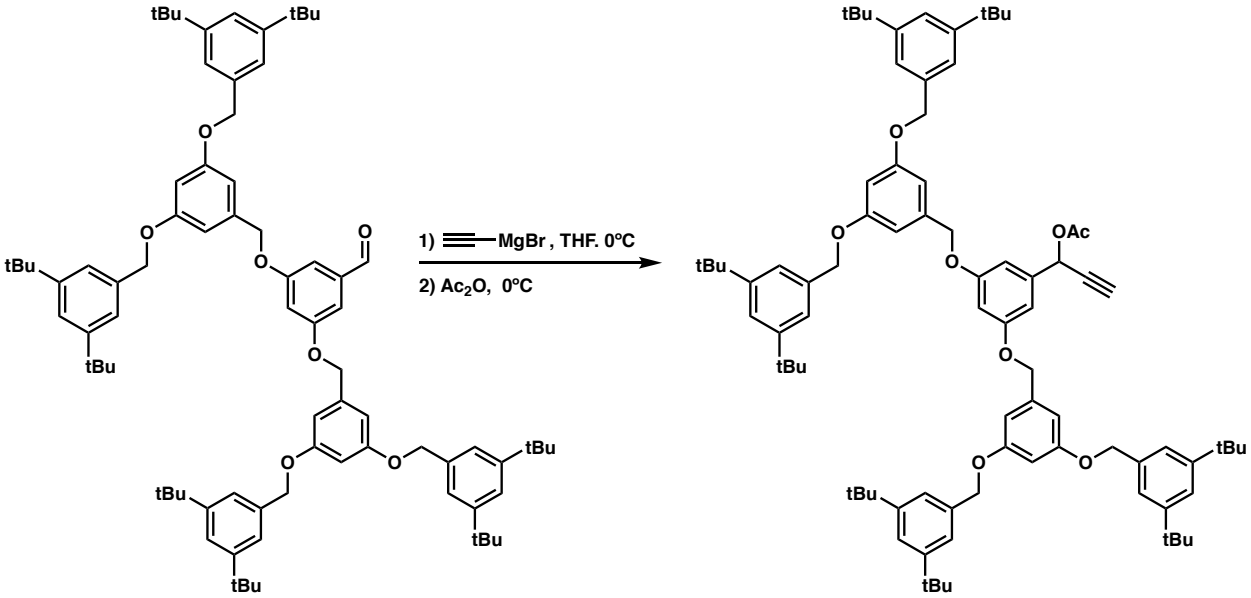

To a flame dried 1 dram vial was added **SI 12** (0.21 g, 0.18 mmol, 1 equiv.) and THF (1.5 mL, 0.12 M). The reaction mixture was cooled to 0°C, and a solution of ethynylmagnesium bromide (0.5 M in THF, 0.54 mL, 1.5 equiv.) was added in a dropwise fashion. The reaction mixture was stirred warming to room temperature for 1 h. The reaction mixture was then cooled to 0°C, and acetic anhydride (0.034 mL, 0.36 mmol, 2.0 equiv) was added in a dropwise fashion. The reaction mixture was stirred warming to room temperature for 1 h, quenched with a saturated aqueous NH_4Cl solution, extracted three times with DCM (5 mL x 3), dried over sodium sulfate, filtered, and concentrated under reduced pressure to yield the title compound as a white solid, which was used in the subsequent reaction without further purification.

5,5',5'',5'''-((((((5-(hex-5-en-1-yn-3-yl)-1,3-phenylene)bis(oxy))bis(methylene))bis(benzene-5,1,3-triyl))tetrakis(oxy))tetrakis(methylene))tetrakis(1,3-di-tert-butylbenzene), 13

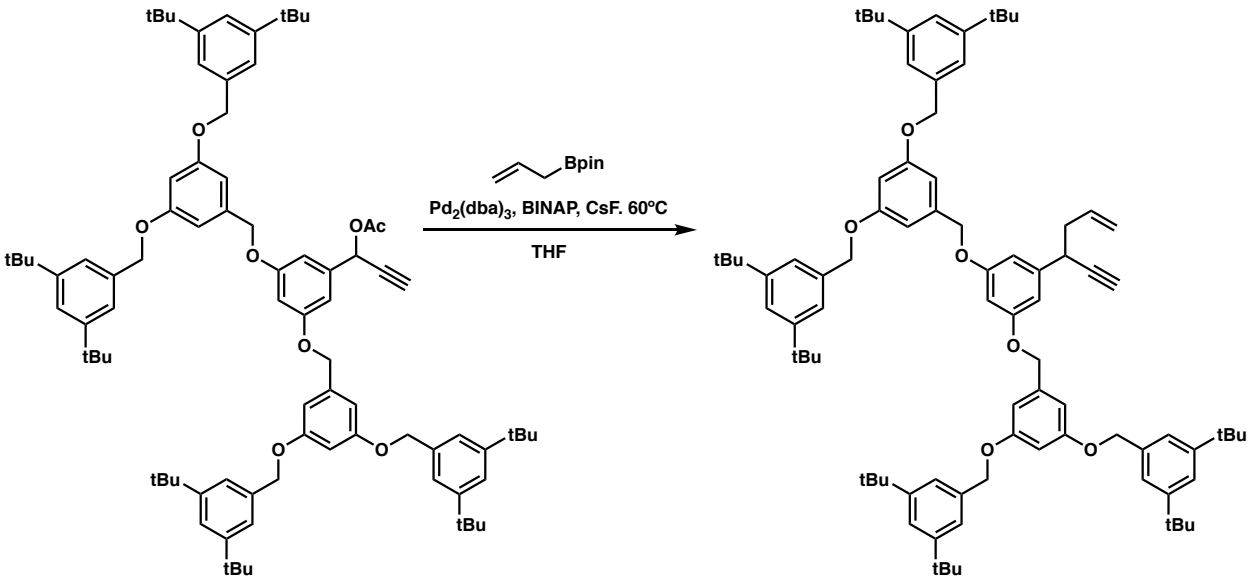

The title compound was synthesized according to a modification of a literature procedure.[42] To a flame dried 1 dram vial was added $Pd_2(dba)_3$ (3.3 mg, 0.0036 mmol, 0.02 equiv.), BINAP (4.5 mg, 0.0072 mmol, 0.04 equiv.), and THF (0.2 mL), and the reaction mixture was stirred for 5 min. To the reaction mixture was added a solution of **SI 13** (0.14 M in THF, 1.3 mL, 1 equiv.), CsF (0.082 g, 0.54 mmol, 3.0 equiv.), and allylboronic acid pinacol ester (0.042 mL, 0.22 mmol, 1.2 equiv.). The reaction mixture was then stirred at 60°C for 13 h, diluted with Et_2O (10 mL), passed through a pad of silica, then concentrated under reduced pressure. The crude product was then purified by column chromatography (30:1 Hexanes/EtOAc), yielding the title compound as a white solid (0.085 g, 38%).

^{1}H NMR (500 MHz, Methylene Chloride-d_2) δ 7.44 (t, J = 1.9 Hz, 4H), 7.31 (d, J = 1.9 Hz, 8H), 6.75 (d, J = 2.3 Hz, 4H), 6.67 (d, J = 2.3 Hz, 2H), 6.65 (t, J = 2.3 Hz, 2H), 6.55 (t, J = 2.3 Hz, 1H), 5.86 (ddt, J = 17.2, 10.1, 6.9 Hz, 1H), 5.13 – 5.05 (m, 2H), 5.03 (s, 12H), 3.68 (td, J = 7.1, 2.5 Hz, 1H), 2.58 – 2.49 (m, 2H), 2.36 (d, J = 2.5 Hz, 1H), 1.36 (s, 72H)

^{13}C NMR (151 MHz, Methylene Chloride-d_2) δ 160.84, 160.39, 151.55, 143.70, 139.80, 136.34, 135.60, 122.81, 122.62, 117.34, 107.26, 106.83, 101.75, 100.84, 85.50, 71.90, 71.44, 70.48, 42.54, 38.24, 35.19, 31.65

HRMS (ESI+) m/z calcd for $C_{86}H_{112}O_6Na$ $[M+Na]^+$: 1263.8351, found: 1263.8384

IR (neat, cm^{-1}) 2954, 2867, 1594, 1457, 1363, 1292, 1249, 1203, 1156, 1053, 895, 870, 832, 738, 712, 684

2.4.6 Synthesis of Bicyclo[3.1.0]hexene Products by Homogeneous Gold(III) Catalysis

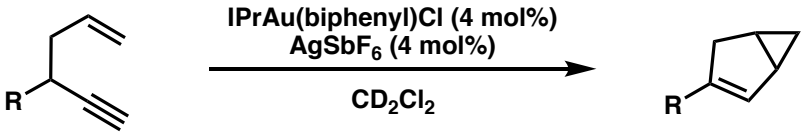

To a 1 dram vial was added IPrAu(biphenyl)Cl (0.04 equiv.), $AgSbF_6$ (0.04 equiv.), and CD_2Cl_2 (0.07 M). The vial was capped and sonicated for 10 minutes. The reaction mixture was passed through a glass fiber filter and collected in a 1 dram vial. 1,5-enyne (1 equiv.) was then added to the reaction mixture, and the mixture was allowed to stir for 22 h to achieve full conversion, which was determined by ^{1}H NMR spectroscopy. The product was then isolated by column chromatography (30:1 hexanes/ethyl acetate).

3-(3,5-bis((3,5-di-tert-butylbenzyl)oxy)phenyl)bicyclo[3.1.0]hex-2-ene, SI 14

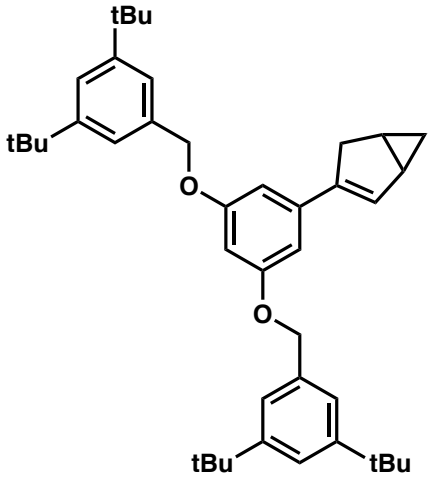

The title compound was prepared according to the general procedure.

^{1}H NMR (600 MHz, Methylene Chloride-d_2) δ 7.42 (q, J = 1.7 Hz, 2H), 7.29 (t, J = 1.5 Hz, 4H), 6.63 (t, J = 1.7 Hz, 2H), 6.52 (t, J = 2.0 Hz, 1H), 6.40 (t, J = 1.9 Hz, 1H), 4.99 (s, 4H), 2.96 (dd, J = 17.0, 7.3 Hz, 1H), 2.69 (d, J = 16.8 Hz, 1H), 1.93 (tt, J = 6.1, 3.2 Hz, 1H), 1.72 (quint, J = 6.9 Hz, 1H), 1.34 (s, J = 1.4 Hz, 36H), 0.93 (td, J = 7.6, 3.6 Hz, 1H), 0.06 (q, J = 3.8 Hz, 1H)

^{13}C NMR (151 MHz, Methylene Chloride-d_2) δ 160.49, 151.53, 140.18, 139.02, 136.49, 130.78, 122.76, 122.57, 105.00, 100.85, 71.37, 36.83, 35.18, 31.63, 24.39, 17.76, 15.82

HRMS (EI+) m/z calcd: 592.4280, found: 592.4282

IR (neat, cm^{-1}) 2954, 2866, 1698, 1585, 1437, 1393, 1363, 1248, 1201, 1154, 1052, 992, 895, 869, 826, 769, 737, 713, 684, 535

3-(3,5-bis((3,5-bis((3,5-di-tert-butylbenzyl)oxy)benzyl)oxy)phenyl)bicyclo[3.1.0]hex-2-ene, SI 15

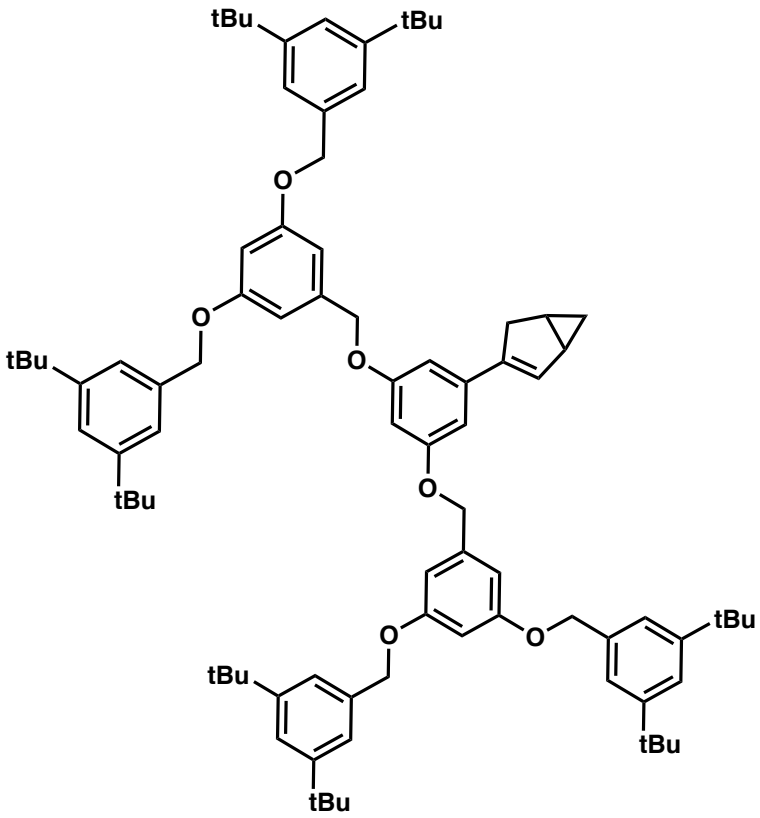

The title compound was prepared according to the general procedure.

^{1}H NMR (600 MHz, Methylene Chloride-d_2) δ 7.44 (t, J = 1.8 Hz, 4H), 7.31 (d, J = 1.8 Hz, 8H), 6.74 (d, J = 2.2 Hz, 4H), 6.67 – 6.62 (m, 4H), 6.51 (t, J = 2.3 Hz, 1H), 6.41 (d, J = 2.3 Hz, 1H), 5.02 (s, 9H), 2.98 (dd, J = 17.0, 7.3 Hz, 1H), 2.75 – 2.66 (m, 1H), 1.94 (td, J = 6.9, 6.5, 2.9 Hz, 1H), 1.73 (quint, J = 7.2 Hz, 1H), 1.35 (s, 72H), 0.94 (td, J = 7.6, 3.7 Hz, 1H), 0.08 (q, J = 3.7 Hz, 1H)

^{13}C NMR (151 MHz, Methylene Chloride-d_2) δ 160.84, 160.25, 151.56, 140.10, 139.93, 139.15, 136.35, 130.97, 122.80, 122.62, 106.77, 105.07, 101.74, 100.91, 71.44, 70.42, 36.84, 35.19, 31.65, 24.45, 17.80, 15.88

HRMS (ESI+) m/z calcd for $C_{86}H_{113}O_6$ $[M+H]^+$: 1241.8352, found: 1241.8567

IR (neat, cm^{-1}) 2954, 2867, 1594, 1450, 1363, 1292, 1249, 1202, 1155, 894, 870, 829, 776, 738, 711, 683

2.4.7 General Procedures for Catalysis with Au(III)-MOFs

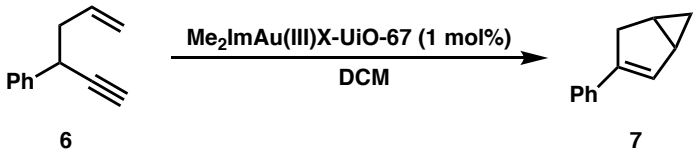

6 7

To a 2 mL vial was added Me_2ImAu(III)Cl-UiO-67 (6% Me_2ImAu(BPDC)Cl loading, 5.0 mg) followed by the addition of a solution of silver salt (0.11 M in $MeNO_2$, 0.3 mL). After 72 h, the crystals were washed with $MeNO_2$ (2 mL x 3) then DCM (2 mL x 5). The crystals were then immersed in DCM (0.3 mL), followed by the addition of 1,5-enyne (1 equiv.). After 22 h, the organic supernatant was removed with DCM (2 mL x 5). Conversion was determined by ^{1}H NMR spectroscopy. ^{1}H NMR spectra of product **7** match those previously reported.[34] For control experiments, an equivalent amount of Me_2ImAu(III)Cl-UiO-67, UiO-67, and/or silver salt was used instead of Me_2ImAu(III)X-UiO-67.

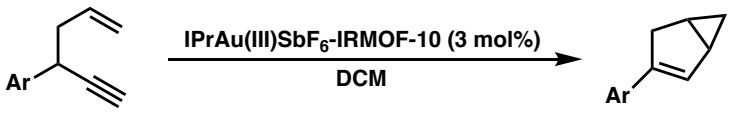

To a 2 mL vial was added IPrAu(III)SbF_6-IRMOF-10 (5% IPrAu(BPDC)Cl loading, 0.03 equiv.) immersed in DCM (0.3 mL), followed by the addition of 1,5-enyne (1 equiv.). After 22 h, the organic supernatant was removed with DCM (2 mL x 5). The washed IPrAu(III)SbF_6-IRMOF-10 crystals were resubjected to the same conditions for recyclability studies. Conversion was determined by ^{1}H NMR spectroscopy. No additional conversion was detected in the supernatant upon removal of IPrAu(III)SbF_6-IRMOF-10. ^{1}H NMR spectra of products **xx** and **xx** match those previously reported.[34] For control experiments, an equivalent amount of IPrAu(III)Cl-IRMOF-10 or IRMOF-9 was used instead of IPrAu(III)SbF_6-IRMOF-10.

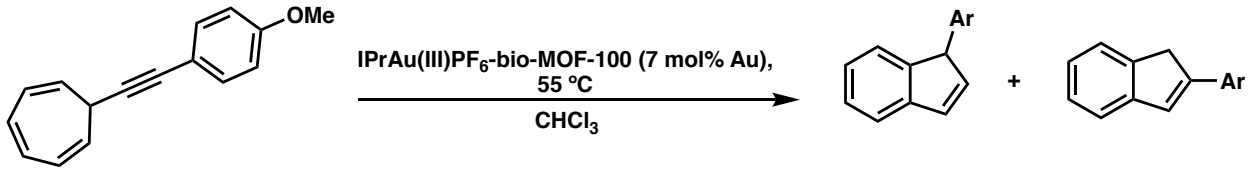

8 9 10

To a 2 mL vial was added IPrAu(III)PF_6-bio-MOF-100 (16% IPrAu(BPDC)Cl loading, 5 mg, 0.0015 mmol, 0.07 equiv.) immersed in DCM (0.1 mL), followed by the addition of substrate **8** (5 mg, 0.022 mmol, 1 equiv.). After heating the reaction mixture at 55°C for 46 h, the organic supernatant was removed with DCM (2 mL x 5). The washed IPrAu(III)PF_6-bio-MOF-100 crystals were resubjected to the same conditions for recyclability studies. Conversion was determined by ^{1}H NMR spectroscopy. ^{1}H NMR spectra of products **9** and **10** match those

previously reported.[32] For control experiments, an equivalent amount of IPrAu(III)Cl-bio-MOF-100 or bio-MOF-100 was used instead of IPrAu(III)PF_6-bio-MOF-100.

2.4.8 Digestion ^{1}H NMR Analysis of Au(III)Cl-MOFs

To a 2 ml vial was added Au(III)Cl-MOF (2 mg), DMSO-d_6 (0.40 mL), and a solution of DCl (25 wt% in D_2O, 0.020 mL). The mixture was sonicated for 10 minutes to digest the crystals. The resulting transparent solution was then used to obtain a ^{1}H NMR spectrum. For Au(III)X-MOF samples analyzed after halide abstraction, the crystals were first treated with a solution of Et_4NCl (0.05 M, 5 equiv. relative to Au) for 2 days, washed with $MeNO_2$ (2 mL x 3) and DCM (2 mL x 5), then dried under reduced pressure prior to digestion. ^{1}H NMR spectra were taken with Bruker spectrometers operating at 500 MHz.

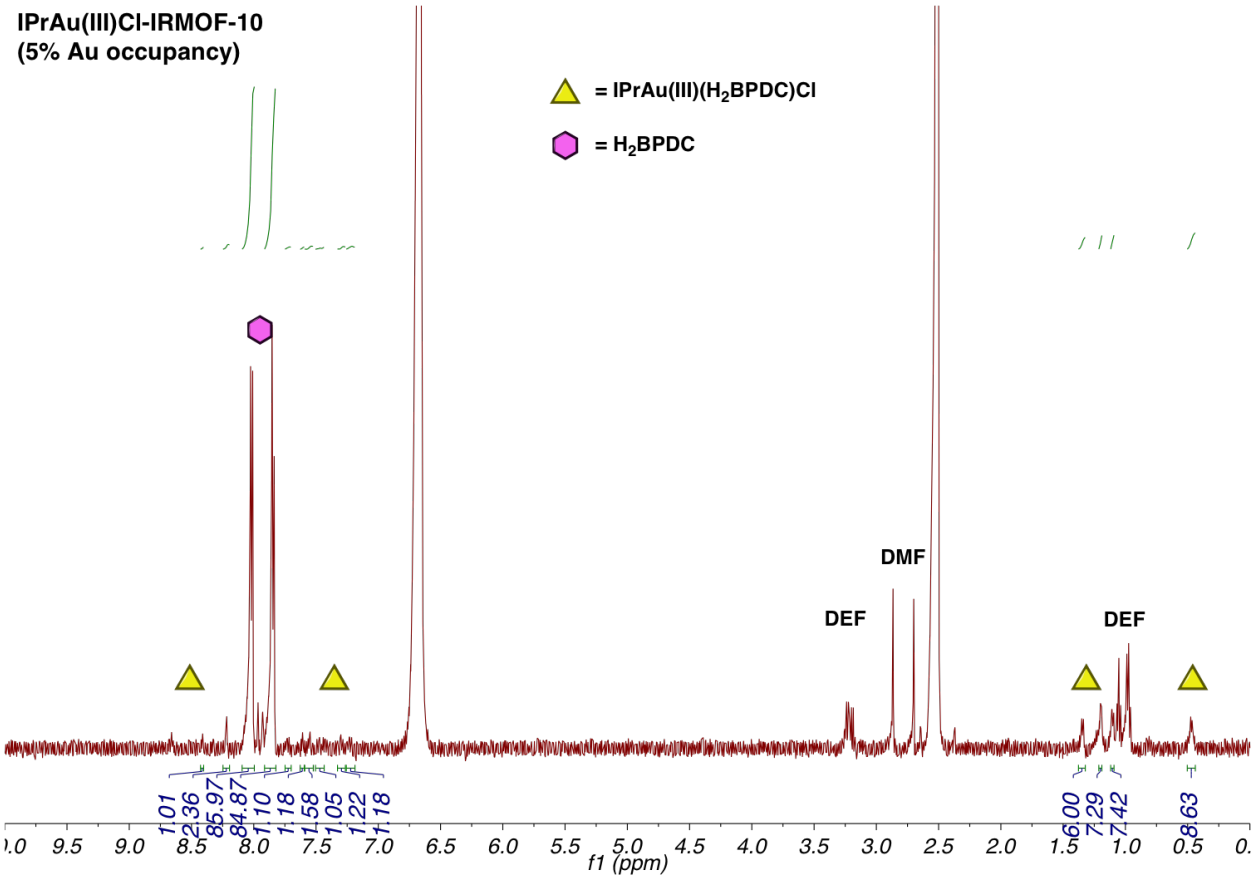

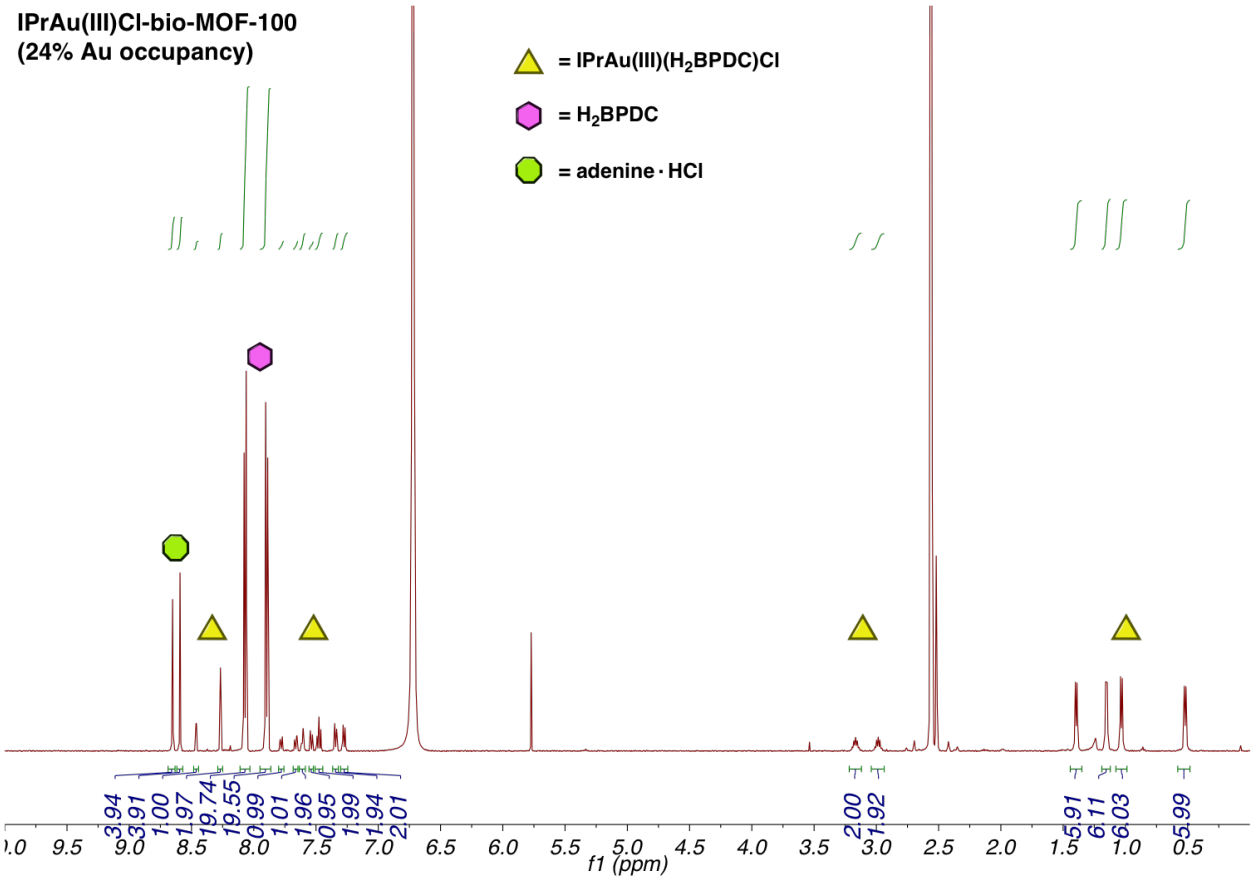
IPrAu(III)Cl-bio-MOF-100
(24% Au occupancy)
= IPrAu(III)(H2BPDC)Cl
= H2BPDC
= adenine · HCl
3.94
3.91
1.00
1.97
19.74
19.55
0.99
1.01
1.96
0.95
1.99
1.94
2.01
2.00
1.92
5.91
6.11
6.03
5.99
f1 (ppm)

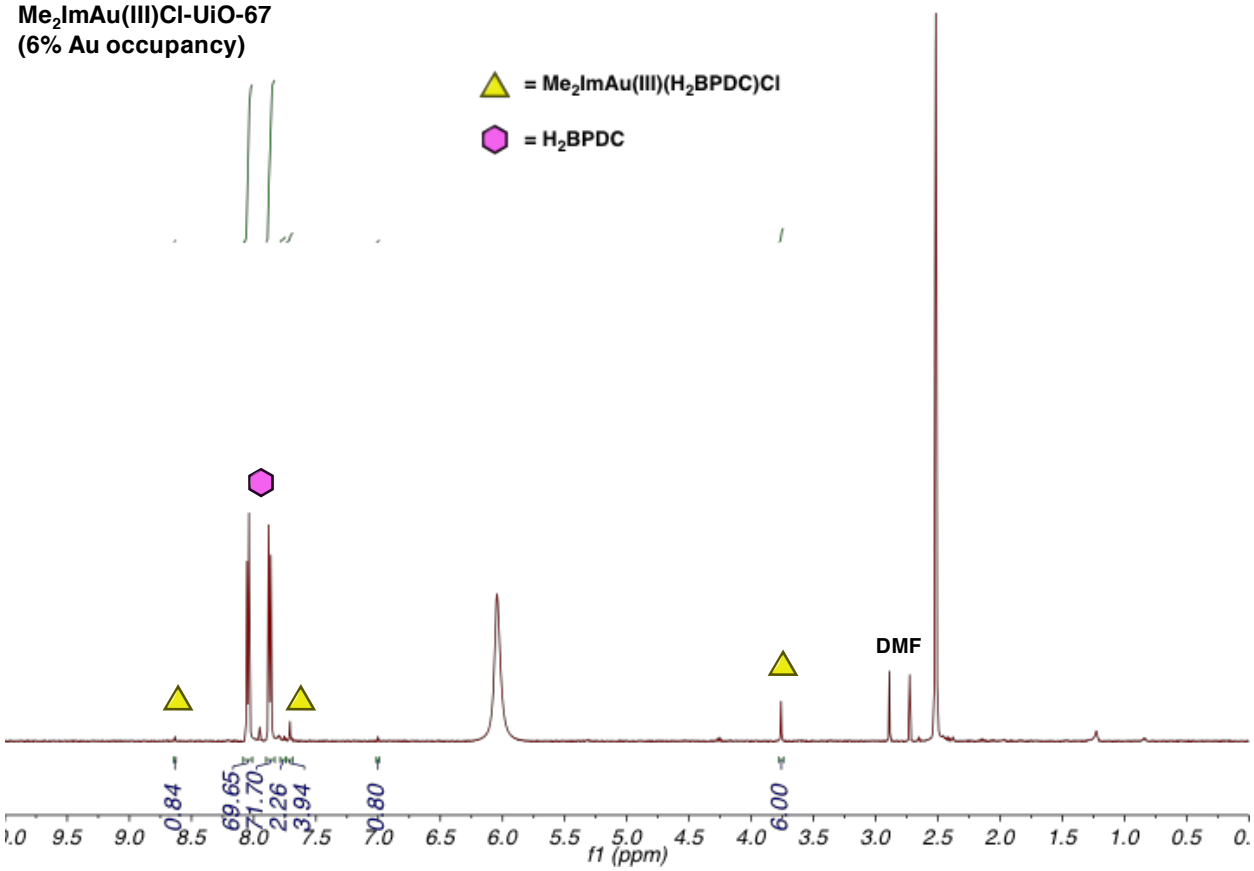
Me2ImAu(III)Cl-UiO-67
(6% Au occupancy)
= Me2ImAu(III)(H2BPDC)Cl
= H2BPDC
DMF
0.84
69.65
71.70
2.26
3.94
0.80
6.00
f1 (ppm)

2.4.9 Single Crystal X-ray Diffraction Data and Analysis

For all samples, the raw data were processed with the Bruker APEX3 software package. The data were first integrated using the SAINT procedure and then corrected for absorption with SADABS procedure. The structures were solved by direct methods (SHELXT-2015) and the refinement was done by full-matrix least squares on F^2 (SHELXL-2014), using the Olex2 software package.[43,44] Mercury software was used for structure visualization.[45]

Table S1. Crystal data, data collection, and structure refinement parameters for **MOF-520-1**.

Name	**MOF-520-1**
Chemical composition	$C_{65.09}H_{37.13}Al_4I_{1.04}O_{18.76}$
Formula mass	1359.64
Crystal system	Tetragonal
Space group	$P4_32_12$
a, Å	19.3244(8)
c, Å	70.518(3)
V, Å^3	26334(2)
d, g cm^{-3}	0.686
μ, mm^{-1}	2.545
Z	8
Measured reflections	89988
Independent reflections	17690
Observed reflections	13405
θ_{min} , º	2.960
θ_{max} , º	57.089
h	-21 to 16

k	-20 to 19
l	-76 to 45
R int	0.1171
R [$F^2>2\sigma(F^2)$]	0.1268
$wR(F^2)$	0.3187
S	1.265
Parameters	860
Restraints	36
$\Delta\rho_{max}$, e Å^{-3}	1.627
$\Delta\rho_{min}$, e Å^{-3}	-0.777
Crystal size, μm^3	80 x 80 x 60
Radiation, Å	Cu/Ka
Temperature, K	273

Table S2. Atomic coordinates of **MOF-520-1**.

Al1	-0.89417(15)	-0.09799(16)	-0.04166(4)
Al3	-0.85966(16)	-0.10461(15)	0.03829(4)
Al4	-0.83379(15)	-0.15528(15)	0.00036(4)
Al5	-0.99482(15)	0.02893(16)	-0.05675(4)
O3	-0.7986(4)	-0.1805(4)	0.04316(9)
O3AA	-0.8134(4)	-0.1513(4)	-0.04346(9)
O11	-0.7562(4)	-0.1506(4)	-0.01599(9)

O15	-0.7834(4)	-0.2255(4)	0.01434(9)
C16	-0.6926(6)	-0.1473(7)	-0.04485(16)
C20	-0.7681(7)	-0.2970(6)	0.04104(15)
C22	-0.1414(6)	0.0220(7)	-0.06173(15)
C23	-0.9569(6)	-0.8464(6)	0.05080(14)
C24	-0.7829(6)	-0.2291(6)	0.03232(14)
C26	-0.6084(7)	-0.5690(6)	0.14969(15)
C27	-0.9125(6)	-0.7863(6)	0.05468(16)
C28	-0.7019(7)	-0.6044(7)	0.12888(17)
H28	-0.7422	-0.6298	0.127
C29	-0.8939(9)	-0.6625(7)	0.0574(2)
H29	-0.9109	-0.6178	0.0561
C30	-0.7861(8)	-0.6143(6)	0.07167(18)
C31	-0.7588(5)	-0.1497(5)	-0.03352(14)
C32	-0.5767(7)	-0.5678(6)	0.16876(14)
C33	-0.6698(8)	-0.6045(7)	0.14674(19)
H33	-0.69	-0.6287	0.1567
C35	-0.7103(8)	-0.5024(6)	0.08541(18)
H35	-0.6848	-0.4649	0.0898
C36	-0.7861(8)	-0.5500(7)	0.06220(18)
H36	-0.8122	-0.5448	0.0512
C37	-0.7579(8)	-0.3570(6)	0.03040(16)
H37	-0.7564	-0.3539	0.0172
C38	-0.7489(8)	-0.4960(6)	0.06869(16)

C39	-0.7518(8)	-0.4265(6)	0.05855(17)
C40	-0.7490(8)	-0.6184(7)	0.08838(18)
H40	-0.7502	-0.6595	0.0952
C41	-0.5726(7)	-0.1461(9)	-0.0664(2)
C42	-0.7607(9)	-0.3668(7)	0.06950(17)
H42	-0.7611	-0.37	0.0827
C43	-0.4647(7)	-0.2962(8)	-0.16048(17)
C44	-0.4587(7)	-0.2233(9)	-0.1259(2)
C45	-0.4303(8)	-0.2325(8)	-0.1592(2)
H45	-0.4097	-0.2136	-0.1699
C46	-0.2014(7)	-0.0792(8)	-0.0763(2)
H46	-0.1589	-0.1013	-0.0776
C47	-0.7096(8)	-0.5633(6)	0.09541(17)
C48	-0.4480(7)	-0.1177(11)	-0.0731(2)
H48	-0.4458	-0.0954	-0.0614
C49	-0.8038(8)	-0.7411(7)	0.0669(2)
H49	-0.7594	-0.7489	0.0715
C50	-0.6956(7)	-0.1424(8)	-0.06421(17)
H50	-0.7384	-0.1386	-0.0702
C51	-0.4645(6)	-0.3357(7)	-0.17766(16)
C52	-0.5697(7)	-0.1516(11)	-0.0469(2)
H52	-0.5272	-0.1572	-0.0409
C53	-0.7500(8)	-0.4210(6)	0.03895(17)
H53	-0.7435	-0.4603	0.0316

C54	-0.6132(8)	-0.5321(7)	0.11723(17)
H54	-0.5933	-0.5071	0.1074
C55	-0.2057(6)	-0.0148(8)	-0.06809(18)
C57	-0.2685(7)	0.0160(9)	-0.0651(2)
H57	-0.2703	0.0596	-0.0596
C58	-0.9349(8)	-0.7189(6)	0.0520(2)
H58	-0.9779	-0.711	0.0465
C59	-0.2618(7)	-0.1101(10)	-0.0824(2)
H59	-0.2586	-0.1513	-0.0892
C60	-0.7688(8)	-0.3027(6)	0.06091(18)
H60	-0.7747	-0.2634	0.0683
C62	-0.5078(9)	-0.1489(12)	-0.0783(2)
C63	-0.6382(8)	-0.1429(11)	-0.0746(2)
H63	-0.6418	-0.1412	-0.0877
C64	-0.3281(7)	-0.0160(11)	-0.0702(2)
H64	-0.3706	0.0052	-0.0681
C65	-0.8288(8)	-0.6729(6)	0.06468(19)
C66	-0.6736(7)	-0.5665(6)	0.11394(16)
C67	-0.4965(8)	-0.3228(9)	-0.14392(19)
H67	-0.5174	-0.3662	-0.144
C68	-0.4535(8)	-0.1844(10)	-0.1079(2)
C69	-0.3246(8)	-0.0839(10)	-0.0791(2)
C70	-0.8466(8)	-0.7969(6)	0.0621(2)
H70	-0.8307	-0.8418	0.064

C71	-0.4265(8)	-0.1976(9)	-0.1421(2)
H71	-0.4021	-0.1562	-0.1415
C72	-0.4956(9)	-0.2823(9)	-0.12748(19)
H72	-0.5217	-0.2967	-0.1171
C73	-0.6296(7)	-0.1489(10)	-0.03621(18)
H73	-0.6269	-0.148	-0.023
C74	-0.5800(8)	-0.5329(7)	0.13480(16)
H74	-0.5386	-0.509	0.1364
C77	-0.5125(7)	-0.1812(10)	-0.0959(2)
H77	-0.5542	-0.2007	-0.0998
C79	-0.3901(7)	-0.1181(11)	-0.0845(2)
C85	-0.3937(7)	-0.1530(10)	-0.1018(2)
H85	-0.3546	-0.155	-0.1095
O2	-0.9741(3)	-0.0464(3)	-0.04141(8)
O6	-0.8832(4)	-0.0966(4)	-0.01558(9)
O8	-0.5211(4)	-0.5357(4)	0.17094(9)
O10	-0.1493(4)	0.0839(4)	-0.05619(10)
O12	-0.6085(4)	-0.5994(4)	0.18171(10)
O13	-0.4419(4)	-0.3089(4)	-0.19237(11)
O17	-0.4877(4)	-0.3975(4)	-0.17640(9)
O18	-0.0850(4)	-0.0109(4)	-0.06243(10)
O21	-1.0183(4)	-0.8344(4)	0.04500(10)
O22	-0.9325(4)	-0.9049(4)	0.05410(11)
O4AA	-0.9025(4)	-0.1558(4)	0.01883(9)

O7	-0.8034(4)	-0.0832(4)	0.01692(9)
C11	-0.7102(10)	0.0037(11)	0.0107(3)
C19	-0.7852(9)	-0.0139(9)	0.0110(3)
H19A	-0.8085	0.0185	0.0193
H19B	-0.8035	-0.0068	-0.0017
I1	-0.47474(13)	0.03079(18)	-0.02839(4)
I0AA	-1.0252(3)	-0.0252(3)	0
C21	-0.6605(11)	-0.0375(14)	0.0194(5)
H21	-0.6732	-0.0785	0.0254
C1AA	-0.5703(12)	0.0453(12)	0.0119(4)
C3AA	-0.5904(14)	-0.016(2)	0.0191(5)
C2AA	-0.6248(15)	0.0888(18)	0.0056(6)
I1AA	-0.6019(3)	0.1927(3)	-0.00517(9)
C14	-0.4455(11)	0.0718(14)	-0.0003(4)
C6AA	-0.3839(10)	0.0964(11)	0.0015(3)
H6AA	-0.3526	0.0928	-0.0085
C0AA	-0.4949(12)	0.0690(16)	0.0135(4)
C5AA	-0.4119(14)	0.133(2)	0.0314(4)
H5AA	-0.4015	0.1583	0.0423
C4AA	-0.4775(14)	0.1031(19)	0.0295(4)
H4AA	-0.5093	0.1066	0.0393
C7AA	-0.3645(10)	0.1273(12)	0.0179(3)
C8AA	-0.2968(10)	0.1647(13)	0.0203(3)
H8AA	-0.2895	0.1733	0.0337

H8AB	-0.2997	0.2091	0.014
C9AA	-0.6876(13)	0.0716(16)	0.0041(6)
H9AA	-0.7193	0.102	-0.0013
O4	-0.2349(4)	0.1252(4)	0.01253(11)
O1	-1.0304(3)	0.0801(3)	-0.03656(9)
O0AA	-0.9469(4)	-0.1849(4)	-0.03938(13)

Table S3. Crystal data, data collection, and structure refinement parameters for $Me_2ImAu(III)(H_2BPDC)Cl$ (**4**).

Name	$Me_2ImAu(III)(H_2BPDC)Cl$ (**4**)
Chemical composition	$C_{41.37}\ H_{35.38}\ Au_2\ Cl_{1.33}\ N_{5.35}\ O_8$
Formula mass	1176.34
Crystal system	Triclinic
Space group	*P*-1
a, Å	8.9818(7)
b, Å	11.3002(8)
c, Å	25.0433(17)
α, º	80.007(4)
β, º	84.613(4)
γ, º	85.061(4)
V, Å^3	2485.9(3)
d, g cm^{-3}	1.572
μ, mm^{-1}	7.448
Z	2
Measured reflections	54104
Independent reflections	18955
Observed reflections	13601
θ_{min} , º	1.806
θ_{max} , º	36.805
h	-13 to 13

k	-17 to 17
l	-38 to 38
R int	0.0483
R [$F^2>2\sigma(F^2)$]	0.0820
$wR(F^2)$	0.2163
S	1.147
Parameters	560
Restraints	0
$\Delta\rho_{max}$, e Å^{-3}	4.408
$\Delta\rho_{min}$, e Å^{-3}	-3.870
Crystal size, μm^3	100 x 80 x 80
Radiation, Å	0.77490
Temperature, K	100

Table S4. Atomic coordinates of Me_2ImAu(III)(H_2BPDC)Cl (**4**).

Au01	0.29971(4)	0.75268(4)	0.80711(2)
Au02	0.25947(4)	0.81284(4)	0.24510(2)
Cl1	0.0892(4)	0.8183(4)	0.75785(14)
Cl00	0.429(3)	0.893(3)	0.2783(11)
O005	0.7810(10)	0.5952(8)	0.9959(3)
H005	0.7713	0.5896	1.0299
O006	-0.1799(9)	0.5970(7)	0.0911(3)

O007	-0.0317(12)	0.7466(8)	0.0642(3)
C008	0.0119(11)	0.5772(12)	0.3648(4)
H008	-0.0615	0.5227	0.3629
N009	0.3094(12)	0.9905(10)	0.1376(4)
N00A	0.1930(11)	0.9556(9)	0.8699(3)
N00B	0.1423(13)	0.7870(9)	0.9180(4)
O00C	0.5967(11)	0.7427(9)	0.9970(3)
O00D	0.2568(11)	0.6283(10)	0.6013(3)
H00D	0.2301	0.6136	0.5719
O00E	0.4747(13)	0.5392(12)	0.5750(4)
O00F	0.1749(13)	0.6033(12)	0.5119(3)
C00G	0.0274(10)	0.6444(10)	0.2631(3)
N00H	0.4264(11)	0.8210(9)	0.1327(4)
C00I	0.1699(12)	0.6664(12)	0.4167(4)
C00J	-0.0858(11)	0.6709(9)	0.0986(3)
C00K	-0.1115(12)	0.5767(10)	0.1973(4)
H00K	-0.1814	0.5252	0.1891
C00L	0.4084(10)	0.6670(9)	0.7483(3)
C00M	-0.0462(11)	0.6579(9)	0.1562(3)
C00N	0.3378(12)	0.8811(10)	0.1663(4)
C00O	0.5485(11)	0.6125(9)	0.7606(4)
C00P	0.0614(10)	0.7277(9)	0.1678(3)

H00P	0.1109	0.7803	0.1392
C00Q	0.0693(10)	0.6490(10)	0.3179(3)
C00R	0.5918(12)	0.6235(9)	0.8145(4)
C00S	0.2041(11)	0.8369(10)	0.8700(4)
C00T	0.5139(12)	0.7031(10)	0.8963(4)
H00T	0.4444	0.75	0.9165
C00U	0.1790(9)	0.7289(9)	0.3195(4)
C00V	0.4860(11)	0.6872(9)	0.8448(4)
C00W	0.0980(10)	0.7218(9)	0.2210(4)
C00X	-0.0761(12)	0.5693(10)	0.2508(4)
H00X	-0.1222	0.5133	0.2789
C00Y	0.6696(15)	0.6636(11)	0.9750(4)
C00Z	0.4437(13)	0.5979(10)	0.6617(4)
O010	0.3212(13)	0.7476(11)	0.4722(4)
C011	0.3558(10)	0.6579(9)	0.6982(4)
H011	0.2595	0.6932	0.6894
C012	0.1213(17)	0.9786(12)	0.9193(5)
H012	0.1008	1.0555	0.9299
C013	0.6459(13)	0.6493(11)	0.9185(4)
C014	0.7490(14)	0.5831(11)	0.8885(4)
H014	0.8362	0.5437	0.9042
C015	0.6386(15)	0.5549(12)	0.7234(4)

H015	0.7357	0.5204	0.7317
C016	0.3921(15)	0.5836(12)	0.6077(4)
C017	0.0636(12)	0.5862(12)	0.4147(4)
H017	0.0259	0.5374	0.4471
C018	0.7244(14)	0.5748(12)	0.8355(5)
H018	0.7986	0.5356	0.8137
C019	0.2482(16)	1.0467(13)	0.8260(6)
H01I	0.3568	1.0316	0.819
H01J	0.2264	1.1265	0.8364
H01L	0.1988	1.0434	0.7931
C01A	0.2261(11)	0.7369(10)	0.3698(4)
H01A	0.2985	0.7919	0.372
C01B	0.0868(19)	0.8734(12)	0.9487(5)
H01M	0.0344	0.8605	0.9837
C01C	0.2066(18)	1.0873(12)	0.1562(6)
H01B	0.1454	1.0538	0.1889
H01C	0.1412	1.1221	0.1274
H01D	0.2652	1.1501	0.1645
C01D	0.5849(15)	0.5485(12)	0.6740(4)
H01N	0.646	0.5096	0.6483
C01E	0.136(2)	0.6565(13)	0.9387(6)
H01O	0.0327	0.6388	0.9515

H01P	0.2005	0.6331	0.9688
H01Q	0.1712	0.6111	0.9094
C01F	0.2264(14)	0.6743(14)	0.4702(4)
C01G	0.4543(18)	0.8900(15)	0.0825(5)
H01G	0.5129	0.8661	0.0521
C01K	0.3811(18)	0.9992(14)	0.0852(5)
H01K	0.379	1.0676	0.0571
C01L	0.4811(19)	0.6945(13)	0.1440(7)
H01E	0.4476	0.6602	0.1814
H01F	0.5909	0.6882	0.1394
H01H	0.4414	0.6503	0.1187
N4	0.413(2)	1.0058(16)	0.2914(7)
N5	0.5567(18)	0.8467(17)	0.2911(7)
C0AA	0.552(3)	1.020(2)	0.3127(8)
H0AA	0.577	1.0893	0.3254
C9	0.619(3)	0.729(3)	0.2837(14)
H9A	0.6031	0.6726	0.3178
H9B	0.7268	0.7318	0.2733
H9C	0.5699	0.7023	0.2551
C10	0.634(3)	0.926(2)	0.3119(9)
H10	0.7322	0.911	0.3235
C8	0.287(4)	1.093(2)	0.2885(12)

H8A	0.2709	1.1262	0.3225
H8B	0.1969	1.0541	0.2833
H8C	0.3055	1.1582	0.2579
C50	0.430(3)	0.922(5)	0.2762(13)

Table S5. Crystal data, data collection, and structure refinement parameters for **Me_2ImAu(III)Cl-UiO-67 (20% Au occupancy)**.

Name	**Me_2ImAu(III)Cl-UiO-67 (20% Au occupancy)**
Chemical composition	$C_{42}H_{12}Au_{0.8}Cl_{0.4}O_{16}Zr_3$ [+ solvent]
Formula mass	1174.99
Crystal system	Cubic
Space group	*F*m-3m
a, Å	26.712(9)
V, Å^3	19060(19)
d, g cm^{-3}	0.819
μ, mm^{-1}	1.588
Z	8
Measured reflections	27263
Independent reflections	882
Observed reflections	676
θ_{min} , º	1.440
θ_{max} , º	27.183
h	-31 to 31
k	-31 to 31
l	-31 to 27
R int	0.2552
R [$F^2>2\sigma(F^2)$]	0.0653
wR(F^2)	0.1848

S	1.012
Parameters	48
Restraints	1
$\Delta\rho_{max}$, e Å^{-3}	1.472
$\Delta\rho_{min}$, e Å^{-3}	-0.611
Crystal size, μm^3	40 x 40 x 40
Radiation, Å	0.7749
Temperature, K	100

Table S6. Atomic coordinates of **Me_2ImAu(III)Cl-UiO-67 (20% Au occupancy)**.

Zr01	0.59249(4)	0.5	0.5
O002	0.63335(18)	0.5	0.57161(19)
C005	0.6170(3)	0.5	0.6170(3)
C006	0.6568(3)	0.5	0.6568(3)
C007	0.6434(5)	0.5	0.7070(4)
H007	0.6099	0.5	0.7166
C008	0.7306(3)	0.5	0.7306(3)
C1	0.6828(5)	0.5	0.7437(4)
O1	0.5537(5)	0.4463(5)	0.4463(5)
Au1	0.81184(17)	0.4840(6)	0.68816(17)
Cl15	0.816(6)	0.5	0.5995(8)
O2	0.5412(4)	0.4588(4)	0.4588(4)

Table S7. Crystal data, data collection, and structure refinement parameters for **Me_2ImAu(III)SbF_6-UiO-67 (20% Au occupancy)**.

Name	**Me_2ImAu(III)SbF_6-UiO-67 (20% Au occupancy)**
Chemical composition	C_{84} H_{24} Au_3 O_{32} Zr_6 [+ solvent]
Formula mass	2683.26
Crystal system	Cubic
Space group	*F*m-3m
a, Å	26.308(12)
V, Å^3	18208(25)
d, g cm^{-3}	0.979
μ, mm^{-1}	3.439
Z	4
Measured reflections	297
Independent reflections	424
Observed reflections	266
θ_{min} , º	1.462
θ_{max} , º	20.774
h	-24 to 10
k	-23 to 23
l	-19 to 24
R int	0.4073
R [$F^2>2\sigma(F^2)$]	0.0849
wR(F^2)	0.2057

S	0.964
Parameters	41
Restraints	30
$\Delta\rho_{max}$, e Å^{-3}	0.946
$\Delta\rho_{min}$, e Å^{-3}	-0.839
Crystal size, μm^3	40 x 40 x 40
Radiation, Å	0.7749
Temperature, K	100

Table S8. Atomic coordinates of **Me_2ImAu(III)SbF_6-UiO-67 (20% Au occupancy)**.

Zr01	0.022(3)	0.032(2)	0.032(2)
O02	0.043(9)	0.042(9)	0.052(10)
O03	0.052(7)	0.052(7)	0.052(7)
Au00	0.146(9)	1.84(13)	0.146(9)
C006	0.056(9)	0.051(12)	0.056(9)
C008	0.094(11)	0.095(14)	0.094(11)
C00B	0.11(3)	0.42(8)	0.05(2)
C00C	0.133(15)	0.155(15)	0.125(15)
C9	0.143(14)	0.151(17)	0.143(14)

Table S9. Crystal data, data collection, and structure refinement parameters for **[(Me$_2$Im)$_2$Au(biphenyl)OH$_2$]SbF$_6$**.

Name	**[(Me$_2$Im)$_2$Au(biphenyl)OH$_2$]SbF$_6$**
Chemical composition	C_{23} H_{25} Au Cl_3 F_6 N_4 Sb
Formula mass	896.55
Crystal system	Monoclinic
Space group	$P2_1/n$
a, Å	12.4660(7)
b, Å	7.2866(3)
c, Å	31.1195(15)
β, º	93.870(2)
V, Å^3	2820.3(2)
d, g cm^{-3}	2.112
μ, mm^{-1}	6.499
Z	4
Measured reflections	12652
Independent reflections	6324
Observed reflections	5005
θ_{min} , º	2.871
θ_{max} , º	28.307
h	-16 to 15
k	-8 to 9
l	-35 to 41

R int	0.0425
$R\ [F^2>2\sigma(F^2)]$	0.0871
$wR(F^2)$	0.1776
S	1.297
Parameters	157
Restraints	0
$\Delta\rho_{max}$, e Å^{-3}	8.311
$\Delta\rho_{min}$, e Å^{-3}	-5.424
Crystal size, μm^3	90 x 60 x 50
Radiation, Å	Mo/Ka
Temperature, K	273

Table S10. Atomic coordinates of **[(Me$_2$Im)$_2$Au(biphenyl)OH$_2$]SbF$_6$**.

Au01	0.27246(5)	1.06890(8)	0.63302(2)
Sb02	0.24562(10)	0.62889(17)	0.47397(4)
Cl03	0.2203(4)	0.0013(8)	0.35702(18)
Cl04	0.2245(5)	0.4016(9)	0.3517(2)
Cl05	0.3035(5)	0.1815(9)	0.2828(2)
C007	0.1415(12)	0.955(2)	0.5969(5)
F008	0.2438(8)	0.3730(15)	0.4639(3)
F009	0.2477(9)	0.8830(16)	0.4843(4)
N00B	0.0898(12)	0.804(2)	0.6044(5)

N00C	0.0805(11)	1.048(2)	0.5668(5)
N00D	0.4429(11)	1.0450(19)	0.5671(4)
F00E	0.3637(13)	0.604(2)	0.5126(5)
C00F	-0.0106(15)	0.945(3)	0.5548(6)
H00F	-0.0645	0.9771	0.534
N00G	0.4462(12)	0.800(2)	0.6051(5)
C00J	0.3917(13)	0.957(2)	0.5970(5)
C00K	0.5292(14)	0.941(3)	0.5556(6)
H00K	0.5772	0.9725	0.5352
F00M	0.1448(14)	0.608(3)	0.5139(6)
C00P	-0.0066(14)	0.790(3)	0.5786(6)
H00P	-0.0567	0.6954	0.5781
F00R	0.1339(13)	0.653(2)	0.4313(5)
F00U	0.3422(13)	0.654(2)	0.4300(5)
C00V	0.5311(14)	0.790(3)	0.5791(6)
H00V	0.5805	0.6948	0.5782
C00Y	0.422(2)	0.666(4)	0.6383(10)
H00A	0.3898	0.7276	0.6615
H00B	0.4866	0.606	0.6489
H00C	0.3721	0.576	0.626
C011	0.1046(16)	1.226(3)	0.5495(6)
H01A	0.1327	1.3048	0.5723
H01B	0.0402	1.2795	0.5362
H01C	0.157	1.2134	0.5284

C013	0.4110(18)	1.224(3)	0.5489(7)
H01D	0.3433	1.2127	0.5325
H01E	0.4646	1.2663	0.5305
H01F	0.4042	1.3107	0.5718
C014	0.2102(18)	0.199(3)	0.3215(7)
H014	0.1382	0.1994	0.3067
C015	0.123(2)	0.664(4)	0.6346(9)
H01G	0.1853	0.6019	0.625
H01H	0.066	0.5769	0.637
H01I	0.1411	0.7181	0.6623
C3	0.1681(12)	1.207(2)	0.6725(5)
C5	0.3459(12)	1.308(2)	0.7040(5)
C9	0.2281(12)	1.307(2)	0.7045(5)
C10	0.3891(12)	1.199(2)	0.6725(5)
C1	0.4985(11)	1.192(2)	0.6700(5)
H1	0.5281	1.1218	0.6488
C2	0.0579(12)	1.197(2)	0.6699(5)
H2	0.0215	1.1243	0.6491
C0AA	0.0030(12)	1.295(2)	0.6985(5)
H0AA	-0.0717	1.293	0.6962
C4	0.1668(13)	1.405(2)	0.7335(5)
H4	0.2022	1.4771	0.7546
C1AA	0.4117(12)	1.408(2)	0.7327(5)
H1AA	0.3825	1.4796	0.7537

C6	0.5236(13)	1.400(2)	0.7296(6)
H6	0.5688	1.4694	0.7483
C7	0.5656(13)	1.293(2)	0.6998(5)
H7	0.6399	1.2847	0.6988
C8	0.0555(14)	1.397(2)	0.7311(6)
H8	0.0167	1.4591	0.7511

IPrAu(III)(H_2BPDC)Cl (5). A prismatic colorless crystal (80 x 50 x 30 μm^3) of IPrAu(III)(H_2BPDC)Cl was measured using a Bruker D-8-Venture diffractometer (λ = 0.71073 Å). According to intensity statistics table for the whole dataset (PRP file), the resolution was cut off to 0.85 Å. The weighting scheme is refined as well as the extinction coefficient. Some reflections were omitted due beam stop clipping and the minor presence of diffuse scattering. Omission of these reflections did not affect the refinement; the fraction of omitted reflections is less than 0.1% of the whole dataset.

Table S11. Crystal data, data collection, and structure refinement parameters for IPrAu(III)(H_2BPDC)Cl (**5**).

Name	IPrAu(III)(H_2BPDC)Cl (**4**)
Chemical composition	C_{41} H_{42} Au Cl N_2 O_4
Formula mass	859.19
Crystal system	Monoclinic
Space group	$P2_1$
a, Å	23.3574(14)
b, Å	13.8095(9)
c, Å	25.9980(18)
α, º	113.200(2)
V, Å^3	7707.6(9)
d, g cm^{-3}	1.481
μ, mm^{-1}	3.928
Z	8
Measured reflections	112638
Independent reflections	26295
Observed reflections	19762
θ_{min} , º	2.286
θ_{max} , º	24.750
h	-27 to 27
k	-16 to 16
l	-30 to 30

R int	0.1853
R [$F^2>2\sigma(F^2)$]	0.0700
$wR(F^2)$	0.1563
S	1.016
Parameters	1796
Restraints	328
Flack parameter	-0.015(10)
$\Delta\rho_{max}$, e Å^{-3}	2.155
$\Delta\rho_{min}$, e Å^{-3}	-2.490
Crystal size, μm^3	80 x 50 x 30
Radiation, Å	Mo/Ka
Temperature, K	100

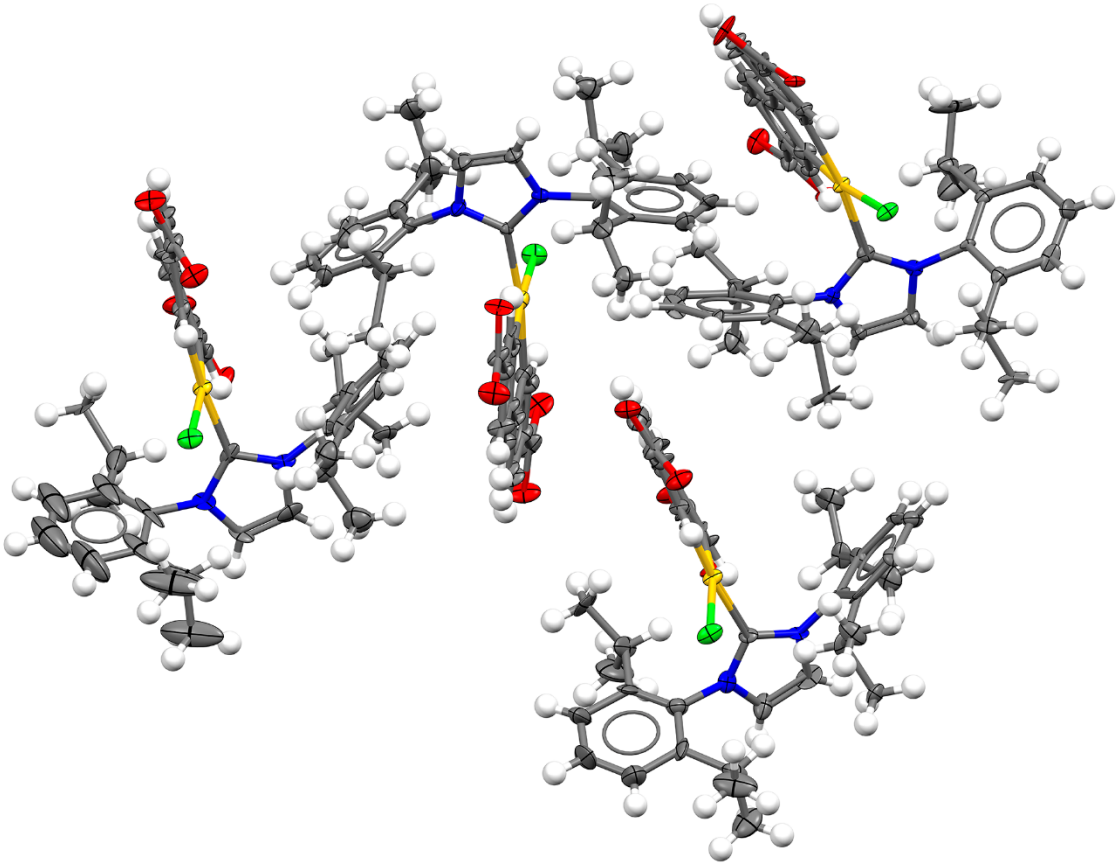

Fig. S1. Asymmetric unit in the single crystal structure of IPrAu(III)(H_2BPDC)Cl (**5**). Thermal ellipsoids are drawn with 50% probability.

IPrAu(III)(Me_2BPDC)Cl (SI 9). A prismatic colorless crystal (70 x 60 x 30 μm^3) of IPrAu(III)(Me_2BPDC)Cl was measured using a Bruker D-8-Venture diffractometer (λ = 0.71073 Å). According to intensity statistics table for the whole dataset (PRP file), the resolution was cut off to 0.75 Å. The weighting scheme is refined as well as the extinction coefficient. Some reflections were omitted due beam stop clipping and the minor presence of diffuse scattering. Omission of these reflections did not affect the refinement; the fraction of omitted reflections is less than 0.1% of the whole dataset.

Table S12. Crystal data, data collection, and structure refinement parameters for IPrAu(III)(Me_2BPDC)Cl (**SI 9**).

Name	IPrAu(III)(Me_2BPDC)Cl (**SI 9**)
Chemical composition	C_{44} H_{50} Au Cl_3 N_2 O_4
Formula mass	974.18
Crystal system	Triclinic
Space group	*P*-1
a, Å	12.3754(16)
b, Å	16.633(2)
c, Å	22.134(3)
α, º	81.284(5)
β, º	74.956(5)
γ, º	78.837(5)
V, Å^3	4291.8(10)
d, g cm^{-3}	1.508
μ, mm^{-1}	3.657
Z	4
Measured reflections	141541
Independent reflections	21130
Observed reflections	16731
θ_{min} , º	2.167
θ_{max} , º	28.422
h	-16 to 16

k	-22 to 22
l	-29 to 29
R int	0.0785
R [$F^2>2\sigma(F^2)$]	0.0964
$wR(F^2)$	0.2522
S	1.033
Parameters	994
Restraints	159
$\Delta\rho_{max}$, e Å^{-3}	5.275
$\Delta\rho_{min}$, e Å^{-3}	-7.800
Crystal size, μm^3	70 x 60 x 30
Radiation, Å	Mo/Ka
Temperature, K	150
CCDC number	

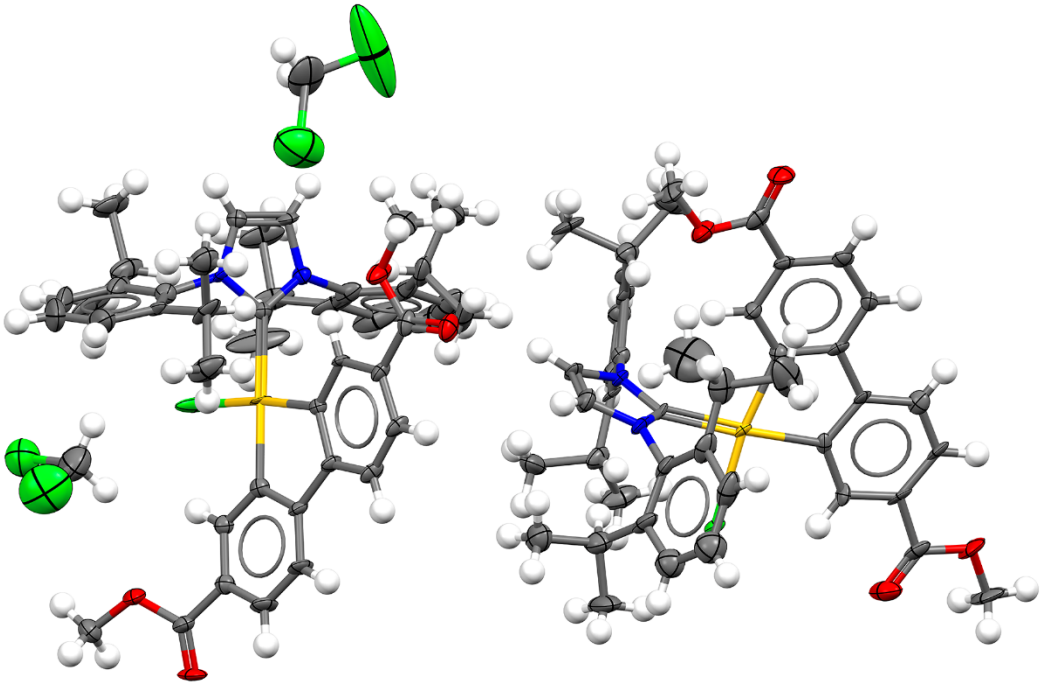

Fig. S2. Asymmetric unit in the single crystal structure of IPrAu(III)(Me_2BPDC)Cl (**SI 9**). Thermal ellipsoids are drawn with 50% probability.

IPrAu(III)Cl-bio-MOF-100 (40% Au occupancy). A cubic colorless crystal (120 x 120 x 120 μm^3) of IPrAu(III)Cl-bio-MOF-100 was measured using a Bruker D-8-Venture diffractometer (λ = 1.54178 Å). The crystal was placed into a capillary filled with DMF in order to prevent crystal degradation. Note that the crystal was measured at 273 K and NOT under nitrogen stream to preserve MOF crystallinity. According to intensity statistics table for the whole dataset (PRP file), the resolution was cut off to 1.45 Å. Solvent masking was applied during structure refinement. Before solvent masking instruction, structure was refined anisotropically (except for the NHC) and hydrogen atoms were placed into positions calculated geometrically. The weighting scheme is refined. Some reflections were omitted due beam stop clipping and the minor presence of diffuse scattering. Omission of these reflections did not affect the refinement; the fraction of omitted reflections is less than 0.1% of the whole dataset. The void volume is estimated to be 267698 $Å^3$ with 32487 electrons removed during masking. The occupancy of the gold, chlorine, and NHC was estimated with a free variable and isotropic displacement parameters were refined freely.

Table S13. Crystal data, data collection, and structure refinement parameters for **IPrAu(III)Cl-bio-MOF-100 (40% Au occupancy).**

Name	**IPrAu(III)Cl-bio-MOF-100 (40% Au occupancy)**
Chemical composition	$C_{167.28}H_{84}Au_{2.62}Cl_{2.62}N_{35.23}O_{39}Zn_{12}$ [+solvent]
Formula mass	4603.99
Crystal system	Cubic
Space group	*I*a-3d
a, Å	69.040(9)
V, Å^3	329075(133)
d, g cm^{-3}	0.372
μ, mm^{-1}	1.458
Z	16
Measured reflections	7710
Independent reflections	4625
Observed reflections	3111
θ_{min} , º	2.394
θ_{max} , º	32.061
h	-30 to 36
k	-40 to 13
l	-47 to 47
R int	0.1216
R [$F^2>2\sigma(F^2)$]	0.1138
wR(F^2)	0.2933

S	1.109
Parameters	348
Restraints	331
$\Delta\rho_{max}$, e Å^{-3}	0.429
$\Delta\rho_{min}$, e Å^{-3}	-0.536
Crystal size, μm^3	120 x 120 x 120
Radiation, Å	Cu/Ka
Temperature, K	273

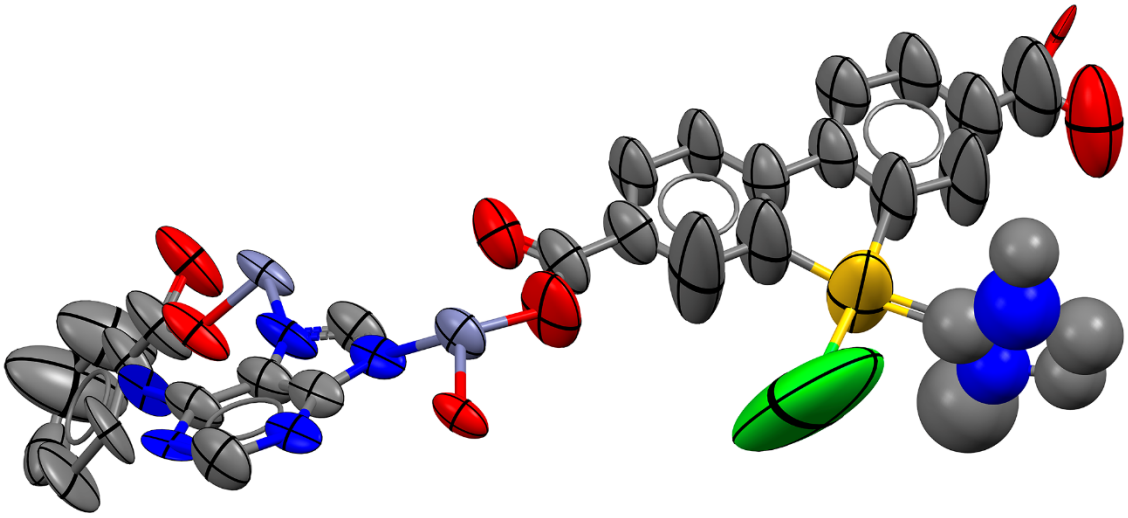

Fig. S3. Asymmetric unit in the single crystal structure of **IPrAu(III)Cl-bio-MOF-100 (40% Au occupancy)**. Thermal ellipsoids are drawn with 50% probability. Hydrogen atoms are omitted for clarity.

IPrAu(III)PF_6-bio-MOF-100 (40% Au occupancy). A cubic colorless crystal (120 x 120 x 120 μm^3) of IPrAu(III)PF_6-bio-MOF-100 was measured using a Bruker D-8-Venture diffractometer (λ = 1.54178 Å). The crystal was placed into a capillary filled with DMF in order to prevent crystal degradation. Note that the crystal was measured at 273 K and NOT under nitrogen stream to preserve MOF crystallinity. According to intensity statistics table for the whole dataset (PRP file), the resolution was cut off to 1.45 Å. It is important to emphasize that the starting model for the structure was taken directly from the final refinement of **IPrAu(III)Cl-bio-MOF-100 (40% Au occupancy)**. Upon first iteration, the positions of the chlorine and carbon atoms adjacent to the NHC could not be refined. Fig. S5 shows the absence of electron density peak next to gold which is evident of successful chloride abstraction. Solvent masking was applied during structure refinement. Structure was refined anisotropically (except for the NHC) and hydrogen atoms were placed into positions calculated geometrically. The weighting scheme is refined. Some reflections were omitted due beam stop clipping and the minor presence of diffuse scattering. Omission of these reflections did not affect the refinement; the fraction of omitted reflections is less than 0.1% of the whole dataset. The occupancy of gold and NHC was estimated with a free variable and isotropic displacement parameters were refined freely.

Table S14. Crystal data, data collection, and structure refinement parameters **IPrAu(III)PF_6-bio-MOF-100 (40% Au occupancy).**

Name	**IPrAu(III)PF_6-bio-MOF-100 (40% Au occupancy)**
Chemical composition	$C_{163.42}H_{84}Au_{2.75}N_{35.51}O_{39}Zn_{12}$ [+solvent]
Formula mass	4495.97
Crystal system	Cubic
Space group	*I*a-3d
a, Å	68.964(11)
V, Å^3	327991(153)
d, g cm^{-3}	0.364
μ, mm^{-1}	1.427
Z	16
Measured reflections	13540
Independent reflections	4161
Observed reflections	1876
θ_{min} , º	2.397
θ_{max} , º	32.085
h	-38 to 4
k	-33 to 29
l	-19 to 47
R int	0.1066
R [$F^2>2\sigma(F^2)$]	0.1115

$wR(F^2)$	0.3163
S	1.093
Parameters	330
Restraints	356
$\Delta\rho_{max}$, e Å^{-3}	0.403
$\Delta\rho_{min}$, e Å^{-3}	-0.280
Crystal size, μm^3	120 x 120 x 120
Radiation, Å	Cu/Ka
Temperature, K	273
CCDC number	

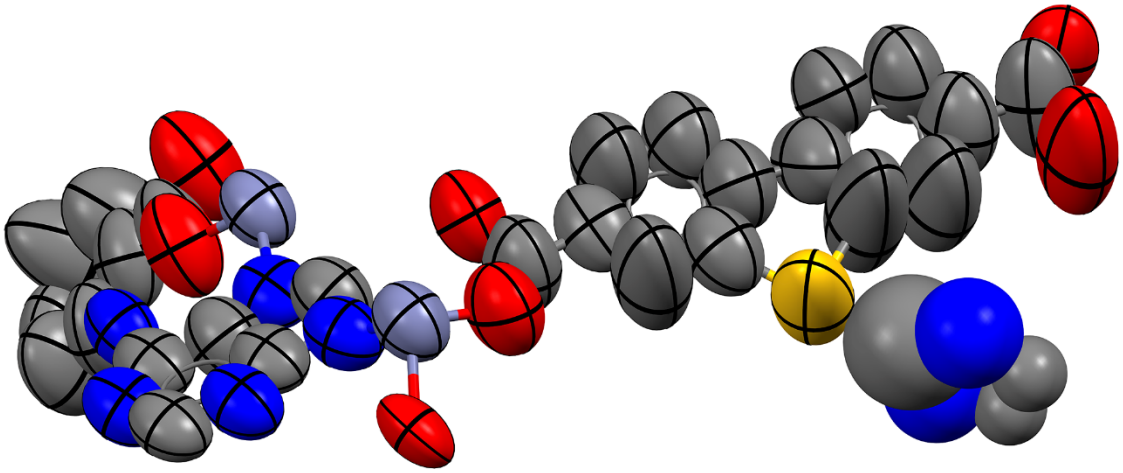

Fig. S4. Asymmetric unit in the single crystal structure of IPrAu(III)PF_6-bio-MOF-100 (40% Au occupancy). Thermal ellipsoids are drawn with 50% probability. Hydrogen atoms are omitted for clarity.

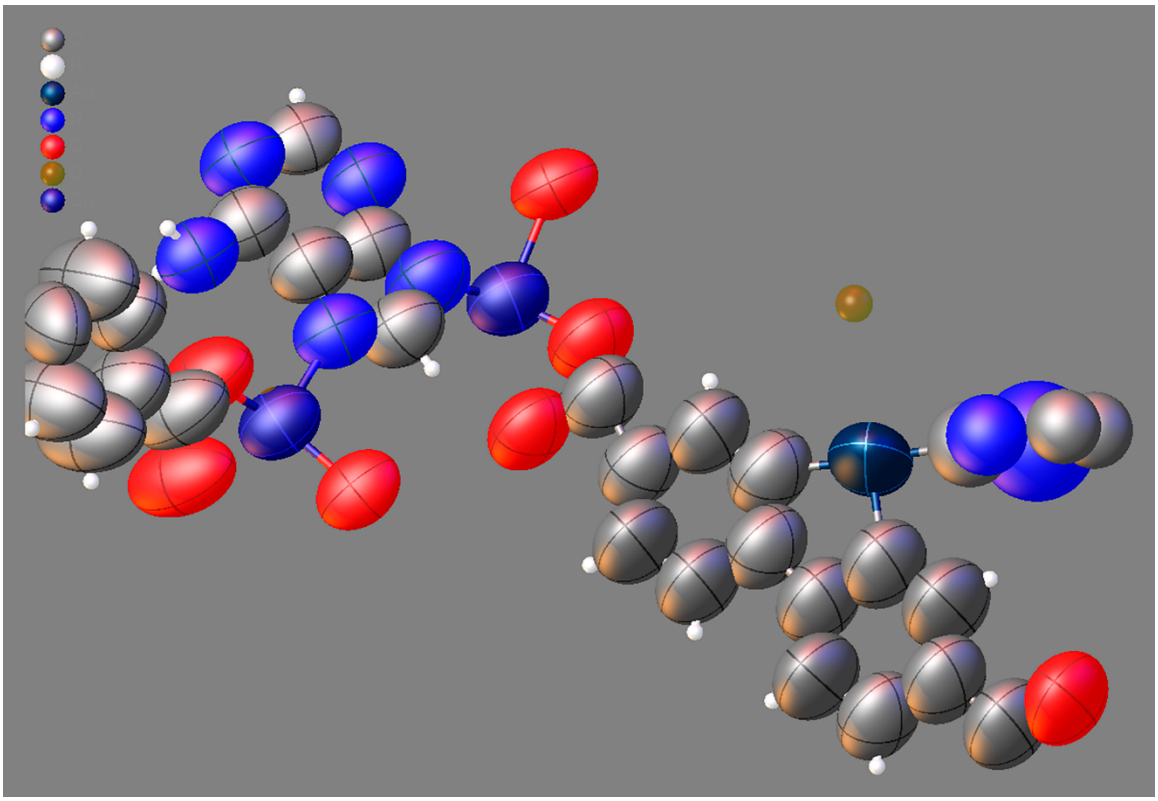

Fig. S5. Asymmetric unit in the single crystal structure of **IPrAu(III)PF_6-bio-MOF-100 (40% Au occupancy)** before solvent masking procedure. The distance between the electron density peak (brown) and gold atom (dark blue) is 2.87 Å, which is much longer than typical Au-Cl bond in both dicarboxylic acid and dimethyl dicarboxylate complexes and IPrAu(III)Cl-bio-MOF-100 (40% Au occupancy).

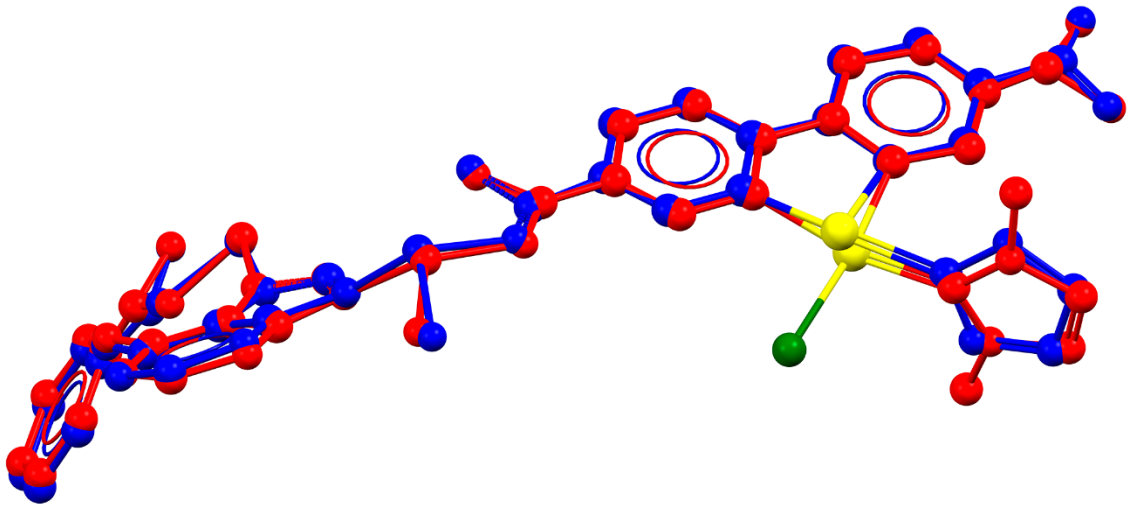

Fig. S6. Overlay of asymmetric units of **IPrAu(III)Cl-bio-MOF-100 (red)** and **IPrAu(III)PF6-bio-MOF-100 (blue).** Atoms of gold and chlorine are shown in yellow and green respectively.

2.4.10 Powder X-ray Diffraction Data

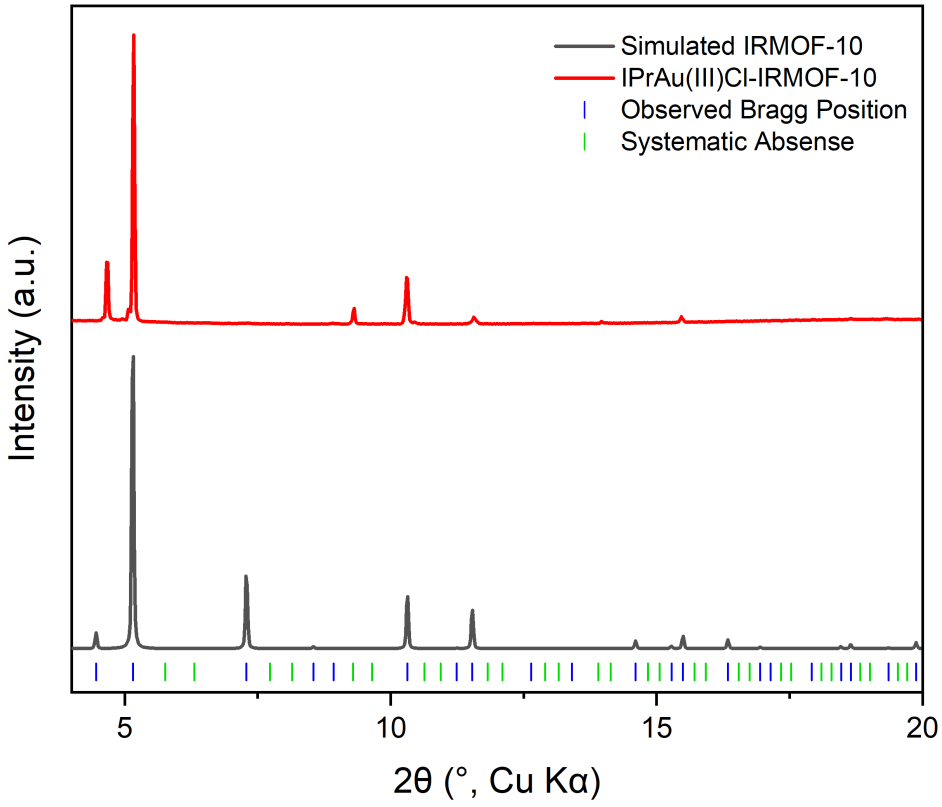

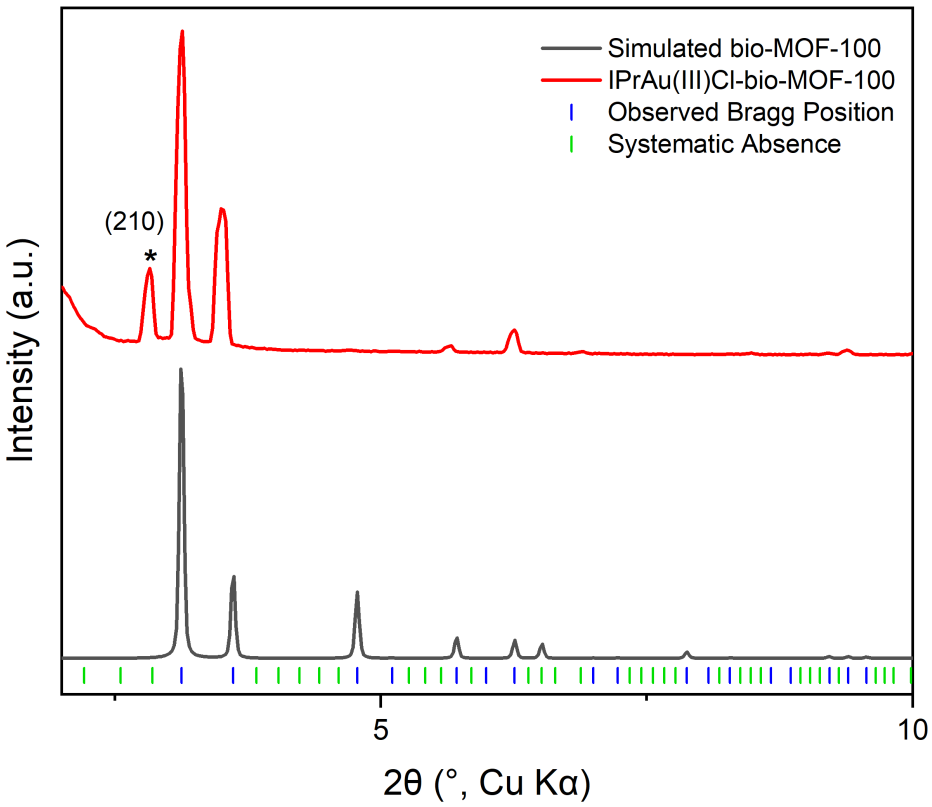

The reflection marked by asterisk was indexed to (210). Although it should have very low intensity because of systematic absence, it is reasoned that the incorporation of IPrAu(III)Cl breaks the space group symmetry of Ia-3d, thus the reflection does not meet the reflection condition. Because gold is a much heavier atom than any other atom in the structure, the reflection arises from systematic absent position is relatively pronounced.

2.4.11 ^{1}H and ^{13}C NMR Spectra of Previously Unreported Compounds

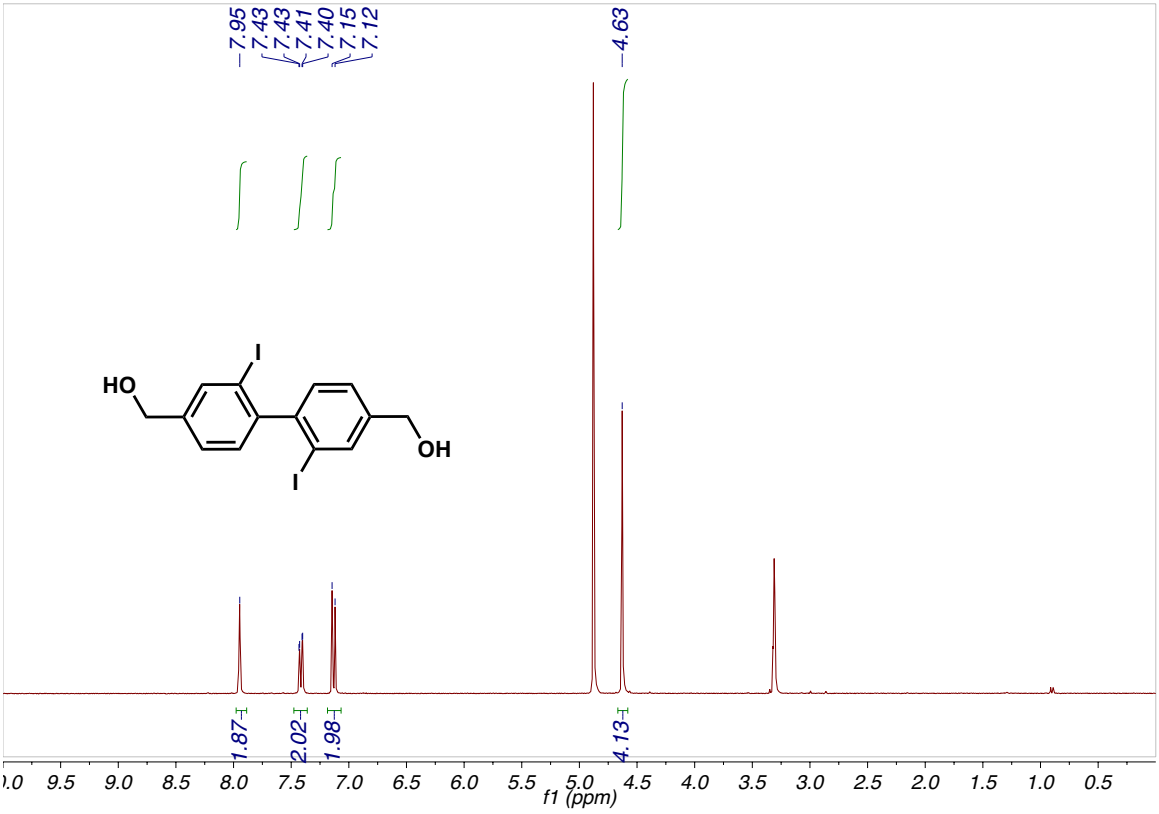

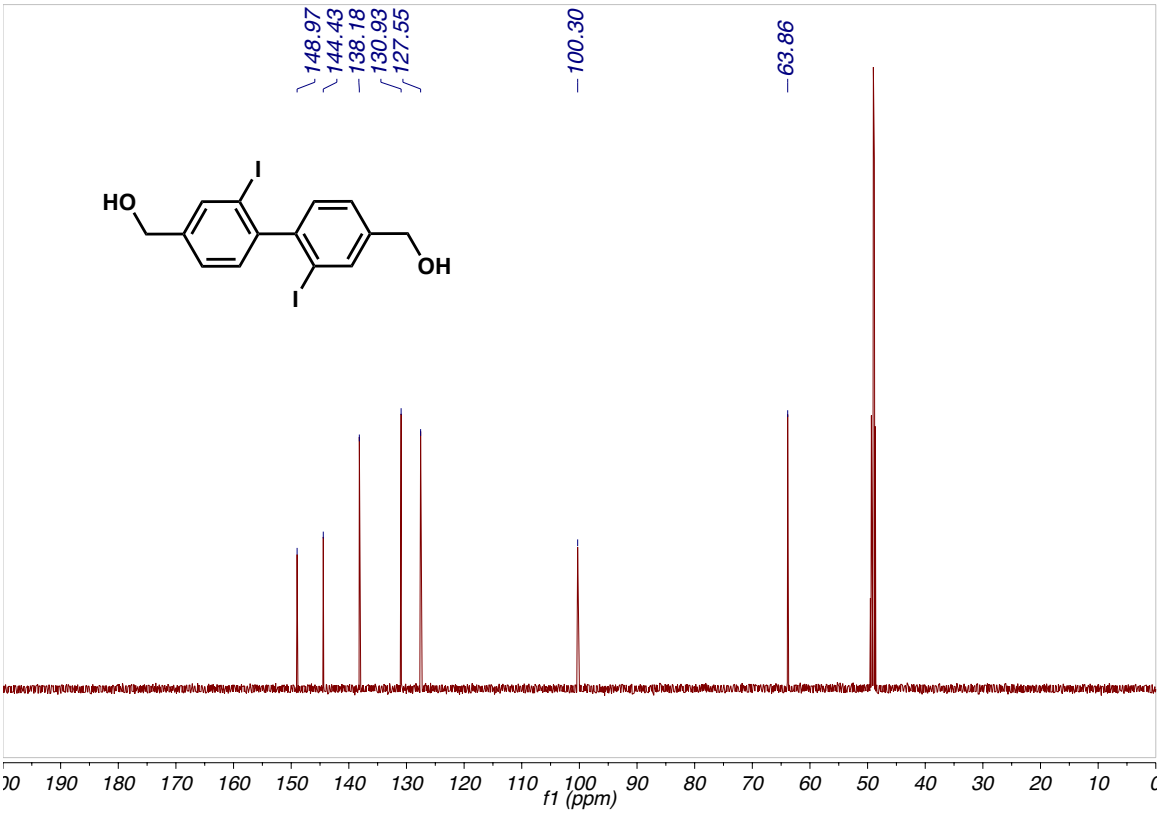

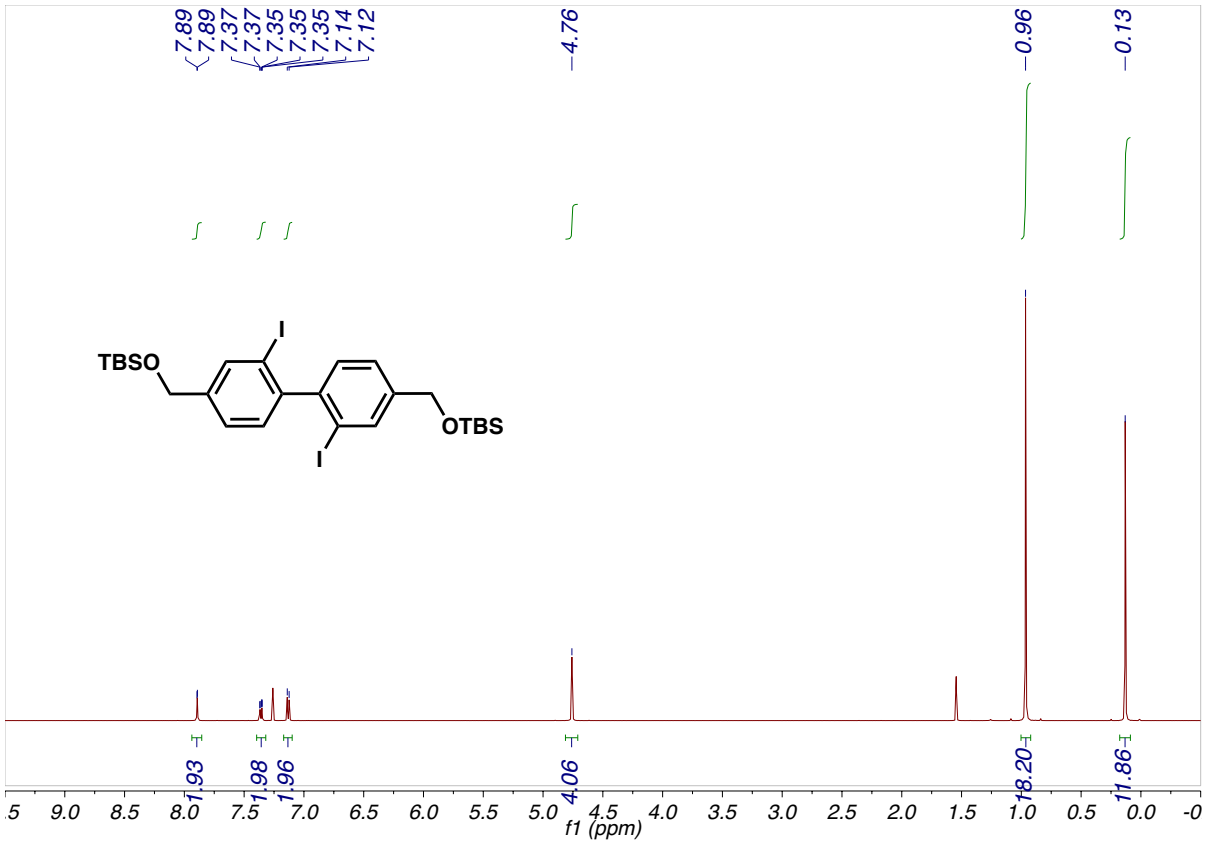
7.89
7.89
7.37
7.37
7.35
7.35
7.35
7.14
7.12
4.76
0.96
0.13
TBSO
I
OTBS
I
1.93
1.98
1.96
4.06
18.20
11.86
f1 (ppm)

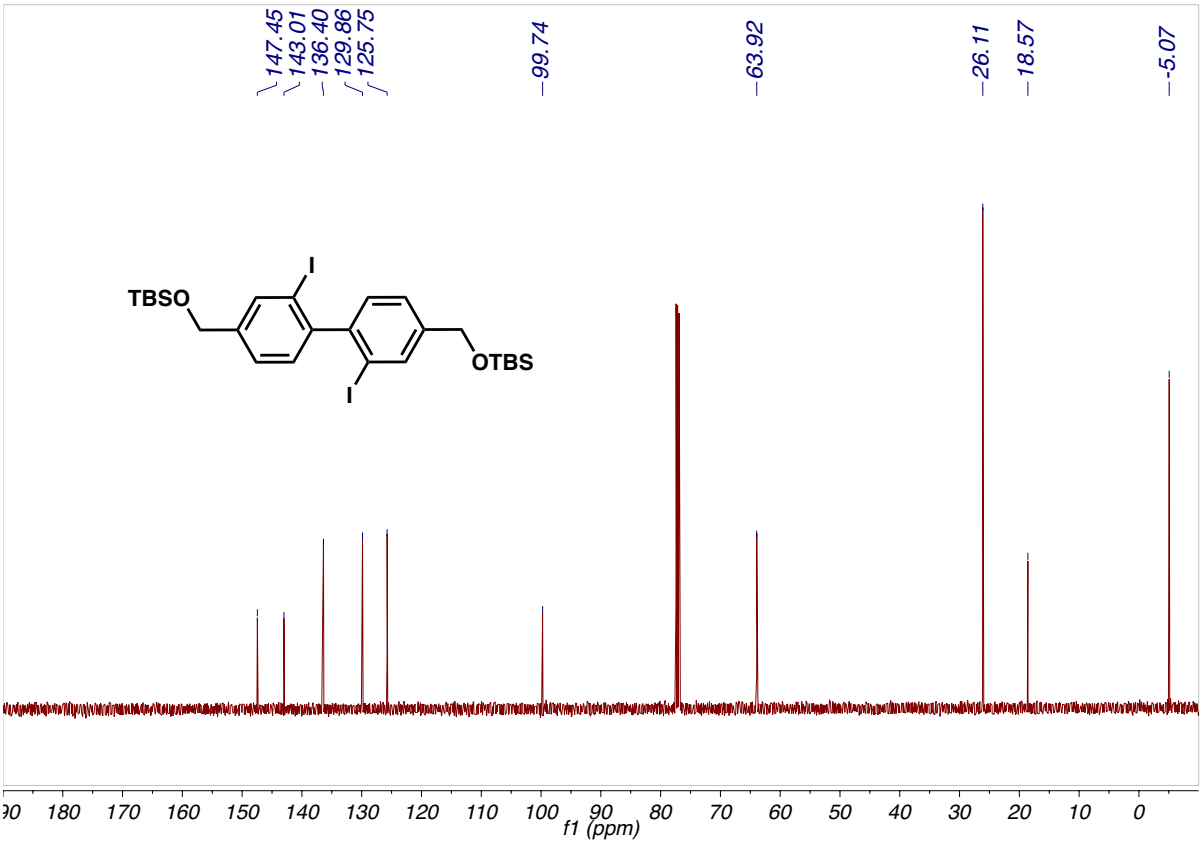
147.45
143.01
136.40
129.86
125.75
99.74
63.92
26.11
18.57
-5.07
TBSO
I
OTBS
I
f1 (ppm)

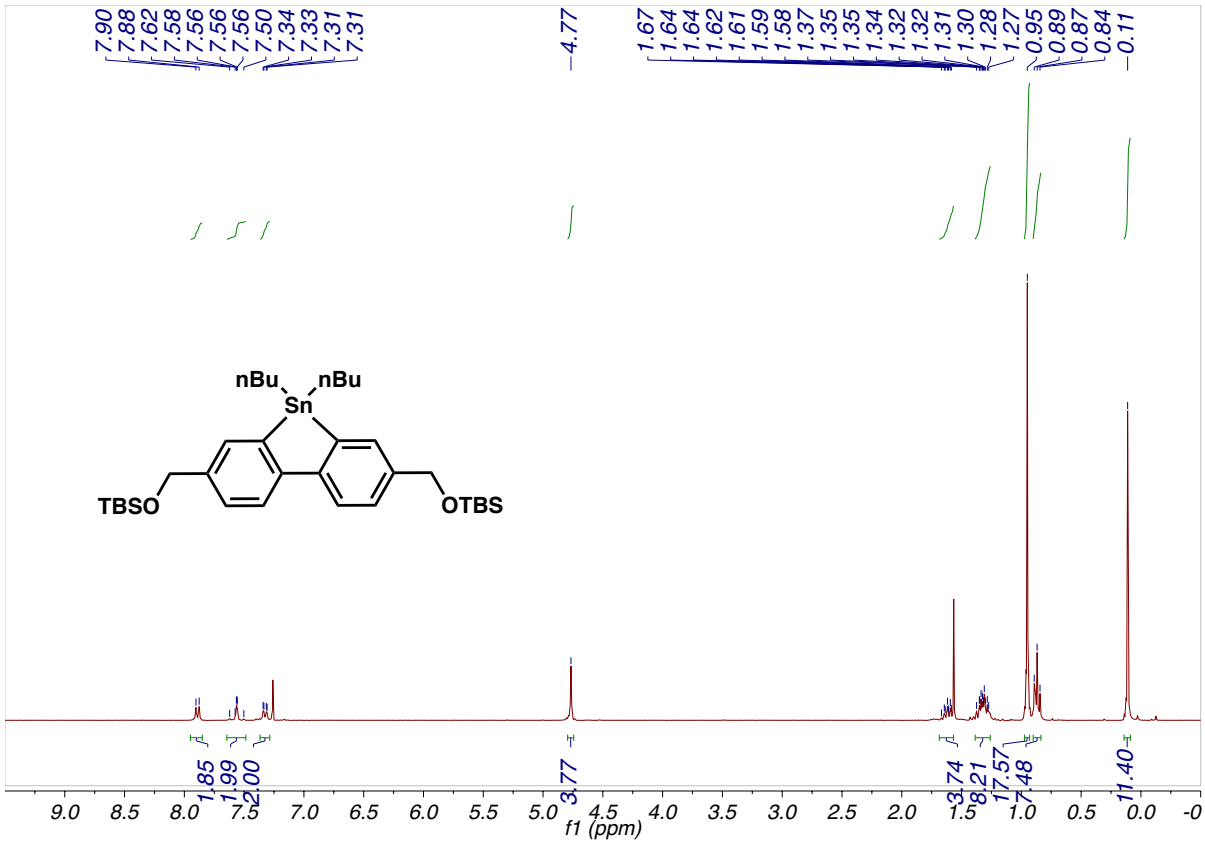
7.90
7.88
7.62
7.58
7.56
7.56
7.56
7.50
7.34
7.33
7.31
7.31
4.77
1.67
1.64
1.64
1.62
1.61
1.59
1.58
1.37
1.35
1.35
1.34
1.32
1.32
1.31
1.30
1.28
1.27
0.95
0.89
0.87
0.84
0.11
nBu
nBu
Sn
TBSO
OTBS
1.85
1.99
2.00
3.77
3.74
8.21
17.57
7.48
11.40
9.0 8.5 8.0 7.5 7.0 6.5 6.0 5.5 5.0 4.5 4.0 3.5 3.0 2.5 2.0 1.5 1.0 0.5 0.0 -0
f1 (ppm)

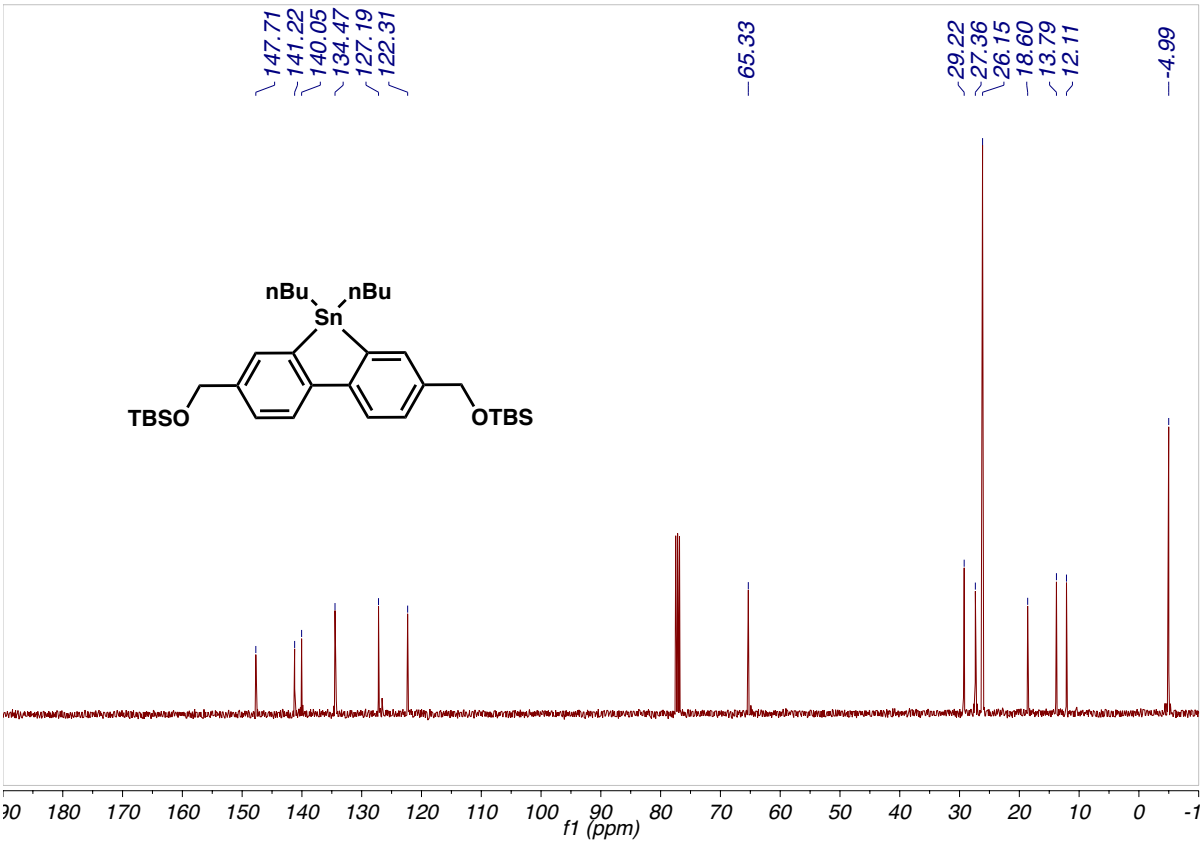
147.71
141.22
140.05
134.47
127.19
122.31
65.33
29.22
27.36
26.15
18.60
13.79
12.11
4.99
nBu
nBu
Sn
TBSO
OTBS
180 170 160 150 140 130 120 110 100 90 80 70 60 50 40 30 20 10 0 -1
f1 (ppm)

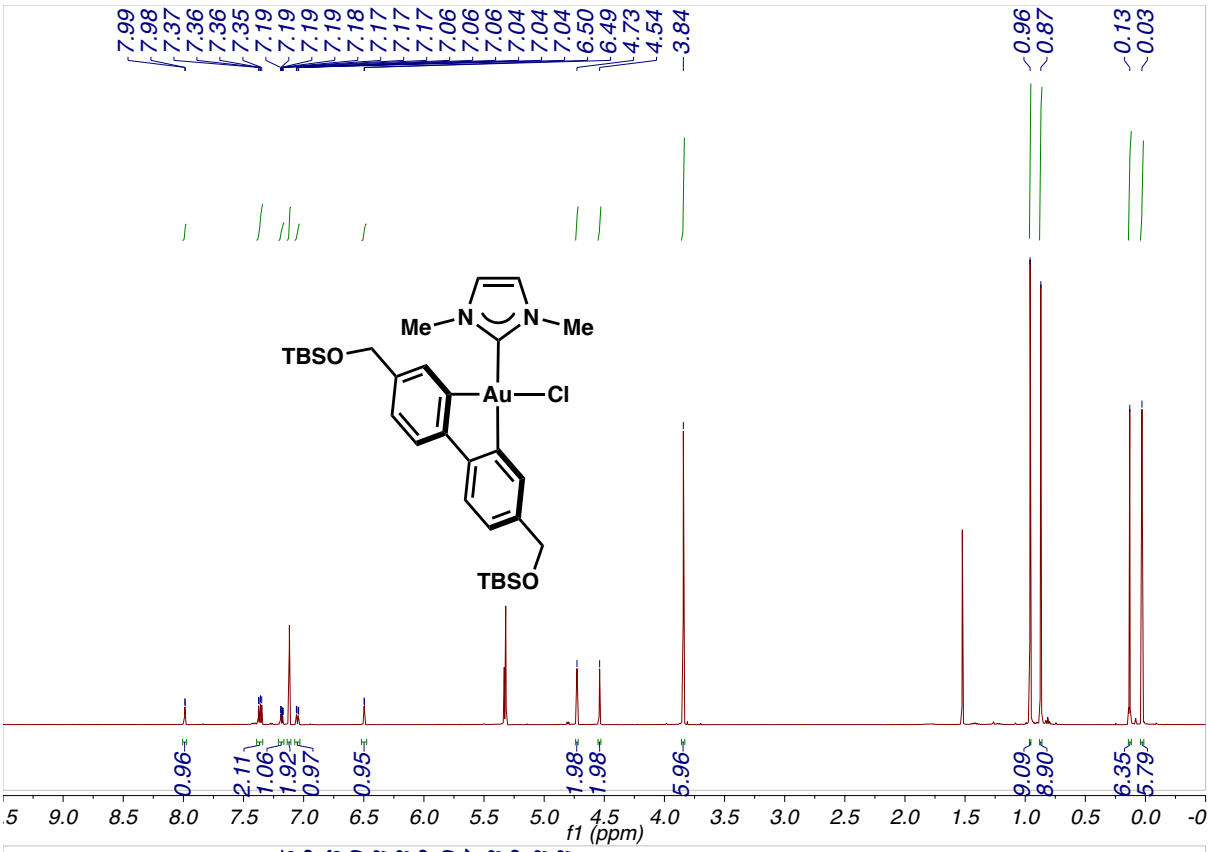
7.99
7.98
7.37
7.36
7.36
7.35
7.19
7.19
7.19
7.19
7.18
7.17
7.17
7.17
7.06
7.06
7.06
7.04
7.04
7.04
6.50
6.49
4.73
4.54
3.84
0.96
0.87
0.13
0.03
Me
N
N
Me
TBSO
Au
Cl
TBSO
0.96
2.11
1.06
1.92
0.97
0.95
1.98
1.98
5.96
9.09
8.90
6.35
5.79
f1 (ppm)

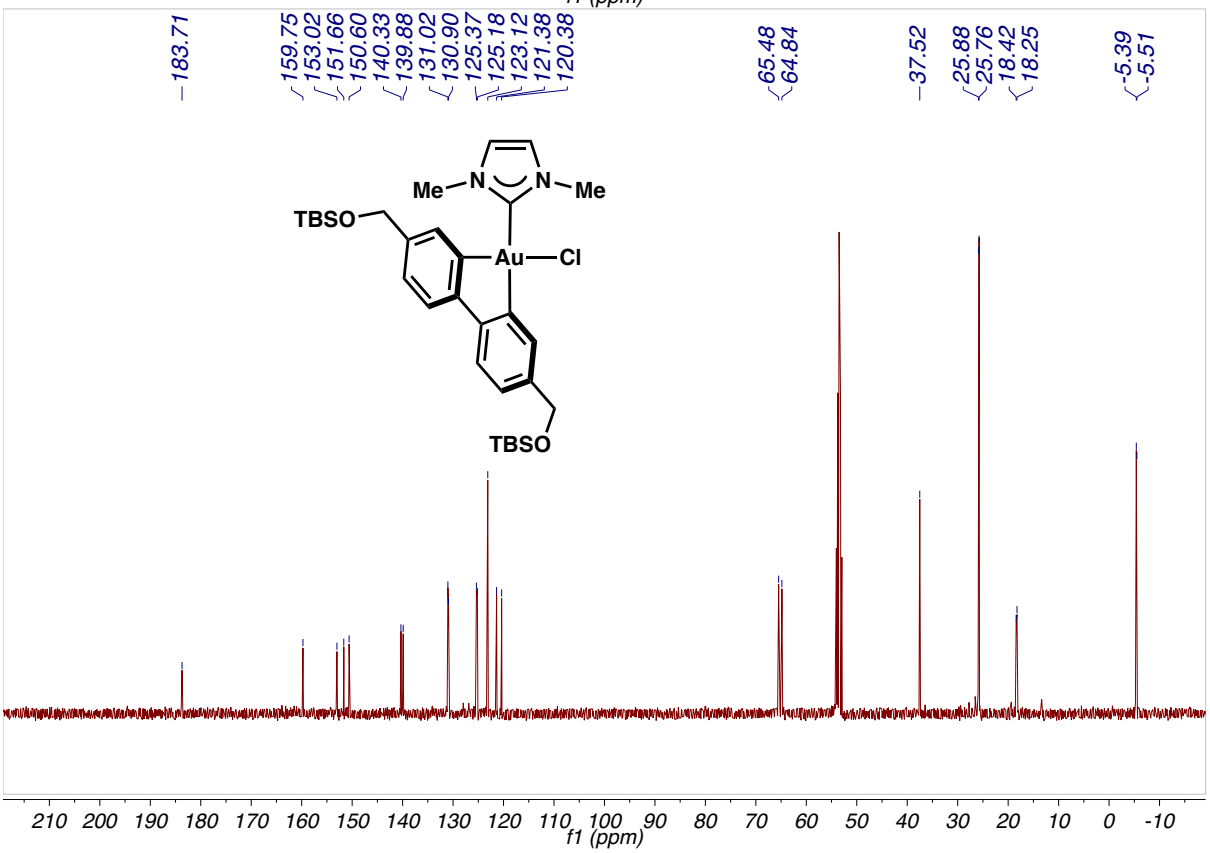
183.71
159.75
153.02
151.66
150.60
140.33
139.88
131.02
130.90
125.37
125.18
123.12
121.38
120.38
65.48
64.84
37.52
25.88
25.76
18.42
18.25
-5.39
-5.51
Me
N
N
Me
TBSO
Au
Cl
TBSO
f1 (ppm)

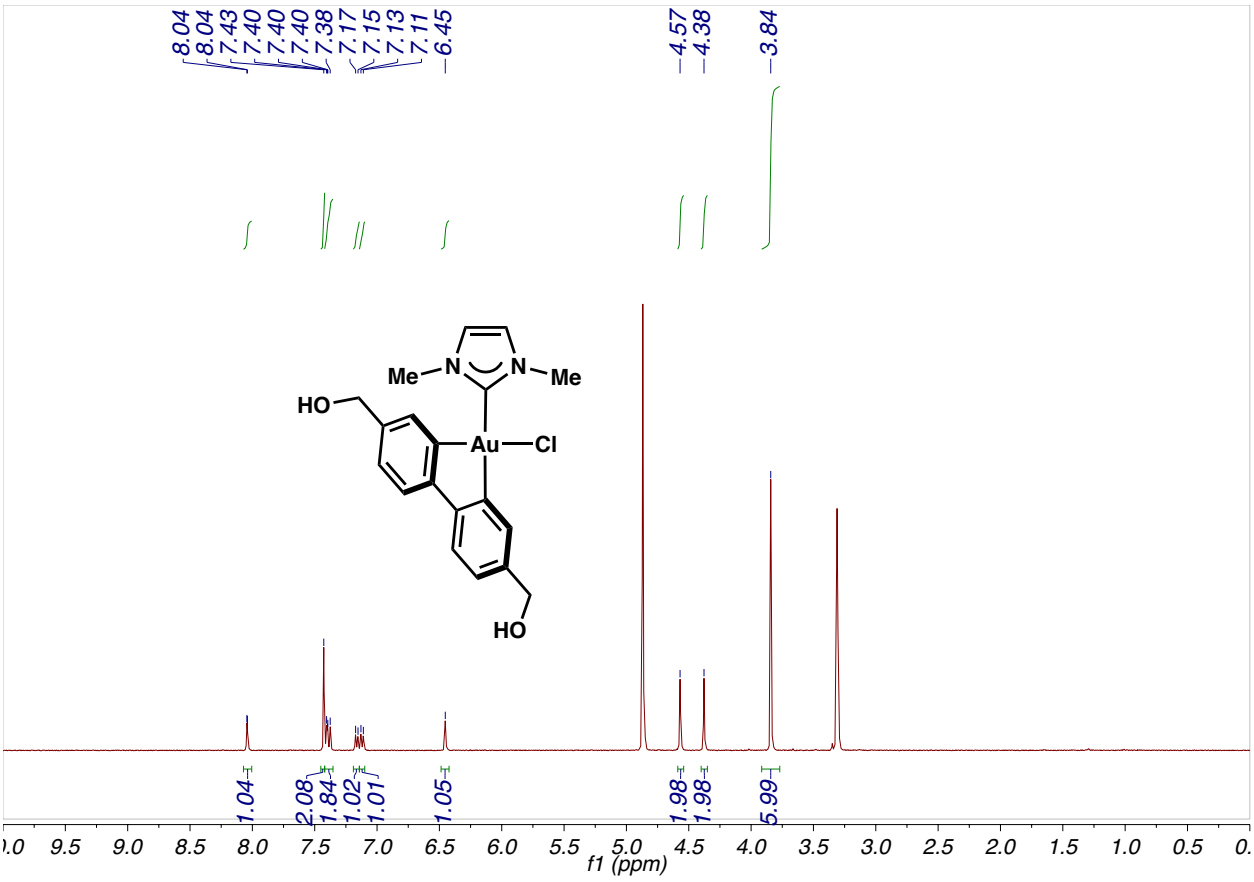
8.04
8.04
7.43
7.40
7.40
7.40
7.38
7.17
7.15
7.13
7.11
6.45
4.57
4.38
3.84
Me
N
N
Me
HO
Au
Cl
HO
1.04
2.08
1.84
1.02
1.01
1.05
1.98
1.98
5.99
f1 (ppm)

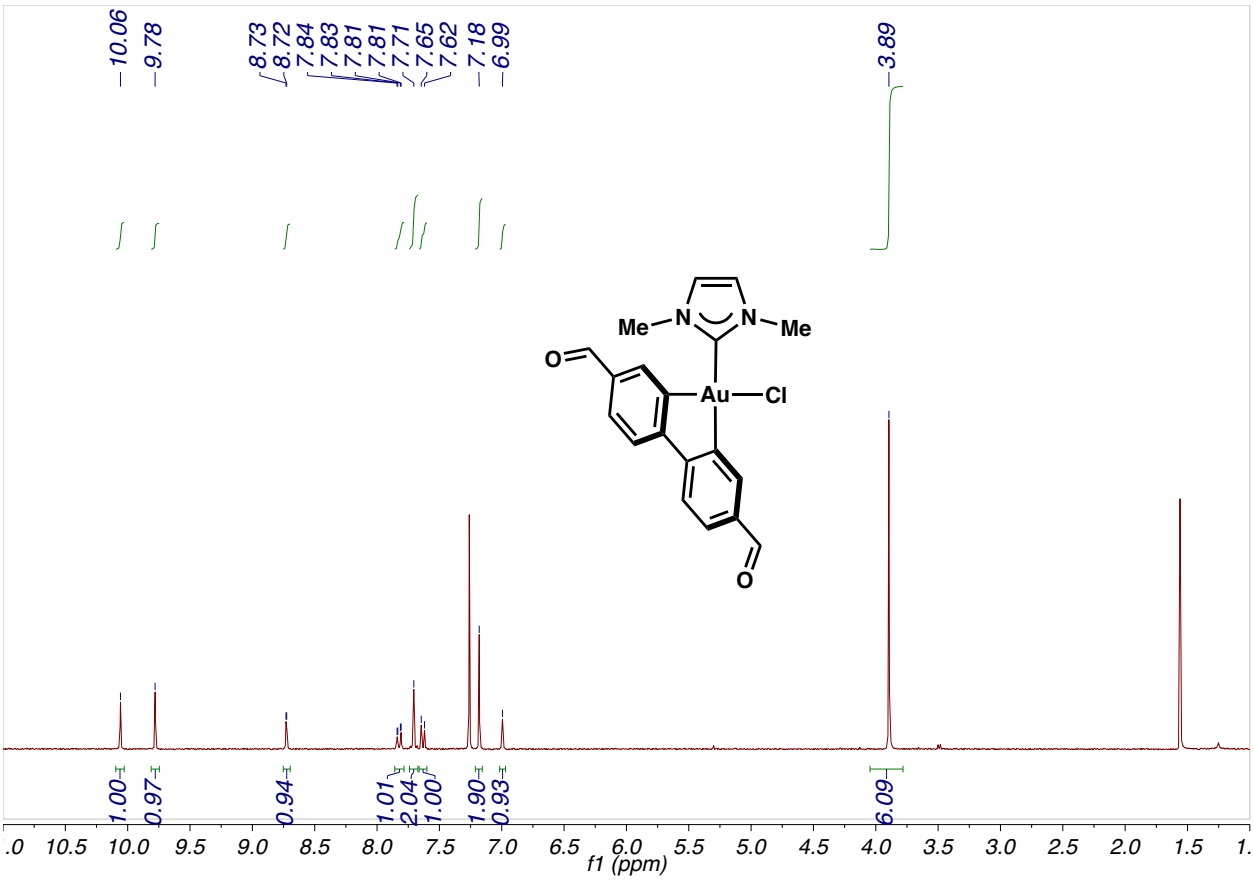
10.06
9.78
8.73
8.72
7.84
7.83
7.81
7.81
7.71
7.65
7.62
7.18
6.99
3.89
Me
N
N
Me
O
Au
Cl
O
1.00
0.97
0.94
1.01
2.04
1.00
1.90
0.93
6.09
f1 (ppm)

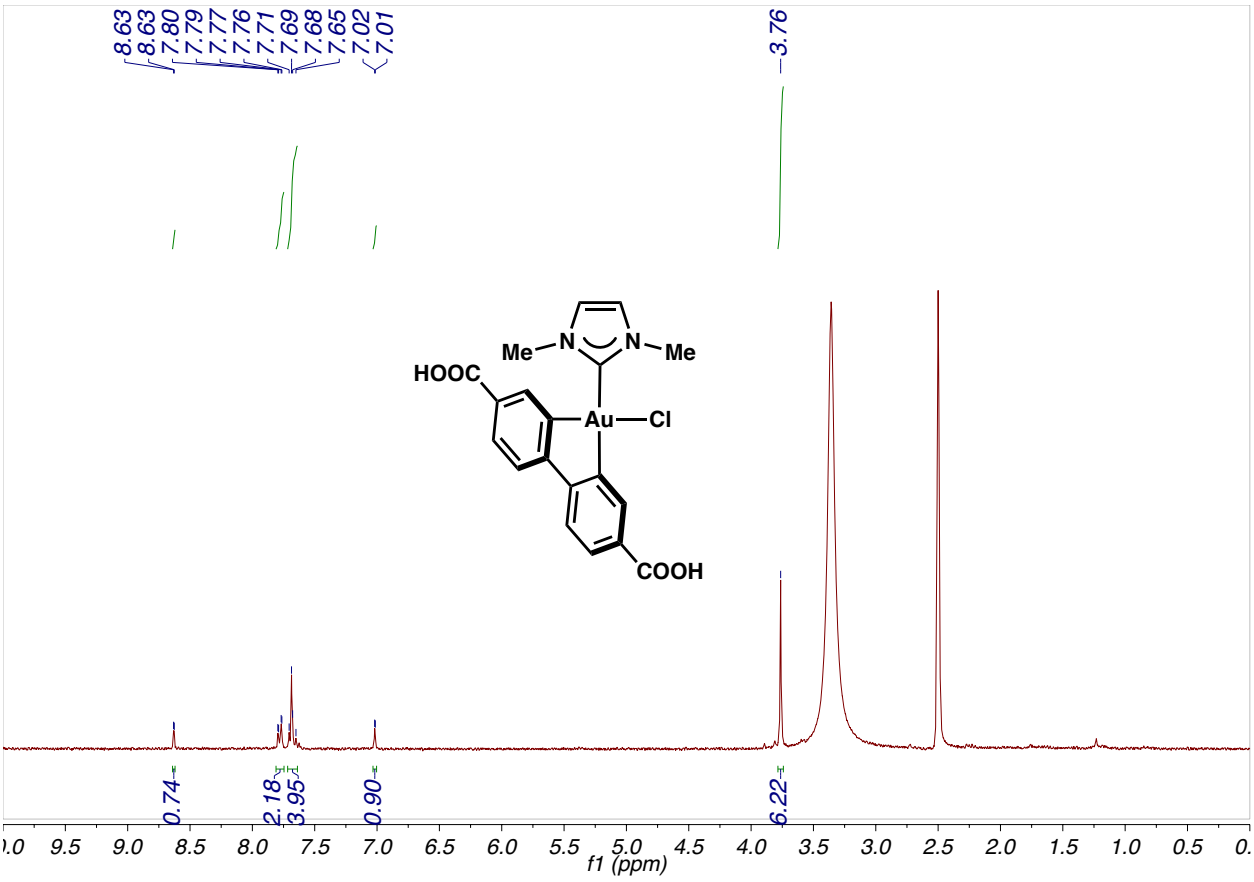
8.63
8.63
7.80
7.79
7.77
7.76
7.71
7.69
7.68
7.65
7.02
7.01
3.76
Me
N
N
Me
HOOC
Au
Cl
COOH
0.74
2.18
3.95
0.90
6.22
f1 (ppm)

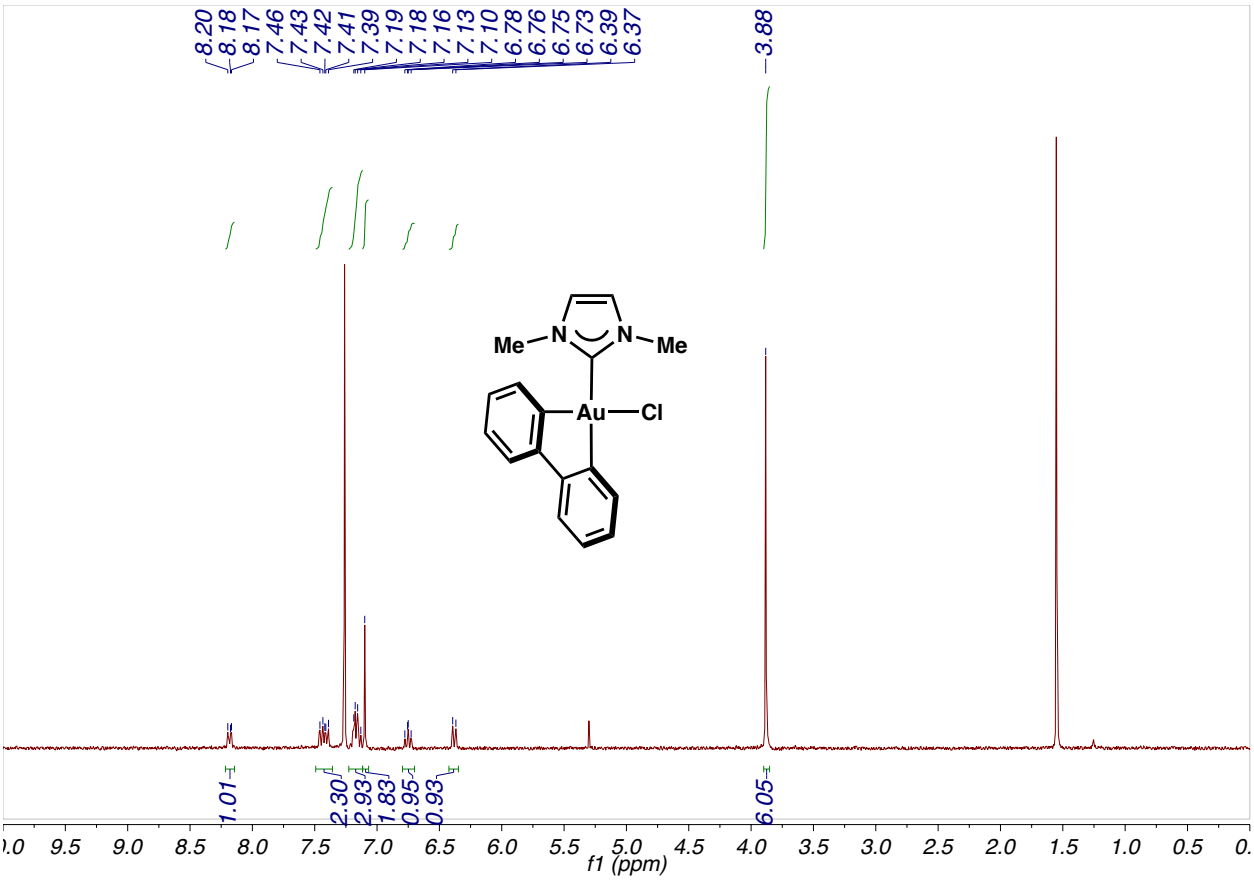
8.20
8.18
8.17
7.46
7.43
7.42
7.41
7.39
7.19
7.18
7.16
7.13
7.10
6.78
6.76
6.75
6.73
6.39
6.37
3.88
Me
N
N
Me
Au
Cl
1.01
2.30
2.93
1.83
0.95
0.93
6.05
f1 (ppm)

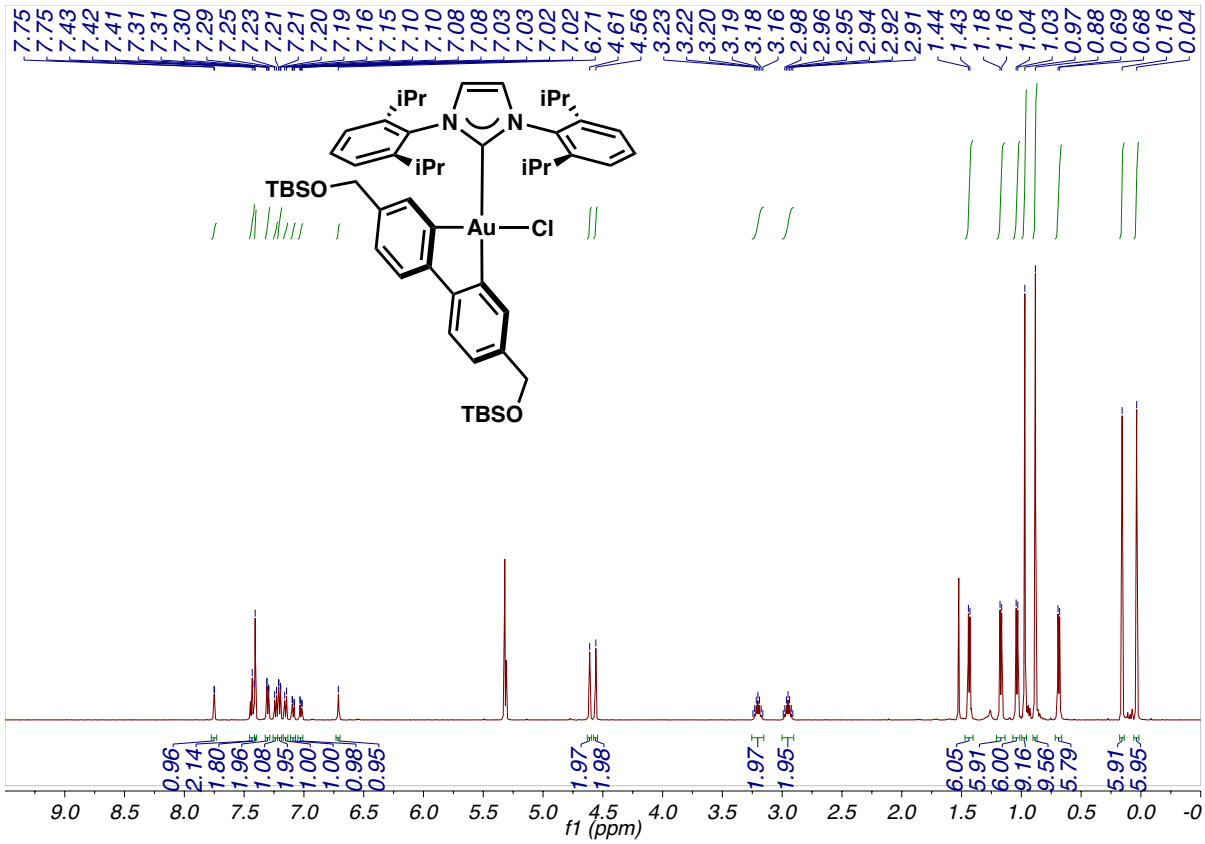
iPr
iPr
iPr
iPr
N
N
TBSO
Au
Cl
TBSO
f1 (ppm)

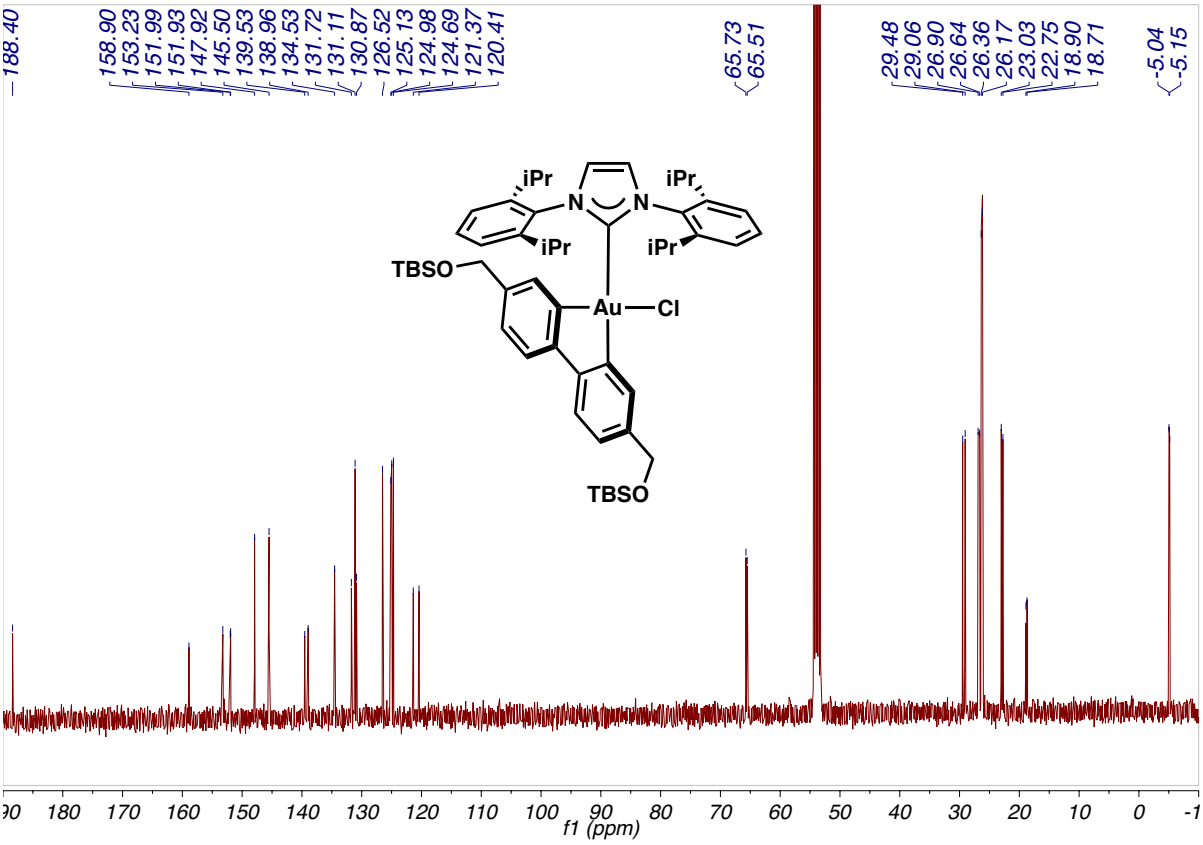
iPr
iPr
iPr
iPr
N
N
TBSO
Au
Cl
TBSO
f1 (ppm)

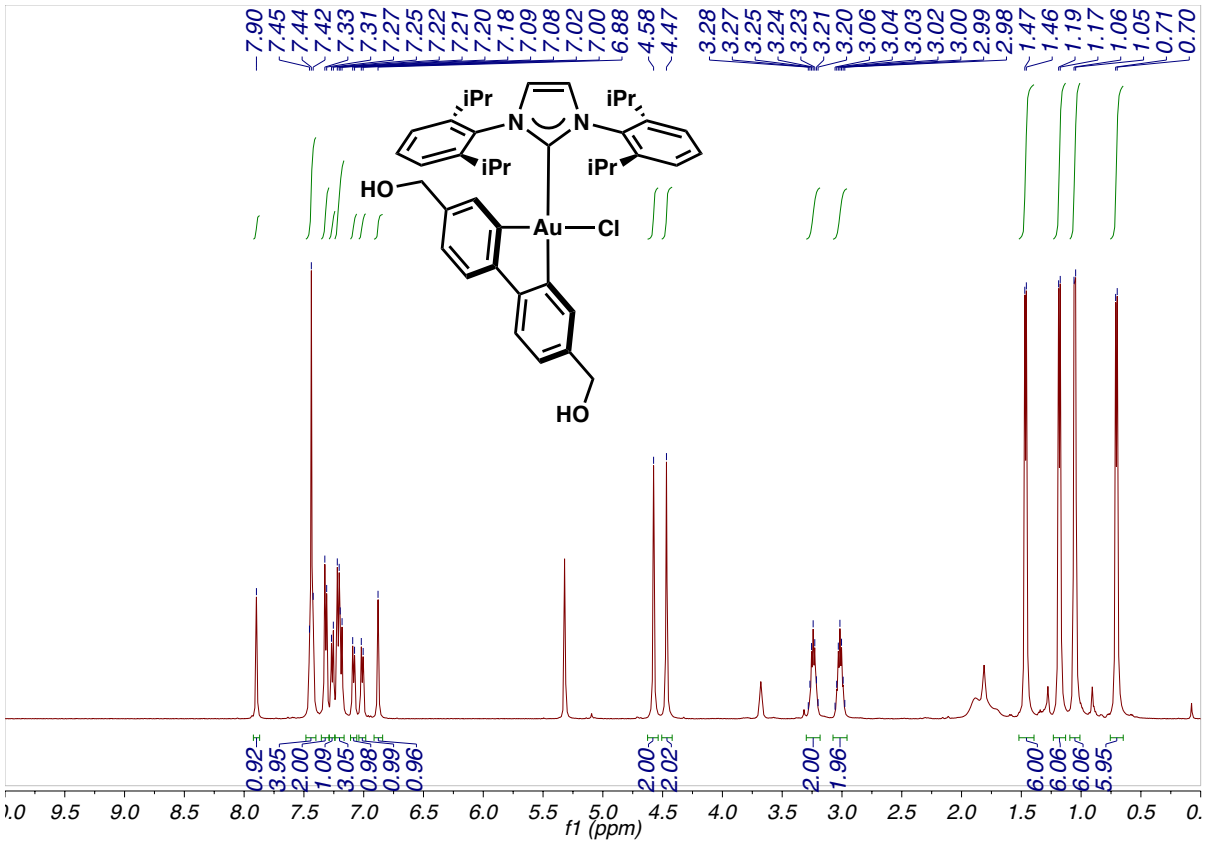
7.90
7.45
7.44
7.42
7.33
7.31
7.27
7.25
7.22
7.21
7.20
7.18
7.09
7.08
7.02
7.00
6.88
4.58
4.47
3.28
3.27
3.25
3.24
3.23
3.21
3.20
3.06
3.04
3.03
3.02
3.00
2.99
2.98
1.47
1.46
1.19
1.17
1.06
1.05
0.71
0.70
iPr
iPr
iPr
iPr
N
N
HO
Au
Cl
HO
0.92
3.95
2.00
1.09
3.05
0.98
0.99
0.96
2.00
2.02
2.00
1.96
6.00
6.06
6.06
5.95
f1 (ppm)

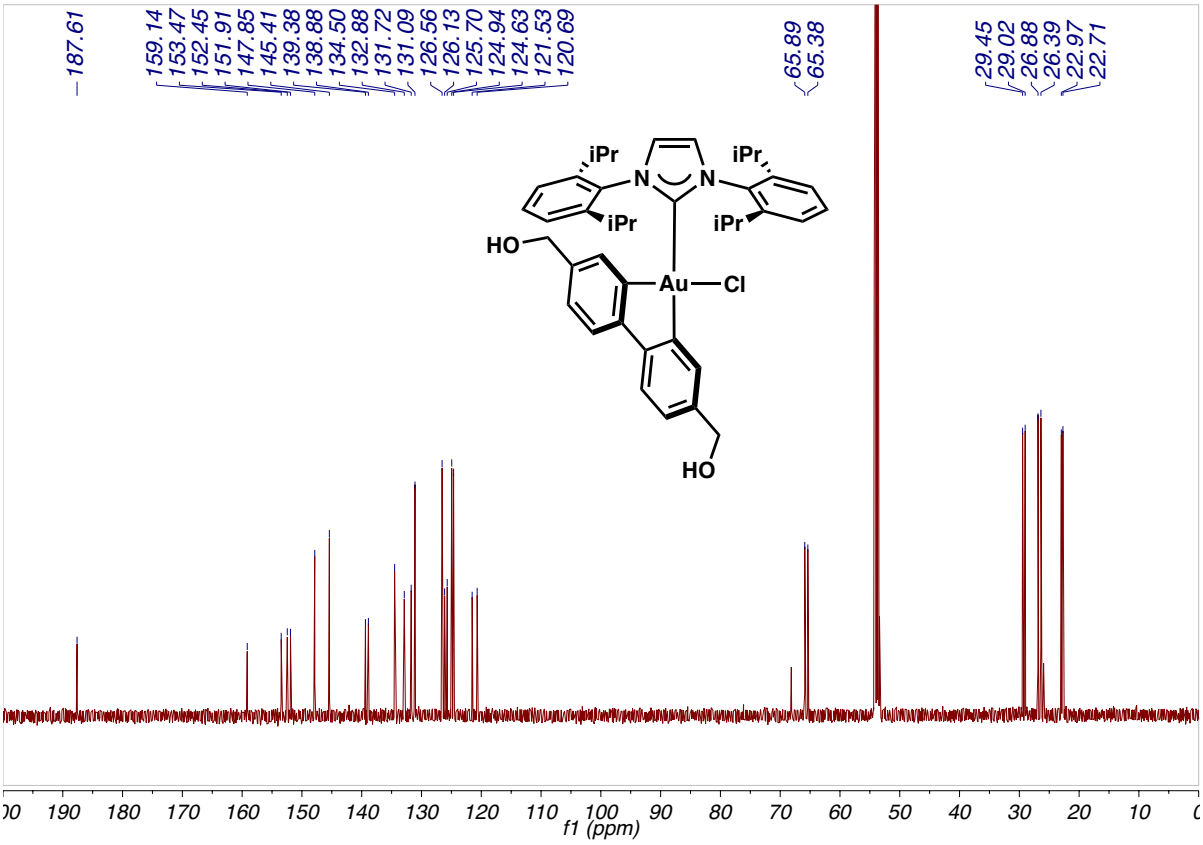
187.61
159.14
153.47
152.45
151.91
147.85
145.41
139.38
138.88
134.50
132.88
131.72
131.09
126.56
126.13
125.70
124.94
124.63
121.53
120.69
65.89
65.38
29.45
29.02
26.88
26.39
22.97
22.71
iPr
iPr
iPr
iPr
N
N
HO
Au
Cl
HO
f1 (ppm)

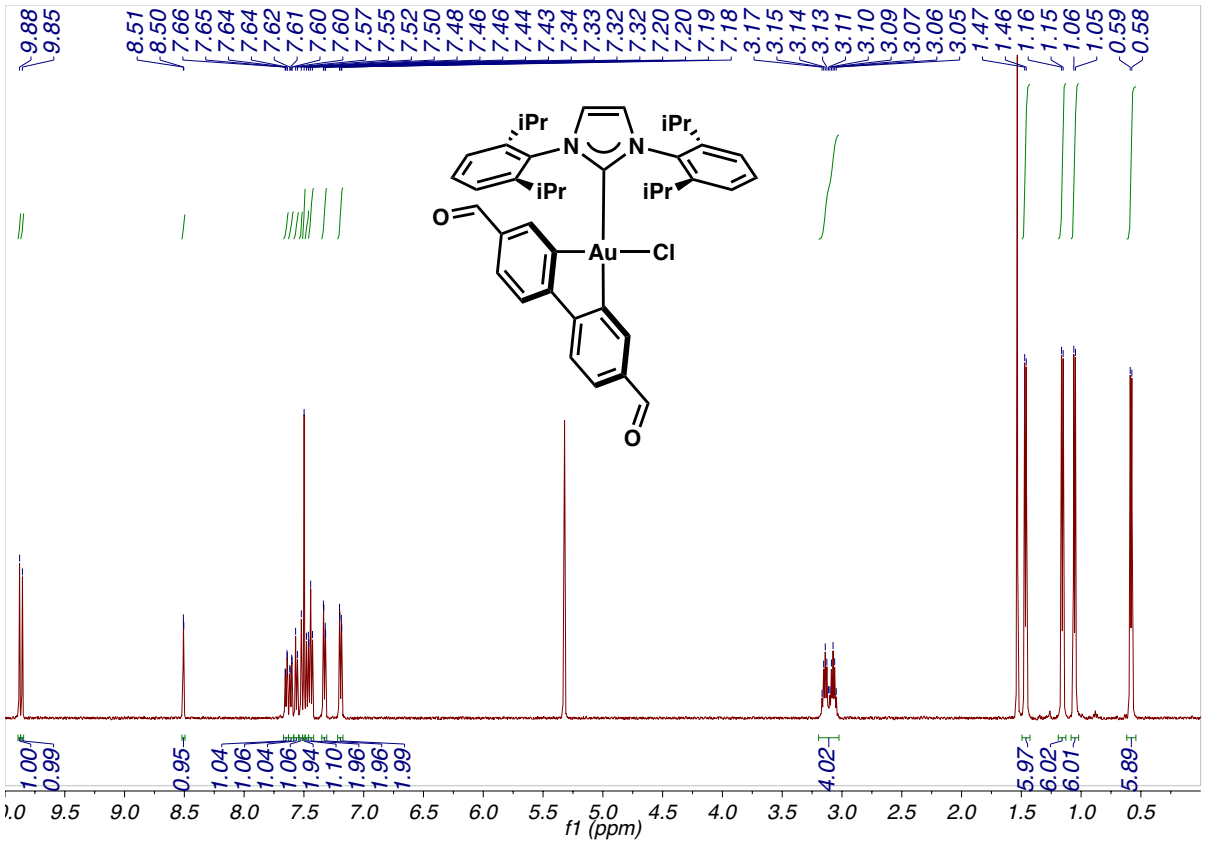
9.88
9.85
8.51
8.50
7.66
7.65
7.64
7.64
7.62
7.61
7.60
7.60
7.57
7.55
7.52
7.50
7.48
7.46
7.46
7.44
7.43
7.34
7.33
7.32
7.32
7.20
7.20
7.19
7.18
3.17
3.15
3.14
3.13
3.11
3.10
3.09
3.07
3.06
3.05
1.47
1.46
1.16
1.15
1.06
1.05
0.59
0.58
iPr
iPr
iPr
iPr
N
N
O
Au
Cl
O
1.00
0.99
0.95
1.04
1.06
1.04
1.06
1.94
1.10
1.96
1.96
1.99
4.02
5.97
6.02
6.01
5.89
f1 (ppm)

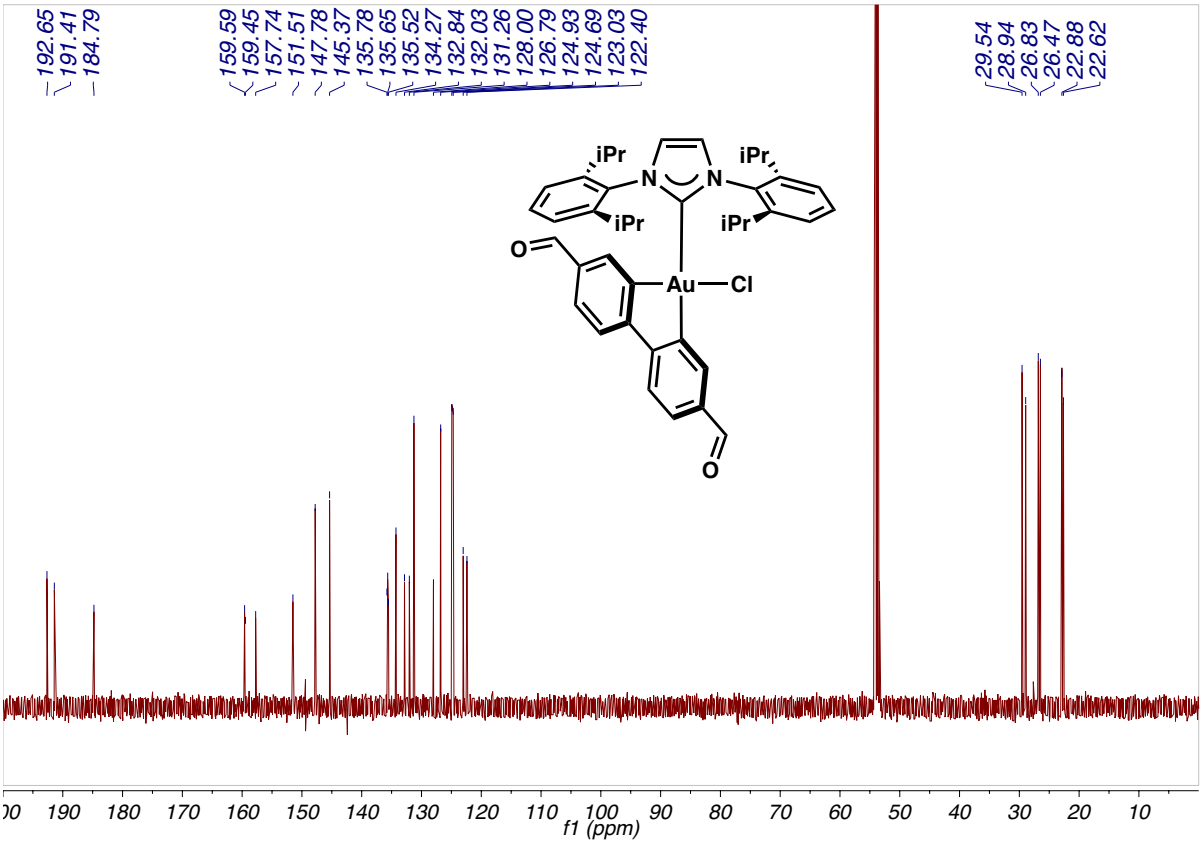
192.65
191.41
184.79
159.59
159.45
157.74
151.51
147.78
145.37
135.78
135.65
135.52
134.27
132.84
132.03
131.26
128.00
126.79
124.93
124.69
123.03
122.40
29.54
28.94
26.83
26.47
22.88
22.62
iPr
iPr
iPr
iPr
N
N
O
Au
Cl
O
f1 (ppm)

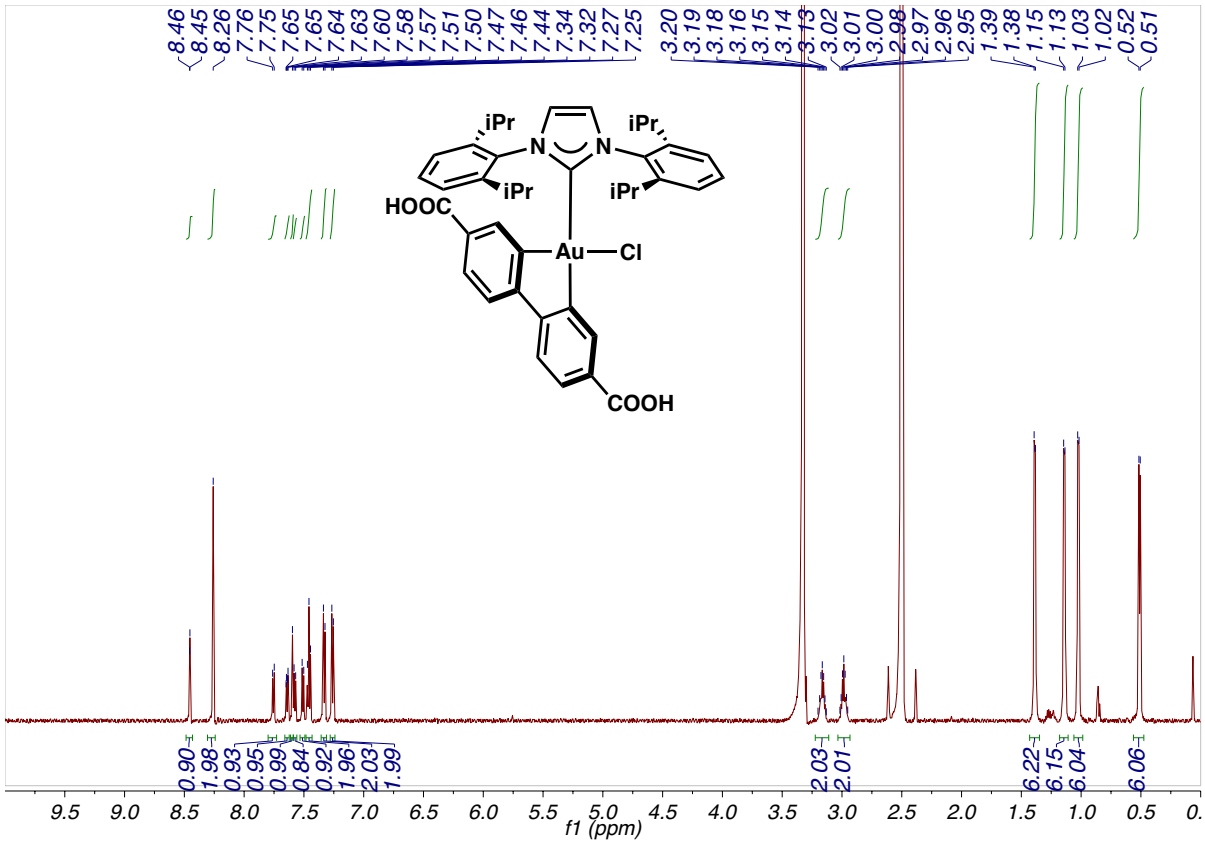
8.46
8.45
8.26
7.76
7.75
7.65
7.65
7.64
7.63
7.60
7.58
7.57
7.51
7.50
7.47
7.46
7.44
7.34
7.32
7.27
7.25
3.20
3.19
3.18
3.16
3.15
3.14
3.13
3.02
3.01
3.00
2.98
2.97
2.96
2.95
1.39
1.38
1.15
1.13
1.03
1.02
0.52
0.51
iPr
iPr
N
N
iPr
iPr
HOOC
Au
Cl
COOH
0.90
1.98
0.93
0.95
0.99
0.84
0.92
1.96
2.03
1.99
2.03
2.01
6.22
6.15
6.04
6.06
9.5
9.0
8.5
8.0
7.5
7.0
6.5
6.0
5.5
5.0
4.5
4.0
3.5
3.0
2.5
2.0
1.5
1.0
0.5
f1 (ppm)

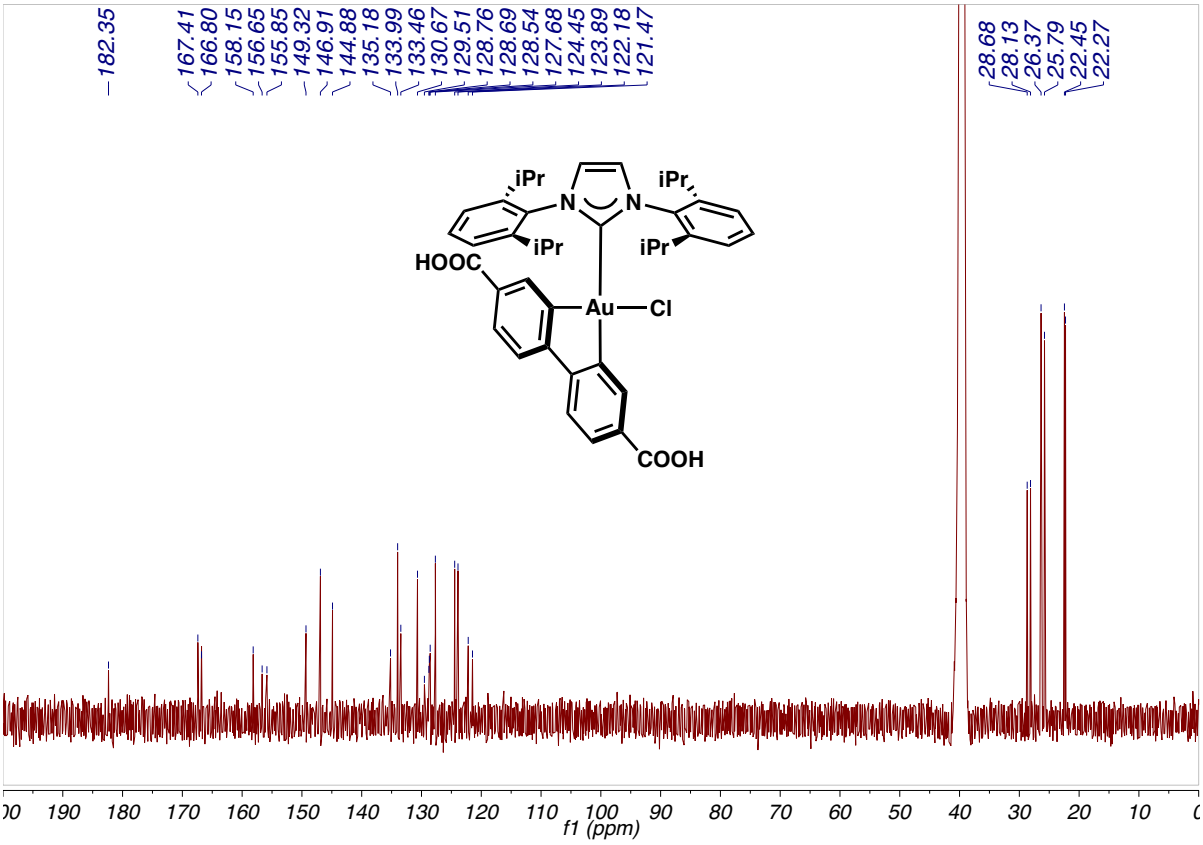
182.35
167.41
166.80
158.15
156.65
155.85
149.32
146.91
144.88
135.18
133.99
133.46
130.67
129.51
128.76
128.69
128.54
127.68
124.45
123.89
122.18
121.47
28.68
28.13
26.37
25.79
22.45
22.27
iPr
iPr
N
N
iPr
iPr
HOOC
Au
Cl
COOH
190
180
170
160
150
140
130
120
110
100
90
80
70
60
50
40
30
20
10
f1 (ppm)

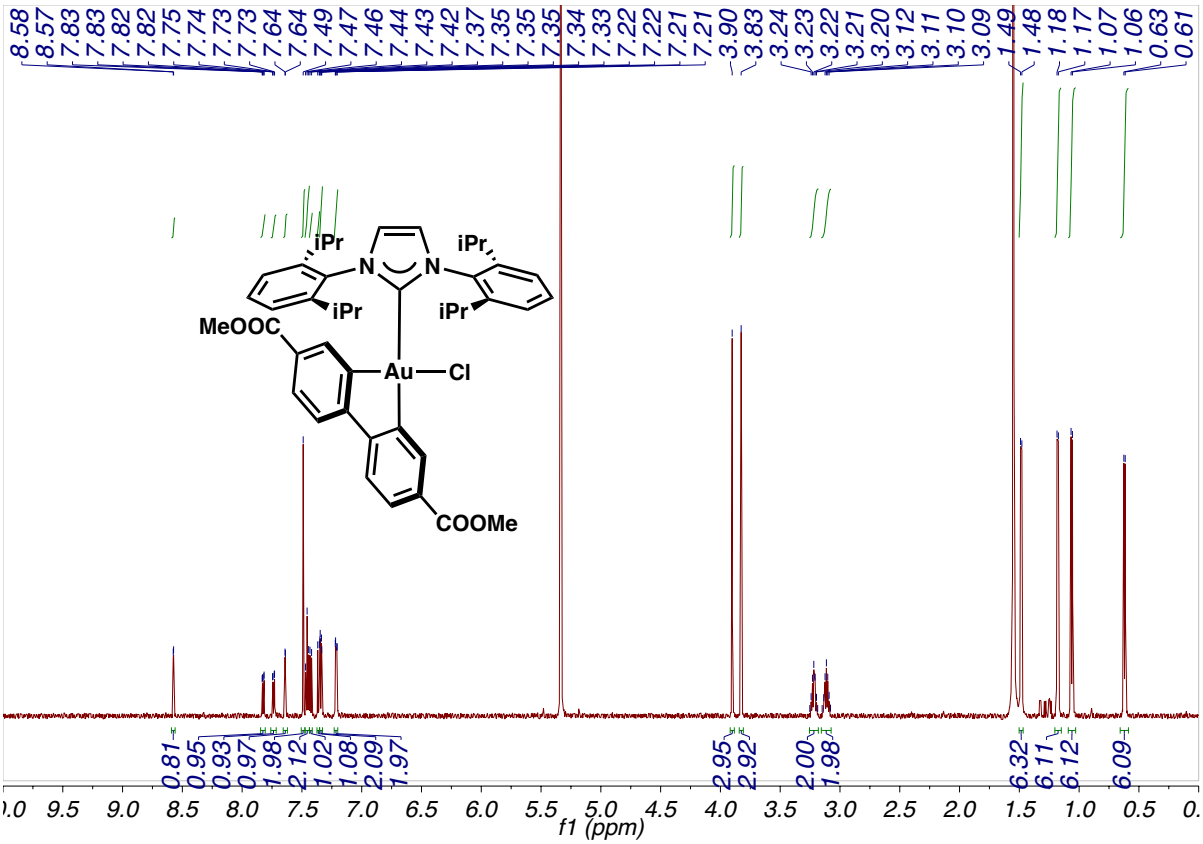
8.58 8.57 7.83 7.82 7.82 7.75 7.74 7.73 7.73 7.64 7.64 7.49 7.47 7.46 7.44 7.43 7.42 7.37 7.35 7.35 7.35 7.34 7.33 7.22 7.22 7.21 7.21 3.90 3.83 3.24 3.23 3.22 3.21 3.20 3.12 3.11 3.10 3.09 1.49 1.48 1.18 1.17 1.07 1.06 0.63 0.61
iPr
iPr
N
N
iPr
iPr
MeOOC
Au
Cl
COOMe
0.81 0.95 0.93 0.97 1.98 2.12 1.02 1.08 2.09 1.97 2.95 2.92 2.00 1.98 6.32 6.11 6.12 6.09
f1 (ppm)

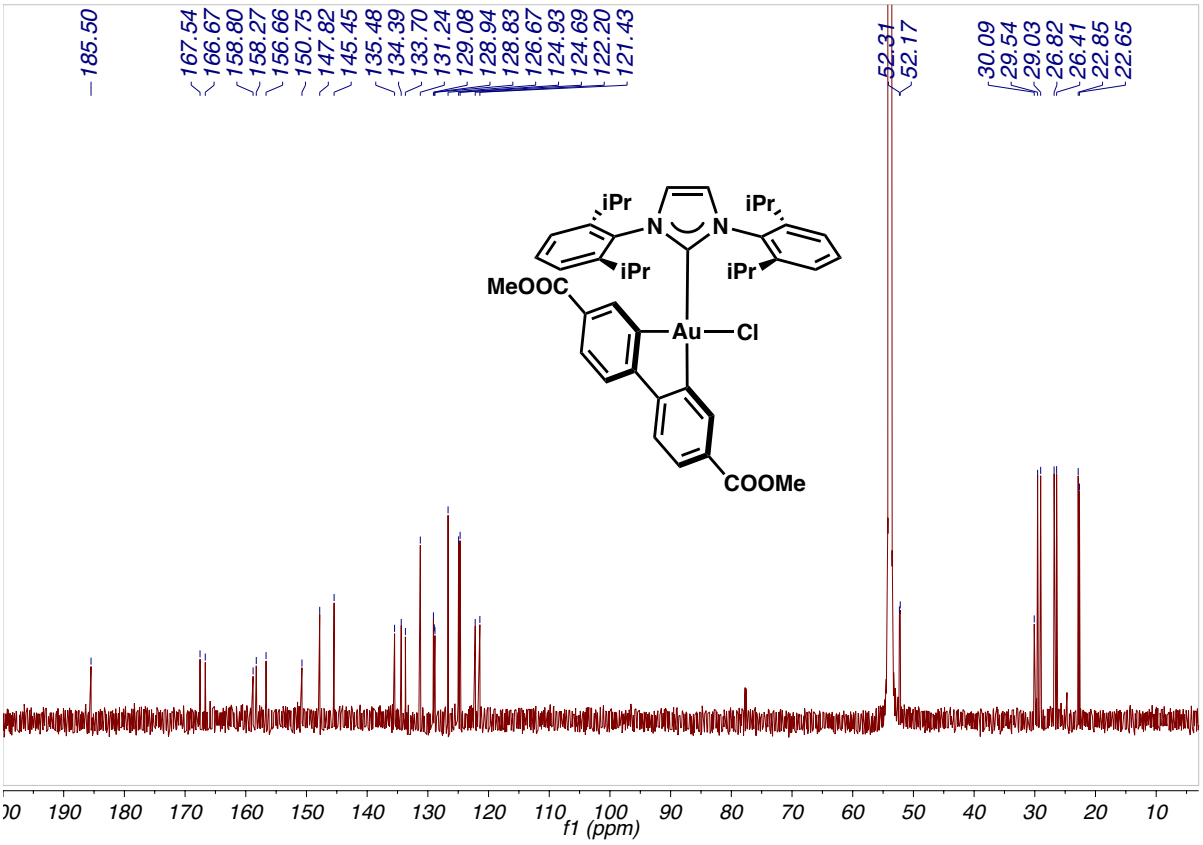
185.50 167.54 166.67 158.80 158.27 156.66 150.75 147.82 145.45 135.48 134.39 133.70 131.24 129.08 128.94 128.83 126.67 124.93 124.69 122.20 121.43 52.31 52.17 30.09 29.54 29.03 26.82 26.41 22.85 22.65
iPr
iPr
N
N
iPr
iPr
MeOOC
Au
Cl
COOMe
f1 (ppm)

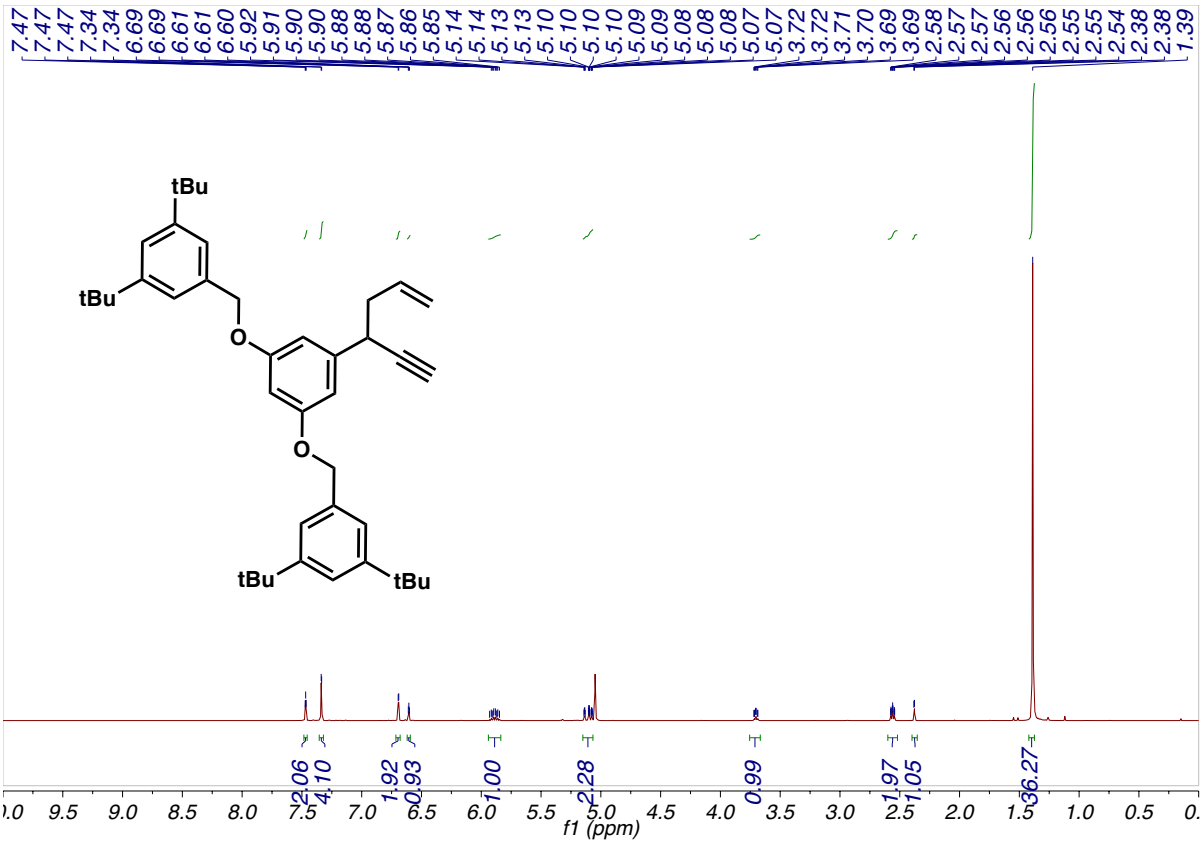
7.47 7.47 7.47 7.34 7.34 6.69 6.69 6.61 6.61 6.60 5.92 5.91 5.90 5.90 5.88 5.88 5.87 5.86 5.85 5.14 5.14 5.13 5.13 5.10 5.10 5.10 5.09 5.09 5.08 5.08 5.08 5.07 5.07 3.72 3.72 3.71 3.70 3.69 3.69 2.58 2.57 2.57 2.56 2.56 2.56 2.55 2.55 2.54 2.38 2.38 1.39
tBu
tBu
O
O
tBu
tBu
2.06 4.10 1.92 0.93 1.00 2.28 0.99 1.97 1.05 36.27
f1 (ppm)

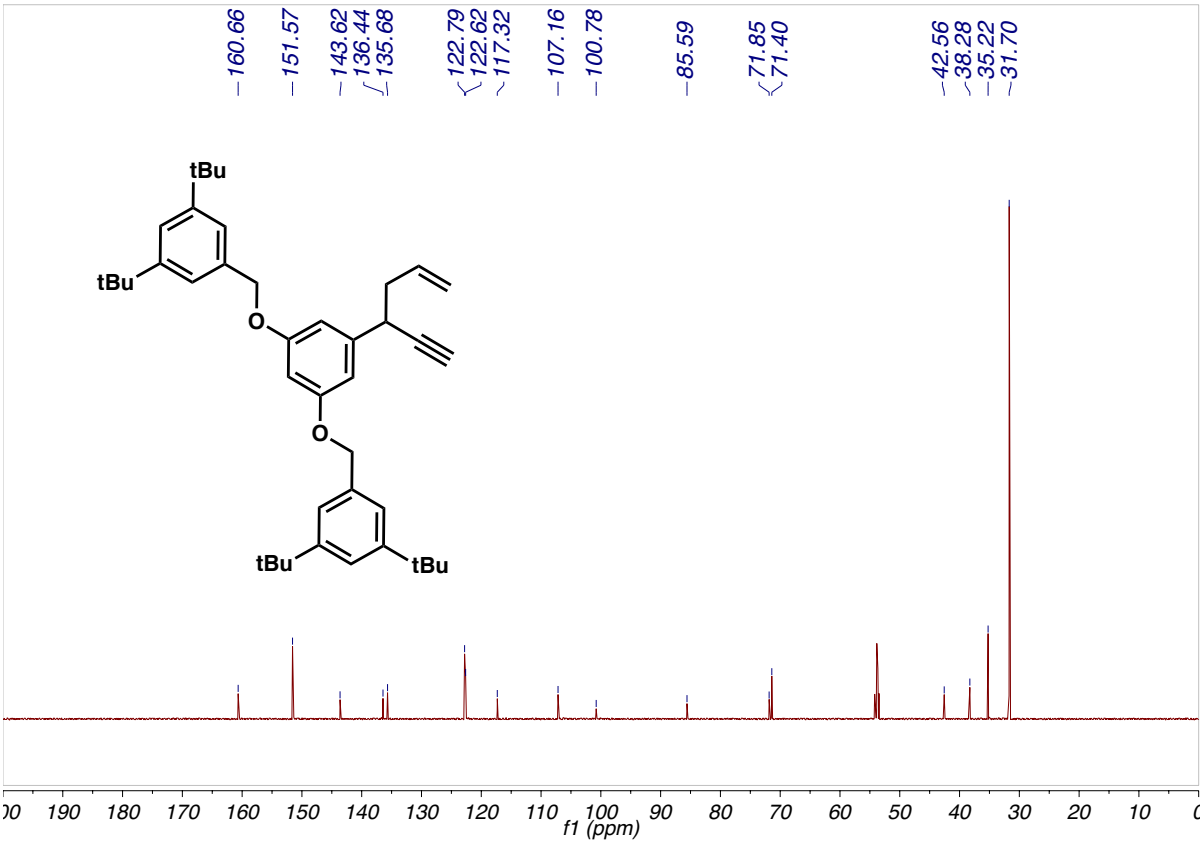
160.66 151.57 143.62 136.44 135.68 122.79 122.62 117.32 107.16 100.78 85.59 71.85 71.40 42.56 38.28 35.22 31.70
tBu
tBu
O
O
tBu
tBu
f1 (ppm)

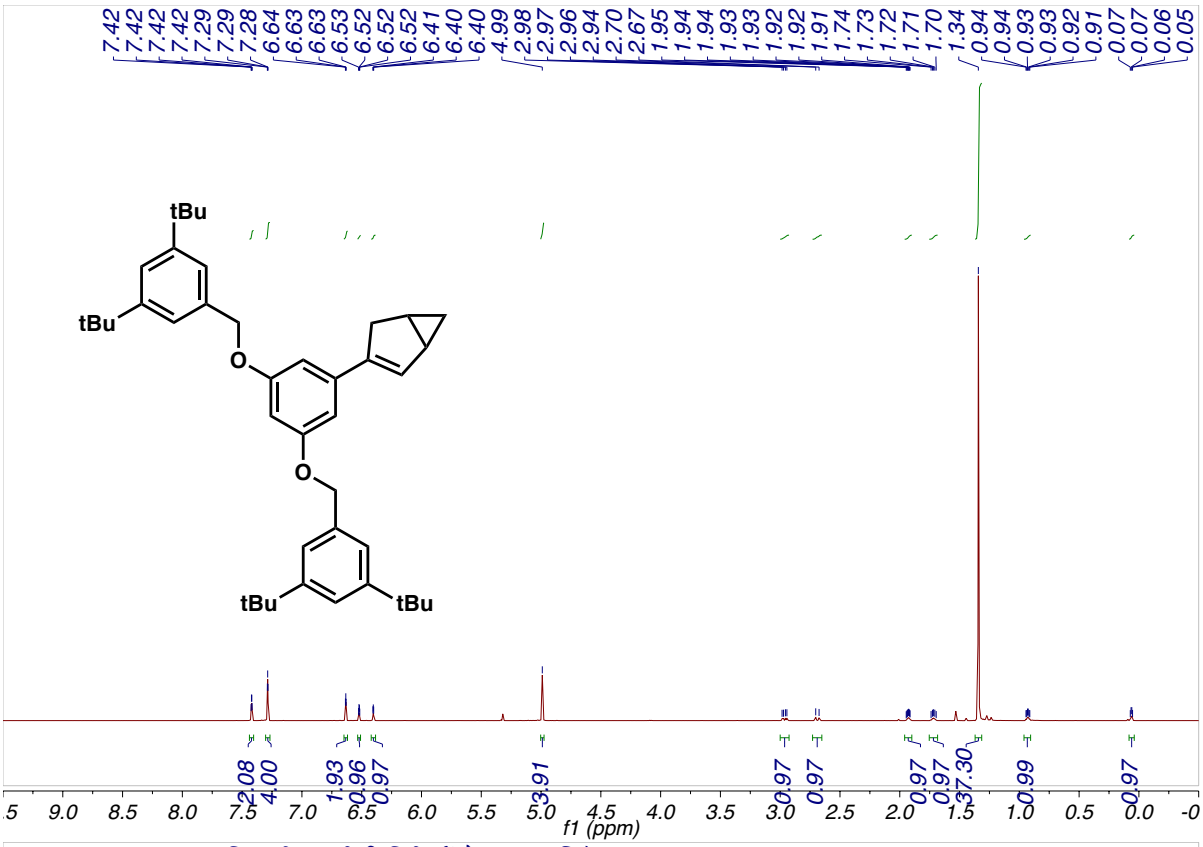
7.42 7.42 7.42 7.42 7.29 7.29 7.28 6.64 6.63 6.63 6.53 6.52 6.52 6.52 6.41 6.40 6.40 4.99 2.98 2.97 2.96 2.94 2.70 2.67 1.95 1.94 1.94 1.93 1.93 1.92 1.92 1.91 1.74 1.73 1.72 1.71 1.70 1.34 0.94 0.94 0.93 0.93 0.92 0.91 0.07 0.07 0.06 0.05
tBu
tBu
O
O
tBu
tBu
2.08 4.00 1.93 0.96 0.97 3.91 0.97 0.97 0.97 0.97 7.30 0.99 0.97
f1 (ppm)

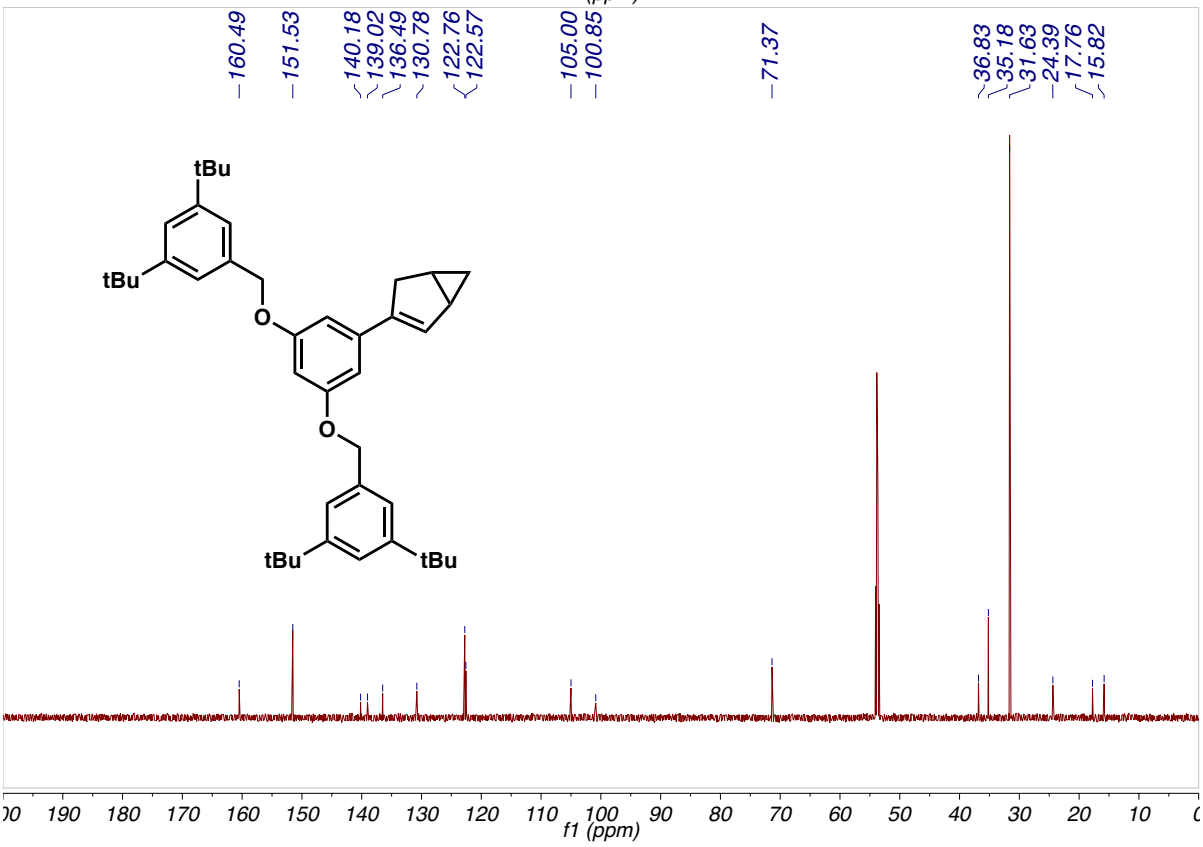
160.49 151.53 140.18 139.02 136.49 130.78 122.76 122.57 105.00 100.85 71.37 36.83 35.18 31.63 24.39 17.76 15.82
tBu
tBu
O
O
tBu
tBu
f1 (ppm)

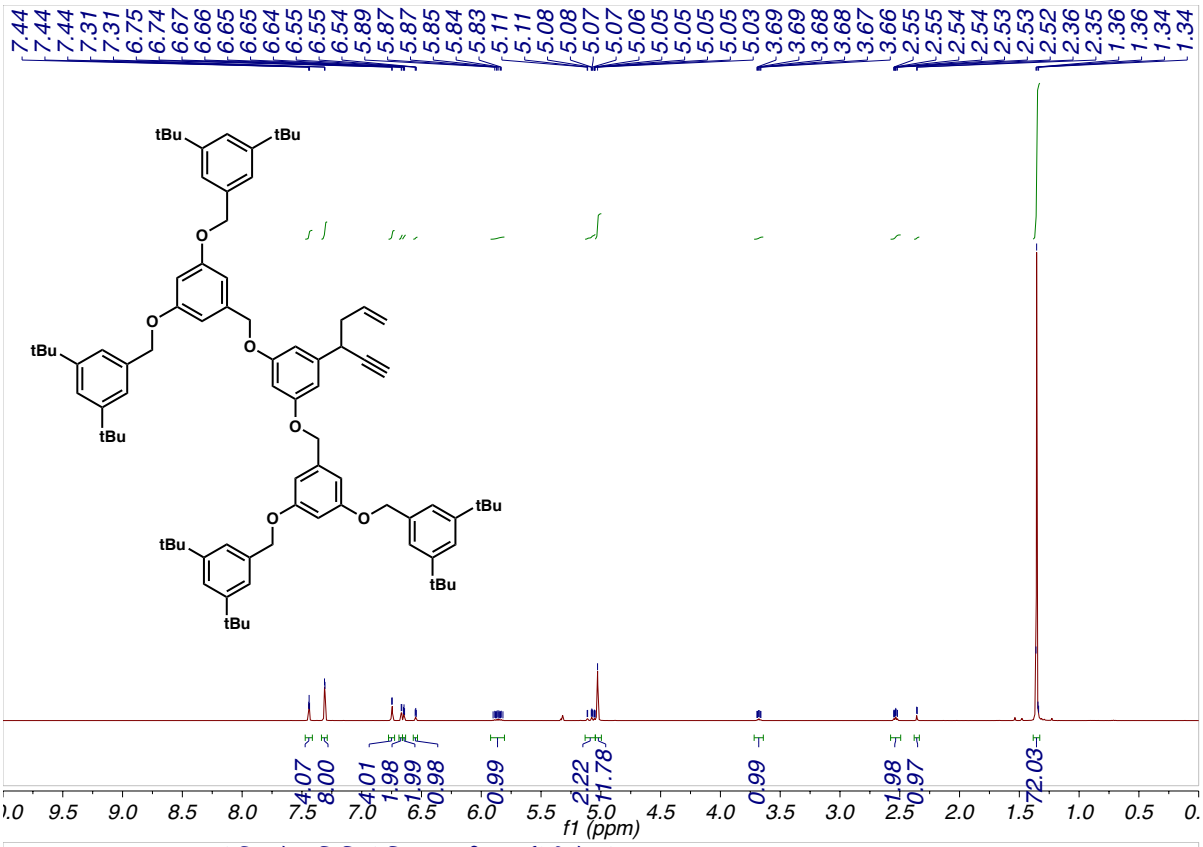
7.44 7.44 7.44 7.31 7.31 6.75 6.74 6.67 6.66 6.65 6.65 6.64 6.55 6.55 6.54 5.89 5.87 5.87 5.85 5.84 5.83 5.11 5.11 5.08 5.08 5.07 5.07 5.06 5.05 5.05 5.05 5.03 3.69 3.69 3.68 3.68 3.67 3.66 2.55 2.55 2.54 2.54 2.53 2.53 2.52 2.36 2.35 1.36 1.36 1.34 1.34
tBu
O
4.07 8.00 4.01 1.98 1.99 0.98 0.99 2.22 11.78 0.99 1.98 0.97 72.03
f1 (ppm)

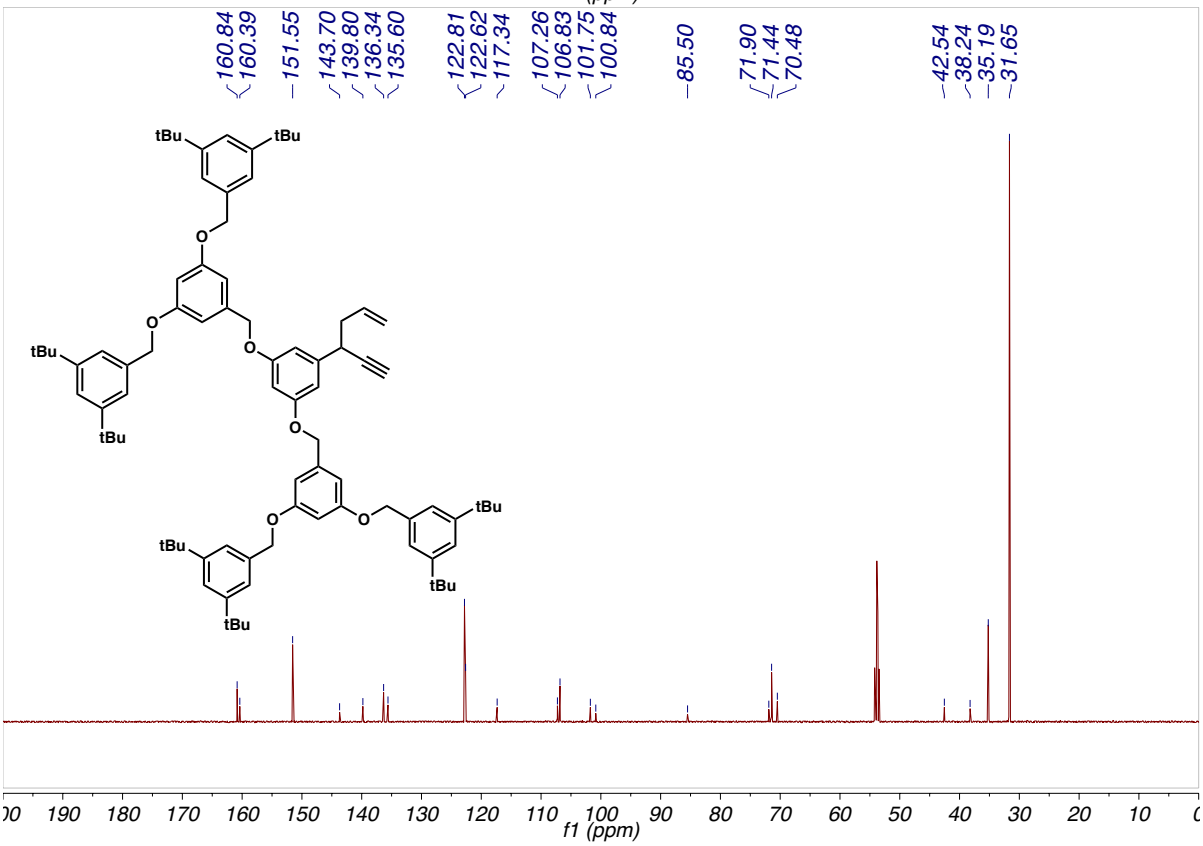
160.84 160.39 151.55 143.70 139.80 136.34 135.60 122.81 122.62 117.34 107.26 106.83 101.75 100.84 85.50 71.90 71.44 70.48 42.54 38.24 35.19 31.65
tBu
O
f1 (ppm)

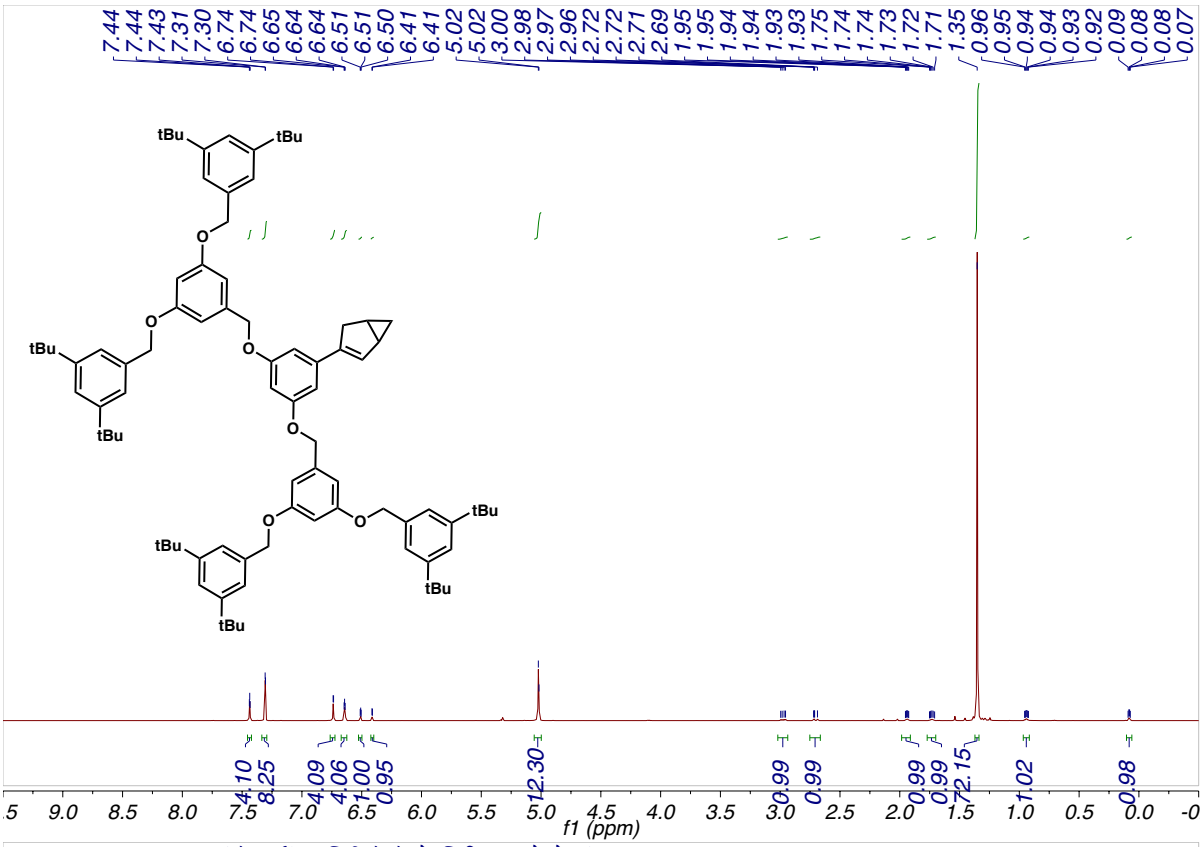
7.44 7.44 7.43 7.31 7.30 6.74 6.74 6.65 6.64 6.64 6.51 6.51 6.50 6.41 6.41 5.02 5.02 3.00 2.98 2.97 2.96 2.72 2.72 2.71 2.69 1.95 1.95 1.94 1.94 1.93 1.93 1.75 1.74 1.74 1.73 1.72 1.71 1.35 0.96 0.95 0.94 0.94 0.93 0.92 0.09 0.08 0.08 0.07
tBu
O
4.10 8.25 4.09 4.06 4.00 0.95 12.30 0.99 0.99 0.99 0.99 12.15 1.02 0.98
f1 (ppm)

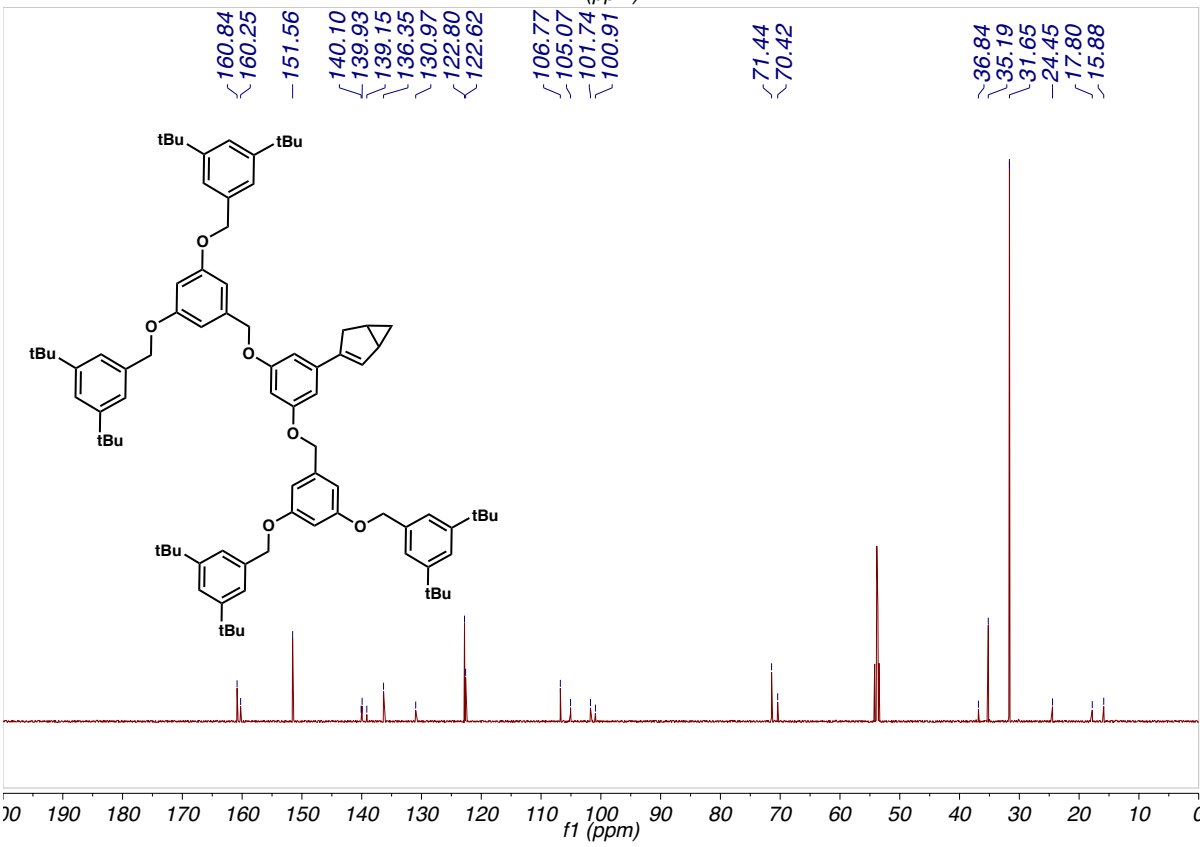
160.84 160.25 151.56 140.10 139.93 139.15 136.35 130.97 122.80 122.62 106.77 105.07 101.74 100.91 71.44 70.42 36.84 35.19 31.65 24.45 17.80 15.88
tBu
O
f1 (ppm)

2.5 References

(1) Davis, D. A.; Moore, J. S.; Caruso, M. M.; White, S. R.; Sottos, N. R.; Odom, S. A.; Shen, Q. *Chem. Rev.* **2009**, *109*, 5755.

(2) May, P. A.; Moore, J. S. *Chem. Soc. Rev.* **2013**, *42*, 7497.

(3) Beyer, M. K.; Clausen-Schaumann, H. *Chem. Rev.* **2005**, *105*, 2921.

(4) Hickenboth, C. R.; Moore, J. S.; White, S. R.; Sottos, N. R.; Baudry, J.; Wilson, S. R. *Nature* **2007**, *446*, 423.

(5) Chen, Z.; Mercer, J. A. M.; Zhu, X.; Romaniuk, J. A. H.; Pfattner, R.; Cegelski, L.; Martinez, T. J.; Burns, N. Z.; Xia, Y. *Science* **2017**, *357*, 475.

(6) Kean, Z. S.; Niu, Z.; Hewage, G. B.; Rheingold, A. L.; Craig, S. L. *J. Am. Chem. Soc.* **2013**, *135*, 13598.

(7) Diesendruck, C. E.; Steinberg, B. D.; Sugai, N.; Silberstein, M. N.; Sottos, N. R.; White, S. R.; Braun, P. V.; Moore, J. S. *J. Am. Chem. Soc.* **2012**, *134*, 12446.

(8) Piermattei, A.; Karthikeyan, S.; Sijbesma, R. P. *Nat. Chem.* **2009**, *1*, 133.

(9) Groote, R.; Jakobs, R. T. M.; Sijbesma, R. P. *Polym. Chem.* **2013**, *4*, 4846.

(10) Huang, W.; Wu, X.; Gao, X.; Yu, Y.; Lei, H.; Zhu, Z.; Shi, Y.; Chen, Y.; Qin, M.; Wang, W.; Cao, Y. *Nat. Chem.* **2019**, *11*, 310.

(11) Segelstein, B. E.; Butler, T. W.; Chenard, B. L. *J. Org. Chem.* **1995**, *60*, 12.

(12) Kawai, H.; Wolf, W. J.; DiPasquale, A. G.; Winston, M. S.; Toste, F. D. *J. Am. Chem. Soc.* **2016**, *138*, 587.

(13) Zhukhovitskiy, A. V.; Kobylianskii, I. J.; Wu, C.-Y.; Toste, F. D. *J. Am. Chem. Soc.* **2018**, *140*, 466.

(14) Rhers, B.; Quadrelli, E. A.; Baudouin, A.; Taoufik, M.; Copéret, C.; Lefebvre, F.; Basset, J.-M.; Fenet, B.; Sinha, A.; Schrock, R. R. *J. Organomet. Chem.* **2006**, *691*, 5448.

(15) Zhang, T.; Manna, K.; Lin, W. *J. Am. Chem. Soc.* **2016**, *138*, 3241.

(16) Choi, K. M.; Kim, D.; Rungtaweevoranit, B.; Trickett, C. A.; Barmanbek, J. T. D.; Alshammari, A. S.; Yang, P.; Yaghi, O. M. *J. Am. Chem. Soc.* **2017**, *139*, 356.

(17) Lee, S.; Kapustin, E. A.; Yaghi, O. M. *Science (80-.).* **2016**, *353*, 808.

(18) Kapustin, E. A.; Lee, S.; Alshammari, A. S.; Yaghi, O. M. *ACS Cent. Sci.* **2017**, *3*, 662.

(19) Yuan, S.; Lu, W.; Chen, Y.-P.; Zhang, Q.; Liu, T.-F.; Feng, D.; Wang, X.; Qin, J.; Zhou,

H.-C. *J. Am. Chem. Soc.* **2015**, *137*, 3177.

(20) Lee, J.; Farha, O. K.; Roberts, J.; Scheidt, K. A.; Nguyen, S. T.; Hupp, J. T. *Chem. Soc. Rev.* **2009**, *38*, 1450.

(21) Yoon, M.; Srirambalaji, R.; Kim, K. *Chem. Rev.* **2012**, *112*, 1196.

(22) Zhang, T.; Lin, W. *Chem. Soc. Rev.* **2014**, *43*, 5982.

(23) Ma, L.; Abney, C.; Lin, W. *Chem. Soc. Rev.* **2009**, *38*, 1248.

(24) Kwong, C.-Y.; Chan, T.-L.; Chow, H.-F.; Lin, S.-C.; Leung, M.-K. *J. Chinese Chem. Soc.* **1997**, *44*, 211.

(25) Yu, X.; Cohen, S. M. *Chem. Commun.* **2015**, *51*, 9880.

(26) McGuirk, C. M.; Katz, M. J.; Stern, C. L.; Sarjeant, A. A.; Hupp, J. T.; Farha, O. K.; Mirkin, C. A. *J. Am. Chem. Soc.* **2015**, *137*, 919.

(27) Wei, Y.-L.; Li, Y.; Chen, Y.-Q.; Dong, Y.; Yao, J.-J.; Han, X.-Y.; Dong, Y.-B. *Inorg. Chem.* **2018**, *57*, 4379.

(28) Huang, Z.; Liu, D.; Camacho-Bunquin, J.; Zhang, G.; Yang, D.; López-Encarnación, J. M.; Xu, Y.; Ferrandon, M. S.; Niklas, J.; Poluektov, O. G.; Jellinek, J.; Lei, A.; Bunel, E. E.; Delferro, M. *Organometallics* **2017**, *36*, 3921.

(29) An, J.; Farha, O. K.; Hupp, J. T.; Pohl, E.; Yeh, J. I.; Rosi, N. L. *Nat. Commun.* **2012**, *3*, 604.

(30) Wu, C.-Y.; Horibe, T.; Jacobsen, C. B.; Toste, F. D. *Nature* **2014**, *517*, 449.

(31) Kleinbeck, F.; Toste, F. D. *J. Am. Chem. Soc.* **2009**, *131*, 9178.

(32) McGonigal, P. R.; de León, C.; Wang, Y.; Homs, A.; Solorio-Alvarado, C. R.; Echavarren, A. M. *Angew. Chem. Int. Ed.* **2012**, *51*, 13093.

(33) Chen, M.; Zhang, Z. M.; Yu, Z.; Qiu, H.; Ma, B.; Wu, H. H.; Zhang, J. *ACS Catal.* **2015**, *5*, 7488.

(34) Bohan, P. T.; Toste, F. D. *J. Am. Chem. Soc.* **2017**, *139*, 11016.

(35) Wu, C.; Hu, A.; Zhang, L.; Lin, W. *J. Am. Chem. Soc.* **2005**, *127*, 8940.

(36) Cesari, C.; Conti, S.; Zacchini, S.; Zanotti, V.; Cassani, M. C.; Mazzoni, R. *Dalton Trans.* **2014**, *43*, 17240.

(37) Hobday, C. L.; Marshall, R. J.; Murphie, C. F.; Sotelo, J.; Richards, T.; Allan, D. R.; Düren, T.; Coudert, F.-X.; Forgan, R. S.; Morrison, C. A.; Moggach, S. A.; Bennett, T. D. *Angew. Chem. Int. Ed.* **2016**, *55*, 2401.

(38) Rowsell, J. L. C.; Yaghi, O. M. *J. Am. Chem. Soc.* **2006**, *128*, 1304.

(39) Liu, C.; Zeng, C.; Luo, T. Y.; Merg, A. D.; Jin, R.; Rosi, N. L. *J. Am. Chem. Soc.* **2016**, *138*, 12045.

(40) Michalska, M.; Grela, K. *Synlett* **2015**, *27*, 599.

(41) Schaub, T.; Radius, U. *Tetrahedron Lett.* **2005**, *46*, 8195.

(42) Ardolino, M. J.; Morken, J. P. *J. Am. Chem. Soc.* **2012**, *134*, 8770.

(43) Sheldrick, G. M. *Acta Crystallogr. Sect. A Found. Crystallogr.* **2008**, *64*, 112.

(44) Dolomanov, O. V.; Bourhis, L. J.; Gildea, R. J.; Howard, J. A. K.; Puschmann, H. *J. Appl. Crystallogr.* **2009**, *42*, 339.

(45) Macrae, C. F.; Edgington, P. R.; McCabe, P.; Pidcock, E.; Shields, G. P.; Taylor, R.; Towler, M.; van de Streek, J. *J. Appl. Crystallogr.* **2006**, *39*, 453.